
Doctoral Dissertations

Student Theses and Dissertations

Summer 2015

Reliability-based optimization design of geosynthetic reinforced embankment slopes

Michelle (Mingyan) Deng

Follow this and additional works at: https://scholarsmine.mst.edu/doctoral_dissertations



Part of the [Civil Engineering Commons](#)

Department: Civil, Architectural and Environmental Engineering

Recommended Citation

Deng, Michelle (Mingyan), "Reliability-based optimization design of geosynthetic reinforced embankment slopes" (2015). *Doctoral Dissertations*. 2407.

https://scholarsmine.mst.edu/doctoral_dissertations/2407

This thesis is brought to you by Scholars' Mine, a service of the Missouri S&T Library and Learning Resources. This work is protected by U. S. Copyright Law. Unauthorized use including reproduction for redistribution requires the permission of the copyright holder. For more information, please contact scholarsmine@mst.edu.

RELIABILITY-BASED OPTIMIZATION DESIGN OF GEOSYNTHETIC
REINFORCED EMBANKMENT SLOPES

by

MICHELLE (MINGYAN) DENG

A DISSERTATION

Presented to the Faculty of the Graduate School of the
MISSOURI UNIVERSITY OF SCIENCE AND TECHNOLOGY

In Partial Fulfillment of the Requirements of the Degree

DOCTOR OF PHILOSOPHY

in

CIVIL ENGINEERING

2015

Approved

Ronaldo Luna, Advisor

Bate Bate

Xiaoming He

Norbert Maerz

Cesar Mendoza

© 2015

Michelle (Mingyan) Deng

All Rights Reserved

ABSTRACT

This study examines the optimization design of geosynthetic reinforced embankment slopes (GRES) considering both economic benefits and technical safety requirements. In engineering design, cost is always a big concern. To minimize the cost, engineers tend to seek an optimal combination of design parameters among the considered alternatives while ensuring the optimal solution is safe. Reliability-based optimization (RBO) is such a technique that provides engineers the optimal design with the minimum cost while all technical design requirements are satisfied. The research goal of this study is to implement a mathematical formulation algorithm of the RBO technique in GRES design. To achieve this goal, slope stability is studied using the limit equilibrium method (LEM). Considering geotechnical uncertainties, the first-order reliability method (FORM) is adopted to perform probabilistic slope stability analysis, address the critical slip surfaces, and assess the reliability of the slope system. The slope stability and reliability are then used as the crucial constraints in the following RBO procedure, wherein the constrained optimization problem will be solved by adopting a genetic algorithm (GA). Sensitivity analysis is carried out on the basis of the probabilistic slope stability analysis to highlight the influence of each involved random variable on the probabilistic performance of the slope system; and thereby, infer the corresponding impact on the optimization design. A framework of how to implement the RBO in GRES design is proposed. An engineering case history is accordingly studied to demonstrate the practical application of the proposed design framework. Compared to the conventional (manual) process, the proposed design framework is more systematic and effective, especially with the large number of design variables involved in geosynthetic reinforced slopes.

ACKNOWLEDGMENTS

I am deeply indebted to my adviser Professor Dr. Ronaldo Luna for his fundamental role in my doctoral work. I would like to express my special appreciation and thanks to Dr. Luna for the tremendous mentor, immeasurable guidance, support, and encouragement over the years. I would also like to thank my committee members, Drs. Bate Bate, Xiaoming He, Norbert Maerz, and Cesar Mendoza for their time and valuable feedback on my Ph.D. defense and the preliminary version of this dissertation.

I gratefully acknowledge the support I received from Missouri University of Science and Technology, and the Department of Civil, Architectural, and Environmental Engineering. I wish to thank Missouri Department of Transportation (MoDOT) and Geosynthetic Institute (GSI) for providing funds for this research. I would also like to thank Dr. David Espinoza, the principal in Geosyntec consultants, for providing the information regarding the Cherry Island Landfill vertical expansion project used in the case study in this research. I wish to thank the graduate students in our geotechnical engineering group for all the great times that we have shared, including the current students: Junnan Cao, Xin Kang, Kerry Magner, Audai Theinat, Jianfeng Zhu; as well as the graduated students: Kyle Kershaw, Nicholas Rocco, Site Onyejekwe, Shuying Wang, and Xiaoyi Zhao.

I am deeply thankful to my parents: Guoxiong Deng and Pinghua Wu. They were the first community that encouraged me find my passion in learning. Without them, this dissertation would never have been written. And finally, I would like to thank Dong Pan for all his love and support.

TABLE OF CONTENTS

	Page
ABSTRACT	iii
ACKNOWLEDGMENTS	iv
LIST OF ILLUSTRATIONS	xiv
LIST OF TABLES	xvii
SECTION	
1 INTRODUCTION	1
1.1 OVERVIEW	1
1.1.1 Reliability-based Optimization.	2
1.1.2 Geosynthetic Reinforced Embankment Slopes.	3
1.2 OBJECTIVES	4
1.3 DISSERTATION ORGANIZATION	5
2 REVIEW OF METHODOLOGIES	6
2.1 OVERVIEW	6
2.2 SLOPE STABILITY ANALYSIS	6
2.2.1 Sliding Block Method.	9
2.2.1.1 Coulomb's theory.	11
2.2.1.2 Rankine's theory.	13
2.2.2 Rotational Method.	14
2.2.2.1 Ordinary method of slices.	14
2.2.2.2 Slip surfaces.	15
2.3 RELIABILITY-BASED ANALYSIS	17
2.3.1 Probability of Failure.	18

2.3.2 Probabilistic Approaches.	19
2.4 CRITICAL SLIP SURFACES	22
2.4.1 Deterministic Analysis.	22
2.4.2 Probabilistic Analysis.	23
2.4.3 Search Approaches.	23
2.5 RELIABILITY-BASED OPTIMIZATION	25
2.6 METHODS EMPLOYED IN THIS RESEARCH	27
3 RELIABILITY-BASED SLOPE STABILITY ANALYSIS	29
3.1 OVERVIEW	29
3.2 STATISTICAL INFERENCE	29
3.2.1 Probability Distribution Models.	30
3.2.2 Probabilistic Parameters.	33
3.2.3 Correlations.	35
3.3 PROBABILISTIC ANALYSIS ALGORITHM	37
3.3.1 MPP-Based FORM.	37
3.3.1.1 Transformation.	37
3.3.1.2 Linearization.	41
3.3.1.3 MPP search.	44
3.3.2 Monte Carlo Simulation.	45
3.4 PROBABILISTIC ANALYSIS IN GRES APPLICATION	47
3.4.1 Multiple Failure Modes.	49
3.4.2 System Reliability.	49
3.4.2.1 Internal failure.	51
3.4.2.2 External failure.	55
3.4.2.2.1 Sliding failure	55

3.4.2.2.2	Deep-seated overall instability	56
3.4.2.2.3	Lateral squeeze failure	57
3.4.2.2.4	Excessive settlement	58
3.4.2.3	Compound failure.	59
3.4.3	Short and Long-Term Conditions.	60
3.5	NUMERICAL EXAMPLE	62
3.5.1	Numerical Example 1: Geotextile Reinforced Road Embankment.	62
3.5.1.1	Deterministic slope stability analysis.	64
3.5.1.2	Probabilistic slope stability analysis.	67
3.5.1.2.1	Uncorrelated random variables	67
3.5.1.2.2	Correlated random variables	70
3.5.1.2.3	System reliability	74
3.5.2	Numerical Example 2: Geogrid Reinforced Embankment Slope.	76
3.5.2.1	Deterministic slope stability analysis.	78
3.5.2.2	Probabilistic slope stability analysis.	80
3.5.2.2.1	Uncorrelated random variables	80
3.5.2.2.2	Correlated random variables	84
3.5.2.2.3	System reliability	86
3.5.3	Discussion.	87
3.6	SUMMARY	92
4	RELIABILITY-BASED SENSITIVITY ANALYSIS	94
4.1	OVERVIEW	94
4.2	PROBABILISTIC SENSITIVITY ANALYSIS ALGORITHM	94
4.2.1	Methods of PSA.	95
4.2.2	MPP-Based PSA.	96

4.2.2.1	Uncorrelated random variables.	98
4.2.2.2	Correlated random variables.	100
4.3	PROBABILISTIC SENSITIVITY ANALYSIS IN GRES DESIGN	102
4.4	NUMERICAL EXAMPLE	104
4.4.1	Uncorrelated Random Variables.	104
4.4.2	Correlated Random Variables.	109
4.5	SUMMARY	113
5	RELIABILITY-BASED OPTIMIZATION DESIGN	115
5.1	OVERVIEW	115
5.2	THE PROBLEMS IN TRADITIONAL DESIGN PROCEDURE	116
5.3	THE PROPOSED RBO DESIGN PROCEDURE	121
5.3.1	RBO Design Algorithm.	122
5.3.2	RBO Design in GRES Application	123
5.3.2.1	Objective functions.	126
5.3.2.1.1	Usage of geosynthetic reinforcements	126
5.3.2.1.2	Cost of geosynthetic reinforcements	131
5.3.2.2	Constraints.	134
5.3.3	RBO Design Procedure.	137
5.4	NUMERICAL EXAMPLE	140
5.4.1	Numerical Example 1: Geotextile Reinforced Road Embankment.	140
5.4.1.1	Design factors.	141
5.4.1.2	Design requirements.	142
5.4.1.3	Design process.	143
5.4.1.3.1	Initial design	144
5.4.1.3.2	Second design	146

5.4.1.4 Results comparison.	149
5.4.1.4.1 Required factor of safety	149
5.4.1.4.2 Target probability of failure	157
5.4.1.4.3 Distribution model	162
5.4.1.4.4 Constraints	168
5.4.2 Numerical Example 2: Geogrid Reinforced Embankment Slope. . .	173
5.4.2.1 Design factors and requirements.	176
5.4.2.2 Design process and results.	177
5.4.3 Discussion.	185
5.5 SUMMARY	190
6 PROPOSED DESIGN FRAMEWORK AND PRACTICAL APPLICATION .	192
6.1 OVERVIEW	192
6.2 PROPOSED FRAMEWORK	192
6.3 CASE STUDY: CHERRY ISLAND LANDFILL	196
6.3.1 Project Description.	197
6.3.2 Current MSE Berm Design.	198
6.3.3 Proposed RBO Framework in MSE Berm Design.	200
6.3.3.1 Sections for analysis.	200
6.3.3.2 Subsurface conditions.	201
6.3.3.3 Simplified model.	203
6.3.3.3.1 Model geometry	203
6.3.3.3.2 Optimized objectives	203
6.3.3.3.3 Loading conditions	204
6.3.3.4 Design parameters.	205
6.3.4 Results and Discussions.	207

6.3.4.1 RBO optimization design.	208
6.3.4.1.1 Two reinforcement zones	210
6.3.4.1.2 Three reinforcement zoens	211
6.3.4.1.3 Four reinforcement zones	213
6.3.4.2 Results comparison.	214
6.4 SUMMARY	217
7 CONCLUSIONS AND RECOMMENDATIONS	218
7.1 CONCLUSIONS	218
7.2 RECOMMENDATIONS FOR FUTURE WORK	221
APPENDICES	
A VARIABLE TRANSFORMATION	223
B LATERAL EARTH PRESSURE THEORY	234
C GEOSYNTHETIC PRODUCTS	241
REFERNCE	249
VITA	257

LIST OF ILLUSTRATIONS

Figure	Page
1.1 Typical components in a GRES structure (Elias et al. 2001)	3
2.1 Various failure mechanisms (Naresh and Edward 2006)	9
2.2 Sliding block method	10
2.3 The two-part wedge mechanism for sliding analysis	11
2.4 The configuration of an unreinforced slope and the forces on a slice with a circular slip surface	16
2.5 The configuration of GRES and the forces on a circular slip surface	17
2.6 A double-loop procedure, adapted from Du et al. (2007)	26
3.1 Pearson's distribution space of β_1 and β_2 coordinates: E - uniform distribution ($\beta_1 = 0, \beta_2 = 1.8$), N - normal distribution, E_x - exponential distribution (Rethati 1988)	32
3.2 The MPP-based FORM in a two-dimensional standard normal space (Du et al. 2010)	38
3.3 Correlated variable transformation	40
3.4 HL-RF search algorithm for locating MPP, adapted from Du et al. (2010)	45
3.5 Monte Carlo Simulation algorithm, adapted from Gasser and Schueller (1997) and Du et al. (2010)	46
3.6 Probabilistic slope stability analysis procedure	48
3.7 Failure modes of reinforced soil slopes (Elias et al. 2001)	49
3.8 Lateral squeezing failure mechanism, adapted from Silvestri (1983)	58
3.9 The configuration of the road embankment in Example 1	63
3.10 The critical deterministic slip surfaces in Example 1	65
3.11 The critical deterministic and probabilistic slip surfaces in Example 1	68
3.12 The comparison of the probabilistic results in Case I to IV in Example 1	71

3.13	The comparison of the probabilistic results in Case V in Example 1	73
3.14	The comparison of the probabilistic results in Case VI in Example 1	73
3.15	The system reliability in Case I to IV in Example 1	75
3.16	The system reliability in Case V in Example 1	75
3.17	The system reliability in Case VI in Example 1	76
3.18	The configuration of the embankment slope in Example 2	77
3.19	The critical deterministic slip surfaces in Example 2	78
3.20	The critical deterministi and probabilistic slip surfaces in Eample 2	81
3.21	The comparison of the probabilistuc results in Case I to IV in Example 2 . . .	83
3.22	The comparison of the probabilistic results in Case V in Example 2	85
3.23	The comparison of the probabilistic results in Case VI in Example 2	86
3.24	The system reliability in Case I to IV in Example 2	88
3.25	The system reliability in Case V in Example 2	88
3.26	The system reliability in Case VI in Example 2	89
5.1	Traditional deterministic design procedure (Elias et al. 2001)	117
5.2	Critical zone defined by rotational and sliding surfaces that meet the re- quired factor of safety (Elias et al. 2001)	118
5.3	Genetic algorithm general framework, adapted from (Coley 1999; Melanie 1999)	124
5.4	Spacing versus reinforcement strength, adapted from Elias et al. (2001) . . .	127
5.5	Developing reinforcement lengths, adapted from Elias et al. (2001)	128
5.6	Primary and secondary reinforcements distribution (Elias et al. 2001)	130
5.7	Unit price vs. allowable tensile strength, collected from US Fabrics	134
5.8	The RBO procedure in GRES design	138
5.9	Slope stability analyses on the original unreinforced slope in Example 1 . . .	141

5.10	The initial design in case 1.3 in Example 1	145
5.11	The second design in case 1.3 in Example 1	148
5.12	The initial and second design in case 1.2 in Example 1	151
5.13	System reliability vs. design trial in case 1.3, 1.2, and 1.1 in Example 1	155
5.14	The usage/cost with different required factor of safety in Example 1	156
5.15	System reliability vs. design trial in case 1.2 ^[0.01] in Example 1	161
5.16	System reliability vs. design trial in case 1.1 ^[0.01] in Example 1	161
5.17	The usage/cost with different target probability of failure in Example 1	162
5.18	System reliability vs. design trial in case 1.3 ^[log] in Example 1	164
5.19	System reliability vs. design trial in case 1.2 ^[log] in Example 1	164
5.20	System reliability vs. design trial in case 1.1 ^[log] in Example 1	165
5.21	The usage/cost with different distribution model in Example 1	165
5.22	The usage/cost with probabilistic constraints only in Example 1	171
5.23	Slope stability analyses on the original unreinforced slope in Example 2	175
5.24	The initial design with $f_{s,req} = 1.5$, $p_{f,internal} = 0.01\%$ in Example 2	179
5.25	The modified design with $f_{s,req} = 1.5$, $p_{f,internal} = 0.01\%$ in Example 2	180
5.26	The modified design with $f_{s,req} = 1.3$, $p_{f,internal} = 0.1\%$ in Example 2	183
6.1	The proposed RBO design framework for GRES system	194
6.2	The location of Cherry Island Landfill	196
6.3	Plan view of Cherry Island Landfill, adapted from Houlihan et al. (2010)	197
6.4	Geometry and reinforcement scheme for MSE berm	199
6.5	The configuration of section A-A'	201
6.6	The configuration of MSE berm model for section A-A'	204
6.7	The critical deterministic and probabilistic slip surfaces for current design	208
6.8	The critical zone and slip surface to be reinforced	209

6.9	The optimized design with two reinforcement zones	211
6.10	The optimized design with three reinforcement zones	212
6.11	The optimized design with four reinforcement zones	213

LIST OF TABLES

Table	Page
2.1 The methods employed in this research work	27
3.1 Failure modes of geosynthetic reinforced slopes and analyzing methods, adapted from Elias et al. (2001) and Naresh and Edward (2006)	50
3.2 The material properties in Example 1	64
3.3 The pullout resistance in deterministic analysis in Example 1	66
3.4 The pullout resistance in probabilistic analysis in Example 1	69
3.5 The probabilistic results in Case I, II, III, and IV in Example 1	70
3.6 The probabilistic results in Case V in Example 1	72
3.7 The probabilistic results in Case VI in Example 1	72
3.8 The system reliability in Example 1	74
3.9 The material properties in Example 2	77
3.10 The pullout resistance in deterministic analysis in Example 2	79
3.11 The pullout resistance in probabilistic analysis in Example 2	82
3.12 The probabilistic results in Case I, II, III, and IV in Example 2	83
3.13 The probabilistic results in Case V in Example 2	84
3.14 The probabilistic results in Case VI in Example 2	85
3.15 The system reliability in Example 2	87
4.1 Sensitivity results in Example 1 (Case I)	105
4.2 Sensitivity results in Example 1 (Case II)	105
4.3 Sensitivity results in Example 1 (Case III)	106
4.4 Sensitivity results in Example 1 (Case IV)	106
4.5 Sensitivity results in Example 1 (Case V: $\rho = 0.1$)	107

4.6	Sensitivity results in Example 1 (Case V: $\rho = 0.5$)	108
4.7	Sensitivity results in Example 1 (Case VI: $\rho = 0.1$)	109
4.8	Sensitivity results in Example 1 (Case VI: $\rho = 0.5$)	110
4.9	Sensitivity results in Example 2 (Case I)	111
4.10	Sensitivity results in Example 2 (Case II)	111
4.11	Sensitivity results in Example 2 (Case V: $\rho = 0.5$)	112
5.1	The disadvantages of traditional design compared to RBO procedure	121
5.2	The unit price and ultimate tensile strength of geosynthetic products	133
5.3	The RBO design requirements in Example 1	144
5.4	The RBO design in Example 1 ($f_{s,req} = 1.3, p_{f_{internal}} = 0.1\%$)	147
5.5	The RBO design in case 1.2 in Example 1	152
5.6	The RBO design in case 1.1 in Example 1	154
5.7	The RBO design in case 1.2 ^[0.01] in Example 1	158
5.8	The RBO design in case 1.1 ^[0.01] in Example 1	160
5.9	The RBO design in case 1.3 ^[log] in Example 1	166
5.10	The RBO design in case 1.2 ^[log] in Example 1	167
5.11	The RBO design in case 1.1 ^[log] in Example 1	169
5.12	The RBO design with probabilistic constraints only in Example 1 ($p_{f_{internal}} = 0.1\%$)	172
5.13	The RBO design with probabilistic constraints only in Example 1 ($p_{f_{internal}} = 0.05\%$)	174
5.14	The RBO design requirements in Example 2	177
5.15	The RBO design in Example 2 ($f_{s,req} = 1.5, p_{f_{internal}} = 0.01\%$)	181
5.16	The RBO design in Example 2 ($f_{s,req} = 1.3, p_{f_{internal}} = 0.1\%$)	184
6.1	Geosynthetic products in the current MSE berm design in the CIL project	200

6.2	The material properties for section A-A' at the CIL site	202
6.3	The reinforcement zones and design variables	205
6.4	Summary of material parameters for design	207
6.5	Summary of slope performance, reinforcement usage and cost	215
6.6	Summary of reinforcement design for the MSE berm in CIL project	215

1. INTRODUCTION

1.1. OVERVIEW

In engineering design, cost is always a big concern. A design should not be only technically feasible, but also economically competent. Usually, there could be various design alternatives to meet the same technical design requirements, but the cost involved could vary significantly. In order to minimize the cost, engineers tend to select an optimal combination of design parameters among the considered alternatives. The process of searching for such an optimal combination is called ‘optimization’. In practical design of geotechnical systems, optimization is always performed manually based on the alternatives selected by engineers experience and judgment. However, a crucial issue faced by designers is: when a large number of design parameters are involved, the design process becomes very time consuming and probably fails to find the ‘best’ optimal result due to the limited number of alternatives the designers can attempt manually.

In light of the preceding issue, a more systematic and effective optimization approach is required so that the cost of a constructed facility is minimized while all technical design requirements are satisfied. Furthermore, due to the unavoidable geotechnical uncertainties which are primarily arising from inherent soil variability, measurement error and transformation uncertainty (Christian et al. 1995; Phoon and Kulhawy 1999b; Phoon and Kulhawy 1999a; Baecher and Christian 2003), reliability-based analysis has been introduced in geotechnical practice with an intention to assess the risk associated with the design of geo-structures. Therefore, to take the reliability requirements into consideration, reliability-based optimization (RBO) needs to be carried out, while optimization is performed by coupling reliability assessment.

1.1.1. Reliability-based Optimization. Theoretically, RBO is a constrained minimization problem, that minimizes an objective function while variables are subject to some reliability constraints. When RBO is applied to the problems of engineering interest, the objective function is always specified as cost function or volume function, while the constraints are determined by design requirements and explicitly model the effects of uncertainties. The idea of RBO is attractive. Substantial studies have been done on solving the RBO problems in past decades as recently summarized by Valdebenito and Schuëller (2010). However, its practical implementation is still challenging because of the coupling between reliability assessment and cost minimization, the high numerical costs involved in its solution, and the interpretation of a specific engineering problem in mathematical and computational language. So far the application of the RBO technique in geotechnical engineering is still very limited. Recent studies mainly focus on the design of pile groups (Chan et al. 2009), foundations (Babu and Basha 2008; Basha and Babu 2008) and retaining walls (Babu and Basha 2008; Basha and Babu 2008; Basha and Babu 2010; Zhang et al. 2011b). Few studies have been carried out on the focus of slope design; particularly in the area of reinforced slopes.

As mentioned by Elias et al. (2001), the use of reinforced soil slope (RSS) structures has expanded dramatically in 1990s; approximately 70 to 100 RSS projects were being constructed yearly in connection with transportation related projects in United States, with an estimated projected vertical face area of 130,000 m²/year. In the last decade, with the developments in reinforcement materials and construction techniques, the use of RSS continuously expands because of its economics and successful performance. Therefore, it can be reasonably expected that great contributions can be made by improving the opti-

mization procedure in the design of reinforced slopes in practice.

1.1.2. Geosynthetic Reinforced Embankment Slopes. Geosynthetic reinforced embankment slope (GRES) is a unique RSS structure which is a form of reinforced soil that incorporates planar geosynthetic reinforcing elements in constructed earth-sloped structures with face inclinations less than 70 degrees. And ‘geosynthetics’ is a generic term that encompasses flexible polymeric materials used in geotechnical engineering (Elias et al. 2001), such as geotextiles, geogrids, geonets, geomembranes, etc.. Among the considered geosynthetic products, geotextiles and geogrids are the two categories used as reinforcement materials most often. A typical GRES structure, as shown in Figure 1.1, generally

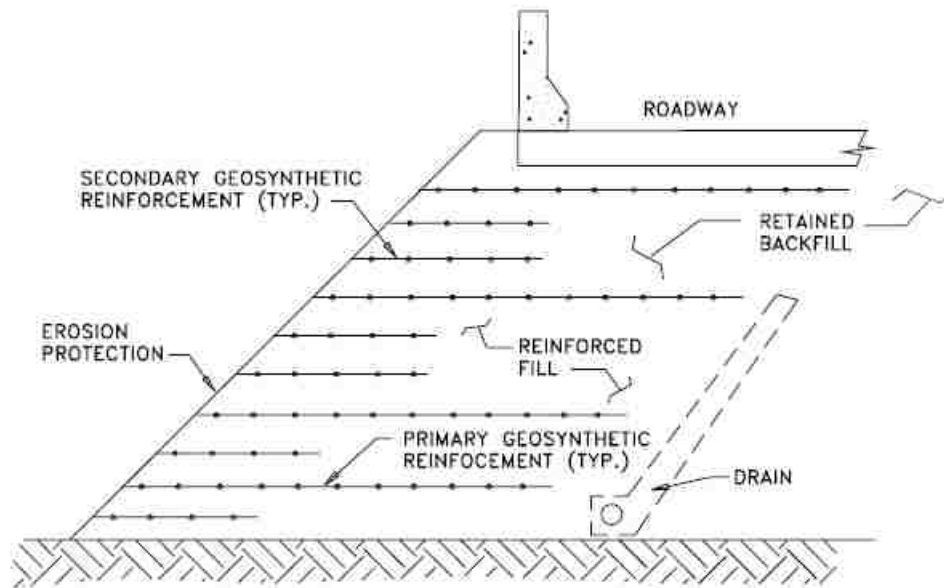


Figure 1.1: Typical components in a GRES structure (Elias et al. 2001)

consists of foundation, retained backfill, reinforced fill, subsurface drainage, primary reinforcements, secondary reinforcements and surface protection. Primary reinforcements are horizontally placed within the slope to provide tensile forces to resist instability. Ei-

ther geotextiles or geogrids with sufficient strength and soil compatible modulus can be used as primary reinforcements. Secondary reinforcements are used to locally stabilize the slope face during and after slope construction. In other words, by placing geosynthetic reinforcements, it is able to construct a slope at an angle steeper than could otherwise be safely constructed with the same soil (Elias et al. 2001). Therefore, the use of GRES is able to increase land usage and decrease site development costs.

Elias et al. (2001) shows a study of the site specific costs of soil-reinforced structures based on a survey of state and federal transportation agencies. In general, the use of GRES results in substantial savings on the order of 25 to 50 percent and possibly more in comparison with a conventional reinforced concrete retaining structure, especially when the latter is supported on a deep foundation system. Furthermore, the study provides an approximation of the actual cost of a specific GRES structure, which is basically depending on the cost of each principal component: 1) reinforcements, 45 to 65 percent of total cost; 2) reinforced fill, 30 to 45 percent of total cost; and 3) face treatments, 5 to 10 percent of total cost. The above are the typical relative costs estimated based on limited data. Details may vary with different projects. But basically it concludes the approximate proportions of expenditures, wherein the reinforcement is obviously the principal part, the optimization design of which is expected to be significant to the total cost.

1.2. OBJECTIVES

This study is primarily focused on the development and implementation of the RBO technique in GRES design with an intention to minimize the geosynthetic reinforcement cost. To achieve this goal, four major research objectives are identified as follows:

1. Perform both deterministic and probabilistic slope stability analyses, in which the

factor of safety and the probability of failure are respectively computed to assess the stability and reliability of the GRES structure;

2. Develop a RBO framework on the focus of GRES design, where the objective function is specified as the geosynthetic reinforcement cost while the crucial constraints are assigned by the previous slope stability analyses;
3. Perform reliability-based sensitivity analysis to evaluate the effects of the uncertainty in each involved random variable on the probabilistic performance and the optimization design of the GRES; and
4. Demonstrate the application of the proposed framework in an engineering case study.

1.3. DISSERTATION ORGANIZATION

This dissertation is organized in seven sections. An introduction to the research topic is presented in Section 1. A comprehensive literature review is presented in Section 2. Through Section 3 to 6, the four major research objectives as mentioned above are respectively addressed in detail. In Section 3, the reliability-based (probabilistic) slope stability analysis and its application to GRES structure are introduced. In Section 4, a reliability-based sensitivity analysis is presented to evaluate the influence of the uncertainty in each random variable on the slope reliability. In Section 5, a reliability-based optimization framework for GRES design is proposed, that incorporates both the traditional deterministic and the proposed probabilistic slope stability analyses along with genetic algorithm (GA) to perform optimization. To demonstrate the proposed RBO framework with a practical application, the Cherry Island Landfill expansion is used as a case study in Section 6. Finally, conclusions and recommendations are presented in Section 7.

2. REVIEW OF METHODOLOGIES

2.1. OVERVIEW

To implement reliability-based optimization (RBO) in the design of geosynthetic reinforced embankment slopes (GRES), it is primarily consisting of three essential tasks: 1) slope stability analysis; 2) reliability-based (probabilistic) analysis; and 3) reliability-based optimization. In general, slope stability analysis is supposed to be embedded as a basic approach to quantify the slope safety; and is traditionally performed on the basis of deterministic soil properties. Three primary methodologies to perform slope stability analysis are reviewed in Section 2.2, wherein limit equilibrium is further discussed based on the various failure mechanisms regarding slope instability. When geotechnical uncertainty is taken into consideration, slope stability should be evaluated along with the reliability-based (probabilistic) analysis to estimate how probable the slope can fail. The methods commonly used to perform probabilistic slope stability analysis are reviewed in Section 2.3. Critical slip surfaces, representing the most dangerous positions within the slope, are routinely searched in most of the practical design and analyses, as stated in Section 2.4. Reliability-based optimization, when introduced in GRES design, intends to minimize the geosynthetic reinforcement cost; meanwhile, the design variables are subject to some reliability constraints and technical requirements. The methods that can be used to address such a constrained minimization problem are reviewed in Section 2.5. And in Section 2.6, the methods to be employed in this research are summarized.

2.2. SLOPE STABILITY ANALYSIS

Currently there are three primary methodologies to perform stability analysis for geosynthetic reinforced slopes: Continuum Mechanics, Limit Analysis (LA), and Limit

Equilibrium (LE). Continuum mechanics approach is numerically based, such as finite element (FE) or finite difference (FD); considers the full constitutive relationships of all the materials involved, e.g., backfills, reinforcements, and face treatments. It satisfies boundary conditions, produces displacements (unavailable in LE and LA) and considers local conditions and the compatibility between dissimilar materials. Generally, it is able to represent a problem in the most realistic fashion. To obtain reliable results, it asks for quality input data, which however is frequently not available in common practice. Furthermore, this approach often requires a designer with good understanding of the possible technical 'traps' that may occur during numerical modeling (Christopher et al. 2005; Leshchinsky et al. 2014). Limit analysis models the soil as a perfectly plastic material obeying an associated flow rule (Yu et al. 1998). It is able to deal with layered soil, complex geometries, groundwater effect, seismicity, and etc.. The numerical upper bound in LA of plasticity yields kinematically admissible failure mechanisms, which means it is not necessary to arbitrarily assume a mechanism as done in LE; and is thereby considered as an advantage when complex problems are involved (Leshchinsky et al. 2014). However, because of its limited familiarity of practicing engineers, this method is not commonly used in routine design.

Limit equilibrium has been the most popular method for slope stability calculations for years by assuming that soil at failure obeys the perfectly plastic Mohr-Coulomb criterion. A major advantage of this approach is its capability to deal with complex soil profiles, seepage and a variety of loading conditions (Yu et al. 1998). As concluded by Christopher et al. (2005), its application to reinforced soil slope (RSS) structures is an extension of the classical approach that has been used for unreinforced slopes for decades. That is, investigates the equilibrium of the soil mass tending to slide down under the in-

fluence of gravity and surcharge, and evaluates the slope stability by producing a factor of safety (f_s) which is defined as the ratio of resisting forces (moments) to driving forces (moments) to maintain a static equilibrium. In geosynthetic reinforced slopes, the stabilizing forces contributed by reinforcement layers are incorporated into the limiting equilibrium equations to determine the factor of safety of the reinforced mass. However, unlike the continuum mechanics approach, a main concern of this method is neither LE nor LA considers the compatibility between dissimilar materials. In unreinforced slopes, this issue is always solved by predetermining the failure surfaces according to the prevailing failure mechanism when vastly different soil layers exist. Similarly, in geosynthetic reinforced slopes, as mentioned by Leshchinsky et al. (2014), the use of LE in conjunction with soils and geosynthetic reinforcements is always not much of an issue. Overall, limit equilibrium is simple to perform and has been adopted in most of the geotechnical specialized software for slope stability analysis, e.g., Slope/W, Slide, SVSlope, Stable, and some RSS design programs, e.g., ReSSA, MiraSlope, SecueSlope, and etc.. Furthermore, LE is the method used in the current design manual: FHWA Mechanically Stabilized Earth Walls and Reinforced Soil Slopes Design & Construction Guidelines (Elias et al. 2001).

Substantial studies have been done on the classical limit equilibrium slope stability analysis for unreinforced slopes. Various approaches have been developed based on different failure mechanisms. For example, planar failure analysis is commonly used in the rock masses that consist of planar joints or bedding planes along which sliding failure may occur (Figure 2.1a). Infinite slope analysis is similar to the planar failure analysis but with a sliding surface parallel to the slope face (Figure 2.1b). Sliding block method, sometimes, is also called wedge method due to the wedge-shaped failure surface predetermined in the slope (Figure 2.1c). And rotational analysis is always performed on a rotational

sliding mass with a non-planar failure surface, such as circular or log spiral (Figure 2.1d), which seems to be more common in most of the soil slopes. In geosynthetic reinforced embankment slopes, planar failure (or infinite failure) hardly occurs due to the relatively homogeneous fill material and the localized reinforcements; but the latter two are commonly implemented in the analyses as demonstrated by Elias et al. (2001).

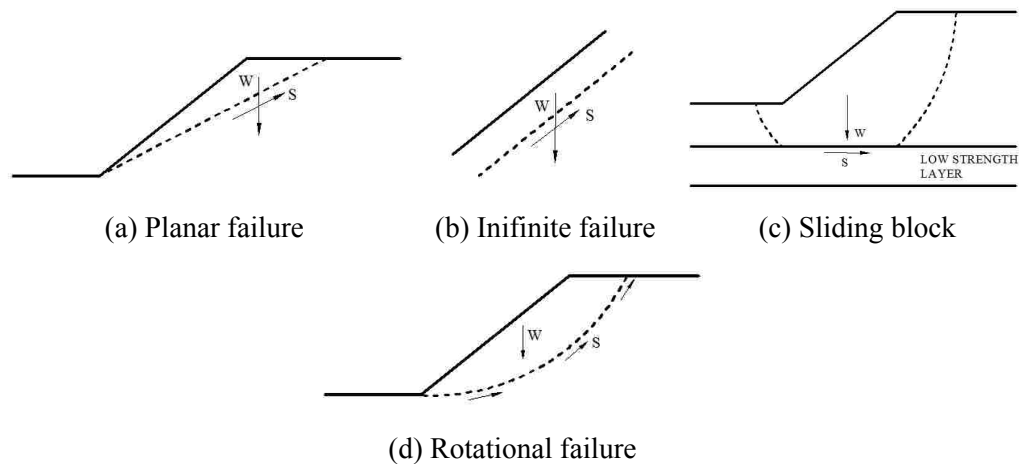


Figure 2.1: Various failure mechanisms (Naresh and Edward 2006)

2.2.1. Sliding Block Method. For the analysis, the potential sliding block is usually divided into three parts: an active wedge at the head of the slide; a central block; and a passive wedge at the toe. As shown in Figure 2.2, P_a is the active force; P_p is the passive force; T is the resisting force due to the interaction between the central block and the bottom layer, simply $= cL + N \tan \phi$, where c and ϕ are the smaller cohesion and friction angle of either the central block or the bottom layer; L is the horizontal width of the central block; and N , the normal force acting on the base of the reinforced mass, can be easily derived by taking vertical equilibrium on the central block. The factor of safety can

be accordingly computed by summing the horizontal forces acting on the central block as given below:

$$f_s = \frac{F_R}{F_D} \quad (2.1)$$

where F_R is the horizontal resisting forces; F_D is the horizontal driving forces (Naresh and Edward 2006). As a result, to determine the minimum factor of safety, various trial locations of the active and the passive wedges need to be checked.

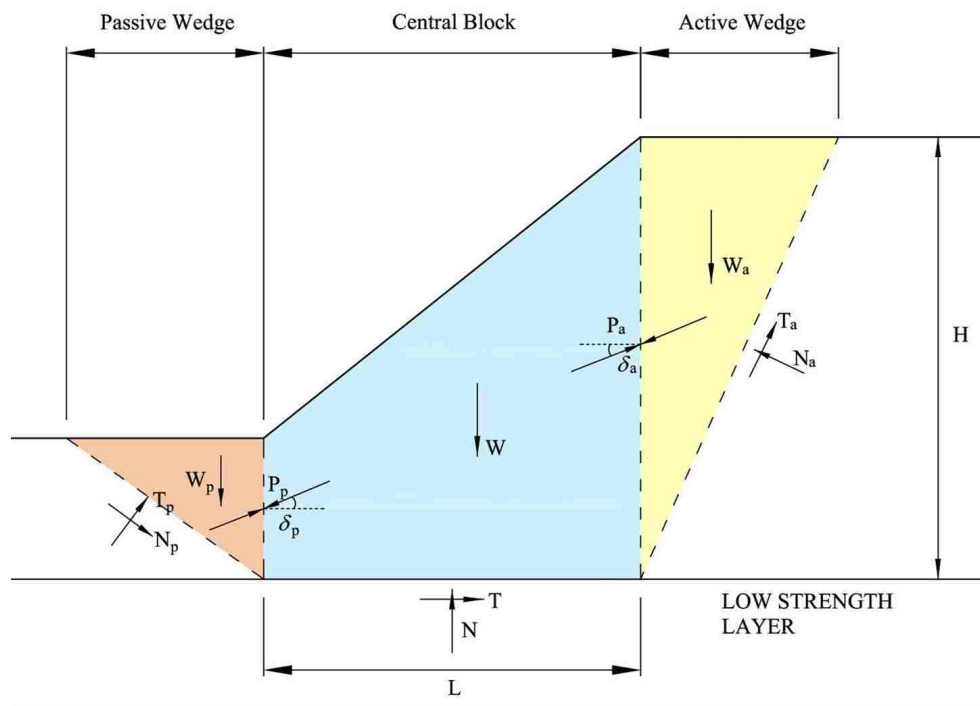


Figure 2.2: Sliding block method

2.2.1.1. Coulomb's theory. To compute the lateral forces, P_a and P_p , two classical theories are commonly involved: Coulomb's theory and Rankine's theory. Coulomb's theory is considered more realistic and generalized compared to the Rankine's, since the latter one assumes a frictionless wall face, that is however, a very ideal situation and can hardly occur. Especially in slope stability analysis, the 'wall' is the central block and the 'wall friction' is contributed by the friction angle of the backfill. Therefore, in Coulomb's theory, the lateral forces acting on the central block are always inclined from the horizontal with an angle that represents the wall-and-soil interface friction, as δ_a or δ_p in Figure 2.2, the value of which is always assumed between $2\phi_w/3$ and ϕ_w , where ϕ_w is the smaller friction angle of either the central block or its neighbor wedge. But in Rankine's theory, since the wall is assumed frictionless, the lateral forces are horizontally acting on the central block. In a geosynthetic reinforced slope system, sliding failure is most likely along the interface between reinforced mass and foundation soil, so that only two wedges are considered as shown in Figure 2.3.

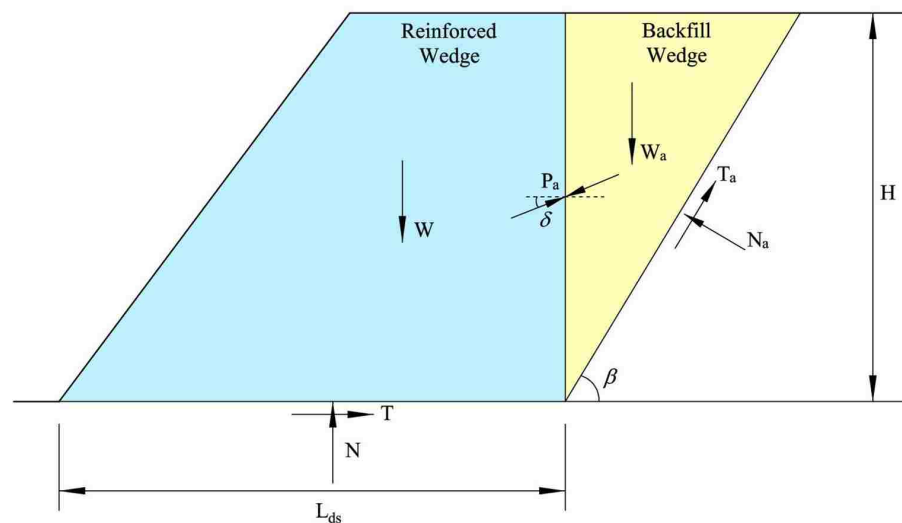


Figure 2.3: The two-part wedge mechanism for sliding analysis

When applied to a uniform granular slope, without considering groundwater effects, Coulomb's theory gives an active force as

$$P_a = \frac{1}{2} K_a \gamma_b H^2 \quad (2.2)$$

where γ_b is the unit weight of the backfill; K_a is the Coulomb's active earth pressure coefficient, give as (Das 2011)

$$K_a = \frac{\cos^2 (\phi'_b - \theta)}{\cos^2 \theta \cos (\delta + \theta) \left[1 + \sqrt{\frac{\sin (\delta + \phi'_b) \sin (\phi'_b - \alpha)}{\cos (\delta + \theta) \cos (\theta - \alpha)}} \right]^2} \quad (2.3)$$

where ϕ'_b is the friction angle of the backfill; θ is the inclination of the back surface of the reinforced zone from vertical; α is the inclination of the backfill from horizontal; and δ is the friction angle between reinforced mass and backfill. According to Figure 2.3, for a vertical reinforced face ($\theta = 0^\circ$) with a horizontal backfill ($\alpha = 0^\circ$), Equation 2.3 can be simplified as

$$K_a = \frac{\cos^2 \phi'_b}{\cos \delta \left[1 + \sqrt{\frac{\sin (\delta + \phi'_b) \sin \phi'_b}{\cos \delta}} \right]^2} \quad (2.4)$$

Considering the equilibrium of the reinforced wedge, the factor of safety against sliding

can be obtained based on Equation 2.1, as (Elias et al. 2001)

$$f_s = \left(\frac{W}{P_a \cos \delta} + \tan \delta \right) \tan \phi' \quad (2.5)$$

where ϕ' is the smaller friction angle of either reinforced mass or foundation soil, and W is the weight of the reinforced wedge.

2.2.1.2. Rankine's theory. In a more generalized case that has cohesive soils and groundwater effects involved, a new active force needs to be derived by taking equilibrium on the reinforced wedge. Therefore, the factor of safety will be redefined. But if multiple layers are involved, Rankine's theory seems a more efficient way to evaluate the lateral earth pressure, since the Coulomb's method asks for more equilibrium conditions. Therefore, in Rankine's theory, a generalized form to compute the active force is given by (Das 2011)

$$P_a = \sum_{i=1}^n \int_0^{h_i} \sigma'_{v_i} K_{a_i} dz + \int_0^H u dz \quad (2.6)$$

where σ'_{v_i} is the effective vertical stress in the i th layer; h_i is the height of the i th layer; u is the pore pressure; n is the number of soil layers; and K_{a_i} is the Rankine's active earth pressure coefficient in the i th layer, given as

$$K_a = \frac{2}{\cos^2 \phi'_b} (1 + M \cos \phi'_b \sin \phi'_b - M \cos \phi'_b - \sin \phi'_b) - 1 \quad (2.7)$$

where $M = c'_b/\gamma_b z$ with c'_b and ϕ'_b representing the cohesion and friction angle of the backfill.

2.2.2. Rotational Method. During last century, more than 10 methods of slices based on limit equilibrium were developed to deal with circular or arbitrarily shaped rotational slip surfaces (Duncan 1996). Using these methods, a potential slip body is divided into a finite number of vertical slices in order to calculate the forces on each slice, thereby, to determine the factor of safety as follows:

$$f_s = \frac{M_R}{M_D} \quad (2.8)$$

where M_R is the resisting moment; M_D is the driving moment. As concluded by Jiang et al. (2003), the existing methods of slices, e.g., ordinary method, Bishop simplified, Janbu simplified, Spencer, Sarma, and etc., involve various assumptions regarding the inter-slice forces along with various combinations of equilibrium conditions (force or/and moment) considered, thus giving different values of factor of safety for the same slip surface.

2.2.2.1. Ordinary method of slices. Ordinary method (Fellenius 1936) is the simplest of all with the simplified assumption that inter-slice forces are neglected. This method satisfies only one condition of equilibrium, and is proved to be relatively conservative and underestimates the factor of safety compared to those more accurate methods (i.e., Bishop simplified, Janbu simplified, and etc.) that satisfy more than one equilibrium conditions. As discussed by Duncan and Wright (1980), its accuracy is good enough for practical purposes in total stress analysis; while the result may be as much as 50% smaller than the 'correct' value that is provided by those more accurate methods for flat slopes with

high pore pressures in effective stress analysis. Regardless of its conditioned accuracy, many researchers are still using this method because of its easy application and computational efficiency especially when combined with reliability-based analysis (Hassan and Wolff 1999; Xue and Gavin 2007; Ching et al. 2009; Zhang et al. 2009).

2.2.2.2. Slip surfaces. The slip surface that may occur in a slope can vary in different conditions. In general, a circular failure analysis is sufficient for a slope in a homogeneous soil layer. But for the slope with heterogeneous multi-soil layers, a non-circular slip surface seems more appropriate (Zolfaghari et al. 2005). According to different slip surfaces, the calculation involved in slope stability analysis varies dramatically. Basically, the more complex the surface, the more complicated the calculation is. Therefore, the circular failure analysis is generally the simplest because of its straight-forward definition of a circular arc. But an arbitrarily shaped anomalous surface requires more efforts on geometry definition and computation; especially when it is to be combined with the reliability-based analysis, difficulties significantly increase. In the ordinary method, the factor of safety along a circular slip surface in an unreinforced slope (Figure 2.4) is derived based on Equation 2.8 as follows:

$$f_s = \frac{\sum_{i=1}^n [c'_i l_i + \tan \phi'_i (W_i \cos \alpha_i - u_i l_i)]}{\sum_{i=1}^n W_i \sin \alpha_i} \quad (2.9)$$

where c'_i and ϕ'_i are the effective cohesion and friction angle at the base of the i th slice; l_i is the arc length of the slip base of the i th slice; W_i is the weight of the i th slice; u_i is the pore water pressure acting on the bottom of the i th slice; α_i is the tangential inclination on

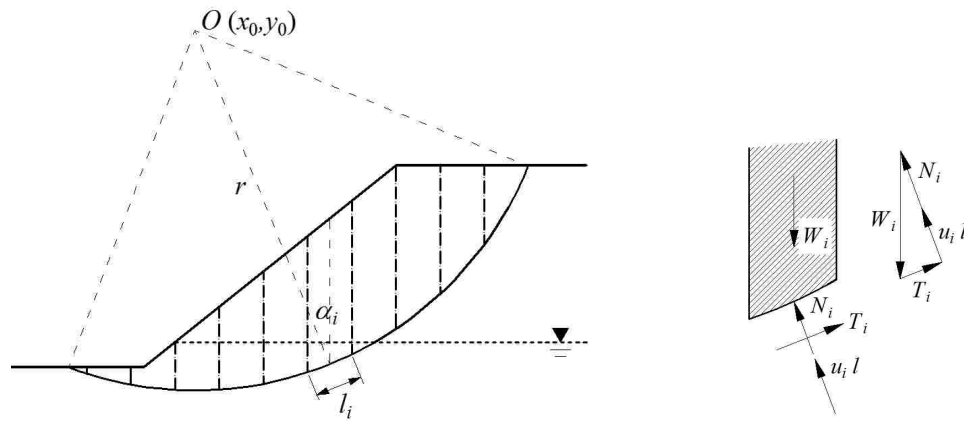


Figure 2.4: The configuration of an unreinforced slope and the forces on a slice with a circular slip surface

the base of the i th slice; and n is the number of slices. When the method is implemented in the stability analysis of geosynthetic reinforced slopes, by adding the contribution of the geosynthetic reinforcements directly to the resisting moment, the factor of safety becomes to

$$f_s = \frac{r \sum_{i=1}^n [c'_i l_i + \tan \phi'_i (W_i \cos \alpha_i - u_i l_i)] + \sum_{j=1}^m T_j d_j}{r \sum_{i=1}^n W_i \sin \alpha_i} \quad (2.10)$$

where T_j is the allowable tensile strength of the j th reinforcement layer; d_j is the moment arm of the j th reinforcement layer; r is the radius of the potential slip surface; and m is the number of reinforcement layers placed within the slope as shown in Figure 2.5. The direction of the tensile forces contributed by reinforcement layers and its corresponding moment arm have been the topic of discussion, because the geosynthetic layer is likely to be distorted as rotational deformation occurs. In the limit, the distortion could orient the

geosynthetics along the potential failure arc, thus changing the tensile forces from horizontal direction to tangential direction, and the moment arm from d_j to r (Koerner 2005). But in practical design, the horizontal tensile force is preferred to be used because of a more conservative d_j .

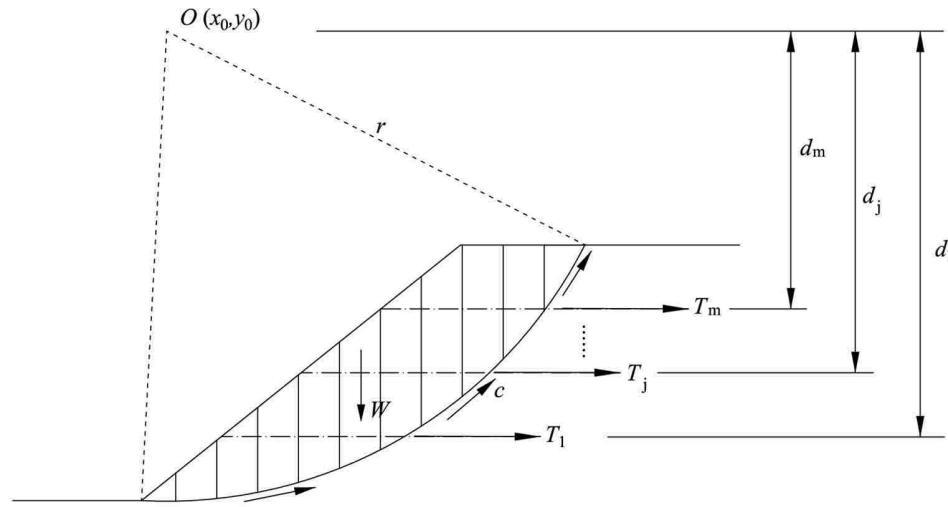


Figure 2.5: The configuration of GRES and the forces on a circular slip surface

2.3. RELIABILITY-BASED ANALYSIS

As demonstrated in Section 2.2, in limit equilibrium analysis, slope safety is conventionally assessed by means of the factor of safety. It is basically developed on the basis of the deterministic soil properties, typically using the mean (average) of the input parameters; and generally fails to be a consistent measure of risk. For example, slopes with the same value of the factor of safety may exhibit different risk levels depending on the uncertainty in soil properties. In other words, it is impossible to say how much safer a slope becomes as the factor of safety is increased (Li and Lumb 1987). To overcome

the preceding shortcoming of the deterministic approach, reliability-based (probabilistic) slope stability analysis is carried out to assess the probabilistic performance considering the relevant uncertainty.

The uncertainty in slope stability is the result of many factors. Some, such as the ignorance of geological details during subsurface exploration, are difficult to treat formally; others, such as the estimates of soil properties are more amenable to statistical analysis (Christian et al. 1995). As mentioned by Baecher and Christian (2003), the uncertainties in soil properties arise from two primary sources: 1) scatter in data, and 2) systematic error in soil property estimation. The former consists of inherent spatial variability in properties and random testing errors in their measurement. The latter consists of systematic statistical errors due to the precision of the correlation model used to transform the test result measurement into desired soil property. To take those uncertainties into consideration, a variety of analyzing methods have been proposed to perform probabilistic slope stability analysis and a concept of ‘probability of failure’ is introduced to assess slope reliability over the years (Cornell 1971; Vanmarcke 1977; Chowdhury and Xu 1994; Christian et al. 1995; Hassan and Wolff 1999; Li and Cheung 2001; Morgenstern and Cruden 2002; Bhattacharya et al. 2003; EI-Ramly et al. 2004; Griffiths and Fenton 2004; Xu and Low 2006; Cho 2007; Ching et al. 2009; Zhang et al. 2011b).

2.3.1. Probability of Failure. Mathematically, the probability of failure (p_f) is evaluated with the integral as follows:

$$p_f = P\{g(\mathbf{x}) < 0\} = \int_{g(\mathbf{x}) < 0} f_{\mathbf{x}}(\mathbf{x}) d\mathbf{x} \quad (2.11)$$

where $\{\mathbf{x}\}$ is the vector of random variables; $g(\mathbf{x})$ is the limit state function; $f_{\mathbf{x}}(\mathbf{x})$ is the joint density function of random variables $\{\mathbf{x}\}$. On the basis of reliability theory, the probability of failure can be expressed as

$$p_f = 1 - \Phi(\beta) \quad (2.12)$$

where β is the reliability index; $\Phi(\cdot)$ is the cumulative distribution function (CDF) of a standard normal distribution. When introduced in engineering design, the probability of failure is a parameter used to evaluate the impact of uncertainties on the performance of a design, where ‘failure’ is a generic term for non-performance (Phoon 2008). As in slope stability analysis, it basically means the driving forces (moments) are over the resisting forces (moments), thereby the static equilibrium state is broken. Thus the limit state function is always set in the form of

$$g(\mathbf{x}) = f_s(\mathbf{x}) - f_{s(r)} \quad (2.13)$$

where $f_{s(r)}$ is the required factor of safety, theoretically set to 1; but may vary with the importance of structures and specific design requirements.

2.3.2. Probabilistic Approaches. A number of probabilistic analysis approaches have been proposed to calculate p_f and β . The most popular methods adopted in probabilistic slope stability analysis are first-order second-moment (FOSM), first-order reliability method (FORM), and Monte Carlo simulation (MCS). Monte Carlo simulation is a

sampling-based method, performing random sampling and conducting a large number of experiments on a computer, thus giving conclusions on the model outputs drawn based on statistical experiments. The procedure of MCS is straightforward and most likely to be adopted in the analysis performed using continuum mechanics method (Morgenstern and Cruden 2002; EI-Ramly et al. 2004; Griffiths and Fenton 2004; Griffiths and Fenton 2007), since it is unable to define a limit state function that is essential to those non-sampling-based probabilistic approaches (i.e., FOSM, FORM). Moreover, because of its high computational costs, MCS is not preferred to be used with the limit equilibrium analysis, where considered repetitive analyses are required to seek the critical surface which will be further introduced in Section 2.4.

FOSM and FORM are both non-sampling-based methods; developed based on the first-order Taylor expansion. In FOSM, the limit state function is approximated with Taylor expansion at the means of random inputs. FOSM is very efficient, convenient and has been adopted in many research works (Chowdhury and Xu 1994; Christian et al. 1995; Hassan and Wolff 1999; Bhattacharya et al. 2003). However, a crucial problem of FOSM is that the method is sensitive to the form of limit state function; that is, the result may change when the limit state function is rearranged to another equivalent form (i.e., Ang and Tang 2007; Zhang et al. 2011b). Thereby it becomes quite tricky to decide which form of the limit state function is most appropriate. In light of the invariant issue, FORM is a desired approach that has the first-order approximation evaluated at a point on the failure surface, thus not influenced by the form of limit state function. In FORM, β can be addressed by

solving a constrained optimization problem:

$$\beta = \min_{\mathbf{u}} \|\mathbf{u}\|, \text{ sub. to } g(\mathbf{u}) = 0 \quad (2.14)$$

where $\{\mathbf{u}\}$ is a set of independent random variables derived by transforming the input variables $\{\mathbf{x}\}$ in Equation 2.13 from their original space to a standard normal space; $g(\mathbf{u})$ is the limit state function in \mathbf{u} -space (standard normal space). Thereby, from Equation 2.12 the probability of failure can be easily obtained.

The major advantage of FORM is its good balance between accuracy and efficiency: it is invariant compared to FOSM and more efficient compared to MCS especially when the probability of failure is low. Therefore, FORM is adopted in many research works (e.g. Low and Tang 1997; Low and Tang 2007; Phoon 2008; Zhang et al. 2011a; Cho 2013). But it should be noticed that since the first-order approximation is embedded, the exact solution is only available when the limit state function is perfectly linear; in nonlinear problems, error arises and the failure in convergence may occur. In probabilistic slope stability analysis, when Mohr-Coulomb strength parameters are considered as probabilistic random variables, from Equation 2.9 and Equation 2.10, it can be noticed ‘ $\tan \phi$ ’ is the major contributor to the nonlinear performance of the limit state function. With the appropriately selected soil properties, the limit state function is always not too nonlinear, or in other words, close to linear performance. Thereby, many researchers keep using FOSM and FORM in probabilistic slope stability analysis due to their computational efficiency and acceptable accuracy.

2.4. CRITICAL SLIP SURFACES

In slope stability analysis, it is routine to search for a slip surface along which the slope is most likely to fail; in other words, it is the most dangerous (or critical) slip surface.

2.4.1. Deterministic Analysis. Conventionally, all the design parameters are deterministic. The conventional analysis is accordingly ‘deterministic’ as well. It requires many calculations performed on different potential slip surfaces in order to arrive at the surface with the lowest factor of safety, denoted as ‘critical deterministic surface’. The problem of locating this surface is formulated as an optimization problem (Li and Cheung 2001):

$$\min_{\text{surface}} f_s \left(\mathbf{p}, x_1^{(k)}, y_1^{(k)}, x_2^{(k)}, y_2^{(k)}, \dots \right) \quad (2.15)$$

where $\{\mathbf{p}\}$ is the collection of input geotechnical parameters; $\{x_1^{(k)}, y_1^{(k)}, x_2^{(k)}, y_2^{(k)}, \dots\}$ is a set of shape variables (location parameters) defining the location of the slip surface for the k th trial; $f_s(\cdot)$ is the factor of safety for a given set of geotechnical parameters and a given geometry of the slip surface defined by location parameters. It is a general form dealing with any shaped surfaces. In a more specific way, for a circular slip surface, there are only three shape variables: x and y ordinates of the center of rotation and the radius of slip surface. Then the problem stated in Equation 2.15 can be simplified as follows:

$$\min_{\text{surface}} f_s \left(\mathbf{p}, x_0^{(k)}, y_0^{(k)}, r^{(k)} \right) \quad (2.16)$$

where $\{x_0^{(k)}, y_0^{(k)}\}$ is the rotation center for the k th trial; $r^{(k)}$ is the radius of the slip circle for the k th trial.

2.4.2. Probabilistic Analysis. Similar to the deterministic analysis, probabilistic analysis tends to address the surface with the highest probability of failure (or the lowest reliability index). Such a surface is called ‘critical probabilistic surface’. The search form is not different in concept from that of critical deterministic surface, and can be formulated in exactly the same way as above (Li and Cheung 2001). Generally, the problem is stated as

$$\max_{\text{surface}} p_f \left(\mathbf{p}, x_1^{(k)}, y_1^{(k)}, x_2^{(k)}, y_2^{(k)}, \dots \right) \quad (2.17)$$

For a circular slip surface, it is

$$\max_{\text{surface}} p_f \left(\mathbf{p}, x_0^{(k)}, y_0^{(k)}, r^{(k)} \right) \quad (2.18)$$

where $p_f(\cdot)$ is the probability of failure for a given set of geotechnical parameters and a given geometry of the slip surface defined by location parameters.

2.4.3. Search Approaches. The critical deterministic and probabilistic surfaces can be located by solving the optimization problems as stated in Equation 2.15, 2.16, 2.17 and 2.18. For a circular slip surface, the most commonly used method is Grid-line search method, in which a predetermined set of grid lines are assigned for the possible locations of the center of slip circle. All the nodal points defined by grid lines are searched to locate

those two critical surfaces with different radii. Grid-line method is simple to implement and is embedded in most of the commercial slope stability programs. Otherwise, a variety of search methodologies were proposed, including: the classical methods, such as the alternating variable technique (Li and Lumb 1987), simplex method (Nguyen 1985; Chen and Shao 1988), conjugate-gradient method (Arai and Tagyo 1985), dynamic programming (Yamagami and Jiang 1997); Monte Carlo technique (Greco 1996); and more recently, the heuristic algorithms, such as simulated annealing algorithm (Cheng 2003; Su 2008), genetic algorithm (McCombie and Wilkinson 2002; Cheng 2003; Zolfaghari et al. 2005; Xue and Gavin 2007; Sengupta and Upadhyay 2009; Talebizadeh et al. 2011) and etc.. But most likely, they are used for non-circular slip surfaces. The number of location parameters is usually much greater than three (for circular surface). Thus, the geometric method, such as grid-line method, becomes inefficient and requires a lot of efforts in defining the solution domain for each location parameter (Phoon 2008).

As discussed by Hassan and Wolff (1999), the critical deterministic and probabilistic surfaces may be located at different positions. But Li and Lumb (1987) emphasized the observation that those two surfaces are very close to each other in homogeneous natural slopes, thus proposed that the location of the critical deterministic surface could be used as a starting location for searching for the critical probabilistic surface. However, as the writers said, this is purely an observation, not universally true; and it is discussed for unreinforced slopes only. As for reinforced slopes, few studies were carried out with such a discussion. Therefore, it is more reasonable to perform a simultaneous search, as stated by Bhattacharya et al. (2003) and Xue and Gavin (2007), for reinforced slopes.

2.5. RELIABILITY-BASED OPTIMIZATION

Reliability-based optimization allows determining the best design solution (with respect to prescribed criteria) while explicitly considering the unavoidable effects of uncertainty. In general, the application of the RBO is numerically involved as it implies the simultaneous solution of an optimization problem and the use of specialized algorithm for quantifying the effects of uncertainties (Valdebenito and Schuëller 2010). A typical formulation of RBO is given by

$$\begin{aligned} \min f(\mathbf{d}, \mathbf{X}, \mathbf{P}) \\ \text{sub. to : } P\{g_i(\mathbf{d}, \mathbf{X}, \mathbf{P}) \leq 0\} \leq p_{f_i}, \quad i = 1, 2, \dots, n_c \end{aligned} \quad (2.19)$$

where f is the objective function; $\{\mathbf{d}\}$ is the set of deterministic design variables; $\{\mathbf{X}\}$ is the set of random design variables; $\{\mathbf{P}\}$ is the set of random design parameters; $g_i(\mathbf{d}, \mathbf{X}, \mathbf{P})$ are the constraint functions; p_{f_i} are the desired probabilities of constraint satisfaction; and n_c is the number of probabilistic constraints. The elements in vector $\{\mathbf{d}\}$ and $\{\mathbf{X}\}$ are the design variables that need to be determined through optimization. The most direct approach for solving a RBO problem is implementing a double-loop strategy (Valdebenito and Schuëller 2010). It employs nested optimization loops as shown in Figure 2.6 to first evaluate the probabilistic constraint (inner loop) and then to optimize the design objective function subject to the reliability requirements (outer loop) (Reddy et al. 1994; Wang et al. 1995; Tu et al. 1999). Because of its easy application, double-loop strategy is implemented in most of the research works regarding the reliability-based optimization design in geotechnical engineering (Wang and Kulhawy 2008; Chan et al. 2009; Wang 2009; Talebizadeh et al.

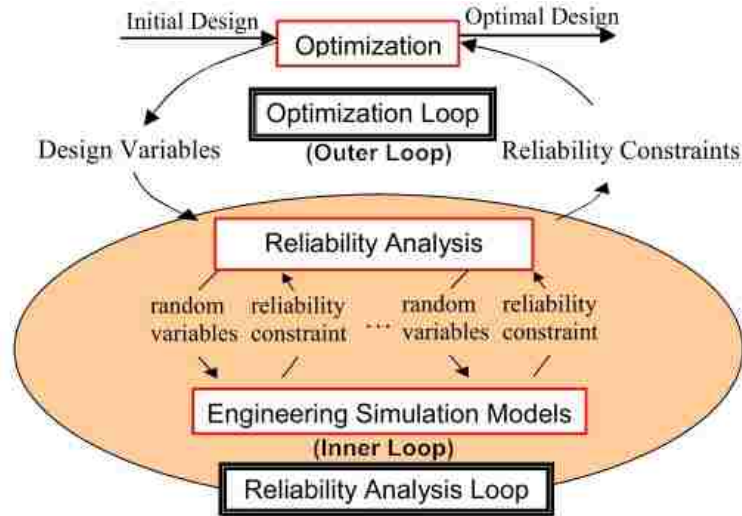


Figure 2.6: A double-loop procedure, adapted from Du et al. (2007)

2011; Zhang et al. 2011b). Otherwise, to improve the efficiency of double-loop strategy, some other techniques were introduced such as to improve the efficiency of uncertainty analysis, e.g., the methods of fast probability integration (Wu 1994), two-point adaptive nonlinear approximations (Grandhi and Wang 1998); or to modify the formulation of probabilistic constraints, e.g., single-loop (Chen and Hasselman 1997), decoupling approach (Li and Yang 1994). But no matter which strategy is employed, it is always the primary task to minimize the objective function subject to the relevant constraints. Such a constrained optimization problem can be solved by implementing the methods as mentioned in Section 2.3.2 as well. However, different from searching for the critical deterministic and probabilistic surfaces that usually comes along with continuous objective functions and smooth constraints, the optimization design of geosynthetic reinforcements includes non-smooth constraints, e.g., the number of reinforcement layers should be integer. Therefore, heuristic algorithms, e.g., simulated annealing algorithm and genetic algorithm, are preferred in design of geo-structures rather than the classical methods (Wang and Kulhawy

2008; Chan et al. 2009; Wang 2009; Talebizadeh et al. 2011; Zhang et al. 2011b).

2.6. METHODS EMPLOYED IN THIS RESEARCH

In summary, the methods to be employed in this research are listed in Table 2.1. The selected ones for implementation in the algorithms developed herein are marked in the “selected” column. Limit equilibrium method is used to perform slope stability calculations, while both sliding block and rotational analyses are to be involved. First-order reliability

Table 2.1: The methods employed in this research work

Analysis Type	Methods		Selected	
Slope Stability Analysis	Continuum Mechanics Method			
	Limit Analysis (LA)			
	Limit Equilibrium (LE)	Sliding Block Method	×	
		Rotational Method	×	
Reliability-based Analysis	First-Order Second Moment (FOSM)			
	First-Order Reliability Method (FORM)		×	
	Monte Carlo Simulation (MCS)		×	
Search Approach	Grid-line Method		×	
	Classical Methods	Alternating variable method; Simplex method; Conjugate-gradient method; etc.		
		Heuristic Methods	Simulated Annealing (SA)	
			Genetic Algorithm (GA)	×
	...			
Reliability-based Optimization	Double Loop Strategy		×	
	Single Loop Strategy			

method is selected as the primary tool for reliability estimate; Monte Carlo simulation is considered as a backup method when FORM fails to converge. Grid-line method is used to search for the critical slip surfaces in both deterministic and probabilistic analyses. In reliability-based optimization, double loop strategy is embedded with genetic algorithm to address the optimal results.

Although the LE method has been generally embedded in most of the geotechnical commercial software as mentioned in Section 2.2, the embedded source code is always unavailable. Furthermore, since those commercial software are currently unable to be combined with the implementation of other algorithms, they can be hardly used in this research work. Therefore, to introduce the reliability-based optimization technique in design of GRES structures, all the above methods are coded in the Matlab, where the genetic algorithm toolbox is directly used to solve the involved reliability-based optimization problem. And the code regarding the slope stability analysis is subsequently bench marked by performing the traditional deterministic slope stability analysis in Slope/W, which is one of the most-widely-used commercial software for slope stability analysis.

3. RELIABILITY-BASED SLOPE STABILITY ANALYSIS

3.1. OVERVIEW

To overcome the shortcoming of the traditional deterministic slope stability analysis that is unable to ensure a consistent risk level of the slopes with a constant factor of safety, reliability-based (or probabilistic) slope stability analysis is carried out. It estimates the probability of failure of a slope system to assess its probabilistic performance considering the relevant geotechnical uncertainties. As mentioned in Section 2.3, the uncertainty of slope stability is the result of many factors, including the lack of information in site investigations and the inherent variability in soil properties. The former is hard to be treated formally, but the latter one is more amenable to statistical analysis. In this study, it is emphasized the uncertainty that arises from the variability of the soil strength and the unit weight of the embankment fill and foundation soil in geosynthetic reinforced embankment slopes (GRES). The estimation of the probabilistic properties of the involved random variables is discussed in Section 3.2. The probabilistic algorithm that is to be embedded in the slope stability analysis is demonstrated in Section 3.3. To thoroughly investigate system reliability, the multiple failure modes that may potentially occur in a GRES structure are taken into consideration in Section 3.4. Two numerical examples are then presented in Section 3.5 to specifically demonstrate the application of the proposed probabilistic analysis in studying the slope stability and reliability of the GRES system.

3.2. STATISTICAL INFERENCE

In general, probabilistic analysis primarily concerns: what events may occur with what probabilities when it is given the probability distribution model and the probabilistic parameters of the random variable whose value is subject to the variations due to chance

(Yates et al. 2003). In other words, probabilistic analysis is efficient provided the involved random variables are well defined. But unfortunately, most of the time, we are in the situation of not knowing the precise distribution from which a set of data can be arisen, but of having to infer a probability distribution from the observed data, which is the main topic of statistical inference. When probabilistic analysis is involved in slope stability assessment, Mohr Coulomb (MC) strength parameters: cohesion (c) and friction angle (ϕ), as well as soil unit weight, including bulk unit weight (γ) and saturated unit weight (γ_{sat}), are commonly considered as the random variables in most of the related studies, since they are supposed to have significant contributions to the resisting forces and the driving forces according to Equation 2.1, 2.9, and 2.10. Their variations, in some ways, reflect the uncertainties involved in soil strength and unit weight and can be generally described by probability distribution models, probabilistic parameters, and the correlations between variables.

3.2.1. Probability Distribution Models. There are a large number of probability distribution models developed so far, but only a few are applied in geotechnical engineering that mainly include normal, log-normal, uniform, exponential, gamma and beta. As concluded by Onyejekwe (2012), to choose an appropriate distribution model, there are two techniques that are commonly used: 1) plotting a histogram of the data and choosing a distribution model that appears to best-fit the histogram; and 2) Pearson's moment-based method, which is developed on the basis of the third- and fourth-moment statistics, such as skewness (C_s) and kurtois (C_k), that are defined by (Rethati 1988; Baecher and Christian

2003)

$$C_s = \frac{n \sum_{i=1}^n (x_i - \bar{x})^3}{(n-1)(n-2)s^3} \quad (3.1)$$

and

$$C_k = \frac{n \sum_{i=1}^n (x_i - \bar{x})^4}{(n-1)(n-2)s^4} - 3 \quad (3.2)$$

where x_i represents each data point in the dataset $\{\mathbf{x}\}$; n is the number of involved data points; \bar{x} and s are the sample mean and standard deviation of the dataset, the derivation of which is to be further discussed in the following Section 3.2.2. According to Pearson's distribution space (Figure 3.1), distribution model can be consequently selected, where β_1 characterizing the skewness and β_2 characterizing the peakiness can be computed as (Rethati 1988)

$$\beta_1 = C_s^2 \quad \text{and} \quad \beta_2 = C_k + 3 \quad (3.3)$$

Laboratory test results indicate most of the soil properties, including unit weight and MC strength parameters, can be considered as the random variables having normal or log-normal distribution (Baecher and Christian 2003; Elkateb et al. 2003; Onyejekwe 2012), which are indeed the most commonly used distribution models in lots of related studies.

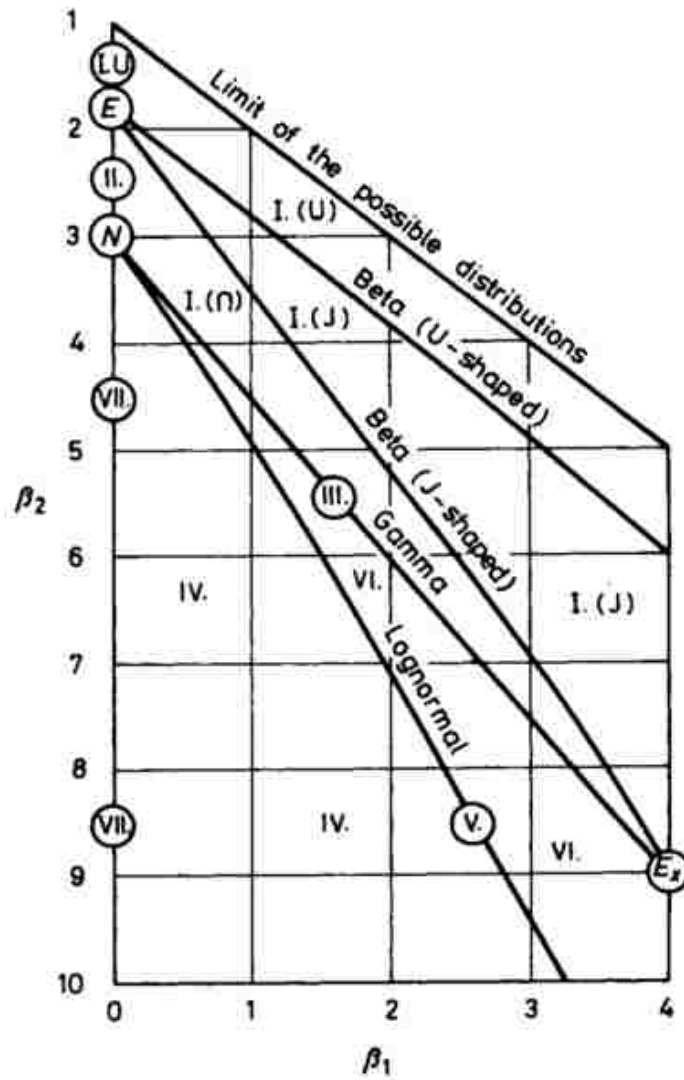


Figure 3.1: Pearson's distribution space of β_1 and β_2 coordinates: E - uniform distribution ($\beta_1 = 0, \beta_2 = 1.8$), N - normal distribution, E_x - exponential distribution (Rethati 1988)

But owing to the fact that distribution is always parameter- and site-specific, it is preferred to select a best fitted distribution model by going through the above procedures, e.g., Pearson's system, if sufficient data are available; otherwise, assumptions have to be made according to previous works and observations. Furthermore, as discussed by Griffiths and Fenton (2008), it is essential to ensure if the distribution model is physically reasonable for the soil property. That is, for example, if the property is strictly non-negative, normal distribution is not physically reasonable since a negative part always exists in such a distribution; only when the probability of negative values is sufficiently small, it may be a reasonable approximation. In principle, the selected distribution model should be as simple as possible while still reflecting the basic nature of the variability (Griffiths and Fenton 2008), that, on the other hand, simplifies parameter estimations and further calculations.

3.2.2. Probabilistic Parameters. Generally, mean and variance are two most important characteristics of a random variable. Mean tells where the probability distribution is 'centered' and variance indicates how 'narrow' or 'wide' the distribution is. In other words, variance is the measurement of the variability of a random variable (Baecher and Christian 2003; Griffiths and Fenton 2008). If there is a random variable X with the probability density function (PDF) $f_X(x)$, its mean (μ_X) and expected value ($E[X]$) are defined as

$$\mu_X = \begin{cases} E[X] = \sum_x x f_X(x), & \text{if } X \text{ is discrete} \\ E[X] = \int_{-\infty}^{\infty} x f_X(x) dx, & \text{if } X \text{ is continuous} \end{cases} \quad (3.4)$$

The standard deviation (σ_X) and variance ($\text{Var}[X]$) are defined as

$$\sigma_X^2 = \text{Var}[X] = \begin{cases} \sum_x (x - \mu_X)^2 f_X(x), & \text{if } X \text{ is discrete} \\ \int_{-\infty}^{\infty} (x - \mu_X)^2 f_X(x) dx, & \text{if } X \text{ is continuous} \end{cases} \quad (3.5)$$

From a collection of data, the above two parameters can be simply estimated based on sample moments by approximating the expectation integrals through a summation over equi-likely samples, each weighted by $1/n$ rather than $f_X(x) dx$ in Equation 3.4 and 3.5 (Griffiths and Fenton 2008). Therefore, sample mean (\bar{x}) and sample standard deviation (s) can be respectively derived as

$$\bar{x} = \frac{1}{n_s} \sum_{i=1}^{n_s} x_i \quad (3.6)$$

and

$$s^2 = \frac{1}{n_s} \sum_{i=1}^{n_s} (x_i - \bar{x})^2 \quad (3.7)$$

Once a distribution has been selected, the fitness must be assessed by means of a number of approaches, that basically include heuristic procedures and goodness-of-fit tests, such as Chi-Square (χ^2) test, Kolmogorov-Smirnov test and Anderson-Darling test (Rethati 1988; Baecher and Christian 2003; Griffiths and Fenton 2008).

3.2.3. Correlations. In the case that multiple random variables are taken into consideration, the relationship between the random variables often has two possibilities: dependent and independent. Basically, say, there are two random variables, if the occurrence of one does not affect the probability of the other, it is called independence; otherwise, they are dependent. Mathematically, two independent random variables, X and Y , have the following property

$$p_{X,Y}(x,y) = p_X(x)p_Y(y) \quad (3.8)$$

which means their joint probability distribution is the product of their marginal probability distributions. If the random variables are dependent, a measurement parameter, correlation coefficient (ρ) ranging between -1 and 1, is introduced to evaluate the degree of linear dependence between the two variables. A positive correlation indicates one tends to go up when another goes up; vice versa, a negative correlation means one tends to go down when another goes up. If the correlation is equal to 1 or -1, the random variables are linearly dependent; otherwise, they are non-linearly dependent; while the correlation is zero, these two variables are uncorrelated, but still can be dependent.

Some of the research works assumed independent random variables for the soil properties, such as MC strength parameters or unit weights, to largely simplify the problem (Xue and Gavin 2007; Ching 2009; Zhang et al. 2013); others considered they are correlated with each other (Wolff 1985; Chowdhury and Xu 1994; Bhattacharya et al. 2003; Griffiths and Fenton 2004; Zhang et al. 2011b). On the basis of soil mechanics, since cohesion and friction angle are two components of soil's shear strength, it is reasonable to

believe they are dependent in some pattern. And most likely, they are negatively correlated, because when a soil has a larger cohesion, friction angle probably tends to go down to maintain the soil's strength within a reasonable range; otherwise, the strength could keep increasing, which is unreasonable and impossible in reality. As discussed by Krounis and Johansson (2011), a reduction in the probability of failure of a soil slope was observed as correlation coefficient changes from 1 to -1. Therefore, if a negative correlation does exist, the probability of failure can be possibly overestimated by assuming independent random variables; on the other hand, a conservative design is to be provided. Moreover, considering the benefits of soil compaction, that is to improve soils engineering properties, shear strength and bearing capacity are generally increased after the soil is compacted and becomes denser. Therefore, it is reasonable to believe a positive correlation existing between soil unit weights and strength parameters, especially the friction angle. After all, the above conclusions are purely observations. The correlations between two or more soil properties have been found to be dependent on the varying degrees of soil type, the testing methods used to obtain the numerical value of the parameter, and the homogeneity of soil (Uzielli et al. 2007). If sufficient data are available, the correlation may be able to be interpreted based on probability theory as follows

$$\rho_s = \frac{\sum_{i=1}^n (x_i - \bar{x})(y_i - \bar{y})}{\sqrt{(x_i - \bar{x})^2} \sqrt{(y_i - \bar{y})^2}} \quad (3.9)$$

where x_i and y_i are the data points in the two datasets for the random variables X and Y ; \bar{x} and \bar{y} are the sample means of the datasets; and ρ_s is the sample correlation coefficient between the random variables X and Y . Otherwise, assumptions have to be made based

on previous investigations and works, or those published correlation models. But in light of the site-specific characteristic regarding the variability of soil properties, inappropriate assumptions may lead to an underestimate or overestimate in the final results.

3.3. PROBABILISTIC ANALYSIS ALGORITHM

To compute the probability of failure, first-order reliability method (FORM) is introduced as the primary probabilistic approach due to its efficiency and effectiveness. The advantages even stand out when FORM is working with the iterative scheme for searching for the critical slip surfaces in slope stability analysis as discussed in Section 2.3 and 2.4. Monte Carlo simulation (MCS), a relatively powerful but computationally costly sampling-based method, is the backup in view of the chances that FORM may fail to converge.

3.3.1. MPP-Based FORM. FORM is developed based on the first-order Taylor expansion evaluated at a point on the failure surface, the shortest distance from which to the origin is defined as the reliability index (β); the probability of failure (p_f) can be accordingly computed from Equation 2.12. In other words, the problem can be easily solved once it is able to locate the most probable point (\mathbf{u}^*), which is the shortest distance point from the origin to the limit state curve $g(\mathbf{u})$ as shown in Figure 3.2. Therefore, the problem can be further transformed into a minimization problem with an equality constraint as described by Equation 2.14, and can be accordingly addressed through some search algorithms that are to be further discussed in Section 3.3.1.3. As a result, since the problem is basically searching for the most probable point (MPP), FORM is considered as an MPP-based method.

3.3.1.1. Transformation. Prior to the MPP search, the random variables need to be transformed from their original random space (\mathbf{x} -space) into a non-dimensional, stan-

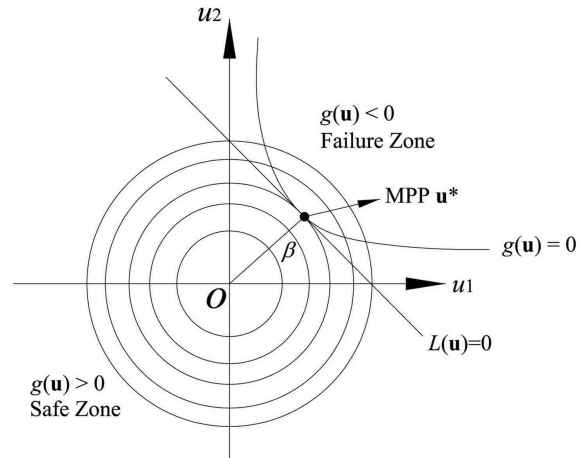


Figure 3.2: The MPP-based FORM in a two-dimensional standard normal space (Du et al. 2010)

dard normal space, as the \mathbf{u} -space in Figure 3.2. If the random variables are independent, Rosenblatt transformation can be directly applied to transform and derive the variables in the standard normal space, denoted as standard variables:

$$u_i = \Phi^{-1} [F_i(x_i)] \quad (3.10)$$

based on which, the probability of failure can be rewritten in an equivalent form as that in Equation 2.11

$$p_f = \int_{g(\mathbf{u}) < 0} \phi_{\mathbf{u}}(\mathbf{u}) d\mathbf{u} \quad (3.11)$$

where x_i is an arbitrary element in $\{\mathbf{x}\}$, a set of random variables in their original space; u_i is an element in $\{\mathbf{u}\}$, a set of standard variables corresponding to $\{\mathbf{x}\}$; $\phi(\cdot)$ and $\Phi(\cdot)$ are

the joint PDF and CDF in standard normal space; and $F(\cdot)$ is the CDF in original space.

If the random variables are dependent, or more specifically, correlated, transformation becomes complicated. The correlated random variables need to be converted into a set of uncorrelated ones by diagonalizing the covariance matrix, whose (i, j) entry can be expressed by

$$\sum_{ij} = \text{COV}[x_i, x_j] = E[(x_i - \mu_{x_i})(x_j - \mu_{x_j})] \quad (3.12)$$

where \sum is the covariance matrix; COV is the covariance operator; x_i and x_j are two arbitrary elements in $\{\mathbf{x}\}$. Similar to the correlated coefficient, covariance represents how much two random variables change together; but differently, the magnitude of the covariance fails to indicate anything regarding the strength of the relationship since it depends on the units and the variability of the random variables. Correlation coefficient is a normalized, non-dimensional quantity (Griffiths and Fenton 2008), defined as

$$\rho_{x_i x_j} = \frac{\text{COV}[x_i, x_j]}{\sigma_{x_i} \sigma_{x_j}} \quad (3.13)$$

From Equation 3.12 and 3.13, the covariance matrix can be expressed in terms of correlation coefficient as

$$\sum_{ij} = \text{COV}[x_i, x_j] = \rho_{x_i x_j} \sigma_{x_i} \sigma_{x_j} \quad (3.14)$$

When sufficient data are available, correlation coefficient can be estimated by Equation 3.9. Covariance matrix is then able to be derived according to Equation 3.14. To complete the transformation, the procedure demonstrated in Figure 3.3 is introduced, wherein an essential step is to decompose the covariance matrix into a lower triangular matrix through Cholesky decomposition, which is only efficient providing a Hermitian, positive-definite matrix. From Equation 3.12 and 3.14, it is not difficult to find the covariance matrix is Hermitian, that has $\Sigma = \overline{\Sigma}^T$, but a positive-semidefinite matrix ($\mathbf{z}^T \Sigma \mathbf{z} \geq 0$ for all \mathbf{z}) instead of positive-definite ($\mathbf{z}^T M \mathbf{z} > 0$ for all non-zero \mathbf{z}). In this situation, Cholesky decomposition still exists, but the theory and the computation are more subtle than for a positive-definite matrix (Higham 2002). More details regarding variable transformation can be referred to Appendix A.

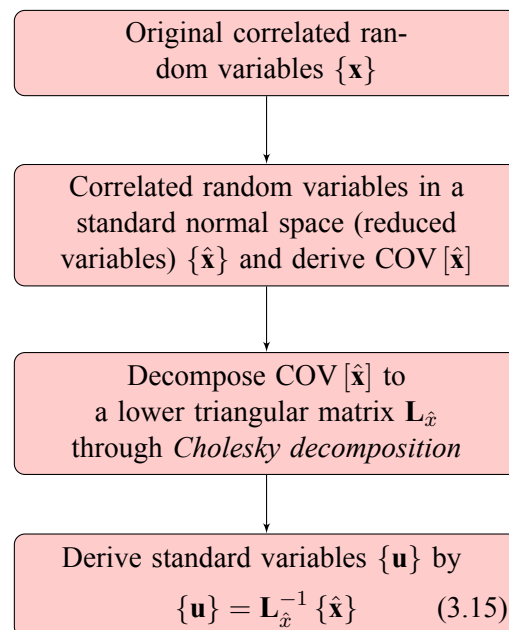


Figure 3.3: Correlated variable transformation

3.3.1.2. Linearization. After the original random variables $\{\mathbf{x}\}$ have been converted into a set of uncorrelated or independent standard normal variables $\{\mathbf{u}\}$, the limit state function can be rewritten as $g(\mathbf{u})$. Since the FORM is developed based on the first-order Taylor expansion, the limit state function is supposed to be linearized at the MPP as follows

$$g(\mathbf{u}) \approx L(\mathbf{u}) = g(\mathbf{u}^*) + \sum_{i=1}^n \left. \frac{\partial g}{\partial u_i} \right|_{\mathbf{u}^*} (\mathbf{u} - \mathbf{u}^*)^T = g(\mathbf{u}^*) + \nabla g(\mathbf{u}^*) (\mathbf{u} - \mathbf{u}^*)^T \quad (3.16)$$

where $\nabla g(\cdot)$ needs to be determined prior to the MPP search since it is going to be continuously recalled in the searching loop. Considering the standard and original random variables are always inter-related in some pattern, through Chain Rule, $\nabla g(\mathbf{u})$ can be given by

$$\frac{\partial g}{\partial u_j} = \sum_{i=1}^n \frac{\partial g}{\partial x_i} \frac{\partial x_i}{\partial u_j} \quad (3.17)$$

or in an equivalent matrix form

$$\nabla g(\mathbf{u}) = \left\{ \begin{array}{c} \frac{\partial g}{\partial x_1} \\ \frac{\partial g}{\partial x_2} \\ \vdots \\ \frac{\partial g}{\partial x_n} \end{array} \right\}^T \left[\begin{array}{cccc} \frac{\partial x_1}{\partial u_1} & \frac{\partial x_1}{\partial u_2} & \cdots & \frac{\partial x_1}{\partial u_n} \\ \frac{\partial x_2}{\partial u_1} & \frac{\partial x_2}{\partial u_2} & \cdots & \frac{\partial x_2}{\partial u_n} \\ \vdots & \vdots & \vdots & \vdots \\ \frac{\partial x_n}{\partial u_1} & \frac{\partial x_n}{\partial u_2} & \cdots & \frac{\partial x_n}{\partial u_n} \end{array} \right] \quad (3.18)$$

wherein $\partial g/\partial x_i$ is based on the limit state function regarding the failure mechanism; while $\partial x_i/\partial u_j$ is primarily depending on the probability distribution of the i th random variable and the correlation between the i th and j th random variables. For normal distribution, the original random variables can be expressed in an inverse form of Equation 3.15 as

$$\{\hat{\mathbf{x}}\} = \mathbf{L}_{\hat{\mathbf{x}}} \{\mathbf{u}\} = \left\{ \frac{x_i - \mu_{x_i}}{\sigma_{x_i}} \right\}_{i=1}^n \quad (3.19)$$

based on which the partial derivative of an original random variable with respect to a standard variable can be derived as

$$\frac{\partial x_i}{\partial u_j} = \sigma_{x_i} \sum_{k=1}^n \mathbf{L}_{\hat{\mathbf{x}}}(i, k) \frac{\partial u_k}{\partial u_j} = \sigma_{x_i} \mathbf{L}_{\hat{\mathbf{x}}}(i, j) \quad (3.20)$$

where $\mathbf{L}_{\hat{\mathbf{x}}}$ is the lower triangular matrix with respect to $\{\hat{\mathbf{x}}\}$, a set of reduced variables that are in standard normal space but still correlated; for log-normal distribution, similar to Equation 3.19, the reduced variables can be derived as

$$\{\hat{\mathbf{x}}\} = \mathbf{L}_{\hat{\mathbf{x}}} \{\mathbf{u}\} = \left\{ \frac{\ln x_i - \mu_{\ln x_i}}{\sigma_{\ln x_i}} \right\}_{i=1}^n \quad (3.21)$$

based on which we have the partial derivative derived as

$$\frac{\partial x_i}{\partial u_j} = x_i \sigma_{\ln x_i} \sum_{k=1}^n \mathbf{L}_{\hat{\mathbf{x}}}(i, k) \frac{\partial u_k}{\partial u_j} = x_i \sigma_{\ln x_i} \mathbf{L}_{\hat{\mathbf{x}}}(i, j) \quad (3.22)$$

since the standard variables $\{\mathbf{u}\}$ are independent,

$$\frac{\partial u_i}{\partial u_j} = \begin{cases} 1, & \text{for } i = j \\ 0, & \text{otherwise.} \end{cases} \quad (3.23)$$

In a special condition that the random variables are independent or uncorrelated, $\nabla g(\mathbf{u})$ can be simplified as

$$\frac{\partial g}{\partial u_i} = \frac{\partial g}{\partial x_i} \frac{\partial x_i}{\partial u_i} \quad (3.24)$$

wherein, according to Appendix A.1, it is easy to obtain

$$\frac{\partial x_i}{\partial u_i} = \sigma_{x_i}, \text{ for normal distribution} \quad (3.25)$$

$$\frac{\partial x_i}{\partial u_i} = \sigma_{\ln x_i} e^M, \text{ for log-normal distribution} \quad (3.26)$$

where $M = u_i \sigma_{\ln x_i} + \mu_{\ln x_i}$. Thereby, from Equation 3.17 and 3.24, it is easy to have $\nabla g(\mathbf{u})$ finally calculated once $\partial g / \partial x_i$ is derived based on the failure mechanism.

In many engineering applications, analytic partial derivatives of the limit state function with respect to the random variables may not be available, or can be hard to derive especially when highly complex limit state function is involved. The numerical methods should be thereby an alternative, such as a two-point estimation with forward, backward or

centered finite difference, through which the limit state function will be called ($2 \times n$) times, where n is the number of involved random variables. If the frequency of function calls is used to measure the computational efficiency, the efficiency of FORM is directly proportional to the dimension of the limit-state function (Du et al. 2010). In view of the truncation error that always exists in numerical differential, centered finite difference is of the order of h^2 in contrast to the forward and the backward approximations that are of the order of h , and consequently implies a more accurate representation of the derivative (Chapra 2008). After all, thinking of computational efficiency and accuracy, it analytic derivative is preferred to use if it is available, so that no additional cost is involved; otherwise, centered finite difference approximation is embedded with highly complex functions. Considering the limit state function is generally defined on the basis of failure mechanisms, the estimation of the partial derivative $\partial g / \partial x_i$ is to be discussed individually in the following Section 3.4.2.

3.3.1.3. MPP search. Provided the transformation and the linearization are done, MPP search is performed to locate the most probable point, the distance from which to the origin is the reliability index. The algorithm as illustrated in Figure 3.4 is modified and extended based on the original Hasofer-Lind method by Rackwitz and Fiessler (1978), denoted as HL-RF method. It is the most popular algorithm due to its effectiveness and capability to converge fast for most situations (Santosh et al. 2006; Du et al. 2010). However, as an iterative scheme, there exists the phenomenon of convergent failure during the iterative calculation of getting the reliability index determined for some limit state functions, typically some highly complex and nonlinear function whose curvature value near the MPP at the limit state surface is large so that the sequential points generated during iterating may oscillate in the domain near the MPP and fail to converge (Santosh et al.

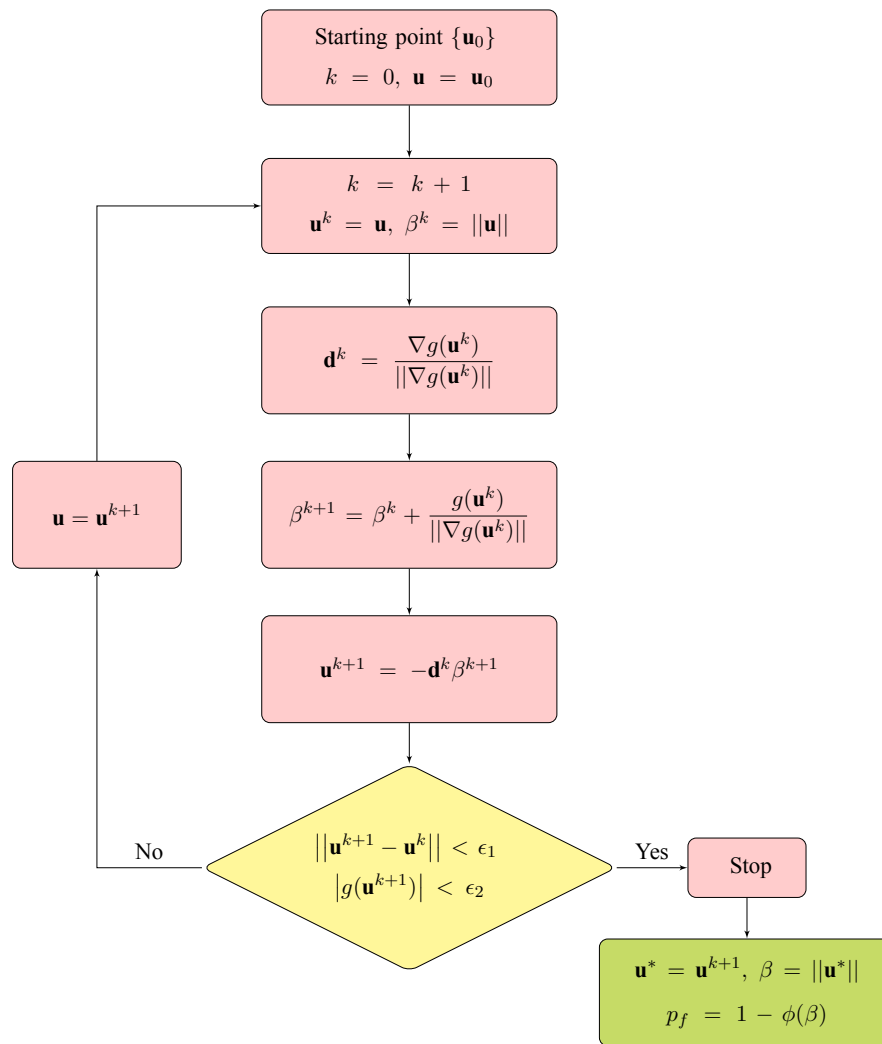


Figure 3.4: HL-RF search algorithm for locating MPP, adapted from Du et al. (2010)

2006; Yang et al. 2006; Du et al. 2010; Gong and Yi 2010). With this in mind, Monte Carlo simulation can be an alternative method to solve the problem.

3.3.2. Monte Carlo Simulation. Monte Carlo simulation is a powerful tool to solve the multi-dimensional probability integral over the failure domain defined by the limit state function $g(\mathbf{x}) < 0$ (Gasser and Schueller 1997). As a sampling-based method, MCS has an outline that is generally described in Figure 3.5, where N is the number of

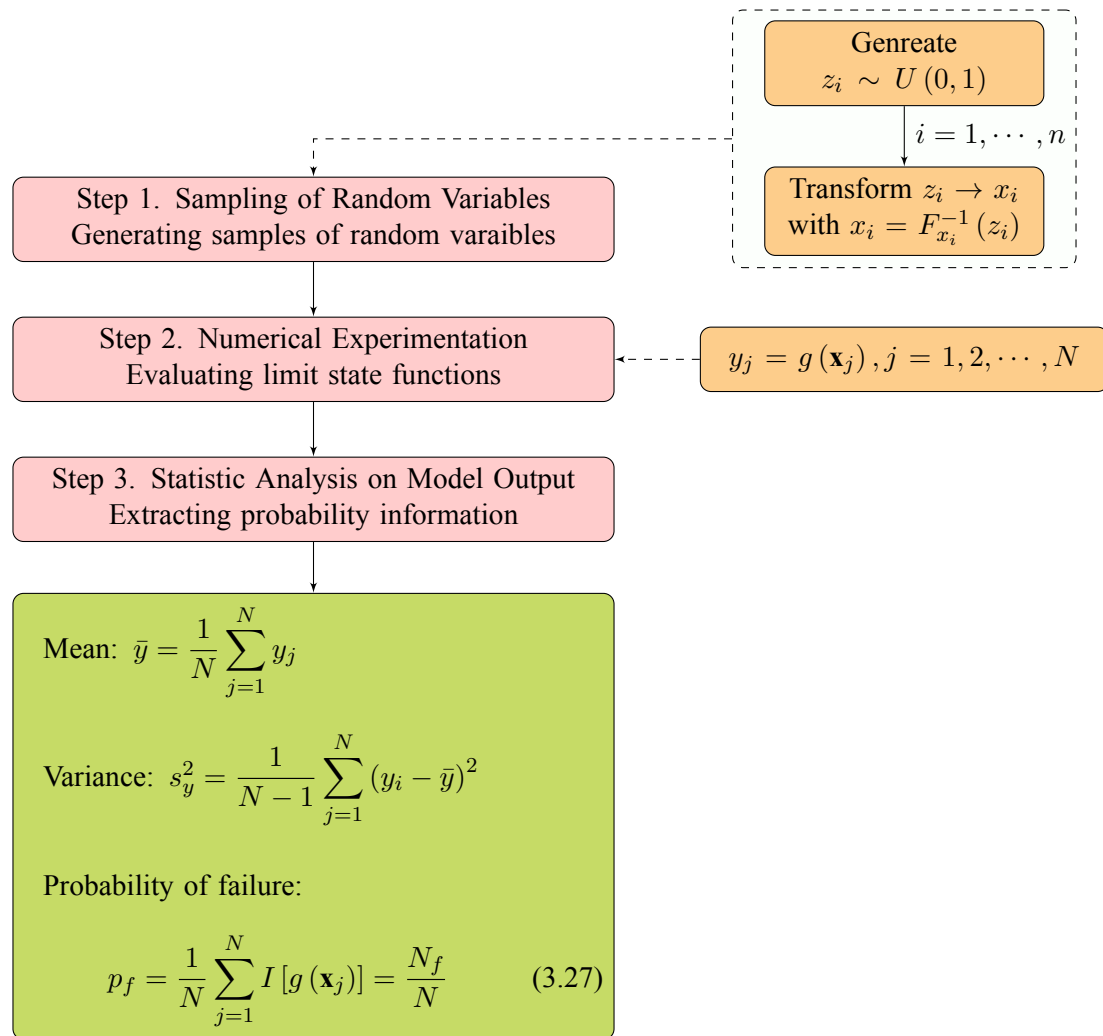


Figure 3.5: Monte Carlo Simulation algorithm, adapted from Gasser and Schueller (1997) and Du et al. (2010)

simulations in MCS; N_f is the number of the samples that have the limit state function less than zero; and n is the number of random variables in the model. The estimation obtained by MCS approaches to the exact solution as $N \rightarrow \infty$; thus, the numerical effort is extremely high especially when the probability of failure is small due to the reason that only the samples that fall into the failure zone can contribute to the probability estimation. Therefore, in view of computational efficiency, HL-RF is selected as the primary method

to locate the MPP; MCS is embedded as a backup in case HL-RF fails to converge.

3.4. PROBABILISTIC ANALYSIS IN GRES APPLICATION

To clearly demonstrate how the proposed probabilistic algorithm as discussed in Section 3.3 can be successfully embedded in the stability analysis of geosynthetic reinforced embankment slopes, a flowchart is illustrated in Figure 3.6. It is required prior to the MPP-based probabilistic analysis that failure mode and potential failure surfaces should be predetermined, based on which the limit state functions can be accordingly defined and the probability of failure can be computed through the MPP-based FORM with respect to the specified failure mechanism. In either deterministic or probabilistic slope stability analysis, it is routine to search for the most dangerous surfaces along which the slope is most likely to fail, denoted as critical slip surfaces, as mentioned in Section 2.4. To achieve this goal, a series of potential failure surfaces are generated within a most probable failure zone that is mainly determined by engineers judgments and experience. Thinking of the phenomenon that critical deterministic and probabilistic slip surfaces may not be located at the same position as discussed in Section 2.4, MPP-based probabilistic analysis is accordingly repeated to locate the critical probabilistic surface with a maximum probability of failure ($p_{f,max}$); meanwhile, deterministic analysis is carried out to locate the critical deterministic surface with a minimum factor of safety ($f_{s,min}$).

In the following sections, the failure modes that may potentially occur in a GRES system will be discussed, followed by the determination of limit state functions. Two numerical examples are consequently carried out in Section 3.5 to demonstrate the application of the proposed probabilistic slope stability analysis.

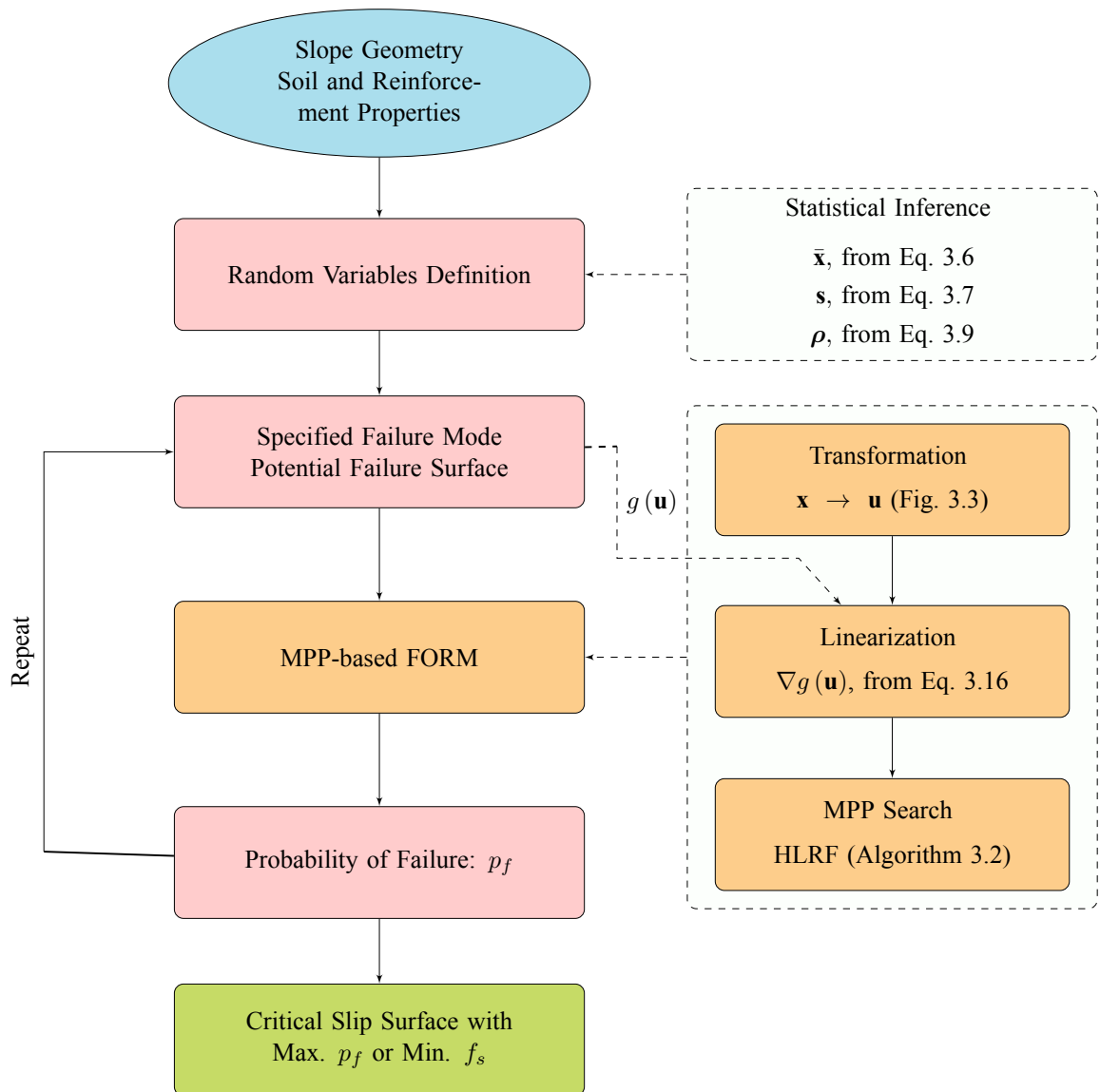


Figure 3.6: Probabilistic slope stability analysis procedure

3.4.1. Multiple Failure Modes. As illustrated in Figure 3.7, a typical GRES structure often has three possible failure modes: 1) internal, where the failure plane crosses all reinforcements; 2) external, where the failure plane is located outside and underneath the reinforced mass; and 3) compound, where the failure plane passes behind and through the reinforced mass. The external failure possibilities also include sliding failure, deep-

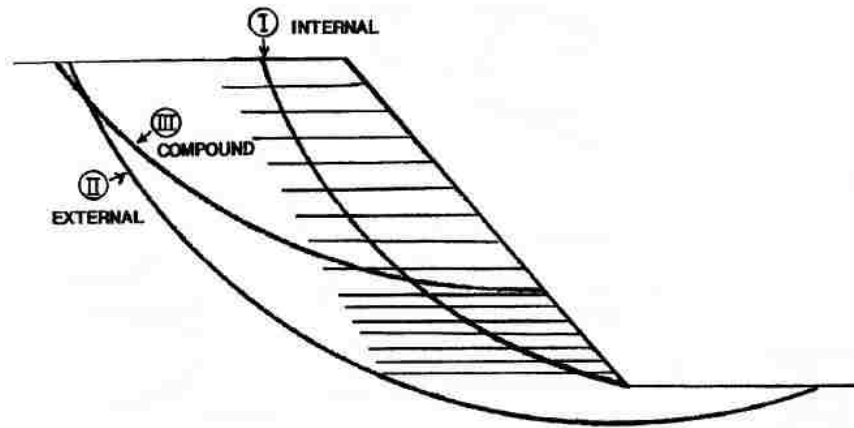
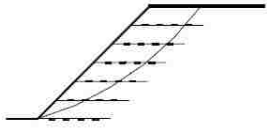
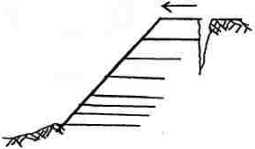
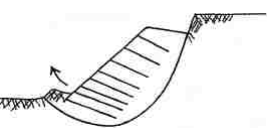
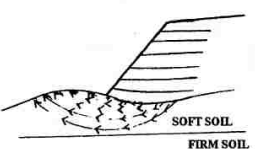
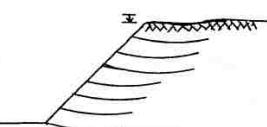
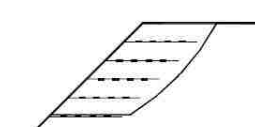


Figure 3.7: Failure modes of reinforced soil slopes (Elias et al. 2001)

seated overall instability, lateral squeezing failure, and excessive settlement (Elias et al. 2001). The design process as well as the analysis should address all the possible failure modes that a GRES system will potentially experience in both short-term and long-term conditions. As recommended by Elias et al. (2001) and Naresh and Edward (2006), the methods used for analyzing the preceding failure modes are summarized in Table 3.1; and embedded in the probabilistic slope stability analysis herein.

3.4.2. System Reliability. As discussed by Basha and Babu (2010), in a series system, the entire system is considered as disabled if even one component fails. The components of the system are so configured that the system failure results from the failure of

Table 3.1: Failure modes of geosynthetic reinforced slopes and analyzing methods, adapted from Elias et al. (2001) and Naresh and Edward (2006)

Failure Modes		Analysis Methods	
Internal		Rotational method ^(a)	
External	Sliding		Sliding block method
	Deep-seated		Rotational method ^(b) or Sliding block method
	Lateral squeeze		Silvestri's approach
	Excessive settlement		Classical geotechnical engineering procedures
Compound		Rotational method ^(b) or Sliding block method	

^(a) Rotational method modified for reinforced slope stability analysis.

^(b) Rotational method for unreinforced slope stability analysis.

any of the failure modes. Thinking of the contributions of the multiple failure modes to the system reliability, the probability of failure can be computed as follows (Basha and Babu 2010) if the failure modes are statistically independent:

$$\begin{aligned}
 p_{f_s} &= P \{ [g_1(\mathbf{x}) \leq 0] \cup [g_2(\mathbf{x}) \leq 0] \cup \dots \cup [g_{n_f}(\mathbf{x}) \leq 0] \} \\
 &= 1 - (\{1 - P[g_1(\mathbf{x}) \leq 0]\} \{1 - P[g_2(\mathbf{x}) \leq 0]\} \dots \{1 - P[g_{n_f}(\mathbf{x}) \leq 0]\})
 \end{aligned}
 \tag{3.28}$$

where p_{f_s} is the system probability of failure; $g_i(\mathbf{x})$ is the limit state function with respect to the i th potential failure mode; and n_f is the number of potential failure modes to be considered. When the probability of failure with respect to each failure mode is computed, the system probability of failure can be obtained from Equation 3.28; and system reliability (R_s) can be obtained by

$$R_s = 1 - p_{f_s} \tag{3.29}$$

As illustrated in Table 3.1, the typical failure modes that may potentially occur in a GRES system include internal, external and compound, all of which should be addressed to thoroughly perform the probabilistic slope stability analysis for a GRES system.

3.4.2.1. Internal failure. The internal failure, where the failure plane crosses all reinforcements, is analyzed by the rotational method that assumes all the geosynthetic layers are effectively working. From Equation 2.10, the limit state function is given by

$$g(\mathbf{x}) = \frac{r \sum_{i=1}^n [c'_i l_i + \tan \phi'_i (W_i \cos \alpha_i - u_i l_i)] + \sum_{j=1}^m T_j d_j}{r \sum_{i=1}^n W_i \sin \alpha_i} - 1 \tag{3.30}$$

where $\mathbf{x} = \{c', \phi', \gamma, \gamma_{\text{sat}}\}$ are the involved random variables with $\{c'\}$ and $\{\phi'\}$ representing the effective MC strength parameters in each layer if multiple layers exist; $\{\gamma\}$ and $\{\gamma_{\text{sat}}\}$ are the bulk unit weight and the saturated unit weight of each soil layer, although not directly shown in Equation 3.30, but significantly contribute to the weight of slice (W_i). All the other parameters in Equation 3.30 have been defined in Section 2.2.2 along with Equation 2.9 and 2.10. Based on the limit state function given by Equation 3.30, the partial derivatives of the limit state function with respect to the strength parameters can be analytically derived as

$$\frac{\partial g}{\partial c'_j} = \sum_{j=1}^{\hat{n}} \frac{l_i}{\sum_{i=1}^n W_i \sin \alpha_i} \quad (3.31)$$

$$\frac{\partial g}{\partial \phi'_j} = \sum_{j=1}^{\hat{n}} \frac{W_i \cos \alpha_i - u_i l_i}{\sum_{i=1}^n W_i \sin \alpha_i} (\tan^2 \phi'_i + 1) \quad (3.32)$$

where c'_j and ϕ'_j are the effective MC strength parameters for the j th layer; and \hat{n} is the number of the layers that the slip surface passes through. Due to the complicated situations that may encounter, such as the location of groundwater table, it is hard to get a general formation of the slice weight in terms of unit weights. Therefore, it is more reasonable to do numerical estimation on the partial derivatives of the limit state function with respect to the unit weights.

Another thing that should be pointed out is the prerequisite of Equation 2.10 and 3.30. That is, all the geosynthetic layers are assumed effectively working without the pullout failure, which always occurs once the load carried by the reinforcement layer exceeds its

pullout resistance capacity; and consequently, instead of tensile strength failure, the reinforcement has been pulled out and fails to work. Therefore, the pullout resistance capacity of the reinforcement layer should be taken as another important factor that controls how much effort the layer can provide as a resistance component. According to FHWA Soils and Foundations Workshop Reference Manual (Naresh and Edward 2006), the unit pullout resistance capacity (P_r) can be computed by

$$P_r = F^* \cdot \alpha \cdot C \cdot \sigma'_v \quad (3.33)$$

where F^* is the pullout resistance factor, the value of which for geosynthetic reinforcement should be conservatively taken as $2/3 \tan \phi$ in absence of test data; ϕ is the peak friction angle of the backfill; α is a scale effect correction factor to account for a non-linear stress reduction over the embedded length of highly extensible reinforcements, usually taken between 0.6 and 1.0 for geosynthetic reinforcements based on laboratory data; C is the reinforcement effective unit perimeter, set as 2 for strips, grids and sheets; and σ'_v is the effective vertical stress at the soil-reinforcement interfaces. Thereby, a factored pullout resistance force (F_r) contributed by the reinforcement layer can be derived as

$$F_r = \frac{P_r L_e}{r_p} \quad (3.34)$$

where L_e is the reinforcement length anchored behind the potential slip surface, denoted as embedment length (or anchorage length); and r_p is a specified reduction factor regarding

the pullout behavior (Elias et al. 2001). Therefore, to better estimate how much effort the reinforcement layer can contribute to the resistance of sliding, T_j in Equation 2.10 and 3.30 should be replaced by the minimal between the factored pullout resistance force and the allowable tensile strength (T_a) of a certain reinforcement layer; and the units of both indicate the force is mobilized per unit width into the out-of-plane dimension. On the other hand, if the tensile strength or the pullout resistance capacity of a geosynthetic reinforcement is actually mobilized is depending on the embedment length anchored behind the slip surface: if the embedded portion is too short, it may cause very limited loading capacity of the reinforcement layer to be carried out. Therefore, it should be guaranteed a required embedment length as (Elias et al. 2001)

$$L_{e(\text{required})} = \frac{T_a r_p}{P_r} \quad (3.35)$$

corresponding to the critical internal failure surface; and as recommended by Elias et al. (2001), the embedment length should be no less than 1 m (or 3.3 ft). The limit state function with respect to the pullout behavior is then given by

$$g(\mathbf{x}) = \frac{P_r L_e}{T_a} - 1 \quad (3.36)$$

where the random variables are selected as the unit weights of the reinforced mass that contribute to the calculation of the effective vertical stress (σ'_v) in determining the unit pullout resistance capacity in Equation 3.33.

3.4.2.2. External failure. The external failure, where the failure plane is located outside and underneath the reinforced mass, has various possibilities: sliding failure, deep-seated overall instability, lateral squeeze failure, and excessive settlement, as illustrated in Table 3.1.

3.4.2.2.1. Sliding failure. The sliding failure that occurs in a GRES system is most likely along the interface between embankment slope and foundation soil. For a uniform granular slope without considering groundwater effects, from Equation 2.5, the limit state function can be directly derived as

$$g(\mathbf{x}) = \left(\frac{W}{P_a \cos \delta} + \tan \delta \right) \tan \phi' - 1 \quad (3.37)$$

where P_a is the active force acting on the reinforced mass and can be derived on the basis of Coulomb's theory from Equation 2.2; W is the weight of the reinforced mass, functional of the reinforced soil unit weight; ϕ' is the smaller angle of either the effective shearing friction between the reinforced soil and reinforcements or the friction of foundation soil; δ is the internal friction angle between the reinforced mass and backfill, generally assigned between $2/3\phi_w$ and ϕ_w , where ϕ_w is the smaller friction angle of either reinforced mass or backfill. In a more generalized way that involves cohesive soils and groundwater effects, the lateral earth force is re-computed on the basis of the equilibrium of reinforced wedge. The factor of safety is accordingly renewed and the limit state function is given by

$$g(\mathbf{x}) = \frac{c' L_{ds} + (W + P_a \sin \delta - u L_{ds}) \tan \phi'}{P_a \cos \delta} - 1 \quad (3.38)$$

where c' is the smaller cohesion of either embankment fill or foundation soil; L_{ds} is the horizontal width of the reinforced mass along foundation; and u is the pore pressure acting on the base of the reinforced mass. The derivation of the new active force and the factor of safety that considers both cohesion and groundwater effects is further discussed in Appendix B.1. When multiple layers are involved, Rankine's theory seems more efficient to be applied with a horizontal active force acting on the reinforced mass; and the limit state function is given by

$$g(\mathbf{x}) = \frac{c' L_{ds} + (W - u L_{ds}) \tan \phi'}{P_a} - 1 \quad (3.39)$$

where P_a is the active force derived on the basis of Rankine's theory according to Equation 2.6. From Equation 2.2 and 2.6, it can be noticed P_a is functional of backfill cohesion (c'_b), friction angle (ϕ'_b) and unit weight (γ_b); while W is determined by the unit weight of the reinforced mass. When the random variables are selected as: $\mathbf{x} = \{c', \phi', \gamma, \gamma_{sat}\}$, numerical estimation needs to be carried out to calculate the partial derivatives of the limit state function with respect to those random variables due to the complexity of the functions. Otherwise, simplification can be made that P_a is assumed as a deterministic variable; thereby, analytic partial derivatives can be derived based on Equation 3.37, 3.38, and 3.39.

3.4.2.2.2. Deep-seated overall instability. A deep-seated failure often occurs underneath the reinforced mass. Therefore, a classical rotational analysis that uses for unreinforced slopes can be implemented to analyze this type of instability by defining a deep-seated failure plane passing through the foundation soil. From Equation 2.9, the limit state

function can be derived as

$$g(\mathbf{x}) = \frac{\sum_{i=1}^n [c'_i l_i + \tan \phi'_i (W_i \cos \alpha_i - u_i l_i)]}{\sum_{i=1}^n W_i \sin \alpha_i} - 1 \quad (3.40)$$

The partial derivatives of the limit state function with respect to the random variables in this situation are same with the ones given by Equation 3.31 and 3.32. When there is a soft layer existing in the foundation soil as shown in Figure 2.2, sliding block method is suitable as well with a failure plane along the soft layer surface; and the partial derivatives $\partial g / \partial x_i$ can be accordingly derived based on the defined limit state function.

3.4.2.2.3. Lateral squeeze failure. If a weak soil layer exists beneath the embankment slope (Figure 3.8) to a limit depth (D_s) which is less than the width of the slope (b), the factor of safety against lateral squeezing can be calculated by (Elias et al. 2001)

$$f_s = \frac{c_u}{\gamma} \left\{ \frac{\lambda}{D_s \tan \theta} + \frac{\pi + 1}{H} \right\} \quad (3.41)$$

where D_s is the depth of the soft layer beneath the embankment slope base; H is the embankment slope height; θ is the slope angle; γ is the unit weight of slope soil; c_u is the undrained shear strength of the soft soil layer; and λ is a factor representing the relative mobilization of the shear strength between the interfaces: $\lambda = 1$ for a perfectly smooth contact at the top interface and a perfectly rough contact at the bottom interface; $\lambda = 2$ for perfectly rough contacts at two interfaces (Silvestri 1983). Based on Equation 3.41, the

are generally not experienced in cohesionless soils where pore water can drain quickly, or in dry or slightly moist cohesive soils where significant amounts of pore water are not present. Therefore, the embankment settlements caused by the consolidation of cohesionless or dry cohesive soil deposits are frequently ignored; but in saturated cohesive soils, consolidation settlement must be discussed (Naresh and Edward 2006). In view of the construction process of a geosynthetic reinforced embankment slope that the fills are placed layer by layer over time, the short-term settlement is always not an issue, and will not be taken into consideration herein. The methods to determine the magnitude and the rate of foundation settlements in various situations (i.e., normally consolidated, over-consolidated) are described in detail in Section 7.4 and 7.5 in FHWA Soils and Foundations Workshop Reference Manual (Naresh and Edward 2006). It shows the settlements are significantly depending on the soil compressibility that always can be evaluated by bearing capacity index (C'), compression index (C_c), recompression index (C_r), coefficient of consolidation (c_v), preconsolidation pressure (σ'_p) and etc.. Based on the allowable foundation settlements that are usually determined from project requirements, the limit state function can be defined in the same way as demonstrated for other failure mechanisms along with the selected random variables.

3.4.2.3. Compound failure. The compound failure, where the failure plane passes behind and through the reinforced mass, can be analyzed by either rotational or sliding block method. In rotational analysis, since the failure plane passes only one or a few reinforcement layers, the limit state function can be modified based on Equation 3.30 as given

below

$$g(\mathbf{x}) = \frac{r \sum_{i=1}^n [c'_i l_i + \tan \phi'_i (W_i \cos \alpha_i - u_i l_i)] + \sum_{j=1}^{m_c} T_j d_j}{r \sum_{i=1}^n W_i \sin \alpha_i} - 1 \quad (3.43)$$

where m_c is the number of the layers through which the failure plane passes; basically, $m_c < m$, but if $m_c = m$, it becomes internal failure. Similarly, if the pullout behavior is taken into consideration, T_j in the above equation should be replaced by the minimum between the factored pullout resistance force and the allowable tensile strength with respect to a certain reinforcement layer. If the failure plane is supposed to occur along a reinforcement layer, sliding block method can be applied with a limit state function modified from Equation 3.37, 3.38, or 3.39, where W is substituted by the weight of the reinforced mass above the failure plane; c' is the effective cohesion of the reinforced soil; ϕ' is the effective friction angle between reinforced soil and reinforcements; and P_a is the active force acting on the wedge that is above the failure plane. The partial derivatives of the limit state function with respect to the random variables can be derived either analytically or numerically.

3.4.3. Short and Long-Term Conditions. As mentioned in Section 3.4.1, to thoroughly evaluate the stability of a GRES structure, both short-term and long-term conditions need to be taken into consideration. In general, if the slope primarily consists of cohesive soils, undrained analysis is always carried out in short-term condition; while drained analysis is performed in long-term condition. In undrained analysis, it is common to use the undrained shear strength (c_u); and a zero undrained friction angle (ϕ_u) is always assumed.

Therefore, the problem can be simplified as: 1) in rotational analysis,

$$g(\mathbf{x}) = \frac{\sum_{i=1}^n c_u l_i}{\sum_{i=1}^n W_i \sin \alpha_i} - 1, \text{ for unreinforced slopes} \quad (3.44)$$

$$g(\mathbf{x}) = \frac{r \sum_{i=1}^n c_u l_i + \sum_{j=1}^m T_j d_j}{r \sum_{i=1}^n W_i \sin \alpha_i} - 1, \text{ for reinforced slopes} \quad (3.45)$$

where $\{c_u\}$ are the undrained shear strengths in multiple soil layers;
and 2) in sliding analysis,

$$g(\mathbf{x}) = \frac{c_u L_{ds}}{P_a \cos \delta} - 1, \text{ from Coulomb's theory} \quad (3.46)$$

$$g(\mathbf{x}) = \frac{c_u L_{ds}}{P_a} - 1, \text{ from Rankine's theory} \quad (3.47)$$

where c_u is the undrained cohesion between reinforced soil and foundation, and P_a is the active force computed with the undrained shear strength. Otherwise, in long term condition, the effective strength parameters are commonly used due to the drained status. If the slope is primarily consisting of granular materials, due to their relatively higher permeability, the drained condition always exists with a zero cohesion assumed regardless of short

term or long term. Thereby, the problem can be simplified as: 1) in rotational analysis,

$$g(\mathbf{x}) = \frac{\sum_{i=1}^n \tan \phi'_i (W_i \cos \alpha_i - u_i l_i)}{\sum_{i=1}^n W_i \sin \alpha_i} - 1, \text{ for unreinforced slopes} \quad (3.48)$$

$$g(\mathbf{x}) = \frac{r \sum_{i=1}^n \tan \phi'_i (W_i \cos \alpha_i - u_i l_i) + \sum_{j=1}^m T_j d_j}{r \sum_{i=1}^n W_i \sin \alpha_i} - 1, \text{ for reinforced slopes} \quad (3.49)$$

and 2) in sliding analysis,

$$g(\mathbf{x}) = \frac{(W + P_a \sin \delta - u L_{ds}) \tan \phi'}{P_a \cos \delta} - 1, \text{ from Coulomb's theory} \quad (3.50)$$

$$g(\mathbf{x}) = \frac{(W - u L_{ds}) \tan \phi'}{P_a} - 1, \text{ from Rankine's theory} \quad (3.51)$$

3.5. NUMERICAL EXAMPLE

To demonstrate the application of the proposed probabilistic slope stability analysis, two numerical examples are carried out in this section, respectively taken from FHWA Mechanically Stabilized Earth Walls and Reinforced Soil Slopes Design & Construction Guidelines (Elias et al. 2001) and Mirafí Geosynthetic for Soil Reinforcement Design Manual.

3.5.1. Numerical Example 1: Geotextile Reinforced Road Embankment. This example is performed on a 1H:1V road embankment that is 5-m high and reinforced by 12 layers of geotextile reinforcements having a unique allowable tensile strength of 4.14

kN/m over the full height of embankment, as shown in Figure 3.9. The groundwater table

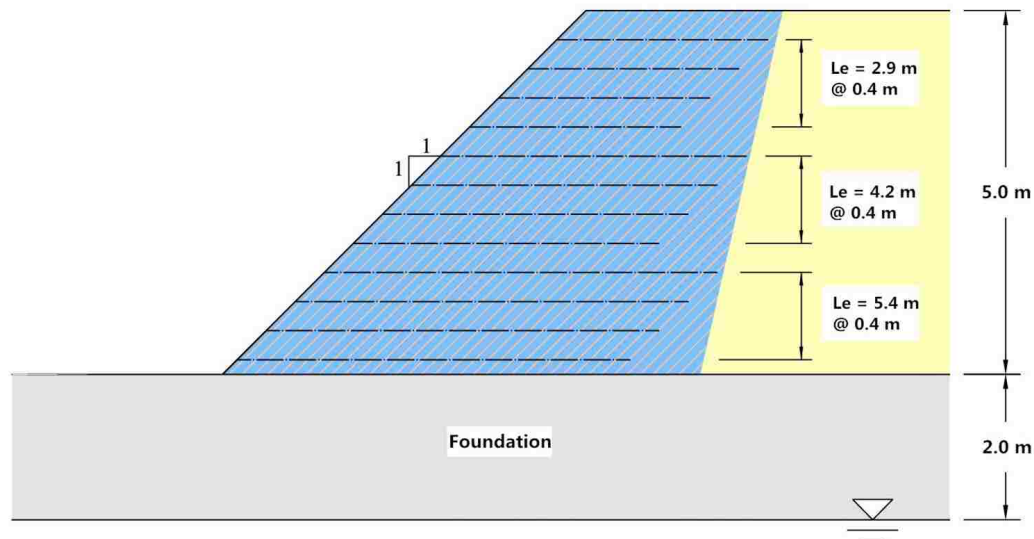


Figure 3.9: The configuration of the road embankment in Example 1

is located 2-m below the foundation, and is not taken into consideration herein. The bottom reinforcement layer is placed after the first lift of the embankment fill with a thickness of 200 mm; afterwards, the reinforcements are evenly placed with an average spacing of 400 mm throughout the whole embankment slope. The foundation soil consists of stiff to very stiff, low-plasticity, silty clay; and the embankment fill is clayey sand and gravel. Their engineering properties are presented in Table 3.2, where some typical COVs are assumed with some published ranges (Baecher and Christian 2003; Houlihan et al. 2010). The design factor of safety regarding the multiple failure modes are all set as 1.3, except for the pullout behavior that is specified as 1.5. Furthermore, the pullout resistance factor, $F^* = 0.43$; and the scale effect correction factor, $\alpha = 0.6$ (Elias et al. 2001).

Table 3.2: The material properties in Example 1

Material	Parameter	Mean	COV
Foundation: stiff to very stiff, low plasticity, silty clay	c_u	100 kPa	30%
	c'	0	Deterministic
	ϕ'	28°	9%
	γ	19 kN/m ³	5%
Embankment fill: clayey sand	c'	0	Deterministic
	ϕ'	33°	8%
	γ	21 kN/m ³	5%

Note: The COVs are assumed based on Baecher and Christian (2003) and Houlihan et al. (2010).

3.5.1.1. Deterministic slope stability analysis. To quickly start the example, deterministic slope stability analysis is first carried out with a total of 2224 rotational slip surfaces being searched, that include 638 for internal, 1551 for compound, and 35 for deep-seated failure. The critical deterministic slip surfaces are accordingly located with respect to the preceding failure modes as shown in Figure 3.10, where the critical deterministic internal failure surface with the minimum factor of safety, $f_{s,i(\min)} = 1.188$, passes all the reinforcements and exits at the toe of the slope; while the critical deterministic compound failure surface has the minimum factor of safety, $f_{s,c(\min)} = 1.213$, and passes 11 out of 12 reinforcement layers in total. Considering the pullout failure that may potentially occur in the reinforced slope, it is summarized in Table 3.3 that the factor of safety against pullout behavior, the tensile force carried by each reinforcement layer, and the corresponding embedment length along the critical deterministic internal failure surface. The minimum factor of safety against the pullout behavior is obtained as 1.66 along the top reinforcement

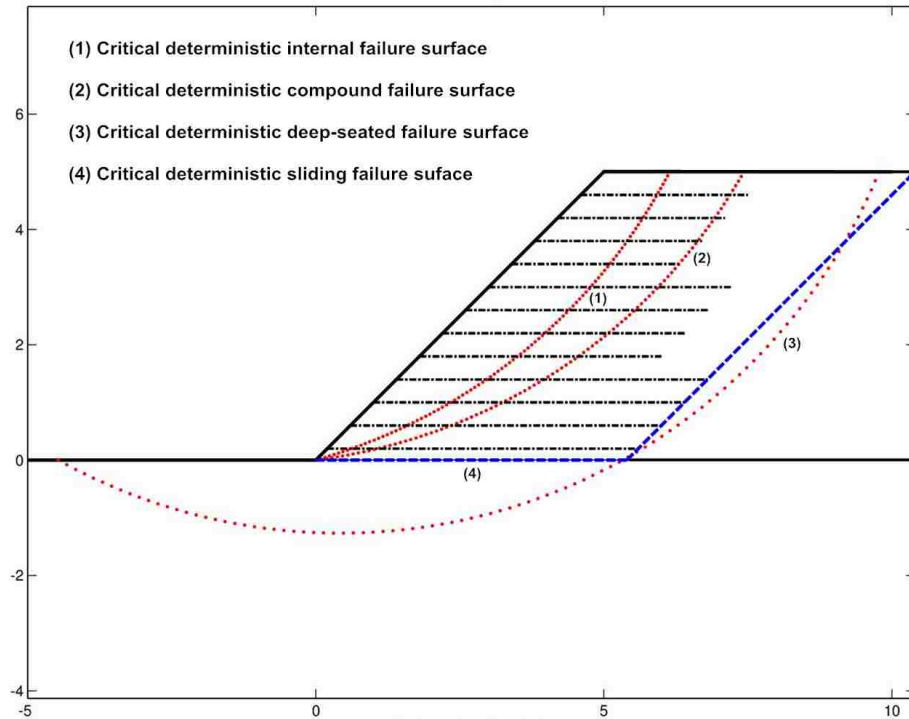


Figure 3.10: The critical deterministic slip surfaces in Example 1

layer and has been big enough compared to the required value of 1.5. The resisting forces provided by the reinforcement layers are all equal to their allowable tensile strength (= 4.14 kN/m), indicating the allowable tensile strength is lower than the pullout resistance force the geotextile reinforcement can provide. In other words, it is more likely to have tensile failure occur in the geotextile reinforcements rather than the pullout failure. Therefore, the allowable tensile strength is considered as a control factor in this example; and is fully mobilized since the anchored portion is long enough with the embedment length greater than the required value, which, except for the top layer, is set to be 1 m, since the calculated value as shown in the parenthesis in Table 3.3 is less than 1 m.

Sliding failure is supposed to occur along the interface between foundation and embankment slope. With 105 sliding surfaces being searched, the critical deterministic

Table 3.3: The pullout resistance in deterministic analysis in Example 1

Layer	f_s	F_r (kN/m)	L_e (m)	$L_{e(\text{required})}$ (m)
1	62.91	4.14	4.97	1 (0.119)
2	51.15	4.14	4.41	1 (0.129)
3	42.78	4.14	4.06	1 (0.142)
4	36.36	4.14	3.83	1 (0.158)
5	21.03	4.14	2.49	1 (0.178)
6	17.88	4.14	2.42	1 (0.203)
7	15.21	4.14	2.40	1 (0.237)
8	12.82	4.14	2.43	1 (0.285)
9	5.04	4.14	1.20	1 (0.356)
10	4.09	4.14	1.29	1 (0.474)
11	3.00	4.14	1.42	1 (0.712)
12	1.66	4.14	1.58	1.423

sliding failure surface is located as shown in Figure 3.10, that has the minimum factor of safety, $f_{s,s(\text{min})} = 1.779$. The critical deterministic deep-seated failure surface is located outside of the reinforced mass with a minimum factor of safety, $f_{s,d(\text{min})} = 1.327$. In summary, through the traditional deterministic slope stability analysis, this geotextile reinforced road embankment doesn't meet the design requirements since the factor of safety against neither internal nor compound failure is greater than the required value of 1.3. In the following sections, probabilistic slope stability analysis is to be carried out, so that it can be evaluated how probable the failure can occur with the calculated factor of safety; and the system reliability is able to be estimated considering the multiple failure modes that may potentially occur.

3.5.1.2. Probabilistic slope stability analysis. As shown in Table 3.2, there are four random variables taken into consideration: the effective friction angle and the unit weight of both foundation soil and embankment fill; while the effective cohesion with zero magnitude is considered as deterministic variable. Since the probabilistic properties of soil strength and unit weight are not available herein, assumptions are made based on some published ranges (Baecher and Christian 2003; Houlihan et al. 2010). As mentioned in Section 3.2.2, normal and log-normal are two most popular distribution models to describe the probabilistic characteristics of the soil properties including MC strength parameters and soil unit weights; therefore, both of them are going to be studied in the following probabilistic analysis as a comparison.

3.5.1.2.1. Uncorrelated random variables. The random variables are assumed uncorrelated and normally distributed (Case I) at first. In view of the chances that the surface with the minimum factor of safety may not coincide with the one having the maximum probability of failure, along with the traditional deterministic analysis, the proposed probabilistic slope stability analysis is simultaneously performed to locate the critical probabilistic slip surfaces with a total of 2224 potential slip surfaces being searched. Along the critical deterministic slip surfaces that have been addressed in Section 3.5.1.1, the probability of failure are respectively obtained as 0.685%, 1.312%, and 0.038% corresponding to internal, compound, and deep-seated failure mode. Meanwhile, the critical probabilistic slip surfaces are located with the maximum probability of failure and the corresponding factor of safety as: 1) $p_{f,i(\max)} = 1.235\%$ and $f_{s,i} = 1.214$, for internal failure; 2) $p_{f,c(\max)} = 1.312\%$ and $f_{s,c} = 1.213$, for compound failure; and 3) $p_{f,d(\max)} = 0.048\%$ and $f_{s,d} = 1.337$, for deep-seated failure. As shown in Figure 3.11, it is only for the compound failure that

two critical surfaces coincide with each other; otherwise, they are located at different positions. Therefore, the pullout behavior should be examined along not only the critical

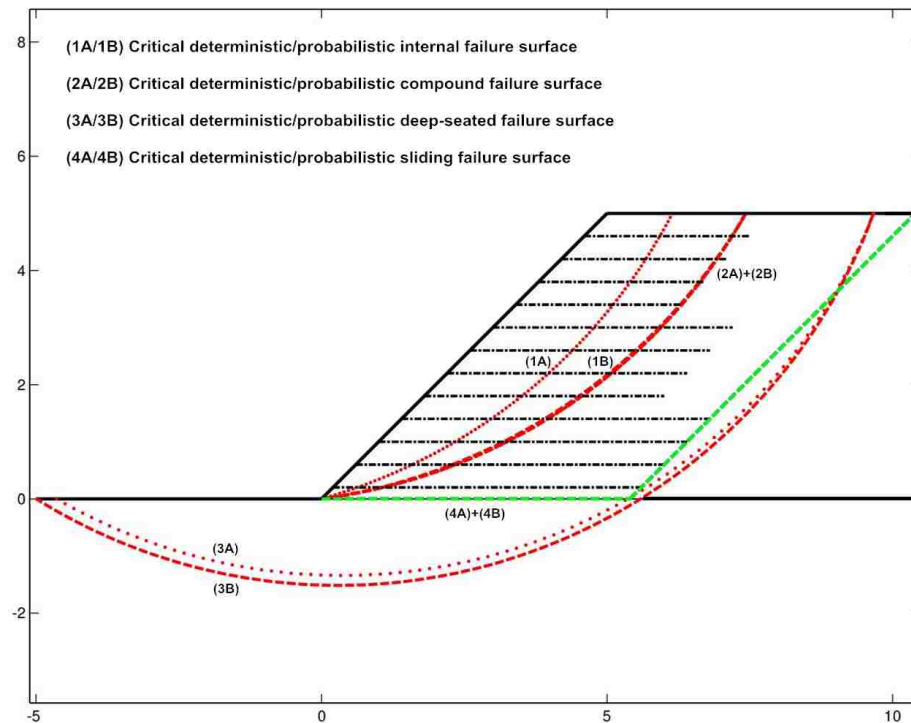


Figure 3.11: The critical deterministic and probabilistic slip surfaces in Example 1

deterministic internal failure surface but also the probabilistic one. The factors of safety against the pullout behavior along the two critical internal failure surfaces are summarized in Table 3.4, where it can be noticed, along the critical probabilistic internal failure surface which is located deeper in the slope compared to the deterministic one, the top four reinforcement layers are most likely to be pulled out since the factors of safety are significantly less than 1.5; and their strengths are not fully mobilized since the anchored portions are not long enough compared to the required embedment lengths. The critical deterministic and probabilistic sliding failure surfaces are located at the same position, that is, along the

Table 3.4: The pullout resistance in probabilistic analysis in Example 1

Layer	Deterministic Internal Surface			Probabilistic Internal Surface			$L_{e(\text{required})}$ (m)
	f_s	F_r (kN/m)	L_e (m)	f_s	F_r (kN/m)	L_e (m)	
1	62.91	4.14	4.97	58.46	4.14	4.62	1 (0.119)
2	51.15	4.14	4.41	43.80	4.14	3.78	1 (0.129)
3	42.78	4.14	4.06	34.58	4.14	3.28	1 (0.142)
4	36.36	4.14	3.83	28.05	4.14	2.96	1 (0.158)
5	21.03	4.14	2.49	13.03	4.14	1.55	1 (0.178)
6	17.88	4.14	2.42	10.43	4.14	1.41	1 (0.203)
7	15.21	4.14	2.40	8.50	4.14	1.34	1 (0.237)
8	12.82	4.14	2.43	6.99	4.14	1.33	1 (0.285)
9	5.044	4.14	1.20	0.21	0.57	0.05	1 (0.356)
10	4.09	4.14	1.29	0.35	0.96	0.11	1 (0.474)
11	3.00	4.14	1.42	0.43	1.18	0.20	1 (0.712)
12	1.66	4.14	1.58	0.34	0.94	0.32	1.423

interface between foundation and embankment slope with a 45-degree inclined back-face; has a maximum probability of failure, $p_{f,s(\text{max})} = 2.1 \times 10^{-4}\%$, along with a minimum factor of safety, $f_{s,s(\text{min})} = 1.779$.

If the random variables are all in log-normal distribution (Case II), the critical surfaces are situated at the same positions as obtained in Case I but with different probabilistic results as summarized in Table 3.5. It is shown a relatively lower probability of failure is obtained in the case of log-normal distribution for any of the discussed failure modes, wherein the sliding failure always has the lowest probability of failure and a highest factor of safety. The comparison is further carried out based on the mixture of normal and log-normal distributions assigned to the random variables: $\phi' \sim N$ with $\gamma \sim LN$ (Case III);

Table 3.5: The probabilistic results in Case I, II, III, and IV in Example 1

Failure Mode	Surface	f_s	p_f (Iterative Steps)			
			Case I	Case II	Case III	Case IV
Internal	Det.	1.188	0.685% (299)	0.329% (298)	0.672% (299)	0.338% (298)
	Pro.	1.214	1.235% (306)	0.728% (306)	1.226% (307)	0.735% (305)
Compound	Det.	1.213	1.312% (306)	0.788% (305)	1.302% (306)	0.795% (305)
	Pro.					
Deep-Seated	Det.	1.327	0.038% (330)	0.008% (329)	0.038% (330)	0.008% (329)
	Pro.	1.337	0.048% (332)	0.009% (331)	0.048% (332)	0.009% (331)
Sliding	Det.	1.779	2.10E-4% (6)	1.31E-5% (6)	2.10E-4% (6)	1.31E-5% (6)
	Pro.					

1. 'Det.' refers to the critical deterministic slip surface;
2. 'Pro.' refers to the critical probabilistic slip surface.

vice versa, $\phi' \sim LN$ with $\gamma \sim N$ (Case IV), as demonstrated in Figure 3.12. By comparing the results in Case I and III, Case II and IV, Case I and IV, and Case II and III, it can be found a greater impact coming from the distribution selection regarding the friction angle rather than the unit weight, which, on the other hand, indicates the probability of failure in each discussed failure mode is primarily controlled by the friction angle instead of the unit weight of foundation soil and embankment fill; especially in the sliding failure, the distribution selection of the unit weight hardly affect the probabilistic results.

3.5.1.2.2. Correlated random variables. If the random variables are considered correlated with each other, a nonzero correlation coefficient should be assigned. As mentioned in Section 3.2.3, the correlation between cohesion and friction angle can possibly be negative; while friction angle and unit weight are most likely in a positive correlation in view of their physical meanings. Since the correlation properties are not available in

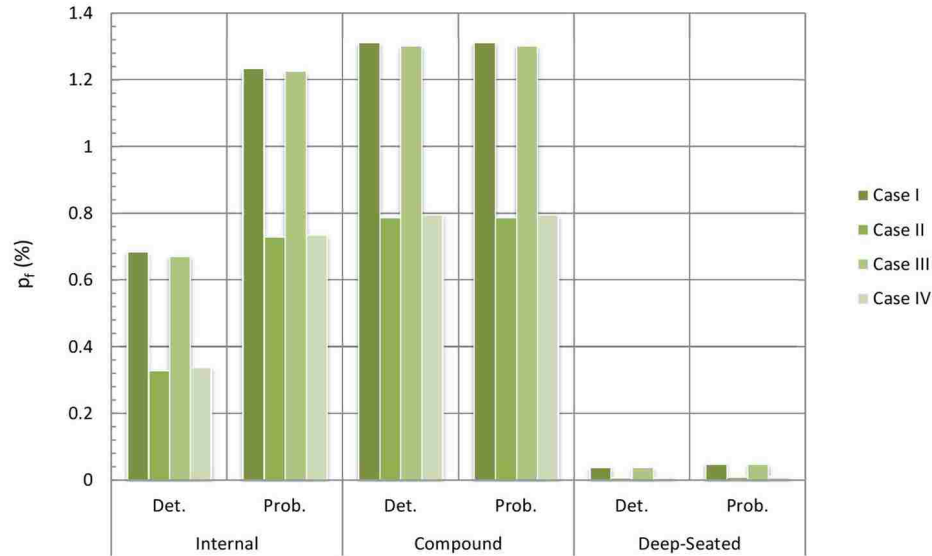


Figure 3.12: The comparison of the probabilistic results in Case I to IV in Example 1

this example, various assumptions are made for comparison to see the effect of the correlation coefficient assigned between the soil properties on the probabilistic results. The MC strength parameters and the soil unit weights are assumed correlated only in the same soil layer. Therefore, there are two sets of correlated random variables herein: $\{\phi'_e, \gamma_e\}$, for the embankment fill; $\{\phi'_f, \gamma_f\}$, for the foundation soil. The analysis is accordingly performed with the correlation coefficient set to be 0.1, 0.2, 0.5 and 0.9 for both foundation soil and embankment fill. The results are listed in Table 3.6 and 3.7; and the comparison is discussed and illustrated in Figure 3.13 and 3.14. The critical surfaces are located at the positions as obtained in the case of uncorrelated random variables (Case I, II, III, and IV), as shown in Figure 3.11. The probability of failure along the two critical surfaces are significantly decreased with the correlation coefficient increasing from 0.1 to 0.9 with respect to the internal and the compound failure in both of the cases with normal (Case V, Figure 3.13) and log-normal distribution (Case VI, Figure 3.14). But it is found slightly

Table 3.6: The probabilistic results in Case V in Example 1

Failure Mode	Surface	f_s	p_f (Iterative Steps)			
			$\rho_{\phi\gamma} = 0.1$	$\rho_{\phi\gamma} = 0.2$	$\rho_{\phi\gamma} = 0.5$	$\rho_{\phi\gamma} = 0.9$
Internal	Det.	1.188	0.564% (307)	0.454% (316)	0.195% (351)	0.028% (430)
	Pro.	1.214	1.154% (310)	1.076% (313)	0.845% (326)	0.559% (348)
Compound	Det.	1.213	1.230% (309)	1.149% (313)	0.912% (325)	0.615% (347)
	Pro.					
Deep-Seated	Det.	1.327	0.040% (329)	0.042% (327)	0.051% (322)	0.065% (315)
	Pro.	1.337	0.053% (329)	0.057% (327)	0.073% (319)	0.101% (309)
Sliding	Det.	1.779	2.10E-4% (6)			
	Pro.					

Table 3.7: The probabilistic results in Case VI in Example 1

Failure Mode	Surface	f_s	p_f (Iterative Steps)			
			$\rho_{\phi\gamma} = 0.1$	$\rho_{\phi\gamma} = 0.2$	$\rho_{\phi\gamma} = 0.5$	$\rho_{\phi\gamma} = 0.9$
Internal	Det.	1.188	0.246% (307)	0.176% (318)	0.045% (361)	0.001% (464)
	Pro.	1.214	0.662% (309)	0.598% (314)	0.425% (328)	0.238% (352)
Compound	Det.	1.213	0.719% (309)	0.653% (313)	0.471% (327)	0.272% (350)
	Pro.					
Deep-Seated	Det.	1.327	0.008% (328)	0.009% (326)	0.012% (322)	0.015% (317)
	Pro.	1.337	0.011% (328)	0.012% (326)	0.017% (320)	0.025% (312)
Sliding	Det.	1.779	2.10E-4% (6)			
	Pro.					

increased along the critical surfaces regarding the deep-seated failure mode; and has no changes along the critical sliding failure surfaces when the correlation coefficient is going up.

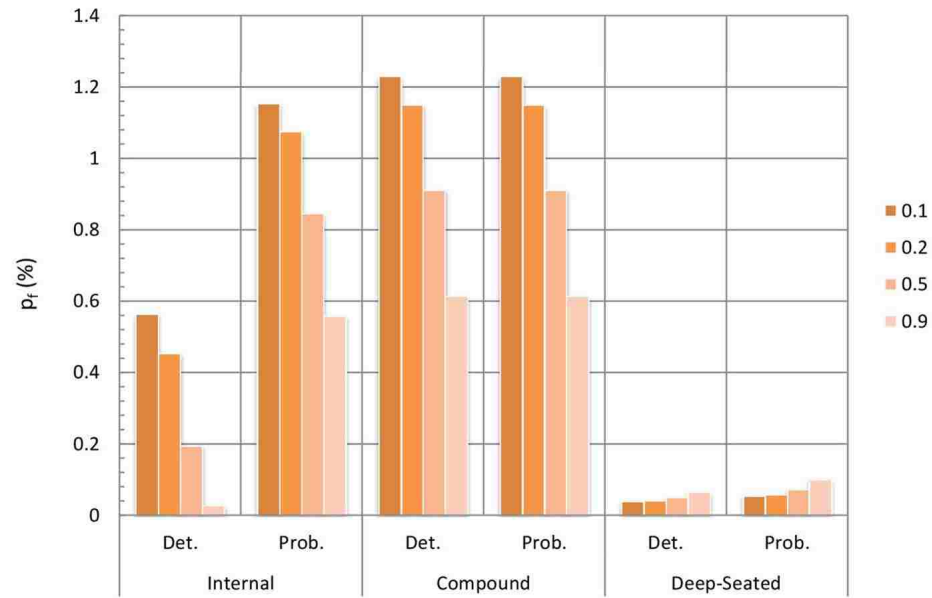


Figure 3.13: The comparison of the probabilistic results in Case V in Example 1

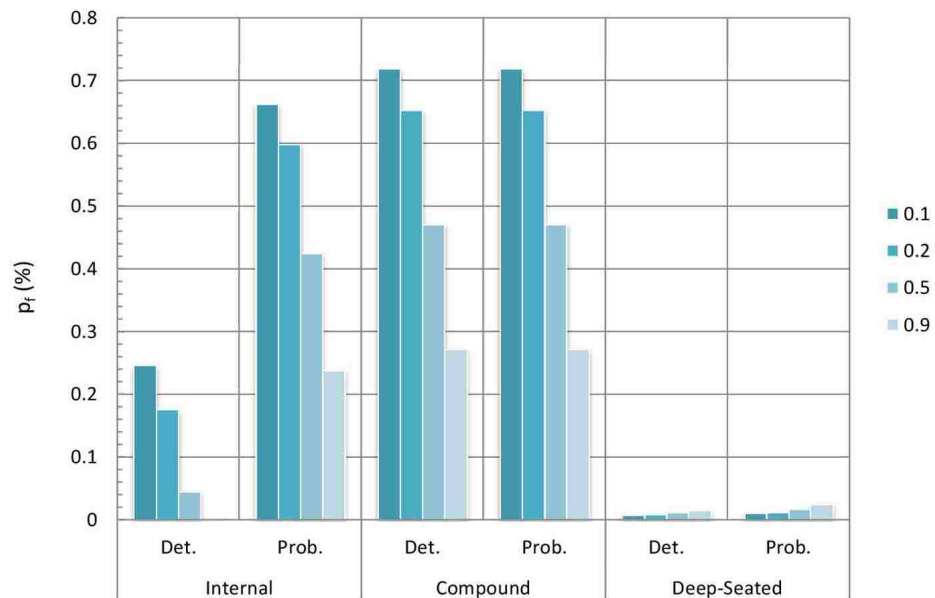


Figure 3.14: The comparison of the probabilistic results in Case VI in Example 1

3.5.1.2.3. System reliability. Based on the probability of failure obtained in different cases, system reliability can be consequently calculated according to Equation 3.28 and 3.29 with respect to the discussed failure modes. The results are listed in Table 3.8 with the comparison demonstrated in Figure 3.15, 3.16 and 3.17. It can be noticed, in this

Table 3.8: The system reliability in Example 1

Case	Internal	Compound	Deep-Seated	Sliding	p_{fs} (%)	R_s (%)
I	30.49	44.30	0.66	2.10E-4	61.54	38.46
II	13.15	14.16	0.11	1.31E-5	25.53	74.47
III	30.13	44.12	0.66	2.10E-4	61.22	38.78
IV	13.37	14.28	0.11	1.31E-5	25.82	74.18
V	0.1	26.65	42.12	2.10E-4	57.85	42.15
	0.2	23.06	39.91		54.11	45.89
	0.5	14.04	33.16		43.07	56.93
	0.9	6.21	24.20		29.77	70.23
VI	0.1	10.75	12.75	1.31E-5	22.22	77.78
	0.2	8.72	10.94		18.81	81.19
	0.5	4.41	7.87		12.08	87.92
	0.9	1.60	4.38		6.13	93.87

example, the compound failure always has the greatest contribution to the system probability of failure; while the sliding failure has the slightest impact. When comparing the results obtained in Case I to IV, by changing the distribution models assigned to the random variables from normal to log-normal, significant reduction can be found in the system probability of failure; meanwhile, the system reliability is highly increased. In Case V and

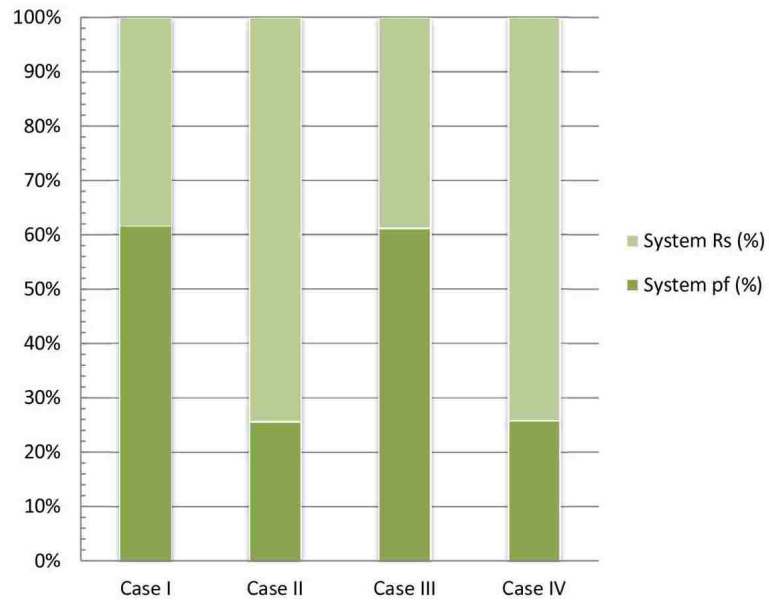


Figure 3.15: The system reliability in Case I to IV in Example 1

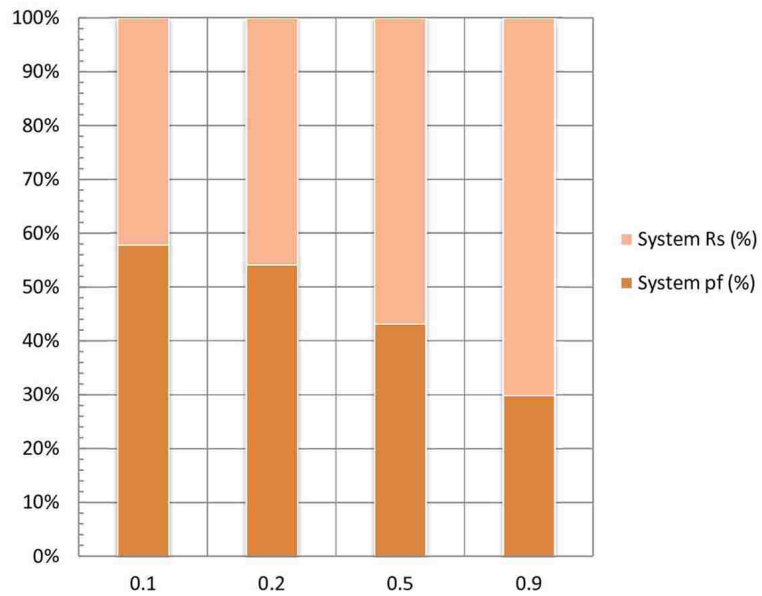


Figure 3.16: The system reliability in Case V in Example 1

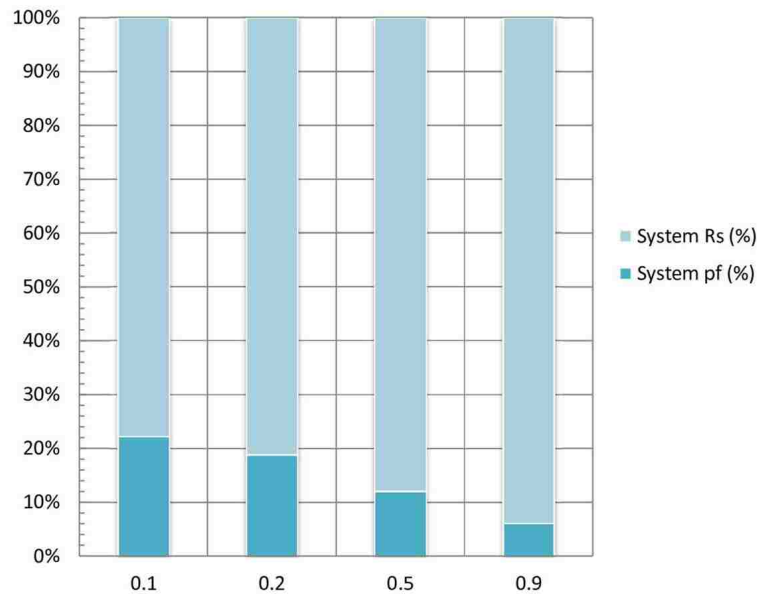


Figure 3.17: The system reliability in Case VI in Example 1

VI, the total probability of failure regarding the internal and the compound failure is greatly decreased with the correlation coefficient increasing from 0.1 to 0.9. But it is found slightly increased in the deep-seated failure mode, and has no changes in sliding failure. Therefore, as a result, with the increase in the correlation coefficient between the friction angle and the soil unit weight, the system probability of failure is decreased while the system reliability is increased.

3.5.2. Numerical Example 2: Geogrid Reinforced Embankment Slope. This example is performed on a 1H:1V embankment slope that is 30-ft high and reinforced by 9 layers of geogrid reinforcements with an average length of 32 ft (Figure 3.18), where the bottom layer is placed along the interface between foundation and embankment slope. Three different geogrid products are installed: Miragrid 5XT for the bottom 4 layers at 3-ft spacing, Miragrid 3XT for the 5th to 7th layers at 3-ft spacing, and Miragrid 2XT for

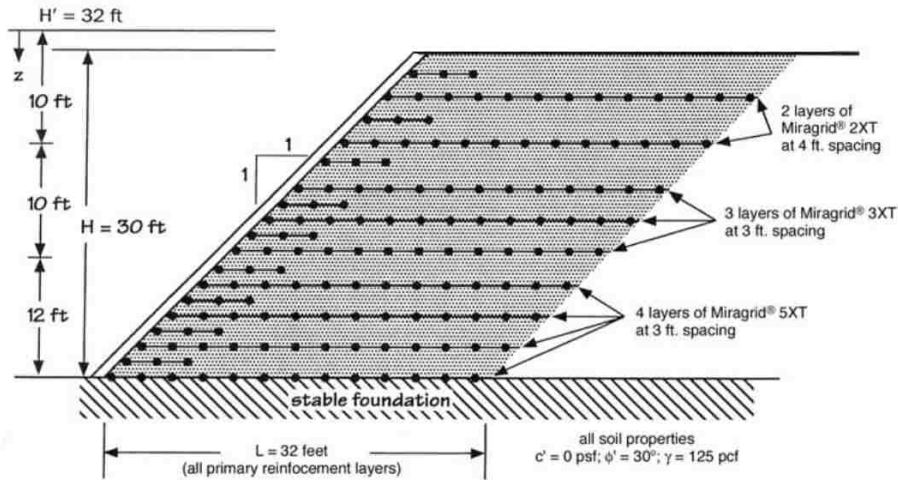


Figure 3.18: The configuration of the embankment slope in Example 2

the top 2 layers at 4-ft spacing. The groundwater is not taken into consideration in this example. The engineering properties of embankment fill, foundation soil and geogrids are summarized in Table 3.9 along with their probabilistic properties. The design factors of

Table 3.9: The material properties in Example 2

Material		Parameter	Mean	COV
Foundation and Embankment		c'	0	Deterministic
		ϕ'	30°	10%
		γ	125 pcf	5%
Geogrids	Miragrid 2XT	T_a	949 lb/ft	Deterministic
	Miragrid 3XT	T_a	1558 lb/ft	Deterministic
	Miragrid 5XT	T_a	2234 lb/ft	Deterministic

Note: The COVs are assumed based on Baecher and Christian (2003) and Houlihan et al. (2010).

safety with respect to the multiple failure modes are all set to be 1.5, including the factor of safety against pullout failure. Furthermore, the pullout resistance factor, $F^* = 0.39$; and the scale effect correction factor, $\alpha = 0.9$. The secondary reinforcements are installed with an intention to locally stabilize the slope face during and after slope construction; but not included in the general slope stability analysis.

3.5.2.1. Deterministic slope stability analysis. To quickly start the example, deterministic slope stability analysis is first carried out with a total of 1953 potential slip surfaces being searched, that include 427 for internal, 762 for compound and 764 for deep-seated failure. The critical deterministic slip surfaces are accordingly located with respect to the preceding failure modes as shown in Figure 3.19, where the critical determinis-

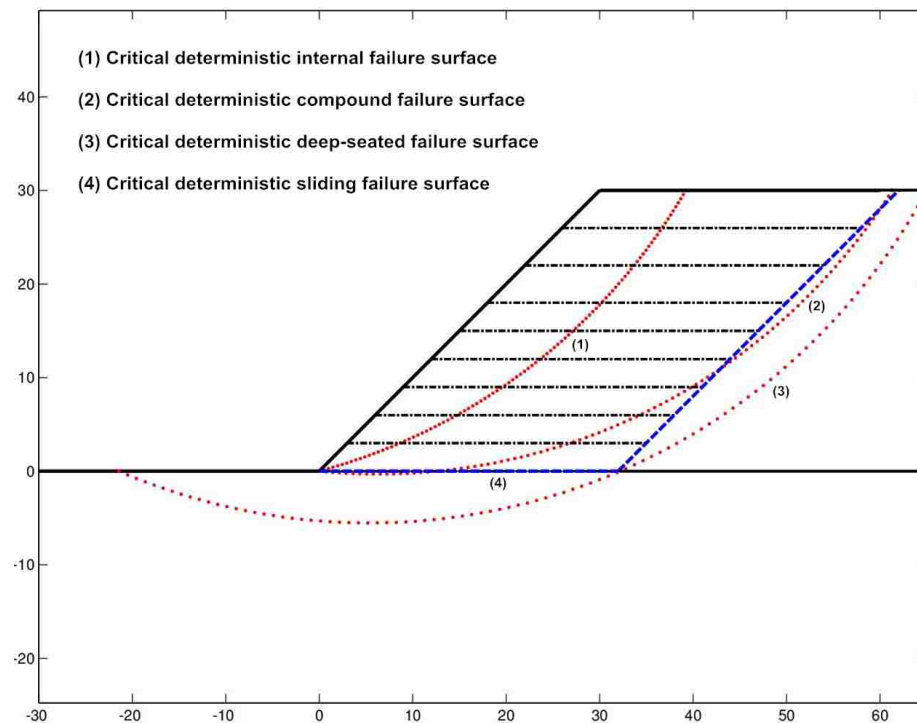


Figure 3.19: The critical deterministic slip surfaces in Example 2

tic internal failure surface with the minimum factor of safety, $f_{s,i(\min)} = 1.225$, passes all the reinforcements and exits at the toe of the slope; while the critical deterministic compound failure surface has the minimum factor of safety, $f_{s,c(\min)} = 1.461$, and passes the bottom four layers only. Considering the pullout failure that may potentially occur in the reinforced slope, it is summarized in Table 3.10 that the factor of safety against pullout behavior, the tensile force carried by each reinforcement layer, and the corresponding

Table 3.10: The pullout resistance in deterministic analysis in Example 2

Layer	f_s	F_r (lb/ft)	L_e (ft)	$L_{e(\text{required})}$ (ft)
1	37.2	2234	32.00	3.3 (1.290)
2	27.6	2234	26.35	3.3 (1.433)
3	21.6	2234	23.25	3.3 (1.612)
4	17.4	2234	21.39	3.3 (1.843)
5	20.3	1558	20.32	3.3 (1.500)
6	16.5	1558	19.84	3.3 (1.800)
7	13.2	1558	19.80	3.3 (2.249)
8	14.9	949	20.30	3.3 (2.055)
9	7.8	949	21.32	4.109

embedment length along the critical deterministic internal failure surface. The minimum factor of safety against the pullout behavior is obtained as 7.80 along the top reinforcement layer and has been significantly higher than the required value of 1.5. The resisting forces are mainly determined by the allowable tensile strengths of the geogrids; and are fully mobilized since the anchored portions are long enough with the embedment lengths greater

than the required values, which, except for the top layer, are all less than the recommended value of 3.3 ft (Elias et al. 2001).

Sliding failure is supposed to occur along the interface between foundation and embankment slope. With 280 potential slip surfaces being searched, the critical deterministic sliding failure surface is located as shown in Figure 3.19, that has the minimum factor of safety, $f_{s,s(\min)} = 1.487$. The critical deterministic deep-seated failure surface is located outside of the reinforced mass with a minimum factor of safety, $f_{s,d(\min)} = 1.450$. In summary, through the traditional deterministic slope stability analysis, this geogrid reinforced embankment slope fails to meet the design requirements since the factors of safety are all lower than the required value of 1.5. In the following sections, the proposed probabilistic slope stability analysis is to be carried out to assess the probability of failure with respect to the discussed potential failure modes and estimate the system reliability in view of the soil variability.

3.5.2.2. Probabilistic slope stability analysis. Although the embankment fill and the foundation soil are both homogeneous with the same soil type, considering the construction process, it is more reasonable to treat them as two layers with two sets of random variables that share the same probabilistic properties: the effective friction angle and the bulk unit weight with the COVs chosen as 10% and 5% according to some published ranges (Baecher and Christian 2003; Houlihan et al. 2010).

3.5.2.2.1. Uncorrelated random variables. Similarly, all the random variables are first assumed uncorrelated and normally distributed (Case I). Along with the traditional deterministic analysis that has been performed in Section 3.5.2.1, a total of 1953 potential slip surfaces are searched in the proposed probabilistic slope stability analysis to locate the critical surfaces with respect to the multiple failure modes, as shown in Figure 3.20.

Along the critical deterministic slip surfaces, the probability of failure are respectively

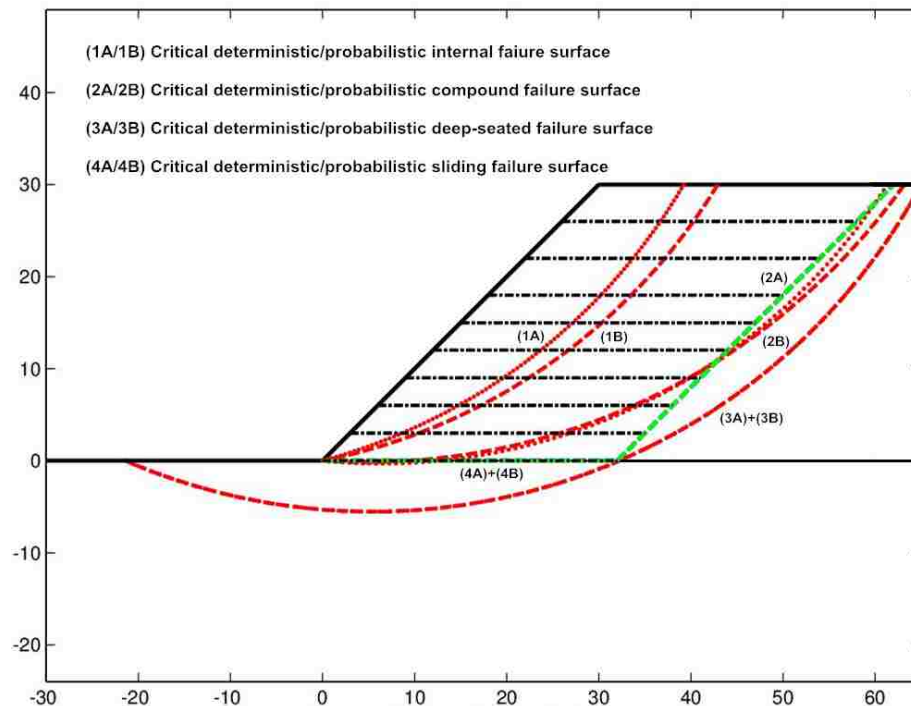


Figure 3.20: The critical deterministic and probabilistic slip surfaces in Example 2

obtained as 0.441%, 0.033% and 0.007% corresponding to internal, compound and deep-seated failure mode. Meanwhile, the critical probabilistic slip surfaces are located with the maximum probability of failure and the corresponding factor of safety as: 1) $p_{f,i(\max)} = 0.658\%$ and $f_{s,i} = 1.238$, for internal failure; 2) $p_{f,c(\max)} = 0.041\%$ and $f_{s,c} = 1.477$, for compound failure; and 3) $p_{f,d(\max)} = 0.007\%$ and $f_{s,d} = 1.450$, for deep-seated failure. As shown in Figure 3.20, the critical probabilistic internal failure surface is situated relatively deeper in the slope compared to the deterministic surface. Therefore, the results regarding the pullout behavior examined along both of the two critical internal failure surfaces are listed in Table 3.11, where it can be noticed, because of the deeper location of the critical

Table 3.11: The pullout resistance in probabilistic analysis in Example 2

Layer	Deterministic Internal Surface			Probabilistic Internal Surface			$L_{e(\text{required})}$ (ft)
	f_s	F_r (lb/ft)	L_e (ft)	f_s	F_r (lb/ft)	L_e (ft)	
1	37.2	2234	32.00	35.1	2234	32	3.3 (1.290)
2	27.6	2234	26.35	25.7	2234	24.55	3.3 (1.433)
3	21.6	2234	23.25	19.4	2234	20.83	3.3 (1.612)
4	17.4	2234	21.39	15.2	2234	18.63	3.3 (1.843)
5	20.3	1558	20.32	17.3	1558	17.33	3.3 (1.500)
6	16.5	1558	19.84	13.9	1558	16.67	3.3 (1.800)
7	13.2	1558	19.80	11.0	1558	16.49	3.3 (2.249)
8	14.9	949	20.30	12.3	949	16.84	3.3 (2.055)
9	7.8	949	21.32	6.5	949	17.74	4.109

probabilistic internal failure surface, the anchored portions are relatively shorter than the ones behind the deterministic surface; and consequently results in a lower factor of safety being computed against the pullout behavior along the critical probabilistic internal failure surface. Nevertheless, with the minimum factor of safety obtained as 6.5 along the top reinforcement layer, the factors of safety have been big enough compared to the required value of 1.5; and therefore, the pullout failure can hardly occur in this slope.

The probabilistic analysis is further carried out with different distribution models assigned to the random variables: ϕ' and $\gamma \sim LN$ (Case II); $\phi' \sim N$ with $\gamma \sim LN$ (Case III); and $\phi' \sim LN$ with $\gamma \sim N$ (Case IV). The results are accordingly listed in Table 3.12; and the comparison is demonstrated in Figure 3.21. It is indicated a lower probability of failure always comes along with the log-normal distributions assigned to the random variables as in Case II and IV. By comparing the results obtained in Case I, II, III, and IV,

Table 3.12: The probabilistic results in Case I, II, III, and IV in Example 2

Failure Mode	Surface	f_s	p_f (Iterative Steps)			
			Case I	Case II	Case III	Case IV
Internal	Det.	1.225	0.441% (309)	0.135% (307)	0.432% (309)	0.139% (307)
	Pro.	1.238	0.658% (312)	0.246% (311)	0.648% (312)	0.252% (311)
Compound	Det.	1.461	0.033% (350)	0.002% (349)	0.033% (350)	0.002% (349)
	Pro.	1.477	0.041% (352)	0.003% (351)	0.041% (352)	0.003% (351)
Deep-Seated	Det.	1.450	0.007% (349)	0.0005% (348)	0.007% (349)	0.0005% (348)
	Pro.					
Sliding	Det.	1.487	1.925% (6)	1.324% (5)	1.925% (6)	1.324% (5)
	Pro.					

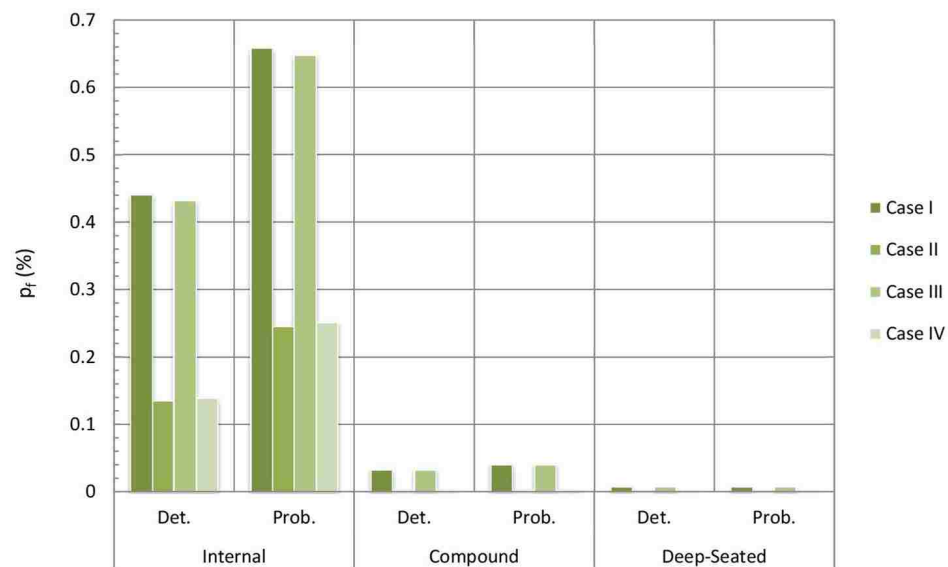


Figure 3.21: The comparison of the probabilistic results in Case I to IV in Example 2

the distribution selection regarding the friction angle is found having a greater impact on the probabilistic results rather than the unit weight. The critical sliding failure surfaces are addressed with the highest probability of failure; thereby, the sliding failure is supposed to have the most significant contribution to the system probability of failure, which can be further demonstrated in Section 3.5.2.2.3.

3.5.2.2.2. Correlated random variables. When the random variables are correlated, the probabilistic results are shown in Table 3.13 and 3.14; and the comparison are demonstrated in Figure 3.22 and 3.23, with the correlation coefficients assigned to both foundation soil and embankment fill changing from 0.1 to 0.9 simultaneously. Significant reduction is found with the increase in the correlation coefficient with respect to the failure modes except for the deep-seated, whose probability of failure is slightly increased but is too small to have affect on the system reliability. Therefore, it can be predicted the system reliability tends to significantly increase when the correlation coefficient is going up.

Table 3.13: The probabilistic results in Case V in Example 2

Failure Mode	Surface	f_s	p_f (Iterative Steps)			
			$\rho_{\phi\gamma} = 0.1$	$\rho_{\phi\gamma} = 0.2$	$\rho_{\phi\gamma} = 0.5$	$\rho_{\phi\gamma} = 0.9$
Internal	Det.	1.225	0.349% (348)	0.268% (328)	0.093% (369)	0.005% (485)
	Pro.	1.238	0.561% (348)	0.471% (326)	0.245% (355)	0.056% (409)
Compound	Det.	1.461	0.032% (351)	0.030% (353)	0.026% (358)	0.019% (366)
	Pro.	1.477	0.038% (354)	0.036% (358)	0.028% (363)	0.018% (369)
Deep-Seated	Det.	1.450	0.0071% (348)	0.0073% (347)	0.0081% (345)	0.0093% (341)
	Pro.	(1.498)			0.0088% (345)	0.0120% (337)
Sliding	Det.	1.487	1.925% (6)			
	Pro.					

For the deep-seated failure, the critical surfaces are located at the same position for the first two cases ($\rho = 0.1$ and 0.2); but separated for the rest of two ($\rho = 0.5$ and 0.9), where the critical probabilistic slip surface has a corresponding factor of safety equal to 1.498.

Table 3.14: The probabilistic results in Case VI in Example 2

Failure Mode	Surface	f_s	p_f (Iterative Steps)			
			$\rho_{\phi\gamma} = 0.1$	$\rho_{\phi\gamma} = 0.2$	$\rho_{\phi\gamma} = 0.5$	$\rho_{\phi\gamma} = 0.9$
Internal	Det.	1.225	0.088% (319)	0.054% (314)	0.006% (391)	0.000% (600)
	Pro.	1.238	0.187% (320)	0.138% (329)	0.042% (367)	0.003% (442)
Compound	Det.	1.461	0.0020% (351)	0.0018% (353)	0.0012% (359)	0.00072% (370)
	Pro.	1.477	0.0024% (354)	0.0020% (357)	0.0013% (361)	0.00073% (370)
Deep-Seated	Det.	1.450	0.00051%	0.00054%	0.00061%	0.00073%
	Pro.		(347)	(346)	(344)	(342)
Sliding	Det.	1.487	1.324% (5)			
	Pro.					

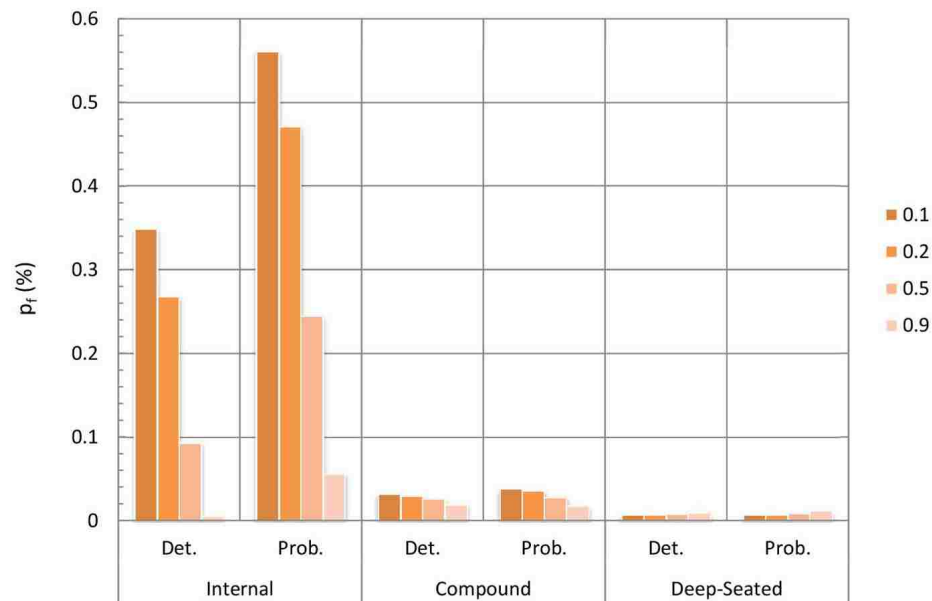


Figure 3.22: The comparison of the probabilistic results in Case V in Example 2

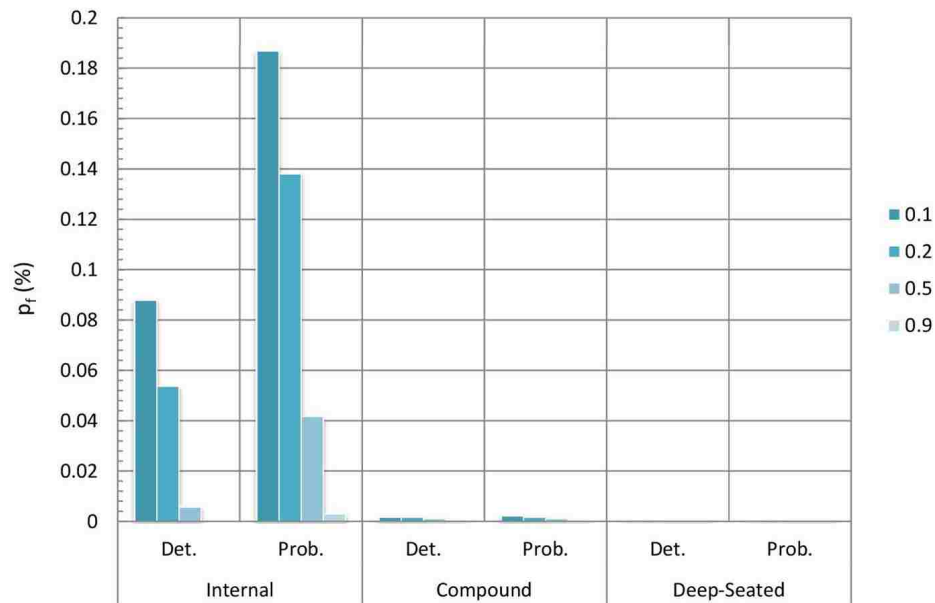


Figure 3.23: The comparison of the probabilistic results in Case VI in Example 2

3.5.2.2.3. System reliability. Based on the probability of failure obtained in different cases, system reliability can be consequently calculated according to Equation 3.28 and 3.29 with respect to the discussed failure modes. The results are accordingly listed in Table 3.15 with the comparison demonstrated in Figure 3.24, 3.25, and 3.26. It can be noticed, in this example, the sliding failure has the greatest contribution to the system probability of failure; while the deep-seated failure has the slightest impact. When comparing the results obtained in Case I to IV, by changing the distribution models assigned to the random variables from normal to log-normal, great reduction can be found in the system probability of failure; thereby, the system reliability is increased. From Case V and VI, it can be concluded, with the increase in the correlation coefficient between the friction angle and the soil unit weight, the system probability of failure is decreased while the system reliability is increased.

Table 3.15: The system reliability in Example 2

Case	Internal	Compound	Deep-Seated	Sliding	p_{fs} (%)	R_s (%)	
I	16.37	1.18	0.20	25.03	38.17	61.83	
II	3.92	0.07	0.01	14.26	17.69	82.31	
III	16.11	1.18	0.20	25.03	37.97	62.03	
IV	4.02	0.07	0.01	14.26	17.78	82.22	
V	0.1	13.56	1.15	0.21	25.03	36.07	63.93
	0.2	11.01	1.11	0.22		34.17	65.83
	0.5	5.13	1.01	0.25		29.77	70.23
	0.9	1.11	0.88	0.29		26.73	73.27
VI	0.1	2.77	0.07	0.01	14.26	16.70	83.30
	0.2	1.88	0.07	0.01		15.94	84.06
	0.5	0.44	0.06	0.01		14.70	85.30
	0.9	0.020	0.05	0.02		14.33	85.67

3.5.3. Discussion. From the above two examples, an observation can be concluded that, in each failure mode, a lower factor of safety always comes along with a higher probability of failure, since both of them intend to evaluate slope stability by sharing the same equilibrium mechanism. However, the factor of safety computed through the traditional deterministic analysis is always unable to consistently measure the risk associated with the uncertainties in soil properties. Thereby, it may happen the slip surface with the minimum factor of safety fails to be the one with the maximum probability of failure. As presented by Li and Lumb (1987), it is observed in an unreinforced, homogeneous slope, critical deterministic and probabilistic slip surfaces are located very close; therefore, to improve searching efficiency, the critical deterministic slip surface is suggested to be the

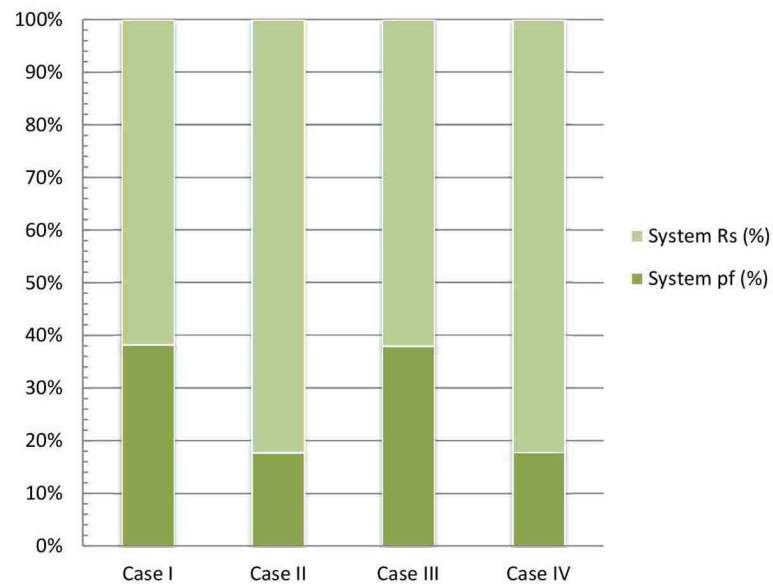


Figure 3.24: The system reliability in Case I to IV in Example 2

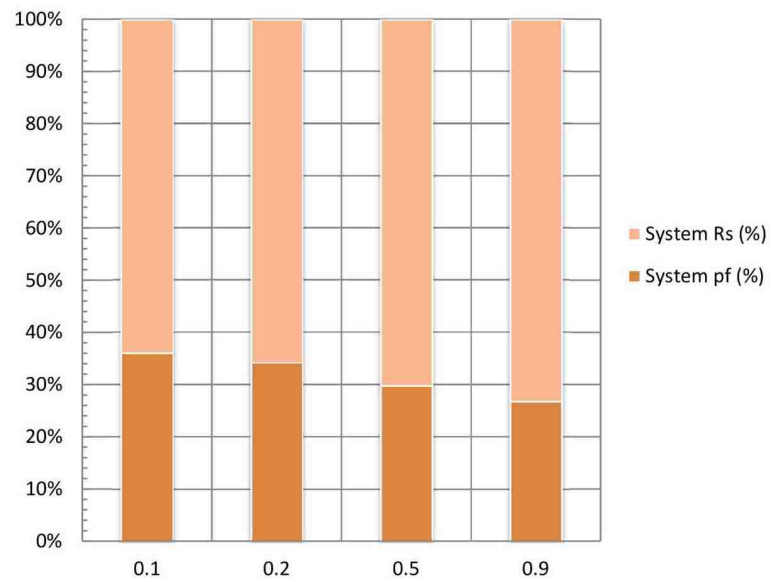


Figure 3.25: The system reliability in Case V in Example 2

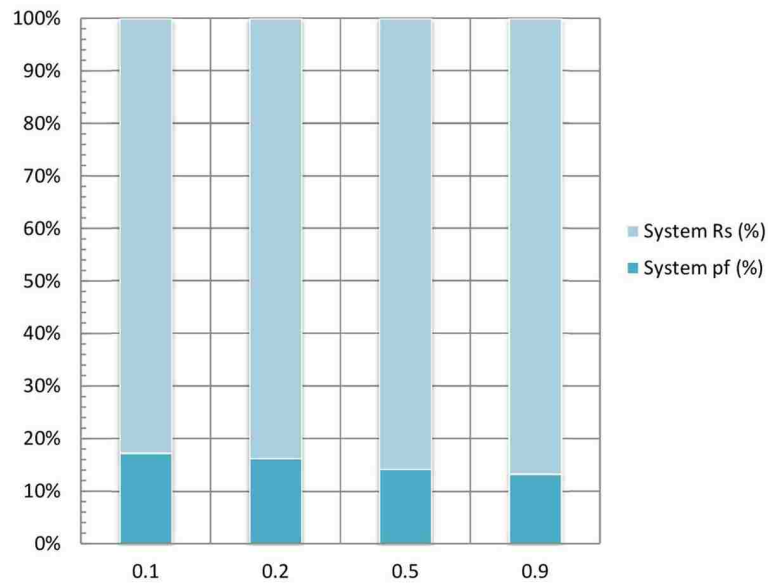


Figure 3.26: The system reliability in Case VI in Example 2

starting location in searching for the critical probabilistic slip surface. From the examples presented in this study, this observation seems applicable in most of the situations but with an exception for the critical internal failure surfaces. In the above two examples, the critical probabilistic internal failure surface is always situated deeper in the slope compared to the deterministic surface. Therefore, the pullout behavior should be examined along both of the two critical surfaces; and the pullout factors of safety corresponding to the probabilistic surface are always lower than the ones obtained along the deterministic surface in view of the embedded lengths behind the critical surfaces. In example 1, the pullout failure can hardly occur along the critical deterministic internal failure surface; but is most likely to appear along the top four reinforcement layers corresponding to the critical probabilistic internal failure surface. In other words, it is indicated the top four reinforcement layers need be extended into a deeper position in the slope to prevent the pullout failure. Therefore, in a GRES system, since the slope stability regarding internal and compound failure

is highly influenced by the reinforcements configuration and their engineering properties, it is more reasonable to do the simultaneous search. That has the probabilistic analysis performed along with the traditional deterministic analysis, to locate the critical slip surfaces with respect to the above two failure modes. The suggestion that presented by Li and Lumb (1987) may be more appropriate in searching for the critical surfaces regarding the deep-seated failure mode.

With the different failure mechanism involved in the slope stability analysis, the formation of the limit state function varies. Therefore, a design with a relatively large factor of safety can probably come along with a high probability of failure. As in example 2, when comparing the factors of safety obtained in various failure modes, the critical sliding failure surface is found with the highest factor of safety, which, in the traditional deterministic analysis, indicates it is supposed to be the safest compared to the critical surfaces in other failure modes. However, through the probabilistic slope stability analysis, the total probability of failure regarding the sliding failure is much greater than the others, which indicates the sliding failure is the most probable failure mode that can potentially occur in such a slope. As a summary, only considering the factor of safety, it is unable to conclude a thorough evaluation regarding the system reliability . On the other hand, in view of the probabilistic approaches employed in this study, MPP-based FORM is proved successfully convergent along every potential slip surface that has been searched in the examples with the iterative steps that are about 300 - 400 in most of the situations. And it seems much more efficient compared to MCS that always asks for much larger amount of samples especially when the probability of failure is low.

System reliability is highly depending on the probability of failure along every potential slip surface. In view of the discussed failure modes, the system reliability is

obtained as 38.46% in example 1 and 61.83% in example 2 with uncorrelated and normally distributed random variables. If we take a look at the results obtained in example 1, there is more than 60% chances the reinforced slope can fail. The system probability of failure is extremely high and unacceptable. Through the traditional deterministic analysis, the minimum factors of safety are obtained as 1.188 and 1.213 with respect to internal and compound failure. It indicates the design doesn't meet the requirements that ask for a factor of safety no less than 1.3; but fails to tell how probable the failure can occur. Through the proposed probabilistic slope stability analysis, the probability of failure is estimated along each potential slip surface. Though it is not a big number, with a series of potential slip surfaces having the probabilistic results at the same level, the total probability of failure regarding the specified failure mode can be huge. For instance, as the compound failure in example 1, the maximum probability of failure is 1.312%; but the total probability of failure is obtained as 44.30% in the case that all random variables are uncorrelated and normally distributed. When the random variables are all assumed in log-normal distribution, the system reliability is significantly increased from 38.46% to 74.47% with the probability of failure along each potential slip surface highly decreased. It indicates the system reliability is very sensitive to the distribution selection regarding the involved random variables. Similar conclusions can be made from example 2, where the primary contributor to the system probability of failure is the sliding failure that has the total probability of failure equal to 25.03% (Case I, III, and V) and 14.26% (Case II, IV, and VI). The system reliability is increased from 61.83% to 82.31% with the log-normal distribution assigned to the random variables as a substitution.

The correlation coefficient between friction angle and unit weight seems have a negative impact on the probability of failure in internal, compound, and sliding failure. As

for the deep-seated failure, the probability of failure is slightly increased when the correlation coefficient goes up. However, as illustrated in the above two numerical examples, the probability of failure regarding the deep-seated failure is much less than the probabilistic results obtained in most of the other failure modes. Therefore, for the entire slope system, a significant reduction is supposed to occur in the probability of failure with the increase in the correlation coefficient between friction angle and unit weight. As discussed in Section 3.2.3, friction angle and unit weight are most likely in a positive correlated relationship; therefore, with an assumption that friction angle and unit weight are uncorrelated, a relatively higher probability of failure is supposed to be derived, based on which a conservative design is to be carried out. From Figure 3.12 and 3.21, it can be found a relatively greater impact on the probabilistic results due to the distribution selection regarding the friction angle rather than the unit weight. In other words, the slope reliability is more sensitive to the probabilistic properties of the friction angle instead of the unit weight. To deeply dig into how sensitive the system reliability is to the involved random variables, sensitivity analysis is to be carried out in the following Section 4 based on the results obtained in this section.

3.6. SUMMARY

In general, probabilistic slope stability analysis can tell us how probable the slope can fail associated with the uncertainties in soil properties. Furthermore, unlike the traditional deterministic slope stability analysis that can only provide the factor of safety individually regarding the potential failure modes that may potentially occur in a geosynthetic reinforced embankment slope, the proposed probabilistic slope stability algorithm is able to estimate the reliability corresponding to the entire system, which is more thor-

oroughly evaluating the safety of the GRES. As illustrated in the numerical examples that are performed in Section 3.5, system reliability seems highly sensitive to the distribution models as well as the correlation coefficients assigned to the involved random variables. Therefore, statistical inference can be a critical step: a better estimation of probabilistic properties of random variables can consequently provide more reliable probabilistic results in the following analysis. However, if there are not enough data available for statistical inference, assumptions have to be made based on some published works and engineering judgment. Therefore, for a more reliable reliability-based design, sensitivity analysis needs to be carried out to tell how much impact those assumptions can have on the probabilistic performance.

4. RELIABILITY-BASED SENSITIVITY ANALYSIS

4.1. OVERVIEW

Sensitivity analysis is an important procedure in engineering design that obtains valuable information about the model behavior, thus provides guidance to the following design process (Liu et al. 2004). For the design with uncertainty (reliability-based design), sensitivity analysis is carried out along with the probabilistic analysis to interpret the relationship between the system reliability and the probabilistic behavior of the involved random variables. In other words, it is to identify the significance that each random variable can contribute to the system reliability; and is consequently called reliability-based (probabilistic) sensitivity analysis (PSA). Three popular methods for conducting the PSA are briefly summarized in Section 4.2, where the MPP-based PSA is further discussed as the method employed in this study. Its practical application in design and analysis of geosynthetic reinforced embankment slopes (GRES) is discussed in Section 4.3, based on which two numerical examples are carried out in Section 4.4 to demonstrate how the proposed MPP-based PSA is working with the probabilistic slope stability analysis.

4.2. PROBABILISTIC SENSITIVITY ANALYSIS ALGORITHM

The basic idea of the probabilistic sensitivity analysis is to evaluate how much influence the probabilistic behavior of the random variable tends to have on the system reliability. In other words, the influence can be directly observed by comparing the results of the probabilistic analysis with different values assigned to the random variables. Therefore, there is a conventional way to conduct the sensitivity analysis, that is, to repeat the probabilistic analysis by changing the probabilistic properties of the random variables and concludes a trend eventually to represent the impacts. This method is very straight-

forward, easy to use; and has been employed in some geotechnical commercial software, such as Slope/W and Slide, along with the deterministic slope stability analysis to examine the effects of those design variables on the factor of safety. When embedded in the probabilistic slope stability analysis, this method becomes very time consuming and inefficient, because: 1) the computational cost is always proportional to the probabilistic dimension (for example, if there are n random variables involved in total, the probabilistic analysis has to be recalled at least $2n(n - 1)$ times to get the trends for all the random variables); and 2) iterative scheme is always embedded in the probabilistic slope stability analysis to locate the critical slip surfaces and estimate the system reliability, especially when the number of random variables is large.

Therefore, three popular alternative categories of PSA techniques are available: 1) variance-based method; 2) probability-based method; and 3) Kullback-Leibler (K-L) entropy-based method.

4.2.1. Methods of PSA. Variance-based method for PSA is based on the decomposition of the variance of a response to its variation sources, that requires two sets of Monte Carlo sampling to estimate the main and total effects of all the random variables (Liu et al. 2004; Jacques et al. 2006; Guo and Du 2009). K-L entropy-based method is developed based on Kullback-Leiber entropy (Kullback and Leibler 1951). Its computational cost is mainly spent on the estimation of two involved joint probability density functions by sampling-based methods, e.g., Monte Carlo simulation (MCS) or Kernel density estimation (KDE) (Martinez and Martinez 2002), as well as the numerical integration on the above density functions. Probability-based method defines a sensitivity measurement as the rate of the change in a probability due to the changes in a statistical parameter of a random input (Melchers 1999; Guo and Du 2009; Deng and Luna 2013). When it is devel-

oped based on the concept of the most probable point (MPP) of failure, the probabilistic information obtained from the MPP-based probabilistic approaches can be directly used to determine the sensitivity measurement so that no additional computational efforts are needed.

It is obvious the last approach is most efficient if the system reliability is evaluated by the MPP-based probabilistic method. Therefore, in view of the computational efficiency, probabilistic-based PSA is selected to be the method used in this study, along with the proposed probabilistic slope stability analysis as demonstrated in Section 3 which is mainly performed by MPP-based first-order reliability method (FORM).

4.2.2. MPP-Based PSA. As introduced above, MPP-based PSA is conducted based on MPP-based FORM to quantify the impact of the uncertainty in each involved random variable on the uncertainty in model output, typically described by the probability of failure (p_f). It is introduced a sensitivity measurement that is defined as the rate of the change in the probability of failure due to the change in a distribution parameter of a random variable as (Melchers 1999; Guo and Du 2009; Deng and Luna 2013)

$$s_p = \frac{\partial p_f}{\partial p} \quad (4.1)$$

where s_p is the sensitivity measurement with respect to the distribution parameter p of the random variable X . From Equation 2.12, Equation 4.1 can be rewritten as

$$s_p = -\phi(-\beta) \frac{\partial \beta}{\partial p} \quad (4.2)$$

where β is the reliability index that can be determined through the MPP-based FORM as discussed in Section 3.3. Considering a set of random variables, $\mathbf{x} = \{x_1, x_2, \dots, x_n\}$, since the reliability index is considered as the distance between the MPP and the original point, it can be computed by

$$\beta = \sqrt{\sum_{k=1}^n (u_k^*)^2} \quad (4.3)$$

where u_k^* is an element in the set of the MPP outputs, $\mathbf{u}^* = \{u_1^*, u_2^*, \dots, u_n^*\}$, in the standard normal space. Then the partial derivative of the reliability index with respect to a specified distribution parameter can be derived as

$$\frac{\partial \beta}{\partial p_j} = \sum_{i=1}^n \frac{\partial \beta}{\partial u_i^*} \frac{\partial u_i^*}{\partial p_j} \quad (4.4)$$

wherein, since the elements in $\{\mathbf{u}^*\}$ are all independent, we have

$$\frac{\partial \beta}{\partial u_i^*} = \frac{\partial}{\partial u_i^*} \left(\sqrt{\sum_{k=1}^n (u_k^*)^2} \right) = \frac{u_i^*}{\beta} \quad (4.5)$$

and Equation 4.4 accordingly becomes

$$\frac{\partial \beta}{\partial p_j} = \frac{1}{\beta} \sum_{i=1}^n u_i^* \frac{\partial u_i^*}{\partial p_j} \quad (4.6)$$

Consequently, for the j th random variable, provided that $\{\mathbf{u}^*\}$ has been determined from the previous MPP-based probabilistic analysis, the sensitivity measurement can be computed by

$$s_{p_j} = -\phi(-\beta) \frac{1}{\beta} \sum_{i=1}^n u_i^* \frac{\partial u_i^*}{\partial p_j} \quad (4.7)$$

once the partial derivative of u_i^* with respect to the specified distribution parameter p_j is derived as discussed in the following sections.

4.2.2.1. Uncorrelated random variables. If the random variables are uncorrelated or independent, Equation 4.7 can be simplified as

$$\frac{\partial \beta}{\partial p_j} = -\phi(-\beta) \frac{u_j^*}{\beta} \frac{\partial u_j^*}{\partial p_j} \quad (4.8)$$

since for $i \neq j$,

$$\frac{\partial u_i^*}{\partial p_j} = 0 \quad (4.9)$$

Otherwise, according to the variable transformation as demonstrated in Section 3.3.1.1 and A.1,

$$u_j^* = \Phi^{-1} [F_j(x_j^*)] \quad (4.10)$$

where x_j^* is the element in the set of MPP outputs, $\mathbf{x}^* = \{x_1^*, x_2^*, \dots, x_n^*\}$, in their original space. For normal distribution, from Equation A.2 and 4.8, the sensitivity measurements with respect to the mean (μ_j) and the standard deviation (σ_j) of the j th random variable are given by (Melchers 1999; Guo and Du 2009)

$$s_{\mu_j} = \phi(-\beta) \frac{u_j^*}{\beta \sigma_j} \quad (4.11)$$

$$s_{\sigma_j} = \phi(-\beta) \frac{(u_j^*)^2}{\beta \sigma_j} \quad (4.12)$$

For log-normal distribution, from Equation A.3, the partial derivatives can be derived as

$$\frac{\partial u_j^*}{\partial \mu_{x_j}} = \frac{1}{\mu_{x_j} \sigma_{\ln x_j}} \left[\frac{\sigma_{x_j}^2}{\mu_{x_j}^2 + \sigma_{x_j}^2} \left(\frac{u_j^*}{\sigma_{\ln x_j}} - 1 \right) - 1 \right] \quad (4.13)$$

$$\frac{\partial u_j^*}{\partial \sigma_{x_j}} = \frac{\sigma_{x_j}}{(\mu_{x_j}^2 + \sigma_{x_j}^2) \sigma_{\ln x_j}} \left[1 - \frac{u_j^*}{\sigma_{\ln x_j}} \right] \quad (4.14)$$

Consequently, the sensitivity measurements can be derived as

$$s_{\mu_j} = -\phi(-\beta) \frac{u_j^*}{\beta} \frac{1}{\mu_{x_j} \sigma_{\ln x_j}} \left[\frac{\sigma_{x_j}^2}{\mu_{x_j}^2 + \sigma_{x_j}^2} \left(\frac{u_j^*}{\sigma_{\ln x_j}} - 1 \right) - 1 \right] \quad (4.15)$$

$$s_{\sigma_j} = -\phi(-\beta) \frac{u_j^*}{\beta} \frac{\sigma_{x_j}}{(\mu_{x_j}^2 + \sigma_{x_j}^2) \sigma_{\ln x_j}} \left[1 - \frac{u_j^*}{\sigma_{\ln x_j}} \right] \quad (4.16)$$

where $\mu_{\ln x_j}$ and $\sigma_{\ln x_j}$ can be computed from Equation A.4 and A.5.

4.2.2.2. Correlated random variables. If the random variables are correlated, for normal distribution, according to the variable transformation as demonstrated in Section 3.3.1.1 and A.2, we have

$$\{\mathbf{u}^*\} = \mathbf{L}_{\hat{x}}^{-1} \{\hat{\mathbf{x}}^*\} \quad (4.17)$$

where $\mathbf{L}_{\hat{x}}$ is the lower triangular matrix obtained by Cholesky decomposition (Appendix A.2.2) with respect to $\{\hat{\mathbf{x}}^*\}$, a set of reduced variables at the MPP as given by

$$\hat{x}_i^* = \frac{x_i^* - \mu_{x_i}}{\sigma_{x_i}} \quad (4.18)$$

Since the elements in $\mathbf{L}_{\hat{x}}$ are only related to the correlation coefficient between the random variables, for the j th random variable, the partial derivatives with respect to its mean, standard deviation and correlation coefficient can be derived as

$$\frac{\partial u_i^*}{\partial \mu_{x_j}} = \sum_{k=1}^n \mathbf{L}_{\hat{x}}^{-1}(i, k) \frac{\partial x_k^*}{\partial \mu_{x_j}} = -\frac{1}{\sigma_{x_j}} \mathbf{L}_{\hat{x}}^{-1}(i, j) \quad (4.19)$$

$$\frac{\partial u_i^*}{\partial \sigma_{x_j}} = \sum_{k=1}^n \mathbf{L}_{\hat{x}}^{-1}(i, k) \frac{\partial x_k^*}{\partial \sigma_{x_j}} = -\frac{\hat{x}_j^*}{\sigma_{x_j}} \mathbf{L}_{\hat{x}}^{-1}(i, j) \quad (4.20)$$

$$\frac{\partial u_i^*}{\partial \rho_{jm}} = \sum_{k=1}^n \frac{\partial \mathbf{L}_{\hat{x}}^{-1}(i, k)}{\partial \rho_{jm}} \hat{x}_k^* = \sum_{k=1}^i \frac{\partial \mathbf{L}_{\hat{x}}^{-1}(i, k)}{\partial \rho_{jm}} \hat{x}_k^* \quad (4.21)$$

based on which, from Equation 4.7, the sensitivity measurements can be derived. For log-normal distribution, the reduced variables at the MPP are given by

$$\hat{x}_i^* = \frac{\ln x_i^* - \mu_{\ln x_i}}{\sigma_{\ln x_i}} \quad (4.22)$$

based on which, the partial derivatives with respect to the mean, standard deviation, and correlation coefficient can be derived by

$$\frac{\partial u_i^*}{\partial \mu_{x_j}} = \frac{\partial u_i^*}{\partial \mu_{\ln x_j}} \frac{\partial \mu_{\ln x_j}}{\partial \mu_{x_j}} + \frac{\partial u_i^*}{\partial \sigma_{\ln x_j}} \frac{\partial \sigma_{\ln x_j}}{\partial \mu_{x_j}} + \sum_{\substack{m=1 \\ m \neq j}}^n \frac{\partial u_i^*}{\partial \rho_{\ln jm}} \frac{\partial \rho_{\ln jm}}{\partial \mu_{x_j}} \quad (4.23)$$

$$\frac{\partial u_i^*}{\partial \sigma_{x_j}} = \frac{\partial u_i^*}{\partial \sigma_{\ln x_j}} \frac{\partial \sigma_{\ln x_j}}{\partial \sigma_{x_j}} + \frac{\partial u_i^*}{\partial \sigma_{\ln x_j}} \frac{\partial \sigma_{\ln x_j}}{\partial \sigma_{x_j}} + \sum_{\substack{m=1 \\ m \neq j}}^n \frac{\partial u_i^*}{\partial \rho_{\ln jm}} \frac{\partial \rho_{\ln jm}}{\partial \sigma_{x_j}} \quad (4.24)$$

$$\frac{\partial u_i^*}{\partial \rho_{jm}} = \frac{\partial u_i^*}{\partial \rho_{\ln jm}} \frac{\partial \rho_{\ln jm}}{\partial \rho_{jm}} \quad (4.25)$$

where the partial derivatives in the natural log-scale are given by

$$\frac{\partial u_i^*}{\partial \mu_{\ln x_j}} = \sum_{k=1}^n \mathbf{L}_{\hat{x}}^{-1}(i, k) \frac{\partial x_k^*}{\partial \mu_{\ln x_j}} = -\frac{1}{\sigma_{\ln x_j}} \mathbf{L}_{\hat{x}}^{-1}(i, j) \quad (4.26)$$

$$\frac{\partial u_i^*}{\partial \sigma_{\ln x_j}} = \sum_{k=1}^n \mathbf{L}_{\hat{x}}^{-1}(i, k) \frac{\partial x_k^*}{\partial \sigma_{\ln x_j}} = -\frac{\hat{x}_j^*}{\sigma_{\ln x_j}} \mathbf{L}_{\hat{x}}^{-1}(i, j) \quad (4.27)$$

$$\frac{\partial u_i^*}{\partial \rho_{\ln jm}} = \sum_{k=1}^n \frac{\partial \mathbf{L}_{\hat{x}}^{-1}(i, k)}{\partial \rho_{\ln jm}} \hat{x}_k^* = \sum_{k=1}^i \frac{\partial \mathbf{L}_{\hat{x}}^{-1}(i, k)}{\partial \rho_{\ln jm}} \hat{x}_k^* \quad (4.28)$$

and

$$\frac{\partial \mu_{\ln x_j}}{\partial \mu_{x_j}} = \frac{1}{\mu_{x_j}} \left(1 + \frac{\sigma_{x_j}^2}{\mu_{x_j}^2 + \sigma_{x_j}^2} \right) \quad (4.29)$$

$$\frac{\partial \sigma_{\ln x_j}}{\partial \mu_{x_j}} = - \frac{\sigma_{x_j}^2}{\sigma_{\ln x_j} \mu_{x_j} (\mu_{x_j}^2 + \sigma_{x_j}^2)} \quad (4.30)$$

$$\frac{\partial \rho_{\ln j m}}{\partial \mu_{x_j}} = - \frac{\rho_{j m} \sigma_{x_j} \sigma_{x_m}}{\sigma_{\ln x_j} \sigma_{\ln x_m} \mu_{x_j} (\mu_{x_j} \mu_{x_m} + \rho_{j m} \sigma_{x_j} \sigma_{x_m})} + \frac{\rho_{\ln j m} \sigma_{x_j}}{\sigma_{\ln x_j}^2 \mu_{x_j} (\mu_{x_j}^2 + \sigma_{x_j}^2)} \quad (4.31)$$

$$\frac{\partial \mu_{\ln x_j}}{\partial \sigma_{x_j}} = - \frac{\sigma_{x_j}}{\mu_{x_j}^2 + \sigma_{x_j}^2} \quad (4.32)$$

$$\frac{\partial \sigma_{\ln x_j}}{\partial \sigma_{x_j}} = \frac{\sigma_{x_j}}{\sigma_{\ln x_j} (\mu_{x_j}^2 + \sigma_{x_j}^2)} \quad (4.33)$$

$$\frac{\partial \rho_{\ln j m}}{\partial \sigma_{x_j}} = \frac{\rho_{j m} \sigma_{x_m}}{\sigma_{\ln x_j} \sigma_{\ln x_m} (\mu_{x_j} \mu_{x_m} + \rho_{j m} \sigma_{x_j} \sigma_{x_m})} - \frac{\rho_{\ln j m} \sigma_{x_j}}{\sigma_{\ln x_j}^2 (\mu_{x_j}^2 + \sigma_{x_j}^2)} \quad (4.34)$$

$$\frac{\partial \rho_{\ln j m}}{\partial \rho_{j m}} = \frac{\sigma_{x_j} \sigma_{x_m}}{\sigma_{\ln x_j} \sigma_{\ln x_m} (\mu_{x_j} \mu_{x_m} + \rho_{j m} \sigma_{x_j} \sigma_{x_m})} \quad (4.35)$$

where $\rho_{j m}$ is the correlation coefficient between the j th and the m th random variable; and $\rho_{\ln j m}$ can be calculated from Equation A.11. Consequently, the sensitivity measurements can be derived based on Equation 4.7, and the equations from Equation 4.23 to Equation 4.35.

4.3. PROBABILISTIC SENSITIVITY ANALYSIS IN GRES DESIGN

As stated by Liu et al. (2004), sensitivity analysis can be utilized in both prior-design stage and post-design stage for different purposes. In prior-design stage, PSA is

performed to identify which variable(s) can be safely eliminated without bringing too much influence to the uncertainty in the design so that the number of random variables can be reasonably decreased, and thus computational efficiency can be improved. When in post-design stage, PSA is mainly used to identify the most significant variable(s) that can have the highest contribution(s) to the system reliability, based on which it can be decided what random uncertainties need to be further controlled to gain the largest improvement on the probabilistic performance of the design. In probabilistic slope stability analysis, Mohr-Coulomb (MC) strength parameters and soil unit weights are always considered as the random variables. By performing PSA following the probabilistic analysis, it can be evaluated how significant each random variable does affect the slope reliability. Compared to those manufacturing in the areas of aerospace, electronics and mechanics, it is extremely hard to improve the probabilistic performance of a slope system by controlling the uncertainties in the involved random variables since the slope is primarily consisting of a natural material: soil. Even though the soil can be improved by compaction or other engineering methods, they are aiming at improving its engineering properties (i.e., to enhance soil strength or bearing capacity) instead of the probabilistic performance (i.e., to decrease its variance). Therefore, when carried out along with the probabilistic slope stability analysis, PSA is primarily working for the prior-design stage to determine whether any of those random variables can be eliminated if its influence on the system reliability is really small and can be ignored to consequently increase the computational efficiency. Furthermore, as discussed in Section 3.6, the probabilistic characteristics regarding the soil properties are frequently unavailable, especially in the prior-design stage where the filling material of the embankment slope has not been decided yet. Therefore, assumptions have to be made based on some published works corresponding to the potential embankment

fills. PSA is accordingly needed in order to estimate how those assumptions can influence the probabilistic performance of the GRES structure.

4.4. NUMERICAL EXAMPLE

To demonstrate the application of the proposed sensitivity analysis in estimating how much impact the random variables can have on the probabilistic performance of a GRES system, two numerical examples are carried out in this section following the probabilistic slope stability analyses presented in Section 3.5. The sensitivity results were accordingly obtained corresponding to the critical deterministic and probabilistic slip surfaces as presented in Table 4.1 to 4.4 for Case I to IV in Example 1 with uncorrelated random variables; Table 4.5 to 4.8 for Case V and VI in Example 1 with correlated random variables; and Table 4.9 to 4.11 for Example 2. In those tables, the first value in each cell is the sensitivity measurement corresponding to the deterministic slip surface, while the second value is for the probabilistic slip surface. When two critical surfaces happened to be located at the same position, there is only one value shown in the cell. According to the definition of the sensitivity measurement in Equation 4.1, a positive value indicates the probability of failure tends to increase with the increase in the certain statistical parameter of the random input; vice versa, a negative sensitivity measurement indicates the probability of failure tends to decrease with the increase in the corresponding parameter.

4.4.1. Uncorrelated Random Variables. The sensitivity measurement with respect to the mean of the friction angle ($s_{\mu_{\phi'}}$) is always negative in either foundation soil or embankment fill, indicating that the probability of failure is going down with the increase of the friction angle in internal, compound and deep-seated failure cases. Otherwise, with a positive sensitivity measurement with respect to the mean of the unit weight in the em-

Table 4.1: Sensitivity results in Example 1 (Case I)

Random Variables		Internal		Compound		Deep-Seated	
		s_μ	s_σ	s_μ	s_σ	s_μ	s_σ
Embankment Fill	ϕ'_e	-7.023E-3	1.740E-2	-1.250E-2	2.791E-1	-2.374E-4	3.812E-4
		-1.101E-2	2.520E-2			-2.405E-4	3.022E-4
	γ_e	8.272E-5	9.602E-7	6.022E-5	2.576E-7	2.680E-6	1.932E-8
		5.519E-5	2.518E-7			3.686E-6	2.824E-8
Foundation	ϕ'_f	NA	/	/	/	-4.607E-4	1.370E-3
						-6.138E-4	1.879E-3
	γ_f	/	/	/	/	-2.965E-6	2.139E-8
						-4.078E-6	3.126E-8

Case I: All random variables are uncorrelated and normally distributed.

Table 4.2: Sensitivity results in Example 1 (Case II)

Random Variables		Internal		Compound		Deep-Seated	
		s_μ	s_σ	s_μ	s_σ	s_μ	s_σ
Embankment Fill	ϕ'_e	-4.429E-3	9.056E-3	-9.557E-3	1.771E-2	-6.862E-5	1.064E-4
		-8.107E-3	1.537E-2			-6.690E-5	8.741E-5
	γ_e	5.339E-5	8.097E-7	4.692E-5	2.520E-7	8.075E-7	8.189E-9
		4.145E-5	2.395E-7			1.066E-6	1.176E-8
Foundation	ϕ'_f	/	/	/	/	-1.321E-4	2.983E-4
						-1.686E-4	3.932E-4
	γ_f	/	/	/	/	-8.935E-7	9.051E-9
						-1.180E-6	1.300E-8

Case II: All random variables are uncorrelated and log-normally distributed.

Table 4.3: Sensitivity results in Example 1 (Case III)

Random Variables		Internal		Compound		Deep-Seated	
		s_μ	s_σ	s_μ	s_σ	s_μ	s_σ
Embankment Fill	ϕ'_e	-6.907E-3	1.716E-2	-1.242E-2	2.777E-2	-2.374E-4	3.812E-4
		-1.094E-2	2.507E-2			-2.405E-4	3.022E-4
	γ_e	8.169E-5	9.012E-7	6.008E-5	2.437E-7	2.687E-6	1.833E-8
		5.505E-5	2.382E-7			3.696E-6	2.678E-8
Foundation	ϕ'_f	/	/	/	/	-4.607E-4	1.370E-3
						-6.138E-4	1.879E-3
	γ_f	/	/	/	/	-2.972E-6	2.026E-8
						-4.088E-6	2.960E-8

Case III: All random variables are uncorrelated with ϕ' in normal and γ in log-normal distribution.

Table 4.4: Sensitivity results in Example 1 (Case IV)

Random Variables		Internal		Compound		Deep-Seated	
		s_μ	s_σ	s_μ	s_σ	s_μ	s_σ
Embankment Fill	ϕ'_e	-4.529E-3	9.236E-3	-9.633E-3	1.782E-2	-6.862E-5	1.064E-4
		-8.176E-3	1.549E-2			-6.690E-5	8.741E-5
	γ_e	5.339E-5	8.097E-7	4.710E-5	2.666E-7	8.055E-7	8.632E-9
		4.164E-5	2.536E-7			1.064E-6	1.239E-8
Foundation	ϕ'_f	/	/	/	/	-1.321E-4	2.983E-4
						-1.686E-4	3.932E-3
	γ_f	/	/	/	/	-8.913E-7	9.561E-9
						-1.177E-6	1.373E-8

Case IV: All random variables are uncorrelated with ϕ' in log-normal and γ in normal distribution.

Table 4.5: Sensitivity results in Example 1 (Case V: $\rho = 0.1$)

Random Variables		Internal		Compound		Deep-Seated	
		s_μ	s_σ	s_μ	s_σ	s_μ	s_σ
Embankment Fill	ϕ'_e	-5.905E-3	1.504E-2	-1.182E-2	2.668E-2	-2.517E-4	4.026E-4
		-1.036E-2	2.398E-2			-2.609E-4	3.261E-4
	γ_e	7.158E-5	-1.736E-5	5.831E-5	-1.291E-5	2.850E-6	-4.344E-7
		5.319E-5	-1.207E-5			3.999E-6	-4.696E-7
	$\rho_{\phi\gamma}$	-3.970E-2		-7.07E-2		3.0E-3	
		-6.350E-2				3.0E-3	
Foundation	ϕ'_f	/	/	/	/	-4.872E-4	1.441E-3
		/	/	/	/	-6.639E-4	2.017E-3
	γ_f	/	/	/	/	-3.174E-6	9.612E-7
		/	/	/	/	-4.464E-6	1.390E-6
$\rho_{\phi\gamma}$	/		/		5.60E-3		
					7.20E-3		

Case V: All random variables are correlated and normally distributed.

bankment fill ($s_{\mu\gamma_e}$), the probability of failure tends to go up corresponding to the increase in the unit weight. Therefore, when selecting the fill material for the embankment slope, the one with higher friction angle and lower unit weight is preferred. The sensitivity measurement with respect to the standard deviation (s_σ) of every involved random variable has a positive value. Since the standard deviation is always reflecting the variability of a random variable as discussed in Section 3.2.2, it is reasonable to have such an observation that the probability of failure is increased when the random variable has a larger standard deviation. As illustrated in Example 1 (Figure 3.11), the critical deterministic and probabilistic slip surfaces with respect to both internal and compound failure are located within the embankment slope so that the foundation soil is not affecting the probabilistic perfor-

Table 4.6: Sensitivity results in Example 1 (Case V: $\rho = 0.5$)

Random Variables		Internal		Compound		Deep-Seated	
		s_μ	s_σ	s_μ	s_σ	s_μ	s_σ
Embankment Fill	ϕ'_e	-2.253E-3	6.537E-3	-9.089E-3	2.156E-2	-3.176E-4	5.000E-4
		-7.755E-3	1.890E-2			-3.586E-4	4.384E-4
	γ_e	3.144E-5	-4.523E-5	4.980E-5	-5.886E-5	3.635E-6	-2.844E-6
		4.439E-5	-5.391E-5			5.494E-6	-3.328E-6
	$\rho_{\phi\gamma}$	-1.98E-2		-6.56E-2		3.0E-3	
		-5.75E-2				4.6E-3	
Foundation	ϕ'_f	/	/	/	/	-6.086E-4	1.762E-3
						-9.014E-4	2.656E-3
	γ_f	/	/	/	/	-4.163E-6	6.049E-6
						-6.359E-6	9.405E-6
	$\rho_{\phi\gamma}$	/		/		7.90E-3	
						1.09E-2	

Case V: All random variables are correlated and normally distributed.

mance regarding either of them. Similarly, in Example 2 (Figure 3.20), the foundation soil has no influence on the probabilistic results along the critical internal failure surfaces. But for the critical surfaces regarding compound and deep-seated failure, the unit weight of the foundation soil has a negative impact on their probability of failure ($s_{\mu_f} < 0$), indicating a denser foundation soil tends to provide a more reliable slope system.

As defined in Section 4.2, the sensitivity measurement is the rate of the change in the probability of failure due to the change in a distribution parameter of a random variable. Therefore, the random variable having a sensitivity measurement with larger magnitude is supposed to have a greater impact on the probabilistic performance. For example, when comparing the sensitivity measurements obtained corresponding to friction angle and unit

Table 4.7: Sensitivity results in Example 1 (Case VI: $\rho = 0.1$)

Random Variables		Internal		Compound		Deep-Seated	
		s_μ	s_σ	s_μ	s_σ	s_μ	s_σ
Embankment Fill	ϕ'_e	-3.414E-3	7.180E-3	-8.833E-3	1.655E-2	-7.414E-5	8.766E-5
		-7.423E-3	1.425E-2			-7.510E-5	9.745E-5
	γ_e	4.253E-5	-1.058E-5	4.451E-5	-1.001E-5	1.145E-6	-1.528E-7
		3.902E-5	-9.019E-6			1.199E-6	-1.685E-7
	$\rho_{\phi\gamma}$	-2.07E-2		-4.79E-2		9.0E-4	
		-4.12E-2				9.0E-4	
Foundation	ϕ'_f	/	/	/	/	-1.424E-4	3.203E-4
		/	/	/	/	-1.888E-4	4.374E-4
	γ_f	/	/	/	/	-9.760E-7	3.030E-7
		/	/	/	/	-1.338E-6	4.317E-7
$\rho_{\phi\gamma}$	/		/		1.4E-3		
					1.8E-3		

Case VI: All random variables are correlated and log-normally distributed.

weight, it is obvious no matter what failure mode is considered, friction angle always has a greater impact on the probability of failure in both embankment fill and foundation soil. Such an observation is identical to the conclusion derived in Section 3.5.3 that the distribution model selection corresponding to the friction angle usually has a much more significant influence on the probabilistic results rather than the unit weights. While, on the other hand, in deep-seated failure, in view of a larger magnitude of the sensitivity measurement, foundation soil appears to have a greater impact on the probabilistic performance when compared to the embankment fill.

4.4.2. Correlated Random Variables. The sensitivity measurements corresponding to the correlation coefficients that exist between the random variables are computed

Table 4.8: Sensitivity results in Example 1 (Case VI: $\rho = 0.5$)

Random Variables		Internal		Compound		Deep-Seated	
		s_μ	s_σ	s_μ	s_σ	s_μ	s_σ
Embankment Fill	ϕ'_e	-7.346E-4	1.765E-3	-6.110E-3	1.203E-2	-9.913E-5	1.506E-4
		-4.921E-3	9.942E-3			-1.149E-4	1.452E-4
	γ_e	1.075E-5	-1.554E-5	3.443E-5	-3.980E-5	1.193E-6	-1.029E-6
		2.902E-5	-3.455E-5			1.843E-6	-1.297E-6
	$\rho_{\phi\gamma}$	-5.8E-3		-3.99E-2		1.3E-3	
		-3.3E-2				1.5E-3	
Foundation	ϕ'_f	/	/	/	/	-1.889E-4	4.179E-4
						-2.858E-4	6.459E-4
	γ_f	/	/	/	/	-1.358E-6	1.891E-6
						-2.121E-6	3.027E-6
$\rho_{\phi\gamma}$	/		/		2.2E-3		
					3.1E-3		

Case VI: All random variables are correlated and log-normally distributed.

herein. In both internal and compound failure, negative numbers are obtained that indicate the probability of failure tends to decrease with the increase of the correlation coefficient; and vice versa, a positive sensitivity measurement is derived in the deep-seated failure situation. The results shown here are identical to the observation obtained in Section 3.5 from Figures 3.13, 3.14, 3.22 and 3.23. When a comparison is carried out between the sensitivity measurements obtained with respect to the friction angle, unit weight, and their correlation coefficient, a larger magnitude indicates the correlation coefficient should have a relatively greater influence on the probability of failure, especially than the unit weight can have. However, according to the definition of the sensitivity measurement, it can be interpreted, the probability of failure is supposed to be changed by the amount equal to

Table 4.9: Sensitivity results in Example 2 (Case I)

Random Variables		Internal		Compound		Deep-Seated	
		s_μ	s_σ	s_μ	s_σ	s_μ	s_σ
Embankment Fill	ϕ'_e	-4.186E-3	1.101E-2	-3.952E-4	1.338E-3	-4.954E-5	1.041E-4
		-6.003E-3	1.494E-2	-4.798E-4	1.609E-3		
	γ_e	1.017E-5	1.354E-7	1.300E-7	3.014E-10	5.336E-8	2.517E-10
		1.106E-5	1.056E-7	2.180E-7	6.917E-10		
Foundation	ϕ'_f	/	/	-4.759E-5	1.939E-5	-7.518E-5	2.398E-4
				-1.409E-5	1.388E-6		
	γ_f	/	/	-5.481E-9	5.359E-13	-5.339E-8	2.520E-10
				-1.037E-9	1.564E-14		

Case I: All random variables are uncorrelated and normally distributed.

Table 4.10: Sensitivity results in Example 2 (Case II)

Random Variables		Internal		Compound		Deep-Seated	
		s_μ	s_σ	s_μ	s_σ	s_μ	s_σ
Embankment Fill	ϕ'_e	-1.846E-4	3.800E-3	-4.196E-5	1.107E-4	-5.318E-6	9.702E-6
		-6.062E-4	8.319E-3	-5.287E-5	1.353E-4		
	γ_e	4.665E-6	9.189E-8	1.472E-8	5.803E-11	6.083E-9	4.493E-11
		1.106E-5	1.056E-7	2.569E-8	1.402E-11		
Foundation	ϕ'_f	/	/	-5.302E-6	2.948E-6	-7.992E-6	1.881E-5
				-1.651E-6	2.488E-7		
	γ_f	/	/	-5.99E-10	9.61E-14	-6.088E-9	4.493E-11
				-1.20E-10	3.08E-15		

Case II: All random variables are uncorrelated and log-normally distributed.

the sensitivity measurement when the corresponding probabilistic parameter is increased by 1 unit. Since the correlation coefficient is unable to be greater than 1 or less than -1,

Table 4.11: Sensitivity results in Example 2 (Case V: $\rho = 0.5$)

Random Variables		Internal		Compound		Deep-Seated	
		s_μ	s_σ	s_μ	s_σ	s_μ	s_σ
Embankment Fill	ϕ'_e	-1.006E-3	3.145E-3	-3.069E-4	1.061E-3	-5.790E-5	1.209E-4
		-2.459E-3	6.949E-3	-3.384E-4	1.169E-3		
	γ_e	2.934E-6	-4.544E-6	1.212E-7	-2.093E-7	6.431E-8	-6.688E-8
		5.320E-6	-7.465E-6	1.849E-7	-3.189E-7		
	$\rho_{\phi\gamma}$	-1.08E-2		-4.1E-3		1.1E-3	
		-2.4E-2		-4.2E-3			
Foundation	ϕ'_f	/	/	-3.714E-5	1.555E-5	-8.728E-5	2.751E-4
				-9.997E-6	1.021E-6		
	γ_f	/	/	-4.665E-9	9.767E-10	-6.620E-8	1.046E-7
			-8.041E-10	4.107E-11			
$\rho_{\phi\gamma}$	/		-1.0E-4		1.6E-3		
			-4.2E-3				

Case V: All random variables are correlated and normally distributed.

such a comparison seems not so reasonable. But basically, the sensitivity measurement corresponding to the correlation coefficient provides us valuable information about how it can influence the probabilistic results.

Another significant difference to be mentioned here is the impact from the standard deviation corresponding to the unit weight of the embankment fill, the sensitivity measurement of which is negative along the critical surfaces regarding internal, compound and deep-seated failure modes. In the above discussion about the uncorrelated random variables (see Section 4.4.1), the probability of failure is supposed to increase when the standard deviation increases; in other words, a greater variability is found in soil properties. However, when the friction angle is correlated with the unit weight in the same

soil layer, the change in one can influence the other. More specifically, with a positive correlation coefficient existing between friction angle and unit weight, according to Equation 3.13, the increase in the standard deviation of the unit weight (σ_{γ_e}) tends to result in a reduction in the standard deviation of the friction angle ($\sigma_{\phi'_e}$). Thereby, the probability of failure is supposed to decrease. Since the friction angle always has a greater impact on the probabilistic performance of the slope, although the increase in σ_{γ_e} has a positive impact on the probability of failure, the corresponding increasing magnitude is less than the reduction resulted from the decrease in $\sigma_{\phi'_e}$. Therefore, a negative sensitivity measurement corresponding to the σ_{γ_e} is consequently obtained.

4.5. SUMMARY

The proposed MPP-based probabilistic sensitivity analysis (PSA) provides the information identical to the observations obtained from the numerical examples presented in Section 3.5. Following the preceding probabilistic slope stability analyses that were carried out with the MPP-based FORM, the MPP-based PSA is very efficient and requires no extra iterative calculations. Through performing PSA, the friction angle seems to have a relatively greater impact on the probabilistic performance of a GRES structure rather than the unit weight of foundation soil and embankment fill. However, it may not be a good choice to eliminate the unit weight as a random variable, since the correlation coefficient existing between the friction angle and the unit weight can also have a great influence on the probabilistic results. Though it is hard to improve the probabilistic performance of a GRES structure by controlling the uncertainties in the involved random variables associated with soil properties, the proposed MPP-based PSA enables a better understanding on the probabilistic slope stability analysis. Moreover, it can provide some guidance to the

GRES design by telling how the assumptions made on the probabilistic characteristics of those random variables can finally influence the probabilistic performance in the GRES structure; and will be further discussed in the following Section 5.

5. RELIABILITY-BASED OPTIMIZATION DESIGN

5.1. OVERVIEW

The traditional deterministic design for geosynthetic reinforced embankment slopes (GRES) is always carried out on the basis of the critical deterministic slip surface that is addressed within the original unreinforced slope by performing deterministic slope stability analysis. As discussed in Section 3.6, although the deterministic analysis successfully quantifies the slope stability, it fails to consider the effects from the uncertainties existing in the soil properties and is accordingly unable to ensure a consistent risk level of the slopes with a constant factor of safety. Therefore, when the geotechnical uncertainties are taken into consideration, through conducting the probabilistic slope stability analysis on a GRES structure, it is often to have the critical deterministic and probabilistic slip surfaces located at different positions. Those two critical surfaces are sometimes very close, but there are still chances that they are far away from each other especially under the affects of geosynthetic reinforcements with different loading capacities and distributions. As a result, there is a need for a reliability-based design approach associated with the soil variability involved in the GRES structure.

Reliability-based optimization (RBO) is such a technique that allows determining the best design solution while ensures higher reliability than an acceptable level. When introduced in the design of a GRES structure, it is primarily working on optimizing the usage of the geosynthetic reinforcements with a purpose of reducing the total cost of the embedded reinforcements while the corresponding technical design requirements are satisfied. So basically, the reliability-based optimization regarding the GRES design can be considered as a constrained minimization problem that is subject to some reliability re-

quirements as well as some technical rules. Compared to the traditional optimizing process which is always performed by manually assigning different values to the design variables, the application of the RBO technique can be expected to intensively improve the design efficiency even with larger amount of alternatives taken into consideration. Therefore, in this chapter, the traditional deterministic design procedure is first briefly introduced in Section 5.2, where the corresponding disadvantages are highlighted. The proposed RBO design procedure is accordingly to be carried out and discussed in Section 5.3, wherein the numerical algorithm to be embedded to solve the preceding optimization problem is briefly discussed in Section 5.3.1. In Section 5.3.2 and 5.3.3, it is demonstrated how the RBO is going to be working with the GRES design considering the technical design requirements that are routinely taken into consideration in the traditional deterministic design procedure. Two numerical examples are finally carried out in Section 5.4 to specifically illustrate the application of the RBO in GRES design.

5.2. THE PROBLEMS IN TRADITIONAL DESIGN PROCEDURE

As illustrated in Figure 5.1, it is provided a step-by-step procedure for GRES design. The design principally assumes the slope is to be constructed on a stable foundation; mainly uses the classical rotational, limit equilibrium slope stability method (Elias et al. 2001). Provided it has been established the geometric, loading, and performance requirements as well as the engineering properties of both in-situ soils and embankment fills, the stability regarding the original unreinforced slope is first evaluated using both circular-arc and sliding-wedge methods to determine if the slope needs to be reinforced and the size of the critical zone to be reinforced. The latter one can be roughly enveloped by the surfaces that just meet the required factor of safety as shown in Figure 5.2. Inside the critical

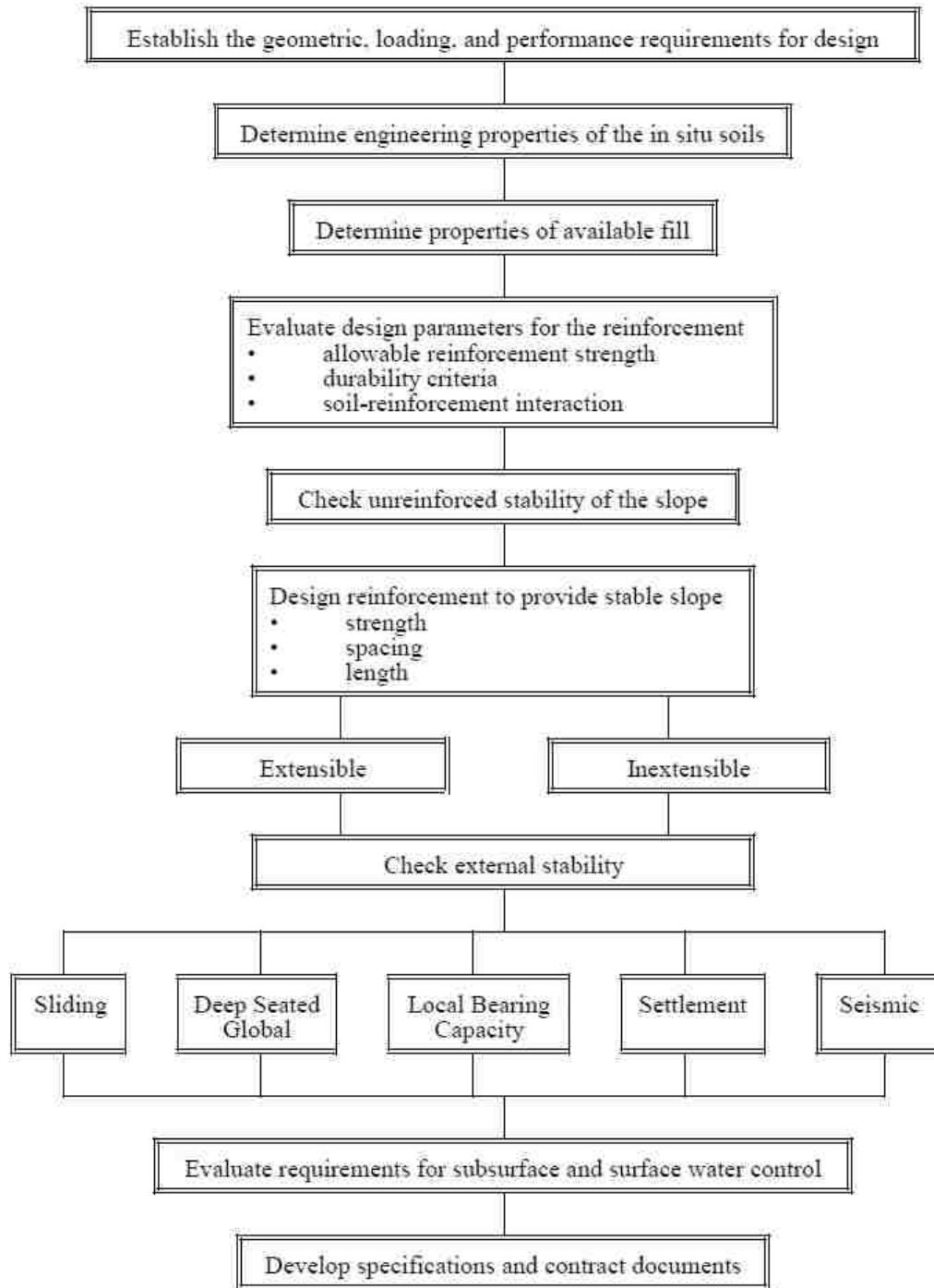


Figure 5.1: Traditional deterministic design procedure (Elias et al. 2001)

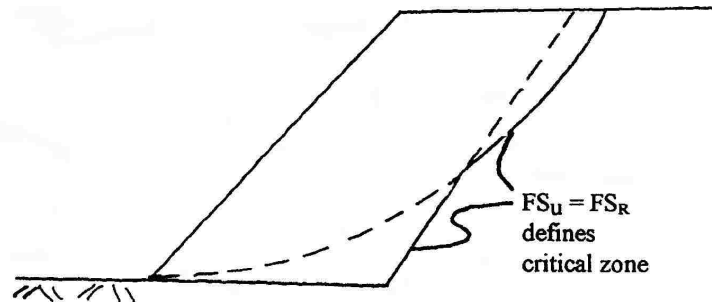


Figure 5.2: Critical zone defined by rotational and sliding surfaces that meet the required factor of safety (Elias et al. 2001)

zone, the total reinforcement tension that needs to be provided by the geosynthetic reinforcements is calculated along each potential failure surface in order to reach the required factor of safety according to Equation 5.1 (Elias et al. 2001),

$$T_s = (FS_R - FS_U) \frac{M_D}{D} \quad (5.1)$$

where T_s is the sum of the required tensile forces per unit width of the reinforcement for all the layers intersecting the failure surface; M_D is the driving moment about the center of the failure circle; D is the moment arm of T_s about the center of the failure circle; FS_R is the required factor of safety; and FS_U is the original unreinforced factor of safety. Among the whole set of T_s obtained corresponding to a series of searching slip surfaces, the largest T_s is considered as the total amount that is to be used to determine the reinforcement strengths, distributions, and required lengths in the GRES design. By comparing Equation 2.10 and 5.1, it is not hard to identify the critical deterministic slip surface is always the surface requiring the largest magnitude of the reinforcement tension (Elias

et al. 2001). Therefore, basically, the reinforcement design in the traditional procedure is mainly developed on the basis of the critical deterministic slip surface addressed within the original unreinforced slope. To be more specific, it is only corresponding to the original critical deterministic surface that such a conventional reinforcement design guarantees the factor of safety above the required level. However, according to the reinforcement design, a new critical surface may be located in the reinforced slope that has a minimum factor of safety lower than the required value. In other words, the critical surface as well as the corresponding minimum factor of safety is supposed to be changing with the reinforcement design. Therefore, if the critical surface is kept updating during the reinforcement design, meanwhile, the minimum factor of safety is strictly controlled above the required level, such a problem can be resolved.

According to the two numerical examples presented in Section 3.5, both of the reinforced slopes are originally designed following the above traditional procedure. It is clearly shown that, when the soil variability is taken into consideration, two critical surfaces are respectively obtained from the traditional deterministic analysis and the proposed probabilistic analysis; and probably located at different positions. In other words, the slip surface with the lowest factor of safety might not be the one with the highest probability of failure; vice versa, the surface with the largest chance to fail may have a factor of safety that is slightly higher than the minimum value. In example 1, along the critical deterministic slip surface, $f_{s, \min} = 1.188$, $p_f = 0.685\%$; along the probabilistic deterministic slip surface, $p_{f, \max} = 1.235\%$, $f_s = 1.214$. In example 2, along the critical deterministic slips surface, $f_{s, \min} = 1.225$, $p_f = 0.441\%$; along the probabilistic deterministic slip surface, $p_{f, \max} = 0.658\%$, $f_s = 1.238$. Therefore, only considering the critical deterministic surface, the traditional procedure can probably lead to a design that fails to meet the requirements

associated with the probability of failure. Furthermore, since the critical probabilistic surface is located deeper than the deterministic one, the required embedment lengths may not be long enough since they are determined on the basis of the deterministic surface. As a result, as shown in Table 3.4, the pullout failure is probably to occur along some reinforcement layers corresponding to the critical probabilistic surface. Therefore, if the design is carried out on the basis of the critical surfaces obtained in both deterministic and probabilistic analyses, such a problem can be resolved.

In general, it rarely has only one unique solution in engineering design. Usually, there could be various design alternatives to meet the same technical design requirements, but the cost involved could be vary significantly. In order to minimize the cost, engineers tend to select an optimal combination of design variables among the considered alternatives. The above traditional procedure is not emphasized on the reinforcement cost but the technical requirements only. Therefore, to search for such an optimal combination, the design procedure needs to be repeated by manually assigning different values to the design variables. But a crucial issue is, when a large number of design variables are involved, meanwhile, not only deterministic but also probabilistic requirements are taken into consideration, the whole design procedure becomes very time consuming; and probably fails to find the 'best' optimal result due to the limited number of alternatives the designers can manually try. As a result, if there is a numerical algorithm that is able to search for the optimal combination that leads to a lowest cost, meanwhile, the technical design requirements are satisfied from both deterministic and probabilistic perspectives, there is no need to manually repeat the design process. And thereby, the preceding problems regarding the design efficiency as well as the optimization accuracy can be resolved. In summary, it is concluded in Table 5.1 that the disadvantages existing in the traditional design procedure

along with how they are supposed to be resolved in the proposed RBO design procedure.

Table 5.1: The disadvantages of traditional design compared to RBO procedure

	Traditional Design Procedure	Proposed RBO Procedure
1	The design is carried out on the basis of a predetermined slip surface that is addressed in the original unreinforced slope so that new critical surface is probably to be located corresponding to the reinforcement design and provides a minimum factor of safety lower than the required level.	The critical surface is to be kept updating during the reinforcement design; meanwhile, the minimum factor of safety is controlled above the required level.
2	Without considering soil variability, the design is carried out on the basis of the critical deterministic slip surface only and probably leads to a design that fails to meet the requirements associated with the probability of failure as well as pullout failure.	The design is to be carried out on the basis of the critical surfaces obtained in both deterministic and probabilistic analyses.
3	The cost issue is not emphasized in the traditional design procedure, so that, to search for an optimal design that has the lowest or a relatively lower cost, the design process needs to be manually repeated based on the considered design alternatives; and thereby, it can be very time consuming and probably fails to locate the 'best' optimal solution.	The optimization design is mathematically concluded as a constrained minimization problem, where the objective function is defined as the total cost regarding the geosynthetic reinforcements; and both deterministic and probabilistic constraints are taken into consideration corresponding to the critical surfaces.

5.3. THE PROPOSED RBO DESIGN PROCEDURE

To solve the problems illustrated in Table 5.1, a more systematic optimization design procedure is proposed. To take the soil variability into consideration, reliability-based optimization, a numerical technique that enables an optimization problem subject to some

probabilistic constraints, is embedded. The algorithm and approaches involved in such a technique are briefly introduced in the following section; and later on, the emphasis is mainly put on the application of the RBO technique in GRES design.

5.3.1. RBO Design Algorithm. To locate the optimal solution while ensure a higher reliability than an acceptable level, a typical RBO problem can be written as

$$\begin{aligned} \min f(\mathbf{d}, \mathbf{X}, \mathbf{P}) \\ \text{sub. to : } P\{g_i(\mathbf{d}, \mathbf{X}, \mathbf{P}) \leq 0\} \leq p_{f_i}, \quad i = 1, 2, \dots, n_c \end{aligned} \quad (5.2)$$

where f is the objective function; \mathbf{d} is the set of deterministic design variables; \mathbf{X} is the set of random design variables; \mathbf{P} is the set of random design parameters; $g(\mathbf{d}, \mathbf{X}, \mathbf{P})$ are the constraint functions; p_f are the desired (target) probabilities of constraint satisfaction; and n_c is the number of probabilistic constraints. The elements in vector \mathbf{d} and \mathbf{X} are the design variables that need to be determined through optimization. To address such a reliability-based constrained optimization problem, double loop strategy is to be implemented herein following the procedure as illustrated in Section 2.5 (Figure 2.6). The probabilistic constraints are evaluated with respect to the specified design variables by performing probabilistic approaches (i.e., FORM or MCS) in the inner loop; and the objective function is optimized subject to the reliability requirements along with some technical design rules in the outer loop. As mentioned in Section 2.5, two branches of optimizing approaches are existing: classical methods, including alternating variable method, simplex method and conjugate-gradient method, are most likely to be used for solving the problems that are not too complicated and have continuous objective function and smooth constraints; how-

ever, in most cases of engineering design, objective function can be complex and not easy defined in view of the various technical design rules that are probably to be involved, meanwhile, the constraints can be non-smooth. Thereby, another branch of methods, the heuristic method, is preferred that includes simulated annealing method, simple harmony search algorithm, tabu search algorithm, anti-colony algorithm, and genetic algorithm which is the one that is to be embedded herein.

Genetic algorithm (GA) is a numerical optimization approach inspired by both natural selection and genetics as well as the evolution of living creatures, in which an optimal solution evolves through a series of generations. Each generation consists of a number of possible selections (or individuals) to the problem, defined by an encoding. The fitness of an individual within the generation is evaluated, and influences the reproduction of the next generation (Coley 1999; Melanie 1999; Cheng and Lau 2008). As concluded by Coley (1999), a typical GA generally consists of the following essential elements: 1) a number or population of guesses of the solution to the problem; 2) a way of calculating how good or bad the individual solutions within the population are; 3) a method for mixing fragments of the better solutions to form new, on average even better solution; and 4) a mutation operator to avoid permanent loss of diversity within the solutions. A general framework regarding the GA process is presented in Figure 5.3, wherein the fitness function $f(x)$ is always identical to the objective function that we are trying to optimize. Accordingly, a global optimum can be located by performing the genetic algorithm provided the problem as expressed in Equation 5.2 is well defined, which is to be further discussed associated with the GRES design in next section.

5.3.2. RBO Design in GRES Application In the optimization design of a GRES structure, provided embankment material and backfill have been selected, it is the pri-

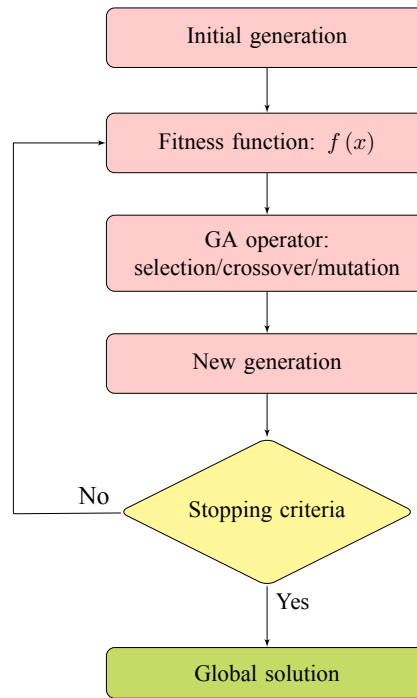


Figure 5.3: Genetic algorithm general framework, adapted from (Coley 1999; Melanie 1999)

primary task to determine the required tensile strength and the distribution of geosynthetic reinforcements with an intention to meet the technical design requirements from both deterministic and probabilistic perspectives while the reinforcement cost is relatively low. Therefore, the objective function is reasonably defined as the total cost with respect to the geosynthetic reinforcements that are to be installed in the slope. Considering the multiple failure modes that may potentially appear in a GRES system as discussed in Section 3.4.1, the problem of optimizing the geosynthetic reinforcement design in a GRES system can be expressed as

$$\min f(\mathbf{d}, \mathbf{X}, \mathbf{P}) = \text{Cost} \quad (5.3a)$$

$$\text{sub. to: } f_{s, \min} \geq f_{s, \text{req}} \quad (5.3b)$$

$$R_{\text{system}} \geq R_{\text{system, req}} \quad (5.3c)$$

$$P \{g_{\text{internal}}(\mathbf{d}, \mathbf{X}, \mathbf{P}) \leq 0\} \leq p_{f_{\text{internal}}} \quad (5.3d)$$

$$P \{g_{\text{compound}}(\mathbf{d}, \mathbf{X}, \mathbf{P}) \leq 0\} \leq p_{f_{\text{compound}}} \quad (5.3e)$$

$$P \{g_{\text{deep}}(\mathbf{d}, \mathbf{X}, \mathbf{P}) \leq 0\} \leq p_{f_{\text{deep}}} \quad (5.3f)$$

$$P \{g_{\text{sliding}}(\mathbf{d}, \mathbf{X}, \mathbf{P}) \leq 0\} \leq p_{f_{\text{sliding}}} \quad (5.3g)$$

$$T_{a(i)} \in [T_{l(i)}, T_{r(i)}] \text{ for } i = 1, 2, \dots, n \in [n_l, n_u]$$

where the deterministic design variables, $\mathbf{d} = \{n, \mathbf{T}_a\}$, consisting of $(n + 1)$ elements with $\{\mathbf{T}_a\}$ representing the allowable tensile strengths of the geosynthetic reinforcements, while, n , as the number of geosynthetic layers, should be a positive integer and bounded within a given range; the random design parameters, $\mathbf{P} = \{\mathbf{c}', \phi', \gamma'\}$, are same with the random variables considered in the previous probabilistic slope stability analysis as demonstrated in Section 3; and the random design variables, \mathbf{X} , are not taken into consideration since the engineering properties of the geosynthetic reinforcements are not considered as the random variables herein. The optimization should yield to both deterministic and probabilistic constraints, including: the minimum factor of safety, $f_{s, \min}$, as constrained in Equation 5.3b should not be lower than the required factor of safety, $f_{s, \text{req}}$; the system reliability, R_{system} , as constrained in Equation 5.3c should not be lower than the required (acceptable) level, $R_{\text{system, req}}$; and the total probability of failure with respect to each involved potential failure mode, as constrained from Equation 5.3d to 5.3g, should be no greater than the desired (target) probabilities of constraint satisfaction, $p_{f_{\text{internal}}}$, $p_{f_{\text{compound}}}$, $p_{f_{\text{deep}}}$, and $p_{f_{\text{sliding}}}$, respectively regarding internal, compound, deep-seated, and sliding fail-

ure modes. To specifically define the objective functions and the constraints regarding the optimization design of a GRES system, more details are to be discussed in the following sections with the consideration of the technical design recommendations used in the traditional design procedure as stated in FHWA Mechanically Stabilized Earth Walls and Reinforced Soil Slopes Design & Construction Guidelines (Elias et al. 2001).

5.3.2.1. Objective functions. As previously mentioned, it is primarily to reduce the total cost of the geosynthetic reinforcements in the proposed reliability-based optimization design of a GRES system. Except for the installation costs, equipment and labor resources, the objective function must be highly depending on two essential factors: the usage and the unit price of the geosynthetic products that are to be used as the reinforcements in the slope system. As introduced in Section 1.1.2, in a GRES system, geosynthetic products are mainly used as: 1) the primary reinforcements, that are horizontally placed within the slope to provide tensile forces to resist slope instability; either geotextiles or geogrids with sufficient strength and soil compatible modulus can be used as the primary reinforcements; and 2) the secondary reinforcements, that are used to locally stabilize the slope face during and after slope construction, generally not taken into consideration in the global slope stability analysis. Therefore, the total cost of the geosynthetic reinforcements in this study is primarily referring to the products cost that should consist of the above two elements in both.

5.3.2.1.1. Usage of geosynthetic reinforcements. For lower slopes with height no larger than 6 m (or 20 ft), a uniform reinforcement distribution is acceptable; but for higher slopes with the total height larger than 6 m (or 20 ft), the slope should be divided into two (top and bottom) or three (top, middle, and bottom) reinforcement zones with equal height (Elias et al. 2001). The deeper the position, the higher the reinforcement strength

should be assigned and the closer the reinforcement layers should be placed as shown in Figure 5.4. Therefore, in the second case, the bounds corresponding to the allowable tensile strength and the number of reinforcement layers should be separately assigned with respect to each reinforcement zone when defining the problem stated in Equation 5.3.

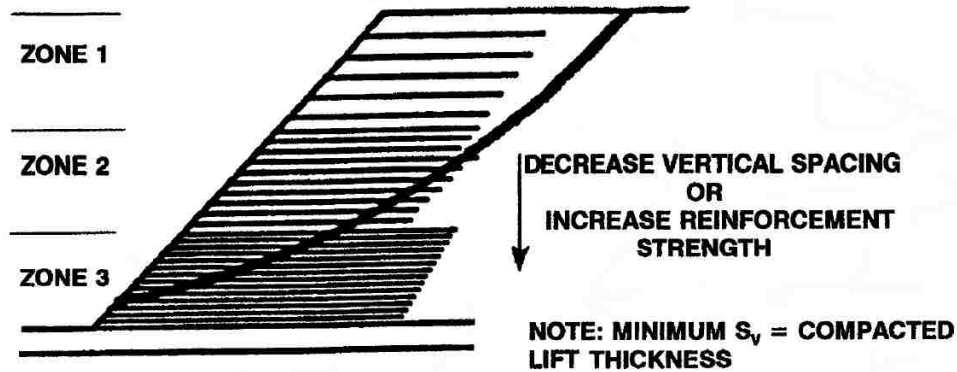


Figure 5.4: Spacing versus reinforcement strength, adapted from Elias et al. (2001)

- Primary reinforcements. Corresponding to a specified GRES cross section with unit width, the usage of the primary geosynthetic reinforcements can be basically calculated by summing the length of each reinforcement layer as

$$L_{\text{primary}} = \sum_{i=1}^{n_p} [L_{e(i)} + L_{\text{slip}(i)}] \quad (5.4)$$

where L_e is the embedment length of the portion anchored behind the slip surface; and L_{slip} is the length of the portion within the slip body. It is obvious the geosynthetic reinforcement length is highly depending on the size of the critical zone and the position of the slip surface that is selected to be the one based on which the reinforcement design is carried out. As

previously mentioned in Section 5.2, the size of the critical zone is generally determined by safety mapping (Leshchinsky et al. 1995; Elias et al. 2001; Leshchinsky et al. 2014), that has the limits of the critical zone roughly enveloped by the surfaces that just meet the required factor of safety. As shown in Figure 5.5, the length required for sliding stability at the base of the embankment generally controls the length of the lower reinforcement levels so that the lower layers must extend at least to the limits of the critical zone. The upper levels of reinforcements may not be required to extend to the limits of the critical zone provided sufficient reinforcements exist in the lower levels to provide the FS_R for all the circles within the critical zone as shown in Figure 5.5; otherwise, it should extend to the

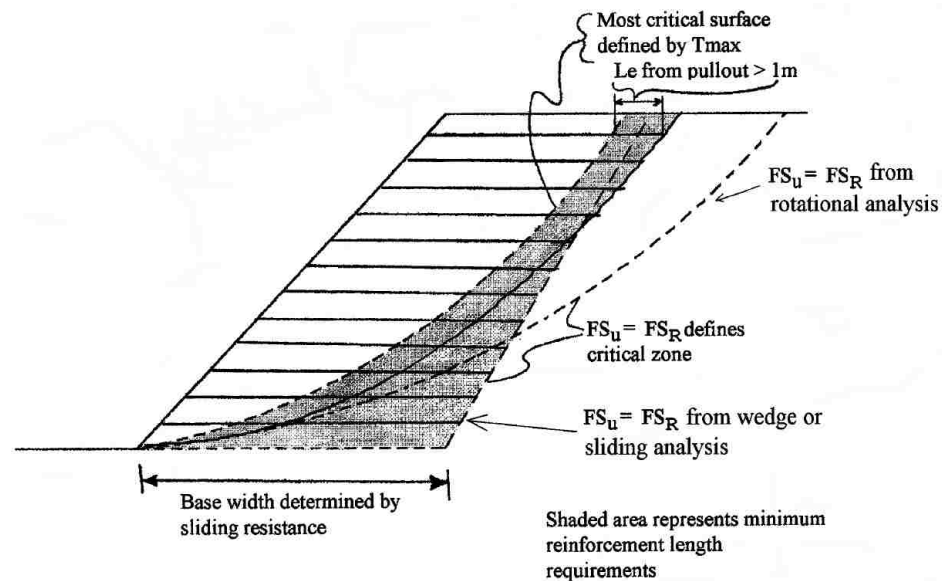


Figure 5.5: Developing reinforcement lengths, adapted from Elias et al. (2001)

limits of the critical zone as well. From the numerical examples presented in Section 3.5, it is shown the critical deterministic and probabilistic slip surfaces can be possibly located at different positions; and the probabilistic surface is observed always situated deeper in the

slope. Therefore, as previously discussed in Section 5.2 and concluded in Table 5.1, both of the two critical surfaces should be taken into consideration in calculating the reinforcement lengths.

In summary, modified from the traditional design procedure proposed by Elias et al. (2001), the length of the primary geosynthetic reinforcements can be determined through the following steps: 1) perform both deterministic and probabilistic slope stability analyses on the original unreinforced slope to locate critical deterministic and probabilistic slip surfaces as well as the target rotational slip surface with FS_R ; the length of the portion within the slip body (L_{slip}) along each reinforcement can be accordingly obtained corresponding to the specified critical surface; 2) compute the required embedment length L_e against the pullout behavior by Equation 3.35 for each reinforcement layer along the specified critical surface; and the L_e should be no less than 1-m (or 3.3-ft) long; 3) compute $L'_p = L_e + L_{slip}$ for each reinforcement layer; 4) perform sliding analysis on the original unreinforced slope to determine the wedge-shaped sliding surface with FS_R ; 5) determine the critical zone by taking the envelop of the wedge-shaped sliding surface and the target rotational slip surface; 6) if the back-surface of the critical zone is located behind the reinforcement with the length of L'_p , the reinforcement should extend to the limits of the critical zone with a larger reinforcement length (L_p); otherwise, $L_p = L'_p$; and 7) finally, the usage of the primary geosynthetic reinforcements can be computed through Equation 5.4.

- Secondary reinforcements. If the spacing between two primary reinforcements is over 800 mm (or 32 inches), secondary reinforcements should be placed between two neighbored primary reinforcement layers with a length typically ranging from 1.2 to 2 m (or 4 to 6.5 ft) to maintain a maximum vertical spacing of 400 mm (or 16 inches) and locally stabilize the slope face. In summary, the total usage of the secondary geosynthetic rein-

forcements can be computed based on the length of each layer placed within the reinforced slope as

$$L_{\text{secondary}} = \sum_{j=1}^{n_s} L_{s(j)} \quad (5.5)$$

where L_s is the length of secondary reinforcement in each layer, and typically set between 1.2 and 2 m (or 4 to 6.5 ft).

- Face wrapping. As recommended by Elias et al. (2001), for the slopes flatter than 1H:1V, closer spaced reinforcements (i.e., every lift or every other lift, but no greater than 400 mm) preclude having to wrap the face in well graded soils. But for steeper slopes and uniformly graded soils, wrapped faces are required to prevent face sloughing as shown in Figure 5.6.

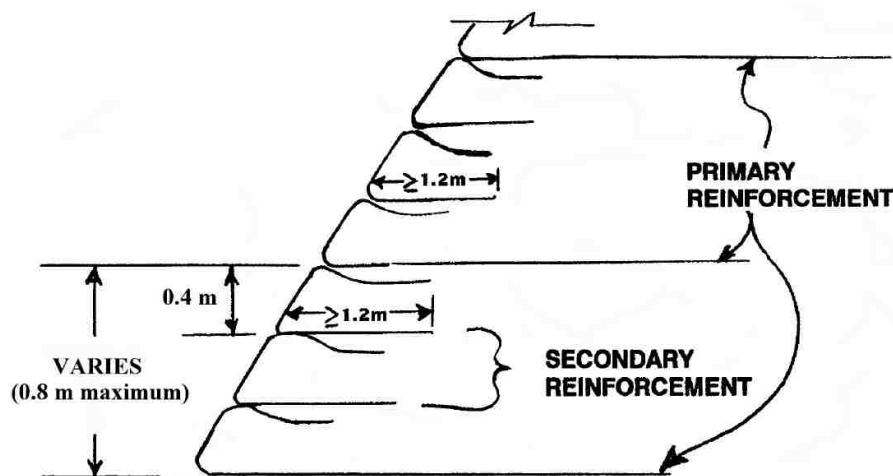


Figure 5.6: Primary and secondary reinforcements distribution (Elias et al. 2001)

• Total usage. When both primary and secondary reinforcements are taken into consideration, for the slopes flatter than 1H:1V and having reinforcements closely placed with a spacing no larger than 400 mm, the total usage of geosynthetic reinforcements is

$$L_{\text{total}} = \sum_{i=1}^{n_p} L_{p(i)} + \sum_{j=1}^{n_s} L_{s(j)} \quad (5.6)$$

where $L_{p(i)}$ and $L_{s(i)}$ are the lengths of primary and secondary reinforcement in each layer. Otherwise, for steeper slopes, face-wrapping should be included in calculating the total usage of geosynthetic reinforcements as

$$L_{\text{total}} = \sum_{i=1}^{n_p} \left[L_{p(i)} + \frac{s_v(i)}{\sin \alpha} + L_w(i) \right] + \sum_{j=1}^{n_s} \left[L_{s(j)} + \frac{s_v(j)}{\sin \alpha} + L_w(j) \right] \quad (5.7)$$

where s_v is the vertical spacing between two neighbored reinforcement layers: when no secondary reinforcements are taken into consideration, s_v is the spacing between two primary reinforcements; otherwise, it is equal to the spacing between two secondary reinforcements; L_w is the embedment length of the face-wrapping; and α is the slope angle.

5.3.2.1.2. Cost of geosynthetic reinforcements. Provided the specified geosynthetic reinforcement distribution, the costs corresponding to the primary and the secondary reinforcements can be generally computed by

$$C_{\text{primary}} = \sum_{i=1}^{n_p} c_{p(i)} L_{p(i)} \quad (5.8)$$

$$C_{\text{secondary}} = \sum_{j=1}^{n_s} c_{s(j)} L_{s(j)} \quad (5.9)$$

where c_p and c_s respectively represent the unit price of the primary and the secondary reinforcements. If the unit price is available with respect to every potential geosynthetic product, c_p and c_s can be specified in detail corresponding to the products that are selected as the reinforcements during optimization. In this case, the algorithm is expected to provide the most precise cost estimation with respect to every potential set of reinforcements that are assigned. Otherwise, in the case that only limited information is available, a function representing the relationship between the unit price and the product properties is to be interpreted through performing interpolation on the given data. In this study it is emphasized the relationship between the unit price and the allowable tensile strength of geosynthetic reinforcement products. Six different products are respectively studied in the two categories that are frequently used as the reinforcements in GRES: woven geotextiles (US2600, US3600, and US4800); and bi-axial knitted geogrids (Microgrid, SG200, and SG550). The engineering properties regarding the above products are available in US Fabrics website and presented in Appendix C. Based on a set of data collected from some geosynthetic distributor as summarized in Table 5.2, the cost functions with respect to the ultimate tensile strengths regarding the preceding geotextiles and geogrids are estimated in Figure 5.7 with different unit systems involved. Based on the relationships obtained from the given data, a higher tensile strength corresponds to a higher price. For a specific reinforcement layer, the unit price can be accordingly calculated based on the estimated cost function with respect to the assigned allowable tensile strength.

In summary, the total cost regarding both primary and secondary geosynthetic re-

Table 5.2: The unit price and ultimate tensile strength of geosynthetic products

Geotextile Products	T_{ult}		Unit Price	
	(kN/m)	(lb/ft)	(\$/m ²)	(\$/ft ²)
US2600	35.9	2460.6	1.72	0.16
US3600	48.2	3303.6	1.94	0.18
US4800	70.0	4797.8	2.26	0.21

Geogrid Products	T_{ult}		Unit Price	
	(kN/m)	(lb/ft)	(\$/m ²)	(\$/ft ²)
Microgrid	29.2	2001.4	1.51	0.14
SG200	52.5	3598.3	1.72	0.16
SG550	118.9	8149.4	3.23	0.30

inforcements can be estimated as: 1) for the slopes flatter than 1H:1V and having closer spaced reinforcements with a spacing no greater than 400 mm,

$$C_{total} = \sum_{i=1}^{n_p} c_{p(i)} L_{p(i)} + \sum_{j=1}^{n_s} c_{s(j)} L_{s(j)} \quad (5.10)$$

and 2) for steeper slopes,

$$C_{total} = \sum_{i=1}^{n_p} c_{p(i)} \left[L_{p(i)} + \frac{s_v(i)}{\sin \alpha} + L_{w(i)} \right] + \sum_{j=1}^{n_s} c_{s(j)} \left[L_{s(j)} + \frac{s_v(j)}{\sin \alpha} + L_{w(j)} \right] \quad (5.11)$$

where c_p and c_s can be the specified unit prices corresponding to the potential geosynthetic

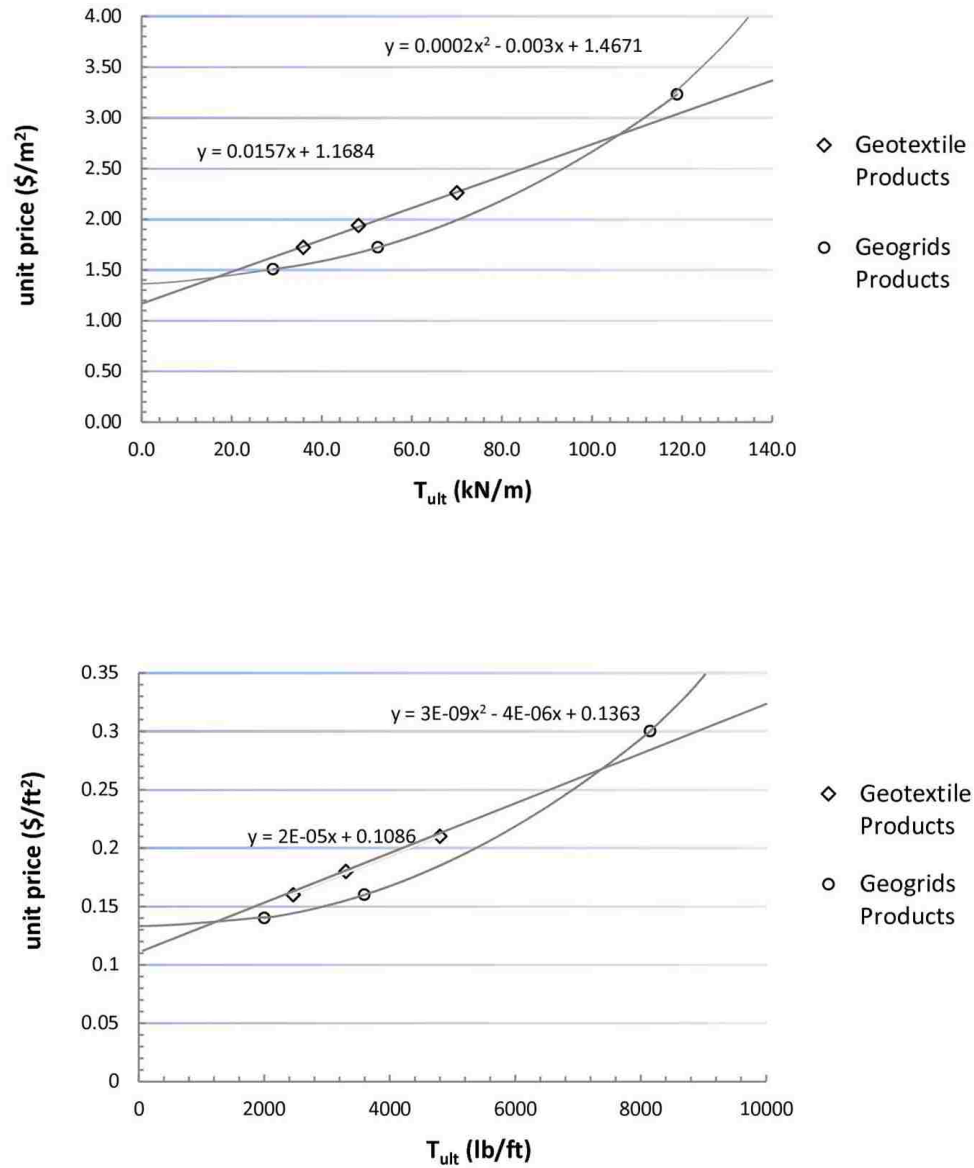


Figure 5.7: Unit price vs. allowable tensile strength, collected from US Fabrics

products or the estimations evaluated from the cost function that represents the relationship between the unit price and product properties.

5.3.2.2. Constraints. As stated in Equation 5.3, the probabilistic constraints can be ideally given on the total probability of failure with respect to each potential failure

mode as well as the system reliability to thoroughly control the level of reliability for the design slope. Therefore, a thorough probabilistic slope stability analysis is required to be embedded in the optimization to evaluate the probabilistic constraints through computing the probability of failure along each potential slip surface. However, due to the iterative scheme embedded in the FORM estimation, plenty of iterative calculations are supposed to be involved in the inner loop in each GA generation with considered potential slip surfaces being searched. Thereby, such an optimization procedure seems dramatically time consuming. In view of the computational efficiency, it can be an alternative to perform the RBO design on the basis of the most dangerous surfaces (i.e., critical deterministic and probabilistic slip surfaces) instead of the entire set of potential slip surfaces. However, as previously discussed in Section 5.2, one of the primary disadvantages existing in the traditional design procedure is the predetermined design surface which is located in the original unreinforced slope prior to the reinforcement design. Based on such a design surface, though the reinforcement design enables a factor of safety above the required level along this surface, a new critical surface can be possibly generated with a minimum factor of safety lower than the required value. Similarly, if it is on the basis of the predetermined design surface only that the RBO design is carried out, same problems can be arisen in either deterministic or probabilistic aspect. As a result, an iterative design process can be considered: 1) the RBO design can be first carried out with the probabilistic constraints assigned to the critical surfaces located in the original unreinforced slope, and obtain an optimal solution denoted as the initial design; 2) a thorough slope stability analysis is accordingly carried out with respect to the initial design to locate the new critical surfaces, which are supposed to be the 'reference' design surfaces in the next RBO trial; 3) on the basis of the updated 'reference' design surfaces, the RBO design procedure is to be repeated

until the optimal design successfully satisfies all the design requirements. By doing so, the computational efforts can be significantly reduced; meanwhile, the preceding problem can be solved.

Furthermore, among the multiple failure modes that may potentially occur in a GRES system, it is only the internal failure that has the failure surface passing all the reinforcement layers. Thereby, it is reasonable to believe the internal failure mode has the most significant influence on the reinforcement design, especially in determining the reinforcement lengths considering the pullout behavior. Therefore, to further simplify the optimization problem and improve the computational efficiency, the probabilistic constraints can be emphasized on the internal slope stability only; and Equation 5.3 can be simplified as

$$\min f(\mathbf{d}, \mathbf{X}, \mathbf{P}) = \text{Cost} \quad (5.12a)$$

$$\text{sub. to: } f_{s, \min} \geq f_{s, \text{req}} \quad (5.12b)$$

$$p_{f_{\text{det},i}} = P \{g_{\text{internal,det}}(\mathbf{d}, \mathbf{X}, \mathbf{P}) \leq 0\} \leq p_{f_{\text{cri, internal}}} \quad (5.12c)$$

$$p_{f_{\text{pro},i}} = P \{g_{\text{internal,pro}}(\mathbf{d}, \mathbf{X}, \mathbf{P}) \leq 0\} \leq p_{f_{\text{cri, internal}}} \quad (5.12d)$$

$$T_{a(i)} \in [T_{l(i)}, T_{r(i)}] \text{ for } i = 1, 2, \dots, n \in [n_l, n_u]$$

where $p_{f_{\text{det},i}}$ and $p_{f_{\text{pro},i}}$ are the probability of failure along critical deterministic and probabilistic internal failure surfaces; and should be no greater than the target probability of failure ($p_{f_{\text{cri, internal}}}$) regarding the above two surfaces. Along with the simplified probabilistic constraints, the GA optimization is carried out considering the deterministic constraint

as well, which is primarily controlled by the minimum factor of safety of the designed slope by implementing a thorough deterministic slope stability analysis in the inner loop.

5.3.3. RBO Design Procedure. On the basis of the objective function, constraints, and technical design rules that have been discussed above, to clearly demonstrate the process of the reliability-based optimization design of GRES systems, a flowchart is presented in Figure 5.8, showing the design procedure. According to the design recommendations stated in Section 5.3.2.1.1, for the slopes with the total height less than 6 m, uniform distribution is acceptable with identical geosynthetic products and design variables as: $\mathbf{d} = \{n, T_a\}$. For the slopes higher than 6 m, if the slope is divided into two reinforcement zones, design variables become as: $\mathbf{d} = \{n_1, T_{a1}, n_2, T_{a2}\}$, where n_1 and n_2 are the numbers of reinforcement layers in bottom and top zones, and T_{a1} and T_{a2} are the allowable tensile strengths of the geosynthetic reinforcements in the two reinforcement zones. If the slope is divided into three reinforcement zones, there are six design variables in total as: $\mathbf{d} = \{n_1, T_{a1}, n_2, T_{a2}, n_3, T_{a3}\}$, where the allowable tensile strength and the number of reinforcement layers are assigned in each reinforcement zone respectively. In order to simplify the problem, geosynthetic products are supposed to have the same tensile strength in each reinforcement zone for both primary and secondary reinforcements. Furthermore, as previously discussed in Section 5.3.2.2, considering the computational efficiency, the probabilistic constraints are emphasized on the internal critical surfaces only.

In summary, the proposed reliability-based optimization design of a geosynthetic reinforced embankment slope can be achieved by:

- 1) Performing deterministic and probabilistic slope stability analyses on the original unreinforced slope to determine the critical zone and the critical surfaces following the steps proposed in Section 5.3.2.1.1.1;

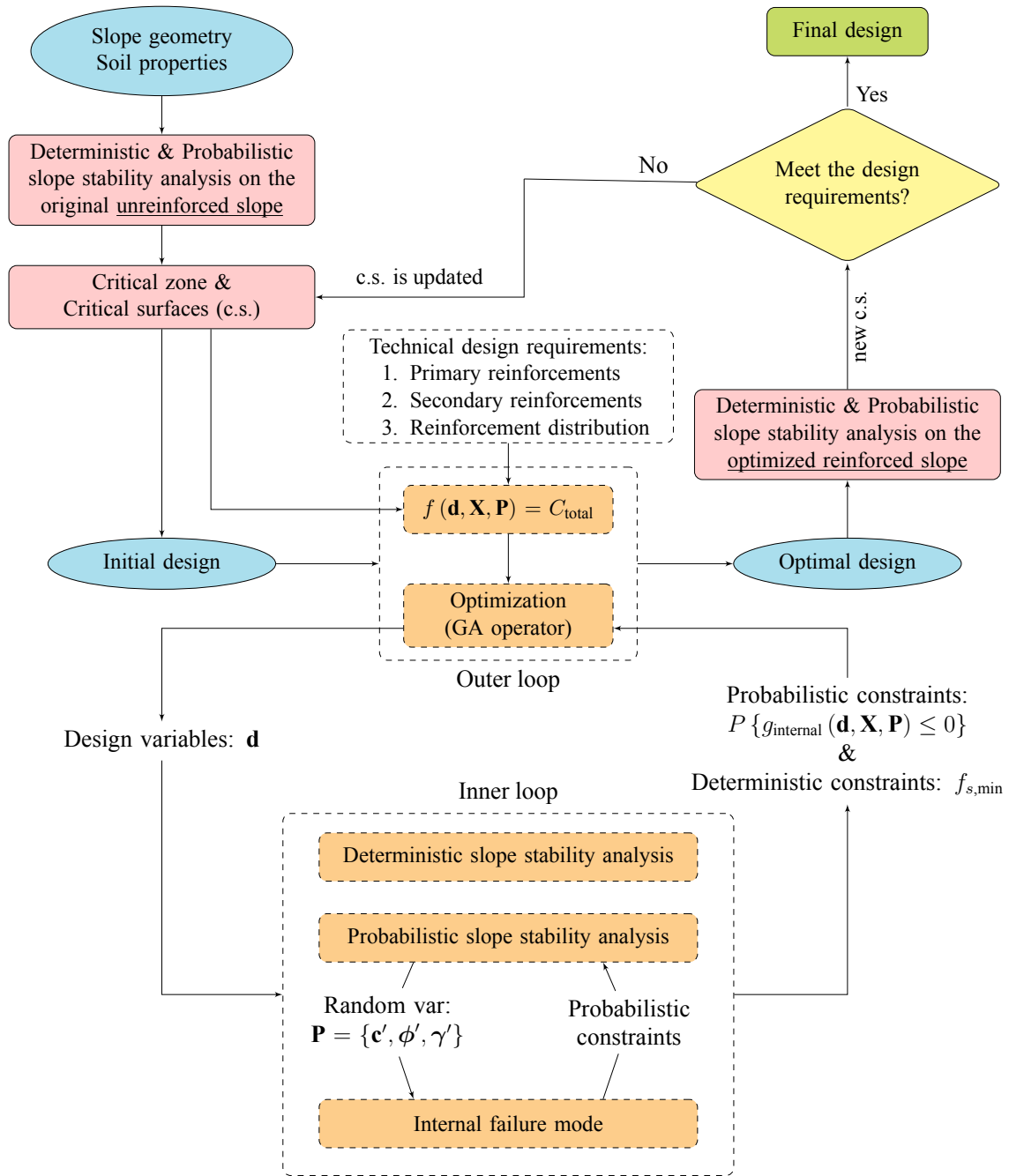


Figure 5.8: The RBO procedure in GRES design

- 2) Determining the objective function based on Equation 5.10 or 5.11 in view of the technical design requirements stated in Section 5.3.2.1.1 and the unit price of the potential geosynthetic products;
- 3) Evaluating the probability of failure along the critical internal failure surfaces as the probabilistic constraints and the minimum factor of safety of the designed slope as the deterministic constraint;
- 4) Performing GA optimization on the basis of the objective function and the constraints defined in step 2) and 3) with the design variables bounded in a predetermined range to obtain the optimal design;
- 5) Performing deterministic and probabilistic slope stability analyses on the optimized reinforced slope to address the new critical surfaces as well as the system reliability considering the multiple failure modes, mainly including internal, compound, and deep-seated failure; and
- 6) Repeating step 2) to step 5) with the updated new critical internal failure surfaces until the design requirements are satisfied.

Based on the optimal design obtained through the above design procedure, sliding stability is accordingly verified, especially on its probability of failure. As previously mentioned in Section 5.3.2.1.1.1, through performing the deterministic analysis on the original unreinforced slope with a required factor of safety specified against sliding failure, the surfaces that just meet the required factor of safety roughly envelope the limits of the critical zone; thereby, the sliding stability is the primary factor that determines the base width of the critical zone and consequently controls the length of the lower reinforcement layers. In other words, with the reinforcement layers extended to the limits of the critical zone, it is always guaranteed a factor of safety against sliding failure above the required

level. But the total probability of failure can be probably beyond the acceptable level since the previous deterministic analysis fails to consider soil variability. In this situation, the lower reinforcement layers may need to be further extended beyond the limits of the critical zone to enhance the sliding stability and consequently decrease the total probability of failure until the design requirements are fully satisfied.

5.4. NUMERICAL EXAMPLE

To demonstrate how the proposed reliability-based optimization procedure can be applied to the design of a GRES system, two numerical examples are carried out in this section. The numerical examples are developed based on the unreinforced slopes defined in the previous chapter of probabilistic slope stability analysis in Section 3.5.

5.4.1. Numerical Example 1: Geotextile Reinforced Road Embankment. As stated in Section 3.5.1, it is required to reinforce a 5-m high, 1H:1V road embankment by placing geosynthetic reinforcements inside. The engineering properties of both embankment fill and foundation soil have been presented in Table 3.2 along with their probabilistic characteristics. Provided the given information, slope stability analyses are first performed on the original unreinforced slope to identify the critical slip surfaces and the critical zone to be reinforced. With a required factor of safety (FS_R) set as 1.3, the critical zone is roughly enveloped by a circular slip surface (2) and a wedge-shaped sliding surface (3) with a 45-degree inclined back-face and a 3.5-m long bottom width as shown in Figure 5.9. The critical rotational slip surfaces are identical in both deterministic and probabilistic analyses, located at a shallow position close to the slope face and passing through the slope toe with a factor of safety that is only 0.663 and a 100% probability of failure. To maintain the slope stability, such an unreinforced slope needs to be reinforced by placing geosynthetic

layers inside.

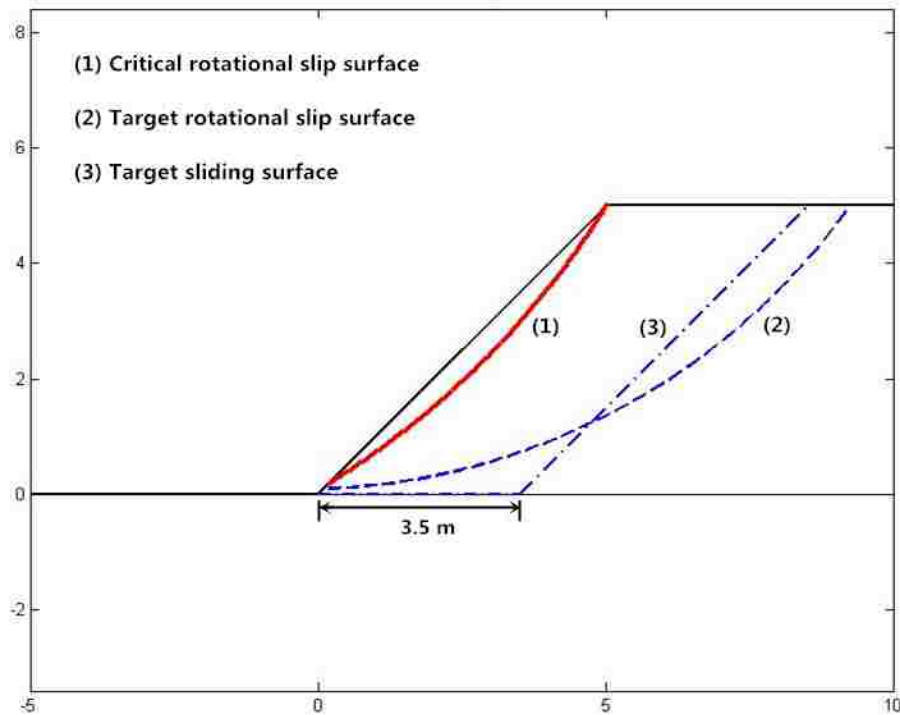


Figure 5.9: Slope stability analyses on the original unreinforced slope in Example 1

5.4.1.1. Design factors. If geotextiles are supposed to be used as the reinforcements in this embankment slope, the strength reduction factors are assumed based on some typical ranges as: 1) $R_{ID} = 1.25$ for installation damage; 2) $R_{CR} = 2.0$ for creep; and 3) $R_{CBD} = 1.2$ for chemical or biological degradation (Koerner 2005). The relationship between allowable tensile strength and ultimate tensile strength are given as

$$T_a = T_{ult} \left(\frac{1}{R_{ID} \times R_{CR} \times R_{CBD}} \right) \quad (5.13)$$

During the optimizing process, since the allowable tensile strength is considered as one of the design variables, from Equation 5.13, the ultimate tensile strength can be computed and accordingly used to estimate the unit price of geotextile products based on the cost function presented in Figure 5.7 as shown below

$$c_{\text{geotextile}} = 0.0157 T_{\text{ult}} + 1.1684 \quad (5.14)$$

where T_{ult} is the ultimate tensile strength of geotextile, in kN/m; and $c_{\text{geotextile}}$ is the corresponding unit price, in \$/m². Since the embankment slope is only 5-m high (< 6 m), according to the design recommendations stated in Section 5.3.2.1.1, reinforcements can be uniformly distributed with an identical tensile strength. Therefore, there are two random variables involved herein: $\mathbf{d} = \{n, T_a\}$, where the allowable tensile strength is set between 3 kN/m and 10 kN/m, and the number of reinforcement layers is a positive integer between 6 and 12.

5.4.1.2. Design requirements. Following the design framework as demonstrated in Figure 5.8, the iterative scheme will be terminated once the following design requirements are fully satisfied: 1) the total probability of failure with respect to the multiple failure modes including: internal, compound, and deep-seated, are no greater than an acceptable level set as 5% in this example; 2) the system reliability is accordingly no less than 85% in view of the above three failure modes; and 3) the minimum factor of safety is above or equal to the required value that is specified as 1.3. If the design successfully meets the above requirements, sliding stability should be accordingly verified to ensure the total probability of failure is no greater than 5% as previously specified to the other failure

modes.

It should be mentioned that, unlike the factor of safety that has been commonly used in the traditional deterministic design of reinforced slope structures, the requirements associated with the level of reliability are not clearly defined in the current design manuals especially when multiple failure modes are taken into consideration. As stated by Baecher and Christian (2003), establishing an appropriate target level of reliability for a project is a complex issue. Generally it involves evaluation of the potential consequences of failure and the required investment and subsequently striking a balance between the risks and the costs to reduce those risks. Basically, in the cases where risks are relatively low (e.g., largely rural areas where failure is not expected to impact structures or humanity, it may be warranted to accept a higher probability of failure, contrasted to cases where risks are higher (e.g. largely urban areas, or cases where failure is likely to impact structure or humanity (Loehr et al. 2006). Selecting an appropriate target level of reliability is beyond the scope of this study, and will not be discussed herein. The values set above, for instance, the acceptable level as 5% for the total probability of failure regarding every potential failure mode, are specified based on the previous probabilistic slope stability analyses presented in Section 3.5.1 with an intention to guarantee an optimal result existing within the constraint ranges as assigned in Section 5.4.1.1.

5.4.1.3. Design process. The reliability-based optimization is first carried out based on the critical zone and the critical surfaces located in the original unreinforced slope (Figure 5.9) with a required factor of safety set as 1.3 and the target probability of failure along the two critical internal failure surfaces set as 0.1%. Thereby, the optimization problem can be mathematically described by modifying the general formation stated

by Equation 5.12 as follows

$$\min f(\mathbf{d}, \mathbf{X}, \mathbf{P}) = \text{Cost} \quad (5.15a)$$

$$\text{sub. to: } f_{s, \min} \geq f_{s, \text{req}} = 1.3 \quad (5.15b)$$

$$p_{f_{\text{det},i}} = P\{g_{\text{internal,det}}(\mathbf{d}, \mathbf{X}, \mathbf{P}) \leq 0\} \leq p_{f_{\text{cri, internal}}} = 0.1\% \quad (5.15c)$$

$$p_{f_{\text{pro},i}} = P\{g_{\text{internal,pro}}(\mathbf{d}, \mathbf{X}, \mathbf{P}) \leq 0\} \leq p_{f_{\text{cri, internal}}} = 0.1\% \quad (5.15d)$$

$$T_a \in [3, 10] \text{ kN/m}, n \in [6, 12] \quad (5.15e)$$

where all the random variables are assumed uncorrelated and normally distributed along with the design requirements as previously specified in Section 5.4.1.2 and clearly summarized in the following Table 5.3.

Table 5.3: The RBO design requirements in Example 1

Deterministic	$f_{s, \min} \geq 1.3$	
Probabilistic	Total Internal, $p_{f_{\text{internal}}}$	$\leq 5\%$
	Total Compound, $p_{f_{\text{compound}}}$	$\leq 5\%$
	Total Deep-Seated, $p_{f_{\text{deep}}}$	$\leq 5\%$
	Total Sliding, $p_{f_{\text{sliding}}}$	$\leq 5\%$
	System Reliability, R_{system}	$\geq 85\%$

5.4.1.3.1. Initial design. Provided the above given information, the initial optimal design is derived with 12 layers of primary reinforcements uniformly distributed within

the critical zone having an identical allowable tensile strength obtained as 5.40 kN/m. No secondary reinforcements are placed inside. The vertical spacing is exactly equal to 400 mm; therefore, it is not needed to wrap the slope face. As shown in Figure 5.10, the rein-

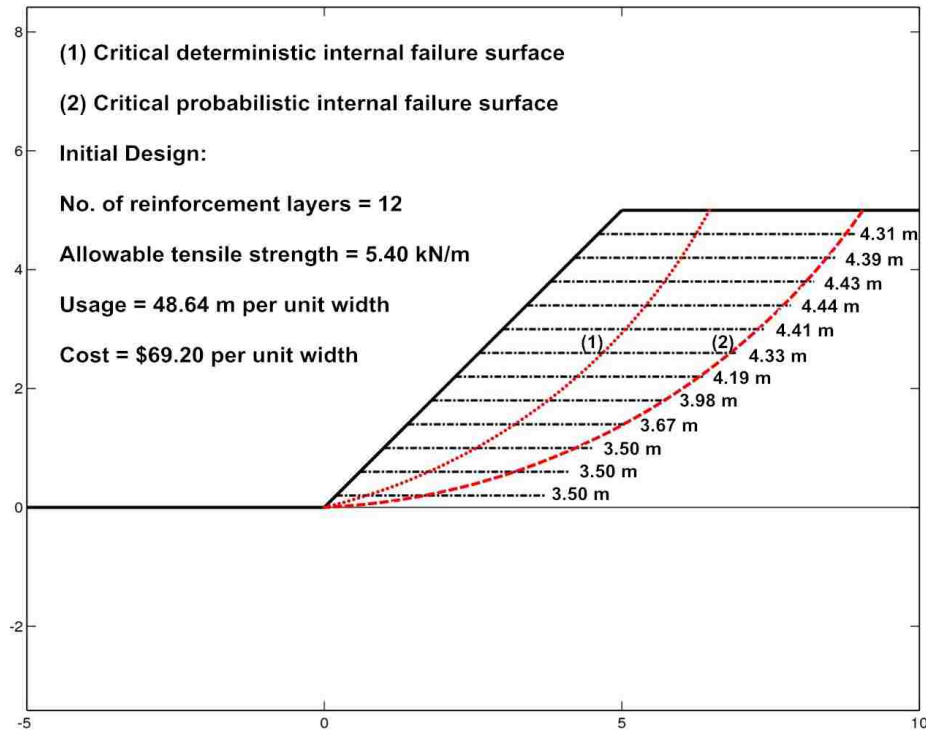


Figure 5.10: The initial design in case 1.3 in Example 1

forcements are all extended to the limits of the critical zone with the length obtained as 3.50, 3.50, 3.50, 3.67, 3.98, 4.19, 4.33, 4.41, 4.44, 4.43, 4.39, and 4.31 m from bottom to top layer. The cost and the usage of the geotextile reinforcements are consequently obtained as \$69.20 and 48.64 m² per unit width of this cross section. Such an optimization guarantees a minimum factor of safety equal to 1.3 and has the probability of failure obtained as zero along the original critical rotational slip surfaces addressed in the previous unreinforced slope. Therefore, the initial optimal design is mainly controlled by the deterministic

constraint instead of the probabilistic constraints regarding the internal probability of failure along the critical surfaces. Through performing a thorough slope stability analysis on the initial optimal design, it is located new critical surfaces with the probabilistic results listed in Table 5.4. With the total probability of failure obtained as 0.2744%, 14.079%, and 3.3650% corresponding to internal, compound, and deep-seated failure mode, the initial design fails to meet the design requirements since the total compound probability of failure exceeds the acceptable level as 5%; meanwhile, the system reliability derived as 82.80% is lower than the required level of 85%. As shown in Figure 5.10, the critical probabilistic internal failure surface is located at a deep position which is very closed to the limits of the critical zone so that the anchored portions behind the critical surface are not long enough and tend to result in the pullout failure along some reinforcement layers. As a result, the initial design is not acceptable and the reinforcements are supposed to be extended.

5.4.1.3.2. Second design. On the basis of the new critical internal failure surfaces updated in the initial design as shown in Figure 5.10, the second optimization trial is accordingly carried out, that has the optimal design derived with 7 layers of primary reinforcements uniformly distributed throughout the embankment slope having an identical allowable tensile strength obtained as 9.14 kN/m without secondary reinforcements placed inside. The vertical spacing is 685.7 mm (> 400 mm); therefore, the slope face should be wrapped up by geotextile reinforcements to prevent face sloughing. Considering the pull-out failure that may potentially occur corresponding to the critical internal failure surface, except for the bottom layer, all the other reinforcements are extended beyond the limits of the critical zone with the length obtained as 3.50, 4.07, 4.77, 5.13, 5.29, 5.31, and 6.06 m as shown in Figure 5.11. Therefore, compared to the initial design, though the number of reinforcement layers is decreased from 12 to 7, the total usage obtained as 49.31 m² in the

Table 5.4: The RBO design in Example 1 ($f_{s,req} = 1.3$, $p_{f,internal} = 0.1\%$)

Trial	RBO Results		Pri. Control	Slope Stability Analyses								
	No. layer			Failure	Critical det.		Critical pro.		Total p_f (%)	System p_f	System R_s	
	T_a (kN/m)		f_s		p_f (%)	f_s	p_f (%)					
1	12	5.40	$f_{s,req} = 1.3$	Internal	1.300	0.0065	1.396	0.0337	0.2744	17.20%	82.80%	
	Usage (m)	48.64		Compound	1.345	0.2033	1.345	0.2033				14.079
	Cost (\$)	69.20		Deep	1.399	0.0272	1.280	0.1810				3.3650
	Face wrap	NO										
2	7	9.14	$f_{s,req} = 1.3$	Internal	1.300	0.0075	1.315	0.0104	0.1620	1.600%	98.40%	
	Usage (m)	49.31		Compound	1.478	0.0021	1.485	0.0037				1.4253
	Cost (\$)	78.84		Deep	1.446	0.0012	1.484	0.0023				0.0192
	Face wrap	YES										

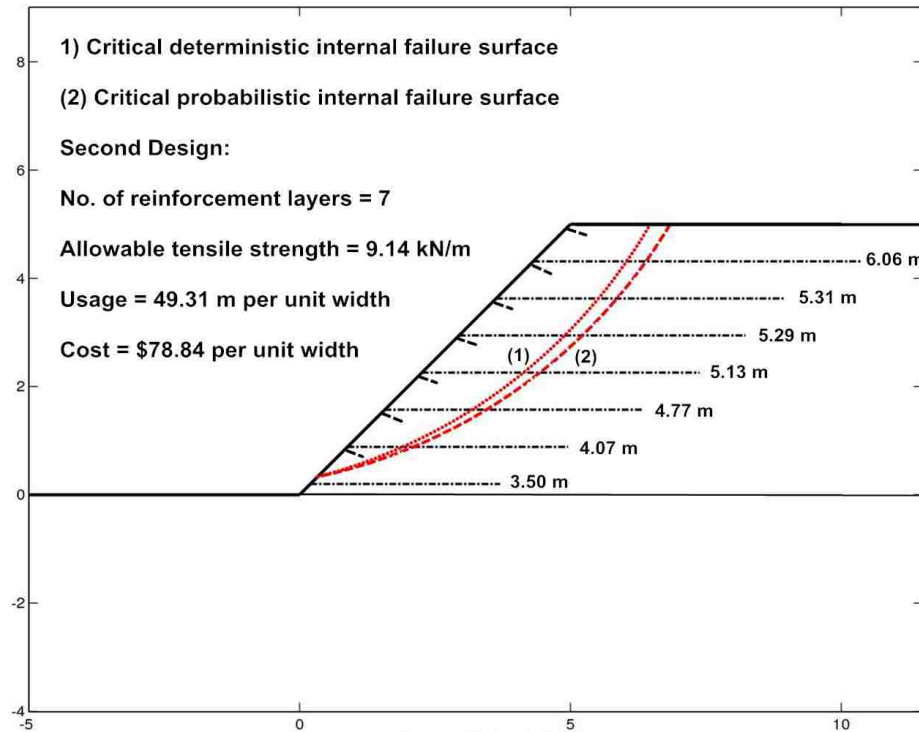


Figure 5.11: The second design in case 1.3 in Example 1

second design is slightly higher than the initial amount. Furthermore, with the required allowable tensile strength increased from 5.40 kN/m to 9.14 kN/m, the total cost is obtained as \$78.84 per unit width, that is \$9.64 higher than the initial cost. Similar to the initial trial, the second optimization is also driven by the deterministic constraint and has a minimum factor of safety obtained as 1.3; while the probabilistic constraints are simultaneously satisfied with the probability of failure along the critical internal failure surfaces derived as 0.0055% and $4.5362 \times 10^{-5}\%$, both of which are greatly less than the target value of 0.1%. A thorough slope stability analysis is accordingly carried out to evaluate if the design is acceptable. As shown in Table 5.4, the total probability of failure is obtained as 0.1620%, 1.4253%, and 0.0192% corresponding to internal, compound, and deep-seated failure mode; meanwhile, the system reliability is derived as 98.40%. Therefore, the de-

sign requirements 1), 2), and 3) as stated in Section 5.4.1.2 are successfully satisfied; and the design process can be accordingly terminated. Based on the optimal design obtained from the second trial, sliding stability is verified with a total probability of failure derived as 0.9001% (< 5%) which is sufficiently small so that it is not needed to extend any lower level of reinforcements to enhance the sliding stability. As a result, the second design can be considered as a more optimal design; and in view of the sliding stability, system reliability is finally obtained as 97.79%.

5.4.1.4. Results comparison. According to the optimization problem as defined by Equation 5.15, the optimal result is supposed to be influenced by many factors. To thoroughly understand how much impact the design factors and requirements can have on the optimization, comparison is carried out focusing on the following aspects: 1) the required factor of safety specified in deterministic constraint; 2) the target probability of failure specified in probabilistic constraints; 3) the distribution model assigned to the random variables; and 4) the constraints involved in the optimization. Since the sliding stability is excluded from the optimizing process, it is not taken into consideration in the following comparisons.

5.4.1.4.1. Required factor of safety. When the target probability of failure is fixed at a constant level of 0.1%, based on the critical zone and the critical surfaces located in the original unreinforced slope, comparison is carried out with the required factor of safety changed to 1.2 and 1.1, as highlighted in the following Equation 5.16; and has the results listed in Table 5.5 and 5.6.

$$\min f(\mathbf{d}, \mathbf{X}, \mathbf{P}) = \text{Cost} \quad (5.16a)$$

$$\text{sub. to: } f_{s, \min} \geq f_{s, \text{req}} = \underline{1.2} \text{ (case 1.2); } \underline{1.1} \text{ (case 1.1)} \quad (5.16b)$$

$$p_{f_{\text{det},i}} = P \{g_{\text{internal,det}}(\mathbf{d}, \mathbf{X}, \mathbf{P}) \leq 0\} \leq p_{f_{\text{cri, internal}}} = 0.1\% \quad (5.16c)$$

$$p_{f_{\text{pro},i}} = P \{g_{\text{internal,pro}}(\mathbf{d}, \mathbf{X}, \mathbf{P}) \leq 0\} \leq p_{f_{\text{cri, internal}}} = 0.1\% \quad (5.16d)$$

$$T_a \in [3, 10] \text{ kN/m, } n \in [6, 12] \quad (5.16e)$$

In the case that the required factor of safety is 1.2 (case 1.2), deterministic constraint works as the primary control factor in the initial optimization trial that generates an optimal design with 7 layers of primary reinforcements uniformly distributed within the critical zone having an identical allowable tensile strength equal to 5.40 kN/m. With such an initial design, system reliability is derived as 71.28%, that is not high enough to meet the required level. Meanwhile, though the probabilistic constraints are satisfied in the initial optimization with the probability of failure obtained as zero along the original critical surfaces, from Table 5.5, it can be noticed, corresponding to the new critical internal failure surfaces updated in the initial design, the probability of failure is derived as 0.43 % for the deterministic surface and 0.55% for the probabilistic surface, both of which exceed the target value specified in the probabilistic constraints as 0.1%. Therefore, a new optimization trial is needed in order to keep the probability of failure along the above two critical surfaces within the target level. In the second optimization trial, the probabilistic constraint becomes the essential factor that controls the optimizing process; and consequently gives an optimal design with the same number of reinforcement layers but a higher allowable tensile strength equal to 8.07 kN/m. As shown in Figure 5.12, the critical internal failure surfaces generated in the second design happen to be located at the same positions as in the initial design; and have the minimum factor of safety obtained

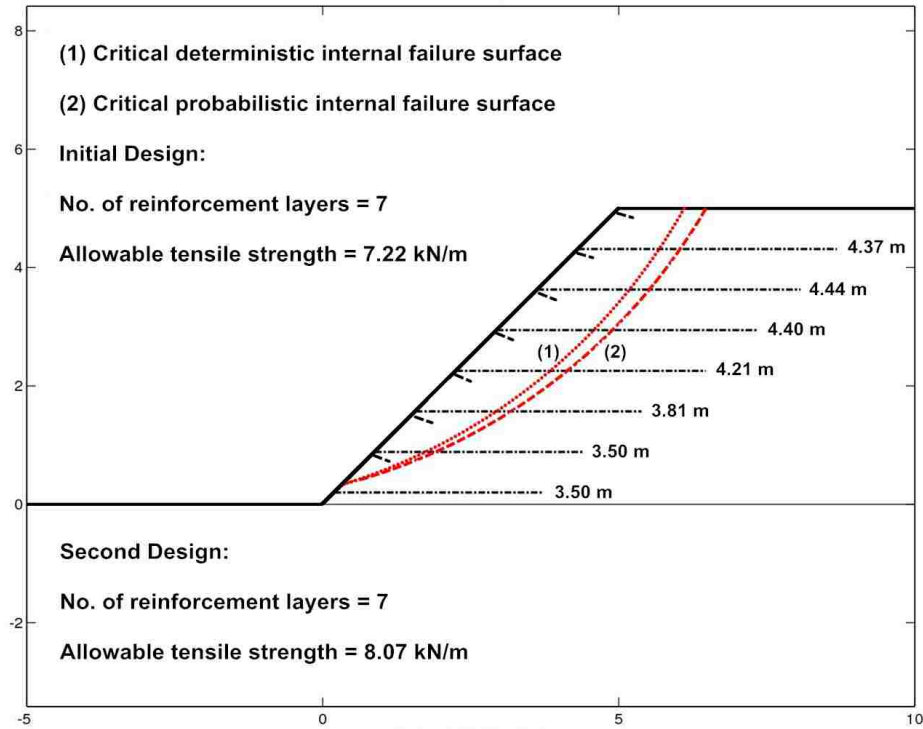


Figure 5.12: The initial and second design in case 1.2 in Example 1

as 1.246 along the deterministic surface and the maximum probability of failure equal to 0.1% along the probabilistic surface. It is obvious the second design successfully meets both deterministic and probabilistic constraints; and more importantly, the probability of failure along the critical probabilistic internal failure surface is exactly equal to the target value specified in the probabilistic constraints. Therefore, it can be expected if the design process continues the same results will be derived. As shown in Table 5.5, such an inference is successfully verified by performing the third optimization trial which gives an optimal result identical to the second design. Therefore, with such a required factor of safety specified as 1.2 in the deterministic constraint, it is unable to provide an acceptable design that meets the design requirements stated in Table 5.3.

When the required factor of safety is specified as 1.1 (case 1.1), similarly, the initial

Table 5.5: The RBO design in case 1.2 in Example 1

Trial	RBO Results		Pri. Control	Slope Stability Analyses							
	No. layer			Failure	Critical det.		Critical pro.		Total p_f (%)	System p_f	System R_s
	T_a (kN/m)		f_s		p_f (%)	f_s	p_f (%)				
1	7		$f_{s,req} = 1.2$	Internal	1.200	0.4340	1.208	0.5457	12.191	28.71%	71.28%
	7.22				Compound	1.334	0.2560	1.336			
	43.42			Deep		1.262	0.1482	1.280	0.1810		
	65.49										
	YES										
2	7		$p_{f,pro,i} = 0.1\%$	Internal	1.246	0.0494	1.249	0.1000	2.5185	19.39%	80.61%
	8.07				Compound	1.338	0.2255	1.341			
	43.42			Deep		1.262	0.1482	1.280	0.1810		
	67.24										
	YES										
3	7		$p_{f,pro,i} = 0.1\%$	Internal	1.246	0.0494	1.249	0.1000	2.5185	19.39%	80.61%
	8.07				Compound	1.338	0.2255	1.341			
	43.42			Deep		1.262	0.1482	1.280	0.1810		
	67.24										
	YES										

optimization trial is mainly controlled by the deterministic constraint; and has the optimal design obtained with 7 layers of primary reinforcements uniformly distributed within the critical zone having an identical allowable tensile strength equal to 5.43 kN/m. The system reliability is consequently derived at an extremely low level as 1.980%; meanwhile, the new critical internal failure surfaces are located at the same position in both deterministic and probabilistic analysis with a minimum factor of safety equal to 1.1 and a probability of failure obtained as 9.91% that significantly exceeds the target value of 0.1%. Therefore, the design process needs to be continued. In the second optimization trial, the probability of failure along the two identical critical internal failure surfaces becomes the controlling factor; and an optimal design is accordingly derived with the same number of reinforcement layers but a higher allowable tensile strength equal to 7.81 kN/m. With a system reliability derived as 78.98%, the second design still fails to meet the design requirements. However, it should be noticed, based on the second design, the critical internal failure surfaces are updated and happen to coincide with the ones obtained in the initial and second design in case 1.2 as shown in Figure 5.12. Therefore, subject to an identical probabilistic constraint that works as the primary control factor with a target probability of failure specified as 0.1%, the third optimization trial gives an optimal design that is exactly the same with the final optimal result obtained in case 1.2. Just as what happened in the last two optimization trials in case 1.2, if the design process continues, the same results will be derived with the system reliability equal to 80.61%. As a result, with such a required factor of safety specified as 1.1 in the deterministic constraint, it is unable to provide an acceptable design.

In summary, with the same target probability of failure assigned in the RBO design, the change in the required factor of safety can significantly influence the final result.

Table 5.6: The RBO design in case 1.1 in Example 1

Trial	RBO Results		Pri. Control	Slope Stability Analyses							
	No. layer			Failure	Critical det.		Critical pro.		Total p_f (%)	System p_f	System R_s
	T_a (kN/m)		f_s		p_f (%)	f_s	p_f (%)				
1	7		$f_{s,req} = 1.1$	Internal	1.100	9.9100	1.100	9.9100	97.439	98.02%	1.980%
	5.43				Compound	1.324	0.3323	1.326			
	43.42			Deep	1.484	0.0023	1.484	0.0023	3.4862		
	61.83										
	YES										
2	7		$p_{f,det,i} = 0.1\%$	Internal	1.232	0.1000	1.236	0.1724	3.9997	21.02%	78.98%
	7.81				Compound	1.337	0.2344	1.339			
	43.42			Deep	1.262	0.1482	1.280	0.1810	3.4862		
	66.62										
	YES										
3	7		$p_{f,pro,i} = 0.1\%$	Internal	1.246	0.0494	1.249	0.1000	2.5185	19.39%	80.61%
	8.07				Compound	1.338	0.2255	1.341			
	43.42			Deep	1.262	0.1482	1.280	0.1810	3.4862		
	67.24										
	YES										

But sometimes, when the required factor of safety is not sufficiently high, the probabilistic constraints become the primary control factor. In this case, though the specified required factor of safety can affect the design process more or less, it may hardly influence the final optimal result. As shown in the cases that have the required factor of safety specified as 1.2 and 1.1 (Figure 5.13), although they have different optimal results obtained in the second

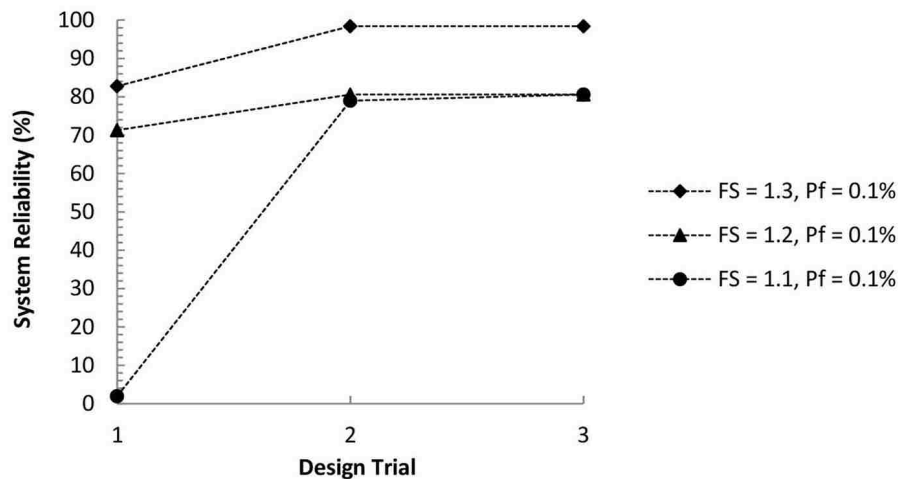


Figure 5.13: System reliability vs. design trial in case 1.3, 1.2, and 1.1 in Example 1

optimization trial, the final designs are identical since the last trials in both cases are driven by the target probability of failure assigned as 0.1% along the same critical internal failure surface. Nevertheless, if we pay attention to the usage of the geotextile reinforcements, it is only in the final design with the required factor of safety equal to 1.3 (case 1.3) that the reinforcement layers extend beyond the limits of the critical zone. As discussed in Section 5.4.1.3.1, this is because the critical probabilistic internal failure surface obtained in the initial design is located at a deep position very closed to the limits of the critical zone. As the reference design surface in the second optimization trial, the required reinforcement

lengths are computed along this surface to prevent the pullout failure; and thereby, the reinforcements are extended beyond the critical zone. Therefore, as shown in Figure 5.14, with the same number of reinforcement layers in the final optimal design, case 1.3 has a relatively higher total usage as well as the total cost of the geotextile reinforcements. Furthermore, if we take a look at the total probability of failure regarding each potential

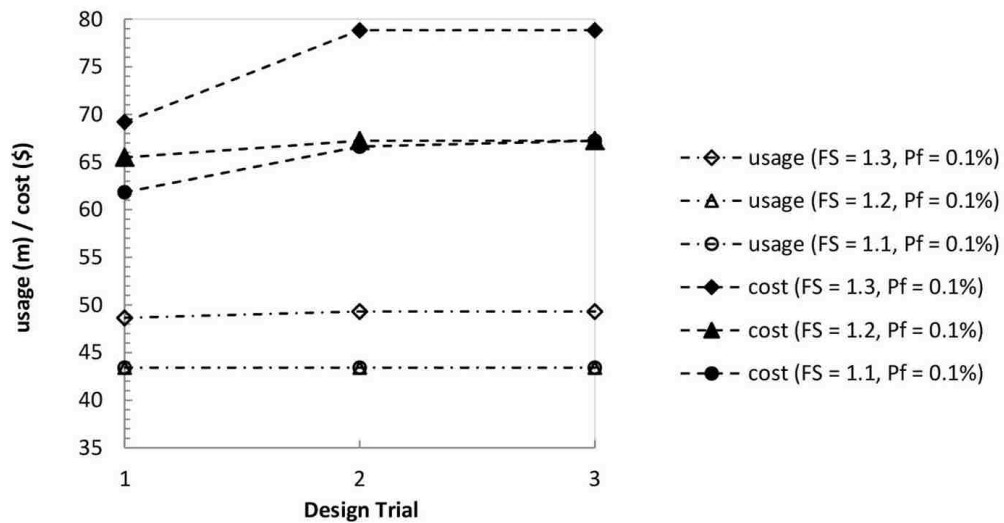


Figure 5.14: The usage/cost with different required factor of safety in Example 1

failure mode in the above three cases, it can be noticed the compound failure seems the primary contributor to the system probability of failure. Especially in the last two optimization trials in case 1.2 and 1.1, though both internal and deep-seated probability of failure successfully meet the design requirements, the compound probability of failure is almost 10% beyond the acceptable level. Thinking of the length of reinforcements, the compound probability of failure is supposed to be decreased by extending some reinforcement layers to a deeper position within the slope.

5.4.1.4.2. Target probability of failure. In the case that the required factor of safety is 1.3, the optimization is always driven by the deterministic constraint instead of the probabilistic constraints so that the target probability of failure specified in the probabilistic constraints can hardly influence the final optimal result. Therefore, to study the impact it can have on the optimal design by assigning different value to the target probability of failure, the comparison is focusing on the cases that have the required factor of safety specified as 1.2 and 1.1 with a target probability of failure significantly reduced from the original value of 0.1% to a lower level of 0.01%, as highlighted in the following Equation 5.17:

$$\min f(\mathbf{d}, \mathbf{X}, \mathbf{P}) = \text{Cost} \quad (5.17a)$$

$$\text{sub. to: } f_{s, \min} \geq f_{s, \text{req}} = 1.2 \text{ (case 1.2}^{[0.01]}\text{); } 1.1 \text{ (case 1.1}^{[0.01]}\text{)} \quad (5.17b)$$

$$p_{f_{\text{det},i}} = P \{g_{\text{internal,det}}(\mathbf{d}, \mathbf{X}, \mathbf{P}) \leq 0\} \leq p_{f_{\text{cri, internal}}} = \underline{0.01\%} \quad (5.17c)$$

$$p_{f_{\text{pro},i}} = P \{g_{\text{internal,pro}}(\mathbf{d}, \mathbf{X}, \mathbf{P}) \leq 0\} \leq p_{f_{\text{cri, internal}}} = \underline{0.01\%} \quad (5.17d)$$

$$T_a \in [3, 10] \text{ kN/m, } n \in [6, 12] \quad (5.17e)$$

According to the results listed in Table 5.7 and 5.8, in both cases, since the deterministic constraint works as the primary control factor in the initial optimization trial, the initial designs are identical to the results obtained in the cases with the target probability of failure set as 0.1% (case 1.2 and 1.1). However, as previously indicated, the probabilistic constraints will control the optimization in the following design; therefore, the change in the target probability of failure is supposed to influence the optimal result since the second

Table 5.7: The RBO design in case 1.2^[0.01] in Example 1

Trial	RBO Results		Pri. Control	Slope Stability Analyses							
	No. layer			Failure	Critical det.		Critical pro.		Total p_f (%)	System p_f	System R_s
	T_a (kN/m)		f_s		p_f (%)	f_s	p_f (%)				
1	No. layer	7	$f_{s,req} = 1.2$	Failure	f_s	p_f (%)	f_s	p_f (%)	12.191	28.71%	71.28%
	T_a (kN/m)	7.22									
	Usage (m)	43.42		Internal	1.200	0.4340	1.208	0.5457	15.885		
	Cost (%)	65.49		Compound	1.334	0.2560	1.336	0.2547			
	Face wrap	YES		Deep	1.262	0.1482	1.280	0.1810	3.4862		
2	No. layer	12	$p_{f_{pro,i}} = 0.01\%$	Failure	f_s	p_f (%)	f_s	p_f (%)	0.8980	18.89%	81.11%
	T_a (kN/m)	4.93									
	Usage (m)	48.64		Internal	1.261	0.0508	1.276	0.0545	15.301		
	Cost (%)	68.12		Compound	1.340	0.2340	1.340	0.2340			
	Face wrap	NO		Deep	1.262	0.1482	1.280	0.1810	3.4862		
3	No. layer	7	$p_{f_{pro,i}} = 0.01\%$	Failure	f_s	p_f (%)	f_s	p_f (%)	0.6210	16.34%	83.66%
	T_a (kN/m)	9.07									
	Usage (m)	43.42		Internal	1.297	0.0091	1.387	0.0462	12.779		
	Cost (%)	69.29		Compound	1.343	0.1938	1.346	0.1944			
	Face wrap	YES		Deep	1.262	0.1482	1.280	0.1810	3.4862		
4	No. layer	7	$p_{f_{det,i}} = 0.01\%$	Failure	f_s	p_f (%)	f_s	p_f (%)	0.0071	0.239%	99.76%
	T_a (kN/m)	9.03									
	Usage (m)	49.28		Internal	1.295	0.0006	1.310	0.0009	0.2310		
	Cost (%)	78.55		Compound	1.477	0.00005	1.484	0.00012			
	Face wrap	YES		Deep	1.437	0.00004	1.465	0.00005	0.0005		

optimization.

When the required factor of safety is specified as 1.2 (case 1.2^[0.01]), neither the second nor the third optimization trial is able to generate an acceptable design since the system reliability always fails to arrive at the required level of 85% mainly due to a total probability of failure obtained over 15% regarding the compound failure mode. On the basis of the third design, the critical probabilistic internal failure surface is located at a deep position very close to the limits of the critical zone, just as in the initial design in case 1.3 (Figure 5.11). Therefore, based on such a reference design surface, the fourth trial gives an optimal result that has the reinforcement layers extended beyond the critical zone to prevent the pullout failure that may potentially occur along some reinforcement layers corresponding to this ‘reference’ surface. As a result, though with the same number of reinforcement layers and an even slightly lower allowable tensile strength, the total compound probability of failure is highly decreased; meanwhile, the system reliability is greatly increased to 99.76%. Similarly, when the required factor of safety is specified as 1.1 (case 1.1^[0.01]), as discussed in the comparison in Section 5.4.1.4.1, though the design process is different, the final optimal result is identical to the final design in case 1.2^[0.01] since the last optimization trial is conducted along the same critical internal failure surfaces with an identical target probability of failure set as 0.01%.

In summary, as illustrated in Figure 5.15 and 5.16, with the same required factor of safety specified in the deterministic constraint, a higher target probability of failure intends to provide a more reliable design; meanwhile, the usage and the cost become relatively higher (Figure 5.17). As demonstrated in Section 5.4.1.4.1, when the required factor of safety is equal to 1.2 and 1.1, with a target probability of failure set as 0.1%, it is unable to provide an acceptable design mainly due to the total probability of failure regarding the

Table 5.8: The RBO design in case 1.1^[0.01] in Example 1

Trial	RBO Results		Pri. Control	Slope Stability Analyses							
	No. layer			Failure	Critical det.		Critical pro.		Total p_f (%)	System p_f	System R_s
	T_a (kN/m)		f_s		p_f (%)	f_s	p_f (%)				
1	No. layer	7	$f_{s,req} = 1.1$	Internal	1.100	9.9100	1.100	9.9100	97.439	98.02%	1.980%
	T_a (kN/m)	5.43			Compound	1.324	0.3323	1.326	0.3357		
	Usage (m)	43.42		Deep	1.484	0.0023	1.484	0.0023	3.4862		
	Cost (%)	61.83									
	Face wrap	YES									
2	No. layer	7	$p_{f_{det,i}} = 0.01\%$	Internal	1.274	0.0034	1.382	0.0088	0.0569	5.729%	94.27%
	T_a (kN/m)	8.60			Compound	1.341	0.0644	1.344	0.0645		
	Usage (m)	43.42		Deep	1.262	0.1482	1.280	0.1810	3.4862		
	Cost (%)	68.32									
	Face wrap	NO									
3	No. layer	7	$p_{f_{det,i}} = 0.01\%$	Internal	1.295	0.0006	1.310	0.0009	0.0071	0.239%	99.76%
	T_a (kN/m)	9.03			Compound	1.477	0.00005	1.484	0.00012		
	Usage (m)	49.28		Deep	1.437	0.00004	1.465	0.00005	0.0005		
	Cost (%)	78.55									
	Face wrap	YES									

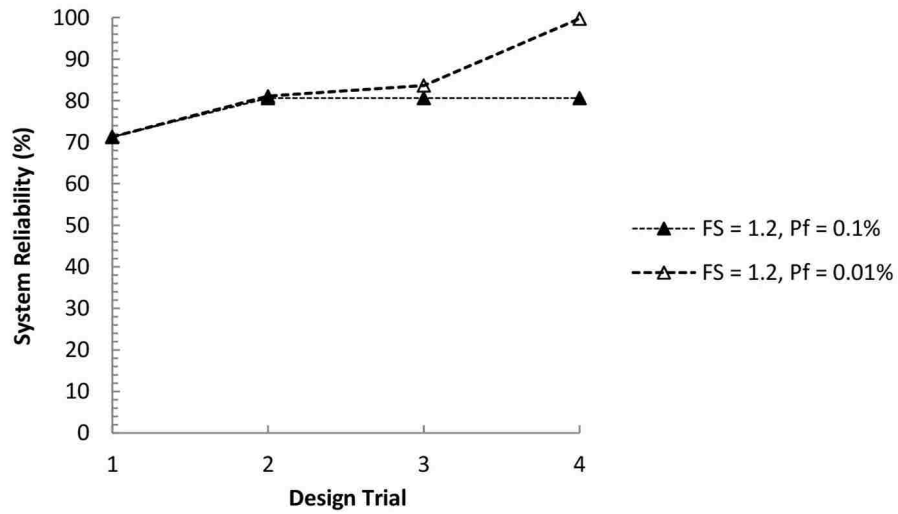


Figure 5.15: System reliability vs. design trial in case 1.2^[0.01] in Example 1

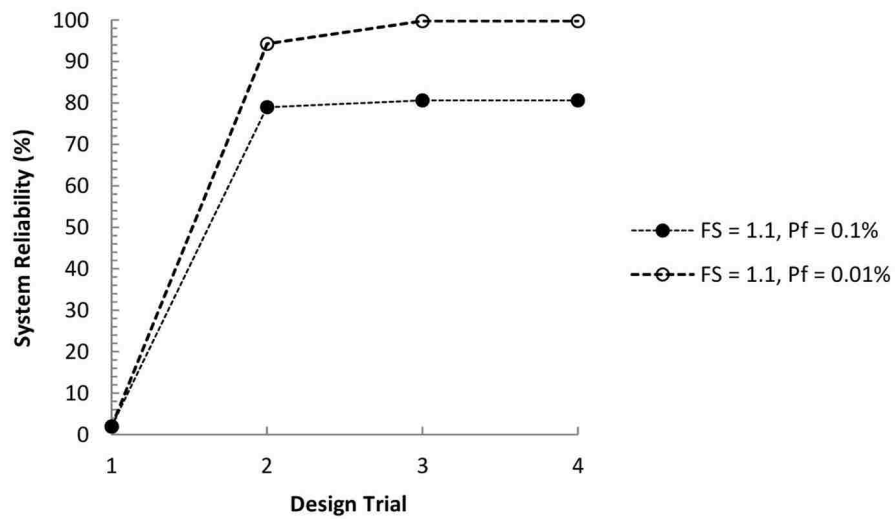


Figure 5.16: System reliability vs. design trial in case 1.1^[0.01] in Example 1

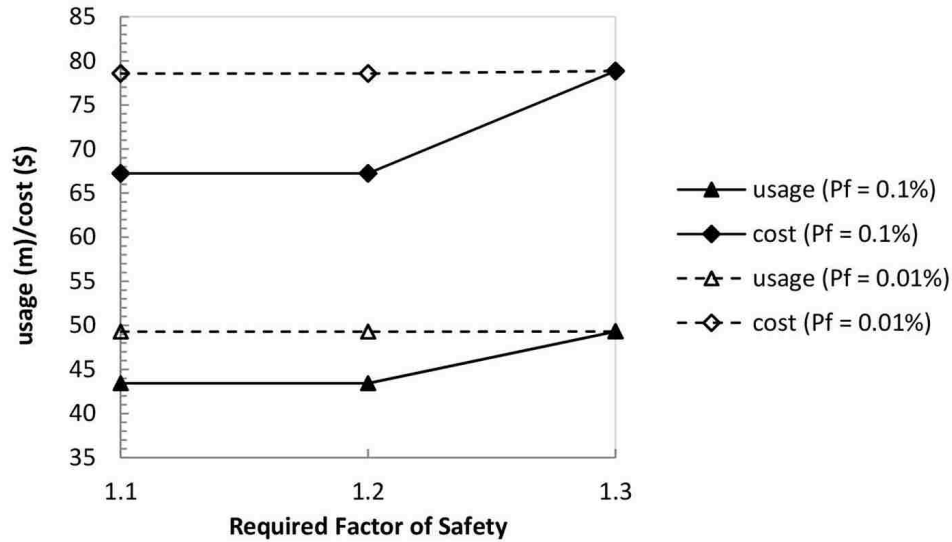


Figure 5.17: The usage/cost with different target probability of failure in Example 1

compound failure mode that exceeds the acceptable level by approximately 10%. When the target probability of failure is lower to 0.01%, such a problem is successfully resolved. Therefore, it can be concluded when the required factor of safety is not sufficiently large, by reducing the target probability of failure assigned in the probabilistic constraints, it is able to obtain an acceptable design.

5.4.1.4.3. Distribution model. As demonstrated in Section 3.5, the selection of the distribution model assigned to the random variables can greatly influence the probabilistic results. More specifically, in this example, when the random variables are changed from normally to log-normally distributed, the probability of failure is largely decreased. Therefore, it can be expected the distribution model selection will influence the reliability-based optimization design more or less. When the required factor of safety is 1.3 (case 1.3^[log]), the deterministic constraint is the primary control factor; therefore, the distribution model selection can hardly influence the final design. As shown in Table 5.9, it is

derived an optimal result in the second optimization trial that is exactly identical to the final design obtained in case 1.3, where all the random variables are in normal distribution. But the differences can be observed by comparing the probabilistic results obtained in both cases with normal and log-normal distribution as listed in Table 5.4 and 5.9. That is, with the same reinforcement design, when the random variables are in log-normal distribution, system reliability is relatively higher than the one obtained with normally distributed random variables.

When the required factor of safety is specified as 1.2 and 1.1, as observed in case 1.2 and 1.1, the probabilistic constraints become the primary control factor since the second and third optimization trial. Therefore, the distribution model is supposed to affect the optimal results in these two situations. When comparing the results listed in Table 5.5 and 5.10, with the same amount of reinforcement usage, the optimized allowable tensile strength is decreased from 8.07 kN/m to 7.55 kN/m in the case that the required factor of safety is 1.2 (case 1.2^[log]). It is because with the same reinforcement design, the log-normal distribution tends to give a lower probability of failure; vice versa, if the target probability of failure is fixed at a constant level, the probabilistic constraints can be satisfied even with a lower allowable tensile strength. Therefore, though the optimized allowable tensile strength is relatively lower in the case with log-normal distribution, the system reliability is obtained as 92.30%, that is approximately 12% higher than the reliability obtained in the case with normal distribution. When the required factor of safety is 1.1 (case 1.1^[log]), as shown in Table 5.11, the final design is identical to the result obtained in case 1.2^[log]; therefore, the same conclusion can be consequently summarized.

In summary, as illustrated in Figure 5.18, 5.19, and 5.20, with log-normally distributed random variables, the system reliability corresponding to the designed reinforced

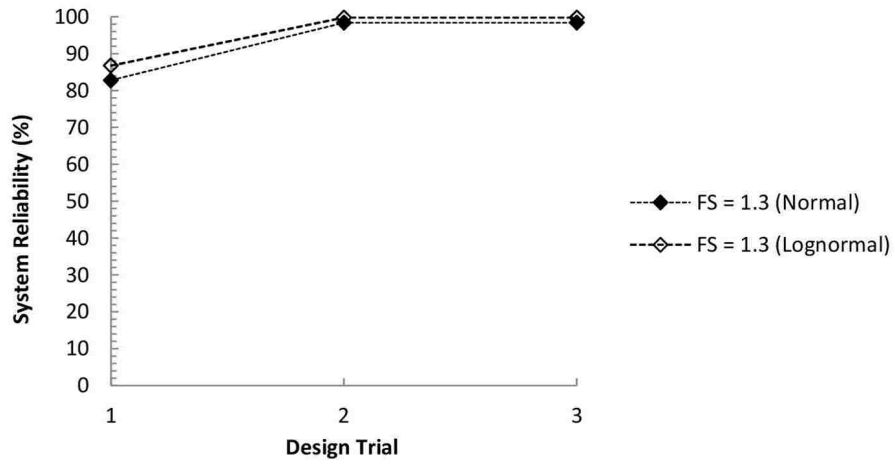


Figure 5.18: System reliability vs. design trial in case 1.3^[log] in Example 1

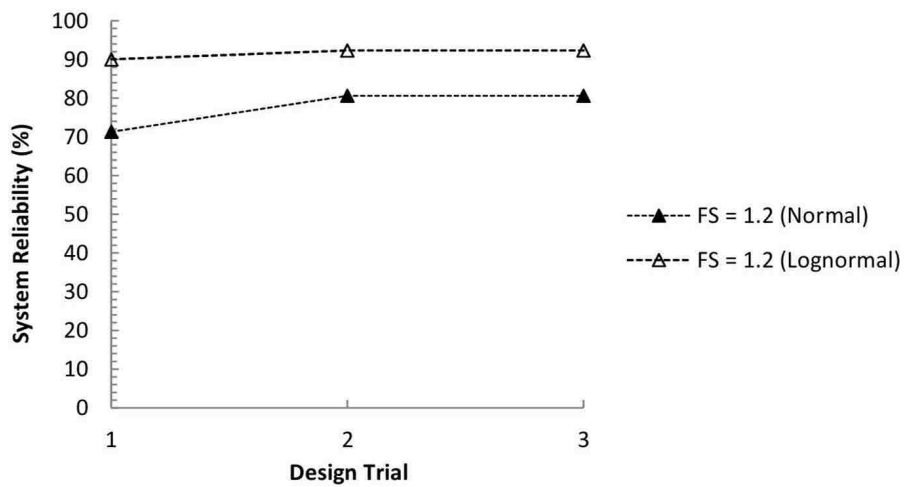


Figure 5.19: System reliability vs. design trial in case 1.2^[log] in Example 1

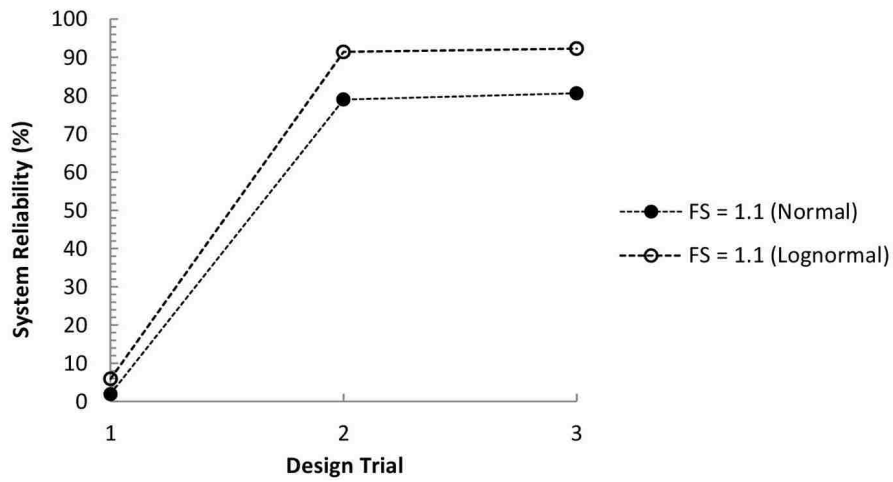


Figure 5.20: System reliability vs. design trial in case 1.1^[log] in Example 1

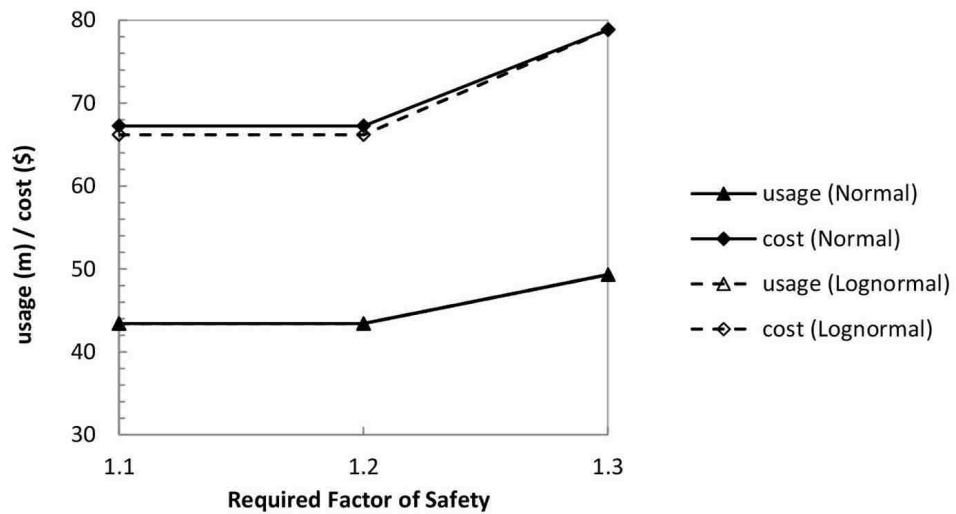


Figure 5.21: The usage/cost with different distribution model in Example 1

Table 5.9: The RBO design in case 1.3^[log] in Example 1

Trial	RBO Results		Pri. Control	Slope Stability Analyses							
	No. layer			Failure	Critical det.		Critical pro.		Total p_f (%)	System p_f	System R_s
	T_a (kN/m)		f_s		p_f (%)	f_s	p_f (%)				
1	7		$f_{s,req} = 1.3$	Internal	1.300	0.0003	1.388	0.0064	0.1343	13.24%	86.76%
	9.16			Compound	1.344	0.0569	1.344	0.0569	13.121		
	43.42			Deep	1.484	0.00007	1.484	0.00007	0.0001		
	69.48										
	YES										
2	7		$f_{s,req} = 1.3$	Internal	1.300	0.0004	1.315	0.0006	0.0046	0.233%	99.77%
	9.14			Compound	1.478	0.00005	1.485	0.0001	0.2277		
	49.31			Deep	1.446	0.000047	1.465	0.000049	0.0004		
	78.84										
	YES										

Table 5.10: The RBO design in case 1.2^[log] in Example 1

Trial	RBO Results		Pri. Control	Slope Stability Analyses							
	No. layer			Failure	Critical det.		Critical pro.		Total p_f (%)	System p_f	System R_s
	T_a (kN/m)		f_s		p_f (%)	f_s	p_f (%)				
1	7		$f_{s,req} = 1.2$	Internal	1.200	0.1764	1.208	0.2425	3.4746	9.986%	90.01%
	7.22			Compound	1.334	0.0865	1.334	0.0865	5.740		
	43.42			Deep	1.262	0.0646	1.280	0.0698	1.0671		
	65.49										
	YES										
2	7		$p_{f,pro,i} = 0.1\%$	Internal	1.218	0.0565	1.224	0.1000	1.3379	7.695%	92.30%
	7.55			Compound	1.335	0.0806	1.338	0.0808	5.4343		
	43.42			Deep	1.262	0.0646	1.280	0.0698	1.0671		
	66.19										
	YES										

slope is relatively higher; especially in the cases with the required factor of safety equal to 1.2 and 1.1 where the probabilistic constraints greatly influence the optimization, the differences relied in the system reliability are most remarkable. Furthermore, as concluded in Figure 5.21, the usage is hardly influenced by the distribution model selection; however, with a lower allowable tensile strength obtained, the design with log-normally distributed random variables leads to a slightly lower cost.

5.4.1.4.4. Constraints. According to Equation 5.12, the optimization as previously performed is simultaneously subject to both deterministic and probabilistic constraints, where the deterministic constraint yields to the minimum factor of safety that can be generally addressed through a thorough deterministic slope stability analysis corresponding to every GA generation; while the probabilistic constraints are mainly determined by the probability of failure along critical deterministic and probabilistic internal failure surfaces that can be evaluated by performing probabilistic analysis with respect to the above two reference design surfaces. Therefore, it is reasonable to believe the computational efforts of the RBO design are directly proportional to the number of constraints; and the computational efficiency can be improved by reducing the number of the constraints that are involved in the optimizing process.

When it is only the probabilistic constraints that are taken into consideration as described by the following Equation 5.18,

$$\min f(\mathbf{d}, \mathbf{X}, \mathbf{P}) = \text{Cost} \quad (5.18a)$$

$$\text{sub. to: } p_{f_{\text{det},i}} = P\{g_{\text{internal,det}}(\mathbf{d}, \mathbf{X}, \mathbf{P}) \leq 0\} \leq p_{f_{\text{cri, internal}}} \quad (5.18b)$$

$$p_{f_{\text{pro},i}} = P\{g_{\text{internal,pro}}(\mathbf{d}, \mathbf{X}, \mathbf{P}) \leq 0\} \leq p_{f_{\text{cri, internal}}} \quad (5.18c)$$

Table 5.11: The RBO design in case 1.1^[log] in Example 1

Trial	RBO Results		Pri. Control	Slope Stability Analyses							
	No. layer			Failure	Critical det.		Critical pro.		Total p_f (%)	System p_f	System R_s
	T_a (kN/m)		f_s		p_f (%)	f_s	p_f (%)				
1	7		$f_{s,req} = 1.1$	Internal	1.102	9.2530	1.102	9.2530	93.4779	94.05%	5.947%
	5.43				Compound	1.324	0.1250	1.326			
	43.42			Deep	1.262	0.0646	1.280	0.0698	1.0671		
	61.83										
	YES										
2	7		$p_{f,det,i} = 0.1\%$	Internal	1.209	0.1000	1.209	0.1000	2.1345	8.581%	91.42%
	7.39				Compound	1.334	0.0834	1.334			
	43.42			Deep	1.262	0.0646	1.280	0.0698	1.0671		
	65.85										
	YES										
3	7		$p_{f,pro,i} = 0.1\%$	Internal	1.218	0.0565	1.224	0.1000	1.3379	7.695%	92.30%
	7.55				Compound	1.335	0.0806	1.338			
	43.42			Deep	1.262	0.0646	1.280	0.0698	1.0671		
	66.19										
	YES										

$$T_a \in [3, 10] \text{ kN/m}, n \in [6, 12] \quad (5.18d)$$

computational efficiency is supposed to be improved mainly due to the elimination of the embedded deterministic slope stability analysis. With the target probability of failure specified as 0.1% in the probabilistic constraints, the results are listed in Table 5.12. After four optimization trials, the design is obtained with 7 layers of primary reinforcements uniformly distributed throughout the embankment slope having an identical allowable tensile strength equal to 7.99 kN/m. Through the probabilistic slope stability analysis, the total probability of failure is obtained as 3.96%, 14.90%, and 3.48% corresponding to internal, compound, and deep-seated failure mode; meanwhile, the system reliability is derived as 78.89%, very closed to the results obtained in case 1.2 and 1.1 that have the system reliability obtained as 80.61%. When the target probability of failure is lower to 0.05%, the results are listed in Table 5.13, that has an optimal design obtained after four optimization trials with the same number of reinforcement layers equal to 7 but a relatively higher allowable tensile strength equal to 8.33 kN/m; and the system reliability is consequently derived as 80.87%. As illustrated in Figure 5.22, with only the probabilistic constraint involved that has the target probability of failure set as 0.1%, the optimal result tends to approach the final design obtained in case 1.2 and 1.1 since the latter two have the probabilistic constraints working as the primary control factor; but it seems more optimization trials are needed. To be more specific, when both deterministic and probabilistic constraints are taken into consideration, only two optimization trials are needed with a required factor of safety equal to 1.2; while three trials are needed when the required factor of safety is 1.1; however, with the probabilistic constraints considered only, at least one more trial is

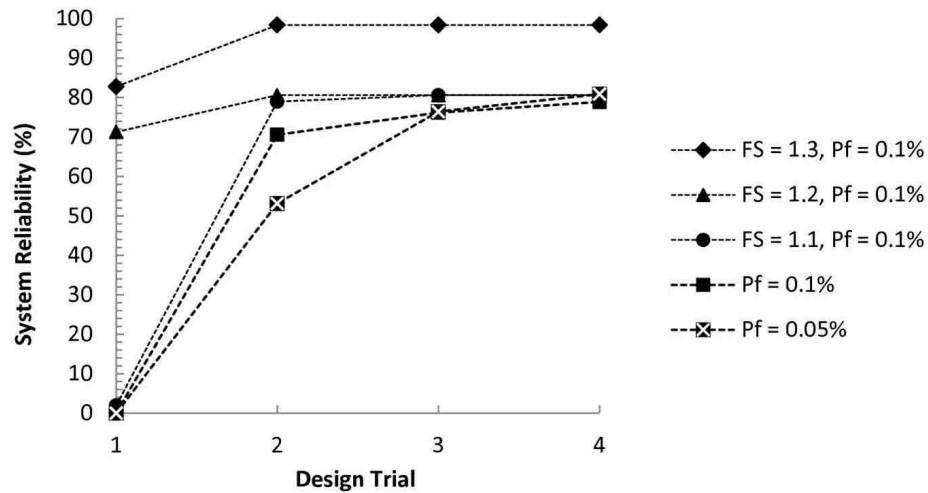


Figure 5.22: The usage/cost with probabilistic constraints only in Example 1

needed to arrive at the level of reliability that is close enough to the results obtained in case 1.2 and 1.1. As a result, though the computational efficiency is improved in every individual optimization trial, with more trials needed, the whole design process requires more computational efforts and becomes more time consuming.

When it is only the deterministic constraint that is taken into consideration as described by the following Equation 5.19,

$$\min f(\mathbf{d}, \mathbf{X}, \mathbf{P}) = \text{Cost} \quad (5.19a)$$

$$\text{sub. to: } f_{s, \min} \geq f_{s, \text{req}} \quad (5.19b)$$

$$T_a \in [3, 10] \text{ kN/m}, n \in [6, 12] \quad (5.19c)$$

computational efficiency is supposed to be improved mainly due to the elimination of the embedded probabilistic analyses that are to be performed on the basis of the two critical

Table 5.12: The RBO design with probabilistic constraints only in Example 1 ($p_{f_{\text{internal}}} = 0.1\%$)

Trial	RBO Results		Pri. Control	Slope Stability Analyses								
	No. layer			Failure	Critical det.		Critical pro.		Total p_f (%)	System p_f	System R_s	
	T_a (kN/m)		f_s		p_f (%)	f_s	p_f (%)					
1	7		$p_{f_{\text{det},i}} = 0.1\%$	Internal	0.966	66.530	0.966	66.530	100	100%	0%	
	3.30				$p_{f_{\text{pro},i}} = 0.1\%$	Compound	1.307	0.400				1.315
	43.42		Deep	1.262			0.148	1.280	0.181			3.486
	57.50			Face wrap			YES					
2	7		$p_{f_{\text{det},i}} = 0.1\%$	Internal	1.198	0.470	1.206	0.581	12.993	29.43%	70.57%	
	7.18				$p_{f_{\text{pro},i}} = 0.1\%$	Compound	1.333	0.257				1.336
	43.42		Deep	1.262			0.148	1.280	0.181			3.486
	65.42			Face wrap			YES					
3	12		$p_{f_{\text{pro},i}} = 0.1\%$	Internal	1.213	0.229	1.217	0.346	5.098	23.72%	76.28%	
	4.4				Compound	1.334	0.273	1.334				0.273
	48.64			Deep		1.262	0.148	1.280	0.181			3.486
	66.92					Face wrap	NO					
4	7		$p_{f_{\text{det},i}} = 0.1\%$	Internal	1.241	0.104	1.249	0.122	3.957	21.11%	78.89%	
	7.99				Compound	1.325	0.316	1.325				0.316
	43.42			Deep		1.262	0.148	1.280	0.181			3.484
	67.08					Face wrap	YES					

internal failure surfaces. When the required factor of safety is 1.3, the optimal results can be hardly influenced since the deterministic constraint works as the primary control factor in both cases. When the required factor of safety is 1.2 and 1.1, the second optimization trial always leads to a result that is similar to the initial design. It is because when both deterministic and probabilistic constraints are taken into consideration, in the second optimization trial, the optimal result is primarily driven by the probabilistic constraints; however, with only the deterministic constraint involved, the initial design has successfully met the constraint; thereby, with identical required factor of safety assigned in the deterministic constraint, same results are given in the second optimization trial.

In summary, in the case that has only the probabilistic constraints taken into consideration, if the target probability of failure is small enough, it is supposed to provide an acceptable design; however, the design efficiency is not as good as in the case that both deterministic and probabilistic constraints are involved while the required factor of safety is reasonably high. In the case that has only the deterministic constraint considered, if the required factor of safety is not sufficiently high, the design process is unable to provide an acceptable design since the optimal results are always identical to the initial design. However, prior to the RBO design, it is hard to identify whether the required factor of safety is high enough or the target probability of failure is sufficiently small corresponding to the upper and lower bounds assigned to the design variables. Therefore, it is more reasonable to perform the RBO design on the basis of both deterministic and probabilistic constraints.

5.4.2. Numerical Example 2: Geogrid Reinforced Embankment Slope. As stated in Section 3.5.2, it is required to reinforce a 30-ft high, 1H:1V embankment slope by placing geosynthetic reinforcements inside. The engineering properties of both embankment fill and foundation soil have been presented in Table 3.9 along with their prob-

Table 5.13: The RBO design with probabilistic constraints only in Example 1 ($p_{f_{\text{internal}}} = 0.05\%$)

Trial	RBO Results		Pri. Control	Slope Stability Analyses							
	No. layer			Failure	Critical det.		Critical pro.		Total p_f (%)	System p_f	System R_s
	T_a (kN/m)		f_s		p_f (%)	f_s	p_f (%)				
1	7		$p_{f_{\text{det},i}} = 0.05\%$	Internal	0.972	64.410	0.972	64.410	100	100%	0%
	3.40										
	43.42		$p_{f_{\text{pro},i}} = 0.05\%$	Compound	1.300	0.606	1.300	0.606	27.379		
	57.60			Deep	1.262	0.148	1.280	0.181	3.486		
	YES										
2	7		$p_{f_{\text{det},i}} = 0.05\%$	Internal	1.177	0.987	1.181	1.181	33.426	46.84%	53.16%
	6.80										
	43.42		$p_{f_{\text{pro},i}} = 0.05\%$	Compound	1.319	0.375	1.319	0.375	17.257		
	64.65			Deep	1.262	0.148	1.280	0.181	3.486		
	YES										
3	12		$p_{f_{\text{pro},i}} = 0.05\%$	Internal	1.224	0.207	1.231	0.234	4.703	23.56%	76.44%
	4.52										
	48.64			Compound	1.334	0.248	1.334	0.248	16.990		
	67.19			Deep	1.262	0.148	1.280	0.181	3.486		
	NO										
4	7		$p_{f_{\text{det},i}} = 0.05\%$	Internal	1.258	0.046	1.377	0.076	2.213	19.13%	80.87%
	8.33										
	43.42			Compound	1.327	0.300	1.327	0.300	14.325		
	67.77			Deep	1.262	0.148	1.280	0.181	3.484		
	YES										

abilistic characteristics. Provided the given information, slope stability analyses are first performed on the original unreinforced slope to identify the critical slip surfaces and the critical zone to be reinforced. With a required factor of safety set as 1.5, the critical zone is enveloped by a circular slip surface (2) and a wedge-shaped sliding surface (3) with a 45-degree inclined back-face and a 30.3-ft long bottom width as shown in Figure 5.23. The critical rotational slip surfaces are identical in both deterministic and probabilistic analyses, located at a shallow position close to the slope face and passing through the slope toe with a factor of safety that is only 0.590 and a 100% probability of failure. To maintain the slope stability, such an unreinforced slope needs to be reinforced by placing geosynthetic layers inside.

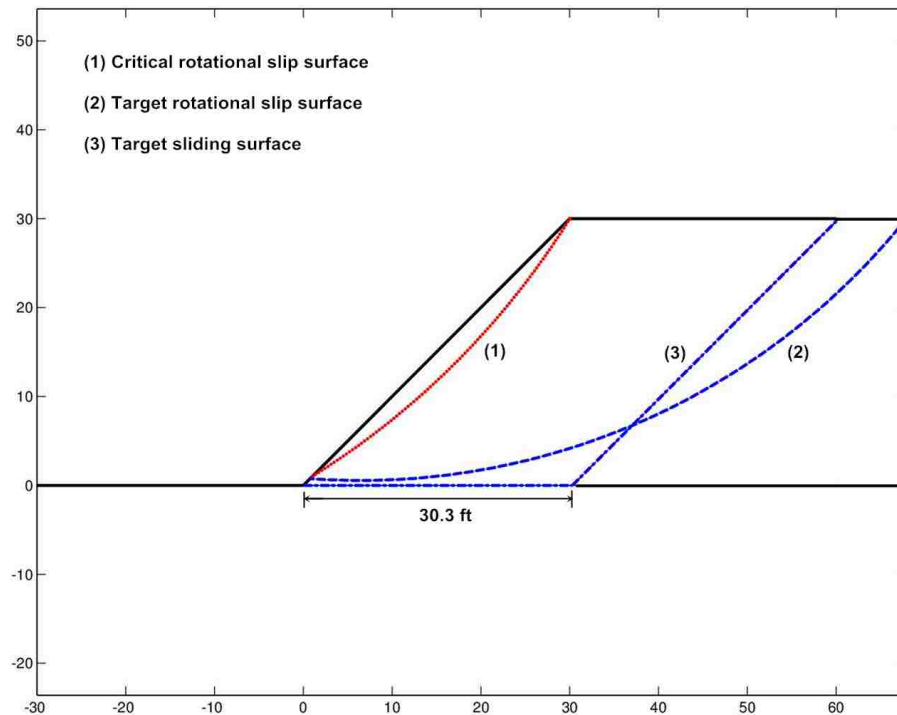


Figure 5.23: Slope stability analyses on the original unreinforced slope in Example 2

5.4.2.1. Design factors and requirements. If geogrids are supposed to be used as the reinforcements in this embankment slope, the strength reduction factors are assumed identical to the ones assigned in the previous numerical example in Section 5.4.1.1. To estimate the unit price of the potential geogrid products, the cost function presented in Figure 5.7 is embedded herein as

$$c_{\text{geogrids}} = (3 \times 10^{-9}) T_{\text{ult}}^2 - (4 \times 10^{-6}) T_{\text{ult}} + 0.1363 \quad (5.20)$$

where T_{ult} is the ultimate tensile strength of geogrids, in lb/ft; and c_{geogrids} is the corresponding unit price, in \$/ft². Since the embankment slope is 30-ft high (> 20 ft), according to the design recommendations stated in Section 5.3.2.1.1, the slope is divided into three reinforcement zones with a total of 6 design variables involved as: $\mathbf{d} = \{n_1, T_{a1}, n_2, T_{a2}, n_3, T_{a3}\}$, where: 1) $n_1 \in [3, 6]$ and $T_{a1} \in [2000, 3000]$ lb/ft, for the bottom zone; 2) $n_2 \in [3, 5]$ and $T_{a2} \in [1600, 2000]$ lb/ft, for the middle zone; and 3) $n_3 \in [1, 5]$ and $T_{a3} \in [1000, 1500]$ lb/ft, for the top zone. Since the required factor of safety is specified as 1.5 in this example, the target probability of failure can be accordingly assigned with a lower value as 0.01% in the probabilistic constraints. Meanwhile, the target level of reliability can be reasonably increased to a higher level; for instance, the total probability of failure should be no greater than 1% corresponding to every potential failure mode; and the system reliability should be no less than 97%. As a conclusion, the optimization problem can be described

by modifying the general formation stated by Equation 5.12 as follows

$$\min f(\mathbf{d}, \mathbf{X}, \mathbf{P}) = \text{Cost} \quad (5.21a)$$

$$\text{sub. to: } f_{s, \min} \geq f_{s, \text{req}} = 1.5 \quad (5.21b)$$

$$p_{f_{\text{det},i}} = P \{g_{\text{internal,det}}(\mathbf{d}, \mathbf{X}, \mathbf{P}) \leq 0\} \leq p_{f_{\text{cri, internal}}} = 0.01\% \quad (5.21c)$$

$$p_{f_{\text{pro},i}} = P \{g_{\text{internal,pro}}(\mathbf{d}, \mathbf{X}, \mathbf{P}) \leq 0\} \leq p_{f_{\text{cri, internal}}} = 0.01\% \quad (5.21d)$$

$$T_{a1} \in [2000, 3000] \text{ lb/ft}, n_1 \in [3, 6] \quad (5.21e)$$

$$T_{a2} \in [1600, 2000] \text{ lb/ft}, n_2 \in [3, 5] \quad (5.21f)$$

$$T_{a3} \in [1000, 1500] \text{ lb/ft}, n_3 \in [1, 5] \quad (5.21g)$$

along with the design requirements summarized in the following Table 5.14.

Table 5.14: The RBO design requirements in Example 2

Deterministic	$f_{s, \min} \geq 1.5$	
Probabilistic	Total Internal, $p_{f_{\text{internal}}}$	$\leq 1\%$
	Total Compound, $p_{f_{\text{compound}}}$	$\leq 1\%$
	Total Deep-Seated, $p_{f_{\text{deep}}}$	$\leq 1\%$
	Total Sliding, $p_{f_{\text{sliding}}}$	$\leq 1\%$
	System Reliability, R_{system}	$\geq 97\%$

5.4.2.2. Design process and results. With the required factor of safety equal to 1.5 and the target probability of failure set as 0.01%, the reliability-based optimization is

first carried out based on the critical zone and the critical surfaces located in the original unreinforced slope (Figure 5.23); and has the initial optimal design derived as: 6 layers of primary reinforcements uniformly distributed in the bottom zone that has the allowable tensile strength obtained as 2291 lb/ft; 4 layers of primary reinforcements in the middle zone that has the allowable tensile strength obtained as 1737 lb/ft; and 3 layers of primary reinforcements in the top zone that has the allowable tensile strength equal to 1349 lb/ft. No secondary reinforcements are placed inside; and the reinforcement layers are distributed close enough so that it is not needed to wrap the slope face. As shown in Figure 5.24, the reinforcements are all extended to the limits of the critical zone with the length obtained as 30.30, 30.30, 30.30, 30.30, 31.89, 33.86, 35.67, 36.93, 37.78, 38.29, 38.52, 38.51, and 38.30 ft from bottom to top layer. The cost and the usage of the geogrid reinforcements are consequently obtained as \$95.63 and 450.95 ft² per unit width of this cross section. Such an optimization guarantees a minimum factor of safety equal to 1.5 and has the probability of failure obtained as zero along the original critical surfaces addressed in the previous unreinforced slope. Therefore, the initial optimization is mainly driven by the deterministic constraint instead of the probabilistic constraints regarding the probability of failure along the critical internal failure surfaces. By performing a thorough slope stability analysis on the basis of the initial design, the critical surfaces are updated with the probabilistic results listed in Table 5.15. Having the total probability of failure obtained as 0.0033%, 0.4199%, and 0.2079% corresponding to internal, compound, and deep-seated failure mode, the initial design has already met the design requirements as stated in Table 5.14 with a system reliability derived as 99.37%. Furthermore, corresponding to the new critical internal failure surfaces located in the initial design (Figure 5.24), the probability of failure is derived as $1.013 \times 10^{-6}\%$ for the deterministic surface and 0.0010% for the probabilistic surface,

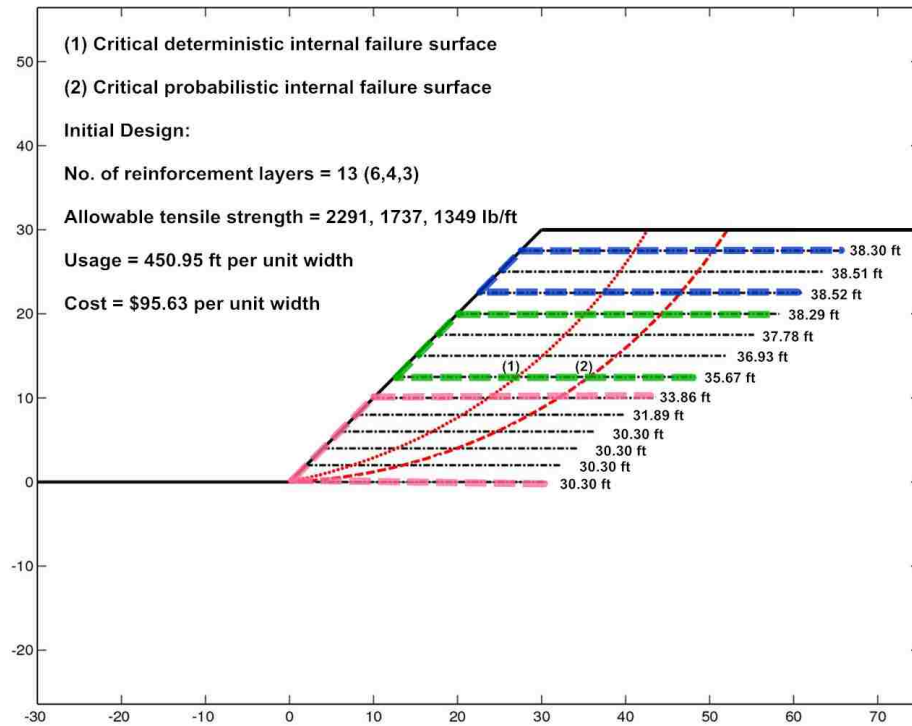


Figure 5.24: The initial design with $f_{s,req} = 1.5$, $p_{f,internal} = 0.01\%$ in Example 2

both of which are greatly lower than the target probability of failure specified in the probabilistic constraints as 0.01%. Therefore, no more optimization trial is needed; and the design process can be terminated with the initial optimal result.

When sliding stability is taken into consideration, provided the reinforced zone has a 30.3-ft long base width, the total probability of failure is derived as 32.12% that greatly exceeds the acceptable level of 1%. Therefore, as shown in Figure 5.25, the lower level of reinforcement layers (1st to 8th) are extended to a length of 37.00 ft to enhance the sliding stability; and the corresponding total probability of failure is significantly decreased to 0.7182%. Based on the modification, probabilistic results are slightly different along with the total probability of failure obtained as 0.0005%, 0.1515%, and 0.0203% corresponding to internal, compound, and deep-seated failure modes; and the system reliability is finally

derived as 99.11%. As a result, after the modification, it can be considered as the final optimal design, that has the total geogrid usage obtained as 487.40 ft and the corresponding cost as \$104.69 per unit width of this cross section.

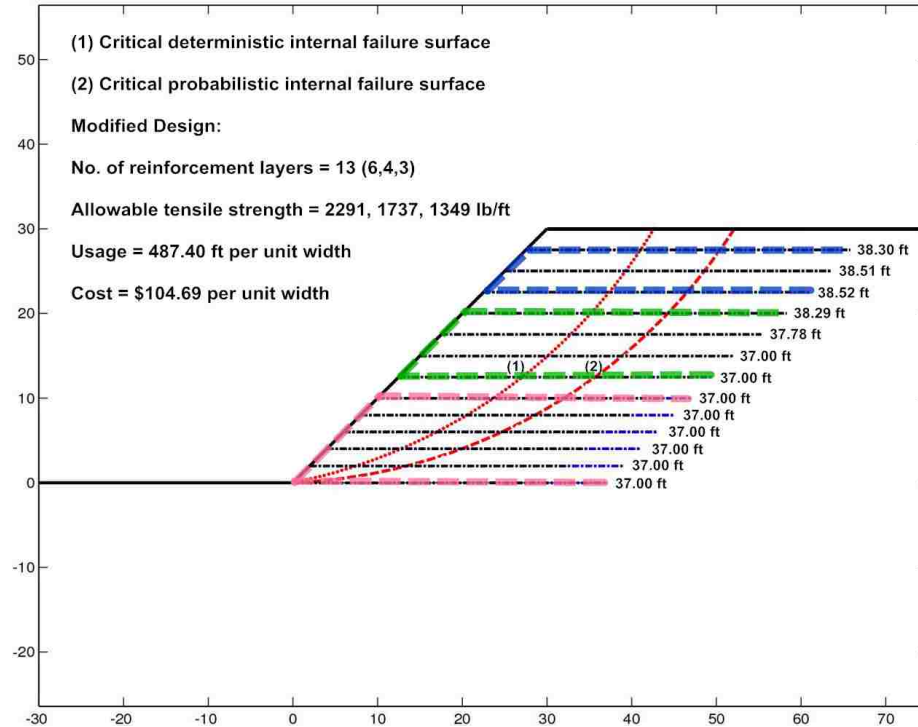


Figure 5.25: The modified design with $f_{s,req} = 1.5$, $p_{f_{internal}} = 0.01\%$ in Example 2

As shown in Table 5.15, when the required factor of safety is 1.5, the level of reliability is extremely high, that has the system reliability above 99% along with the probability of failure approaching zero along the critical surfaces. Therefore, it may worth it to seek an optimal design that has the system reliability around the same level but with a lower required factor of safety specified in the deterministic constraint that consequently leads to a lower reinforcement cost. As a comparison, the RBO design is performed with the required factor of safety lower to 1.3 and the target probability of failure increased to 0.1%,

Table 5.15: The RBO design in Example 2 ($f_{s,req} = 1.5$, $p_{f,internal} = 0.01\%$)

Trial	RBO Results		Slope Stability Analyses									
	No. layer	6,4,3	Failure	Critical det.		Critical pro.		Total p_f (%)	System p_f	System R_s		
T_a (lb/ft)	2291,1737,1349	f_s		p_f (%)	f_s	p_f (%)						
1	Usage (ft)	450.95	Internal	1.500	1.013E-6	1.661	0.0010	0.0033	0.630%	99.37%		
	Cost (\$)	95.63	Compound	1.554	0.0010	1.575	0.0077	0.4199				
	Face wrap	NO	Deep	1.525	0.0006	1.637	0.0007	0.2079				
	Final Design		Failure	Critical det.		Critical pro.		Total p_f (%)			System p_f	System R_s
	No. layer	6,4,3		f_s	p_f (%)	f_s	p_f (%)					
M	T_a (lb/ft)	2291,1737,1349	Internal	1.500	1.013E-6	1.661	0.0010	0.0005	0.889%	99.11%		
	Usage (ft)	487.40	Compound	1.669	9.221E-6	1.688	1.333E-5	0.1515				
	Cost (\$)	104.69	Deep	1.575	0.0004	1.637	0.0007	0.0203				
	Face wrap	NO	Sliding	1.902	0.0515	1.902	0.0515	0.7182				

Note: M - Modified optimal design

as described in the following Equation 5.22

$$\min f(\mathbf{d}, \mathbf{X}, \mathbf{P}) = \text{Cost} \quad (5.22a)$$

$$\text{sub. to: } f_{s, \min} \geq f_{s, \text{req}} = 1.3 \quad (5.22b)$$

$$p_{f_{\text{det},i}} = P \{g_{\text{internal,det}}(\mathbf{d}, \mathbf{X}, \mathbf{P}) \leq 0\} \leq p_{f_{\text{cri, internal}}} = 0.1\% \quad (5.22c)$$

$$p_{f_{\text{pro},i}} = P \{g_{\text{internal,pro}}(\mathbf{d}, \mathbf{X}, \mathbf{P}) \leq 0\} \leq p_{f_{\text{cri, internal}}} = 0.1\% \quad (5.22d)$$

$$T_{a1} \in [1600, 2400] \text{ lb/ft}, n_1 \in [3, 6] \quad (5.22e)$$

$$T_{a2} \in [1200, 1800] \text{ lb/ft}, n_2 \in [3, 5] \quad (5.22f)$$

$$T_{a3} \in [900, 1000] \text{ lb/ft}, n_3 \in [1, 5] \quad (5.22g)$$

where the upper and the lower bounds with respect to the design variables are correspondingly modified. The optimal results are listed in Table 5.16, where 5 layers of primary reinforcements are uniformly distributed in the bottom zone with the allowable tensile strength equal to 1788 lb/ft; 4 layers in the middle zone with the allowable tensile strength equal to 1458 lb/ft; and 3 layers in the top zone with the allowable tensile strength equal to 991 lb/ft. If the reinforcement layers are all extended to the limits of the critical zone, the total probability of failure is consequently obtained as 0.9027%, 0.3264%, and 0.2079% corresponding to internal, compound, and deep-seated failure; meanwhile, the system reliability is derived as 98.57% considering the above three failure modes. When sliding stability is taken into consideration, as shown in Figure 5.26, the lower reinforcement layers (1st to 7th) are extended beyond the critical zone with a length of 37.00-ft to enhance the sliding stability and decrease the corresponding total probability of failure to the acceptable level.

Therefore, based on the modification made on the reinforcement lengths, the final optimal design is derived with a total usage of 450.40-ft and a total cost of \$81.08 per unit width of this cross section. Compared to the results obtained in the previous case with the required

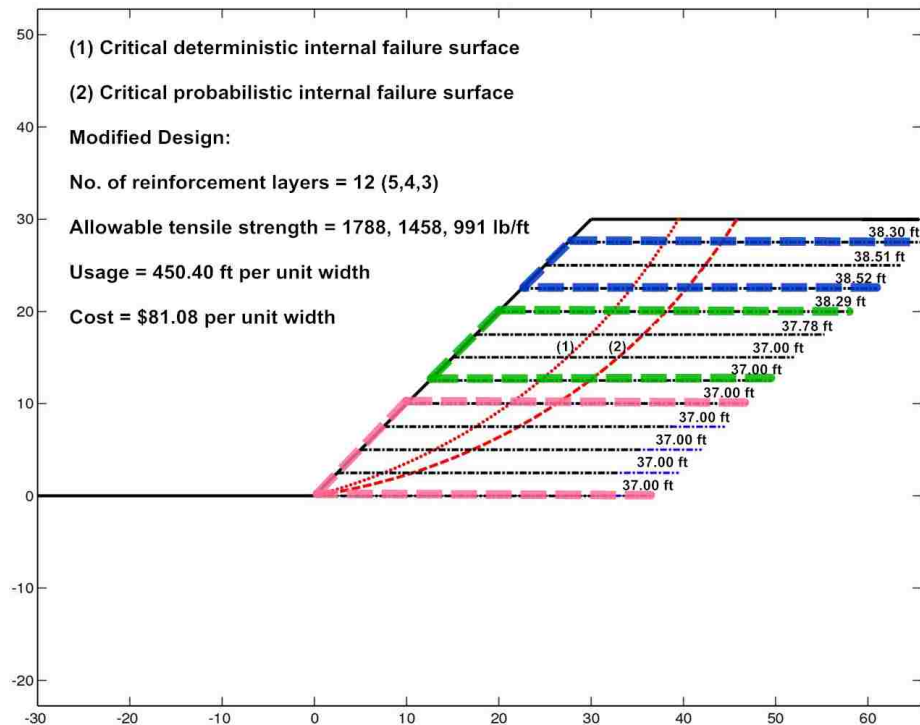


Figure 5.26: The modified design with $f_{s,req} = 1.3$, $p_{f_{internal}} = 0.1\%$ in Example 2

factor of safety specified as 1.5 (case 1.5), the system reliability is derived as 98.23% with a required factor of safety set as 1.3 (case 1.3), that is approximately 0.88% lower than the value obtained in case 1.5; while the total usage of the geogrids is decreased by 37-ft per unit width, and the total cost is correspondingly reduced from \$104.69 to \$81.08 with a set of lower allowable tensile strengths obtained in the optimization. Therefore, with a required factor of safety reasonably decreased from 1.5 to 1.3, the level of reliability is slightly influenced, but the reduction in the total cost is significant.

Table 5.16: The RBO design in Example 2 ($f_{s,req} = 1.3$, $p_{f,internal} = 0.1\%$)

Trial	RBO Results		Slope Stability Analyses									
	No. layer	5,4,3	Failure	Critical det.		Critical pro.		Total p_f (%)	System p_f	System R_s		
T_a (lb/ft)	1788,1458,991	f_s		p_f (%)	f_s	p_f (%)						
1	Usage (ft)	420.06	Internal	1.300	0.0205	1.326	0.0682	0.9027	1.432%	98.57%		
	Cost (\$)	75.01	Compound	1.440	0.0018	1.490	0.0131	0.3264				
	Face wrap	NO	Deep	1.525	0.0006	1.637	0.0007	0.2079				
	Final Design		Failure	Critical det.		Critical pro.		Total p_f (%)			System p_f	System R_s
	No. layer	5,4,3		f_s	p_f (%)	f_s	p_f (%)					
M	T_a (lb/ft)	1788,1458,991	Internal	1.300	0.0205	1.326	0.0682	0.9365	1.766 %	98.23 %		
	Usage (ft)	450.40	Compound	1.624	0.0002	1.679	0.0016	0.1006				
	Cost (\$)	81.08	Deep	1.575	0.0004	1.637	0.0007	0.0203				
	Face wrap	NO	Sliding	1.902	0.0515	1.902	0.0515	0.7182				

Note: M - Modified optimal design

5.4.3. Discussion. Compared to the traditional design procedure for geosynthetic reinforced embankment slopes, the proposed reliability-based optimization design framework has three primary advantages as demonstrated in Table 5.1. That is, in summary, it enables an optimal design that guarantees a lower cost regarding the geosynthetic reinforcements; meanwhile, the technical design requirements are fully satisfied in both deterministic and probabilistic aspects.

As discussed in Section 5.2, the critical deterministic rotational slip surface located in the original unreinforced slope is traditionally the only reference design surface used to determine the reinforcement length and the resistance force that needs to be provided by the reinforcements to maintain the slope stability. However, from the above two numerical examples, it is shown that the critical surfaces in a reinforced slope are probably changing with the reinforcement design. For instance, in example 1, the critical internal failure surfaces obtained in the initial design (Figure 5.10) are different from the original critical surfaces located in the unreinforced slope (Figure 5.9); and are continuously updated according to the second design (Figure 5.11). Similarly, in example 2, the same observation can be made for the critical surfaces as illustrated in Figure 5.23, 5.24, and 5.25. As a conclusion, though the initial design enables the factors of safety along the original critical surfaces above the required value, a new critical deterministic surface is most likely to be generated at a different position with a minimum factor of safety which can be probably lower than the acceptable level. Therefore, with a predetermined critical deterministic surface used as the only reference design surface in the traditional procedure, it may lead to an unacceptable design that fails to meet the design requirements. But with the proposed RBO design framework, such a problem can be successfully resolved since the optimiza-

tion yields to the deterministic constraint where the required factor of safety is specified. More specifically, a thorough deterministic slope stability analysis is carried out with every GA generation during the optimization to search for the new critical deterministic surface along with the minimum factor of safety. In other words, the proposed RBO design is performed on a 'flexible' critical deterministic surface that varies with the reinforcement design. Therefore, through performing the proposed RBO procedure, an optimal design is always guaranteed that has a minimum factor of safety no less than the required value.

If we take a look at the two numerical examples presented in the previous chapter regarding the reliability-based slope stability analysis in Section 3.5, both of the reinforced slopes are originally designed following the traditional procedure (Elias et al. 2001). In example 1 (Section 3.5.1), to achieve the design factor of safety specified as 1.3, 12 layers of geotextile reinforcements are uniformly distributed throughout the embankment slope with an identical allowable tensile strength equal to 4.14 kN/m. However, as previously discussed, the traditional design is developed on the basis of the critical surfaces addressed within the original unreinforced slope. After placing geotextile reinforcement layers inside of the embankment, a new critical deterministic internal failure surface is generated along with a minimum factor of safety derived as 1.188, which is lower than the required value. On the other hand, it indicates the resistance force provided by the current reinforcements is not enough. To enhance the slope stability, modification can be made by either placing more reinforcement layers inside or increasing the tensile strength of the reinforcements. Therefore, the problem still exists as how many layers are needed and how strong the reinforcements should be; and is supposed to be even more complicated when both soil variability and economic benefits regarding the reinforcement design are taken into consideration. In general, through performing the proposed RBO design procedure, the preceding

problems can be automatically resolved provided reasonable upper and lower bounds are assigned to the design variables. As for example 1, with a required factor of safety set as 1.3 and a target probability of failure specified as 0.1%, the final optimal result is given by 7 layers or primary reinforcements uniformly distributed throughout the embankment slope with an identical allowable tensile strength equal to 9.14 kN/m, based on which the minimum factor of safety is exactly equal to the required value as 1.3; and the system reliability is obtained as 97.79%, approximately 60% higher than the level of reliability corresponding to the traditional design. As previously mentioned in Section 5.4.1.3.2, with a required factor of safety specified as 1.3, the optimal design is primarily controlled by the deterministic constraint instead of the probabilistic constraints; in other words, it is indicated such a required factor of safety is sufficiently high corresponding to this example so that the probability of failure along the two critical internal failure surfaces are both lower than the target value specified in the probabilistic constraints. Therefore, one could repeat the traditional design procedure with different values assigned to the design variables until the minimum factor of safety arrives at the required level, meanwhile, the system reliability meets the target level of reliability. As previously demonstrated in Section 3.5, the critical internal failure surfaces are probably located at different positions in deterministic and probabilistic analysis, where the probabilistic surface is always situated deeper than the deterministic one; and thereby, the reinforcements designed based on the probabilistic surface should be accordingly longer. Since the traditional procedure is always carried out based on the deterministic surface without considering soil variability, some reinforcement layers may not be long enough. And thereby, the total probability of failure regarding the compound failure is relatively high and exceeds the acceptable level, just as what happened in the initial design in case 1.3 as illustrated in Section 5.4.1.3.1. As

a result, though it is possible to make the minimum factor of safety arrive at the required level by repeating the traditional design procedure with various design alternatives, it may still fail to guarantee the slope reliability above the target level.

Provided the technical design requirements are satisfied in both deterministic and probabilistic aspects, economic benefits becomes an important factor that influences the reinforcement design. In the proposed RBO procedure, the total cost corresponding to geosynthetic reinforcements is considered as the objective function; and is minimized through the optimization. As previously demonstrated in Section 5.4.1.4, in general, a higher required factor of safety and a lower target probability of failure tends to achieve a higher cost. However, if the optimization is mainly controlled by the deterministic constraint, the cost can be hardly influenced by the target probability of failure specified in the probabilistic constraints; vice versa, the cost is affected mainly due to the target probability of failure when the probabilistic constraints work as the primary control factor. Furthermore, in view of the distribution model assigned to the random variables, as discussed in Section 5.4.1.4.3, with the same reinforcement design, log-normal distributions tend to provide a lower probability of failure; in other words, a lower allowable tensile strength is supposed to be derived with the target probability of failure fixed at a constant level. Therefore, the total cost in the case of log-normal distribution is slightly lower than the amount obtained in the case of normal distribution. Similarly, when the correlation coefficient is taken into consideration, as previously discussed in Section 3.5.3, the system reliability increases when the correlation coefficient between friction angle and soil unit weight changes from 0 to 1. Therefore, it is reasonable to believe with a target probability of failure fixed at a constant level, a lower allowable tensile strength is supposed to be derived with a higher correlation coefficient assigned between the random variables. As

a conclusion, the total cost obtained with correlated random variables is supposed to be lower than the amount obtained with uncorrelated random variables; and tends to decrease with the increase of the correlation coefficient of soil properties for the embankment fill and the foundation soil.

Compared to the conventional way that seeks an optimal design by manually repeating the design process with various design alternatives, the proposed RBO design framework is more systematic, effective, and efficient especially when a large number of design variables are involved. For instance, in example 1, two design variables are involved, including the number of reinforcement layers and the corresponding allowable tensile strength. Assuming the number of potential alternatives as n_1 and n_T respectively for the above two design variables, the traditional design procedure needs to be repeated by a total of $(n_1 \times n_T)$ times to address an optimal result. However, in example 2, there are three reinforcement zones along with six design variables involved in total, including: the number of reinforcement layers and the corresponding allowable tensile strength in each reinforced zone. Assuming the number of potential alternatives as: n_{11} and n_{T1} for the bottom zone; n_{12} and n_{T2} for the middle zone; and n_{13} and n_{T3} for the top zone, the number of trials that are needed to obtain the optimal result is significantly increased to $(n_{11} \times n_{T1} \times n_{12} \times n_{T2} \times n_{13} \times n_{T3})$. Therefore, to enhance design efficiency, the number of design alternatives may need to be reduced; but meanwhile, the ‘best’ optimal result can be probably missed. To be more specific, for example, if the required factor of safety is specified as 1.3, with limited number of design alternatives involved in the optimization process, it is probably to address an ‘optimal’ design that provides a minimum factor of safety greatly higher than the required value, say 1.4; though the design still successfully meets the design requirements and has the lowest cost among the whole set of alternatives,

a better ‘optimal’ design seems available with a lower minimum factor of safety or even identical to the required value. To address such a better optimal result, more design alternatives are needed. In other words, to increase the optimization accuracy, the conventional design process can be very time consuming with a large amount of design alternatives involved, especially when the slope reliability is taken into consideration. As a comparison, through performing the proposed RBO procedure, as in example 1, when the required factor of safety is specified as 1.3, the deterministic requirement is always satisfied with a minimum factor of safety exactly equal to the required value since the optimization is primarily controlled by the deterministic constraint. Similarly, in example 2, with a sufficiently large required factor of safety specified in the deterministic constraint, the minimum factor of safety obtained based on the final optimal design is identical the required value as well. On the other hand, if the probabilistic constraints are working as the primary control factor during the optimization, the probability of failure obtained along the critical internal failure surfaces are always equal to the target probability of failure specified in the probabilistic constraints. As a conclusion, provided the reasonable upper and lower bounds assigned to the design variables, the proposed RBO design framework is more advanced since it is able to address a ‘real’ optimal result which is bounded by the technical design requirements embedded in either deterministic or probabilistic constraints.

5.5. SUMMARY

The optimization design is traditionally performed by manually assigning various design alternatives to address an optimal solution with the lowest cost regarding the geosynthetic reinforcements. Compared to such a conventional way, the proposed RBO design procedure is more systematic and effective. It is able to maximize the economic

benefits regarding the geosynthetic reinforcement design, meanwhile, enables the technical design requirements successfully satisfied in either deterministic or probabilistic aspect. Furthermore, since the proposed reliability-based optimization design framework is developed based on the traditional design procedure stated in FHWA Mechanically Stabilized Earth Walls and Reinforced Soil Slopes Design & Construction Guidelines (Elias et al. 2001), it is convenient to apply in practical design of geosynthetic reinforced embankment slopes.

6. PROPOSED DESIGN FRAMEWORK AND PRACTICAL APPLICATION

6.1. OVERVIEW

Generally speaking, the proposed reliability-based optimization (RBO) design framework for geosynthetic reinforced embankment slopes (GRES) primarily incorporates: 1) traditional deterministic slope stability analysis, 2) reliability-based (probabilistic) slope stability analysis, and 3) reliability-based optimization. The applications of the preceding analyses and algorithms have been demonstrated in the previous chapters with two hypothetical numerical examples selected from FHWA Mechanically Stabilized Earth Walls and Reinforced Soil Slopes Design & Construction Guidelines (Elias et al. 2001) and Mirafi Geosynthetics for Soil Reinforcement Design Manual, respectively. To further discuss how the proposed design framework can be applied in practical, a case study is carried out in this chapter on a practical engineering project: the design of the expansion of the Cherry Island Landfill, Delaware. The landfill expansion involves the installation of pre-fabricated vertical drains (PVDs) and the construction of a mechanically stabilized earth (MSE) berm over very soft river sediments and dredged materials (Houlihan et al. 2010). In the project, the MSE berm plays a dual role, compressing and consolidating foundation soils while providing new disposal space. It was designed to be constructed with a steep outer slope (1H:3V), to achieve which geosynthetic reinforcement techniques were required. Therefore, the proposed design framework is mainly emphasized on the design of the geosynthetic reinforcements in the MSE berm for the landfill expansion.

6.2. PROPOSED FRAMEWORK

The proposed reliability-based optimization design framework is developed on the basis of the traditional deterministic design procedure as stated in FHWA Mechani-

cally Stabilized Earth Walls and Reinforced Soil Slopes Design & Construction Guidelines (Elias et al. 2001). Implemented with probabilistic analysis and reliability-based optimization technique, the whole design framework is summarized in Figure 6.1, wherein:

- In step 1, provided well-defined geometric and loading requirements, performance requirements are established from both deterministic and probabilistic perspectives, including: 1) the required factor of safety against internal, compound, deep-seated, and sliding failure; 2) the maximum allowable total probability of failure regarding internal, compound, deep-seated, and sliding failure; and 3) the acceptable level of system reliability in view of the preceding multiple failure modes.
- In step 2 and 3, the engineering properties of both in-situ soils and embankment fills are determined. Conventionally, the general engineering properties are usually taken as the average properties based on field exploration and lab testing. But from a reliability perspective, probabilistic characteristics are needed as well, including: 1) distribution model; 2) probabilistic parameters (i.e., standard deviation); and 3) the correlation between random variables. As for the in-situ soils (i.e., foundation soils), evaluation can be generally made of the amount data that would be needed to characterize the subsurface conditions with a reasonably high degree of accuracy (Houlihan et al. 2010). Increasing the number of tests increases the confidence that the range of possible values has been determined and also increases the confidence that the standard deviation on the mean is accurate (Baecher and Christian 2003; Houlihan et al. 2010). But for the embankment fills (i.e., reinforced and retained fills), since the embankment hasn't been built during the design stage, the range of the possible values and the standard deviations of their engineering properties can be hard to obtain through field exploration or lab testing. In this situation,

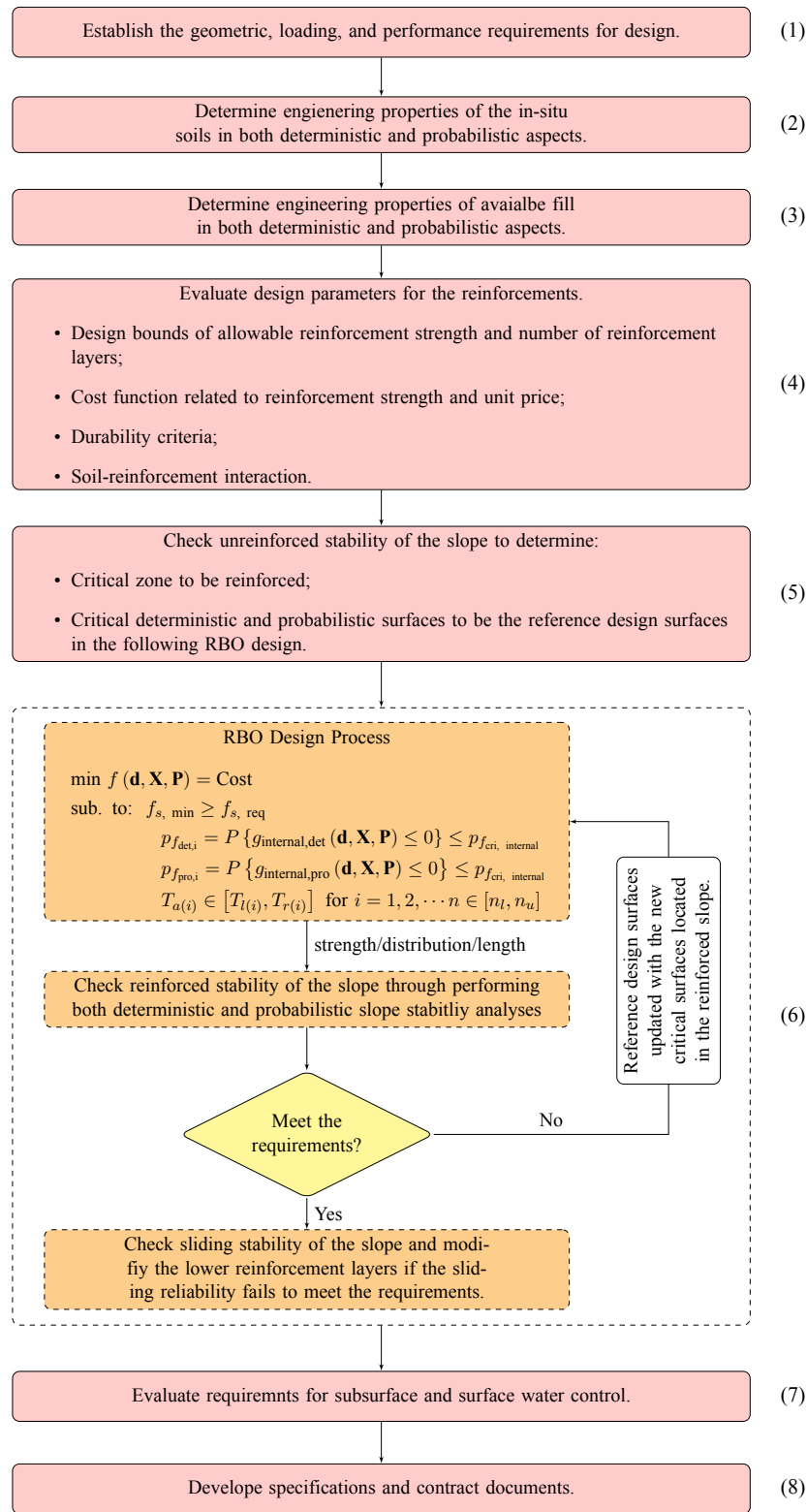


Figure 6.1: The proposed RBO design framework for GRES system

estimations have to be made based on available fills.

- In step 4, referring to the technical design requirements stated in Section 5.3.2.1 and current design manual (Elias et al. 2001), the design variables are defined, including: 1) how many reinforcement zones are needed according to the slope height; and thereby, how many design variables are to be involved; 2) the upper and lower bounds of the design variables, that mainly include the allowable reinforcement strength and the number of reinforcement layers; if multiple reinforcement zones exist, the design bounds need to be assigned separately in each zone; and 3) the cost function related to the reinforcement strength and the corresponding unit price.
- In step 5, a thorough slope stability analysis from both deterministic and probabilistic perspectives is first carried out on the unreinforced slope to determine the critical zone to be reinforced as well as the critical surfaces that are to be used as the reference design surfaces in the following optimization design process.
- In step 6, reliability-based optimization is accordingly performed on the basis of the critical surfaces located in the original unreinforced slope, followed by a thorough slope stability analysis performed on the optimal solution to check whether the reinforced slope meets the performance requirements established at the beginning. If the requirements are successfully satisfied, sliding stability is to be further checked especially from the probabilistic perspective; otherwise, the RBO is to be repeated with the new critical surfaces updated in the reinforced slope along with the optimized reinforcement design until the performance requirements are finally satisfied.
- In step 7 and 8, the requirements for subsurface and surface water control are evaluated. And the specifications and contract documents are finally developed.

6.3. CASE STUDY: CHERRY ISLAND LANDFILL

Cherry Island Landfill (CIL), owned and operated by Delaware Solid Waste Authority (DSWA), has been used for municipal solid-waste (MSW) disposal since 1985. Built on an old dredge disposal site at the confluence of the Delaware and Christina rivers in Wilmington, DE., the subsurface conditions at the site of the landfill consist of extremely soft, compressible materials. By the early 2000s, the Cherry Island Landfill was nearing its waste capacity and the DSWA needed to develop a plan to extend the life of the landfill. However, as shown in Figure 6.2, the original landfill was geographically confined by the Delaware River on the east, the Christina River on the south, Interstate 495 to the west, and by dredge lagoons to the north, so horizontal land expansion of the facility was not an option. The only option to increase the waste capacity of the landfill was a vertical expan-

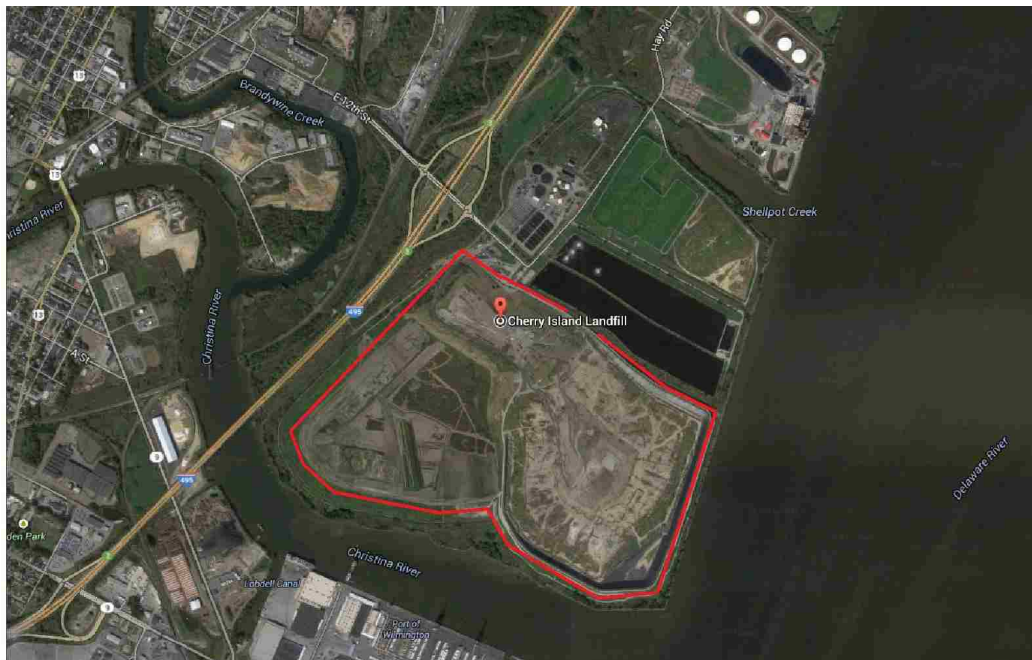


Figure 6.2: The location of Cherry Island Landfill

sion. As a result, in order to expand vertically, significant ground improvement measures and reinforcement techniques would be required (Houlihan et al. 2010; Bygness 2012).

6.3.1. Project Description. Generally speaking, the expansion project was to increase the disposal capacity of the landfill by raising the height of the waste by approximately 70-ft while providing the required stability (Houlihan et al. 2010). Considering the soft subgrade at the site of the landfill, the expansion work primarily includes the installation of prefabricated vertical ‘wick’ drains in the foundation soils of the disposal area to accelerate consolidation and soil strength gain; and the construction of a MSE berm, having heights ranging from 30 to 60 ft. The wick drains and MSE berm are both to be constructed around the perimeter of Phases III, IV, and V, as shown in Figure 6.3, and will have a length of over 8,000 ft (Houlihan et al. 2010). The purpose of the perimeter MSE berm were to 1) consolidate, and thus increase the shear strength of the foundation soils; and 2) counterbalance the lateral load caused by the waste in the landfill (Houlihan

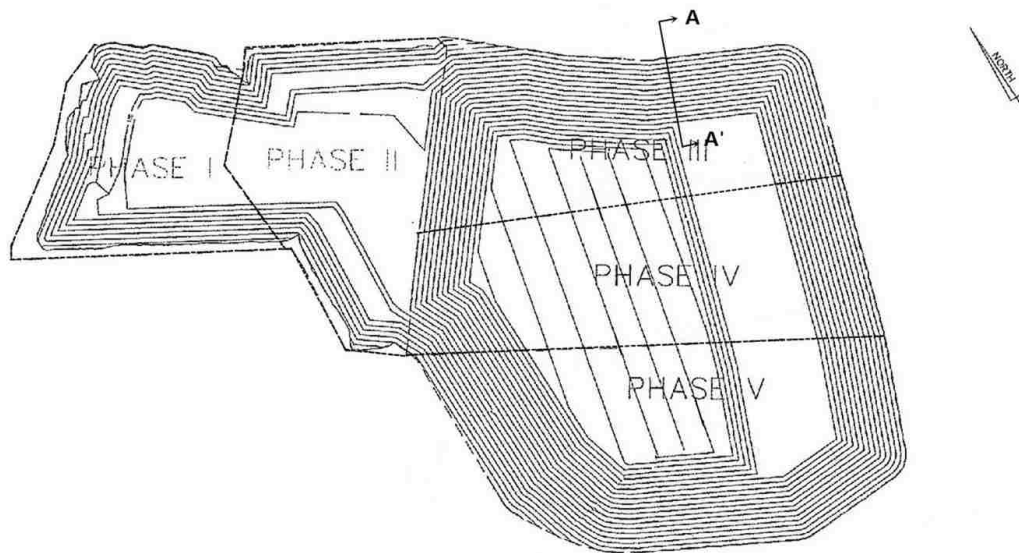
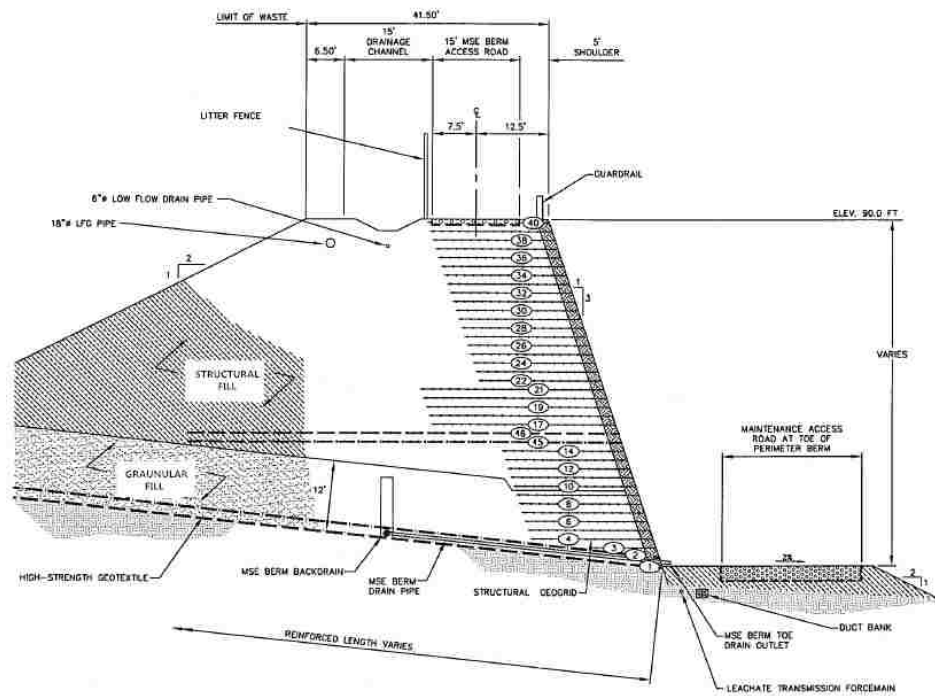


Figure 6.3: Plan view of Cherry Island Landfill, adapted from Houlihan et al. (2010)

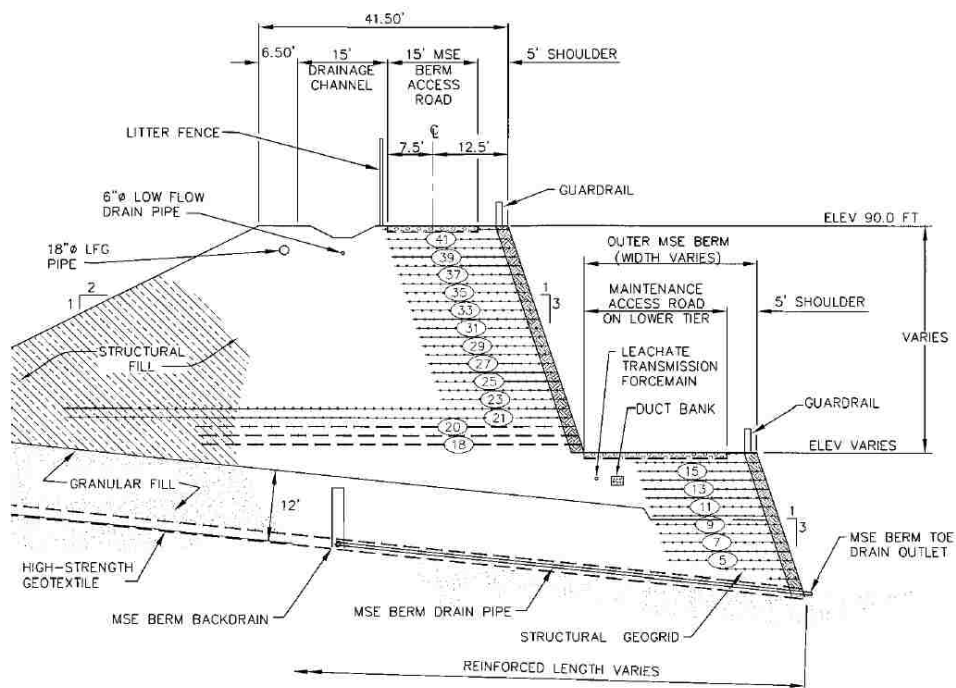
et al. 2010). Therefore, to maximize the strength gain in the foundation and because of the horizontal space constraints, the berm was designed to be constructed having a steep outer slope (1H:3V), and a mild internal slope (2H:1V). From the perspective of both cost-effective and construction friendly, to maintain the stability of the berm, high-performance geosynthetic materials were selected for reinforcement.

6.3.2. Current MSE Berm Design. As shown in Figure 6.4, the current design of the MSE berm has high-strength polyester geotextile reinforcements installed at the base of the berm with drainage sand to provide quality backfill and allows water to drain from the PVDs. The bottom two layers of reinforcement played an extremely important role in providing stability to the reinforced berm. As concluded in Table 6.1, these two layers consisted of TenCate Mirafi® PET1170 geotextile that has an extremely high ultimate strength equal to 1,170 kN/m (80,000 lb/ft); and extended to a deep position with an embedment length of 140-ft. At the mid-height of the berm, two additional long embedment lengths of the high-strength Mirafi® PET1170 geotextile were used for additional stability. The remainder of the berm was constructed using TenCate Miragrid® 20XT polyester geogrids with the embedment lengths ranging from 20 to 80-ft. The face detail consisted of L-shaped wire baskets acting as a form for fill placement and woven polypropylene small-aperture geogrid (TenCate Miramesh® GR) wrapped around the slope face for stability and erosion control (Bygness 2012).

In summary, over 380,000 square yards of Mirafi® PET1170, 670,000 square yards of Miragrid® 20XT, and 315,000 square yards of Miramesh® GR were required to construct the MSE berm with the heights of 60 to 70 feet and a total perimeter length of approximately 8,700 feet (Houlihan et al. 2010; Bygness 2012).



(a) Single-tier MSE berm



(b) Two-tier MSE berm

Figure 6.4: Geometry and reinforcement scheme for MSE berm

Table 6.1: Geosynthetic products in the current MSE berm design in the CIL project

Type	T_{ult}	Usage	Detail
Mirafi® PET1170	1,170 kN/m (80,000 lb/ft)	380,000 yd ²	High-strength polyester geotextile placed at the base and mid-height of the berm for external stability.
Miragrid® 20XT	200 kN/m (13,705 lb/ft)	670,000 yd ²	Polyester geogrid placed within the berm for internal (local) stability.
Miramesh® GR	21 kN/m (1,440 lb/ft)	315,000 yd ²	Polypropylene geogrid for face treatment and erosion protection.

6.3.3. Proposed RBO Framework in MSE Berm Design. In view of the large amount of geosynthetic reinforcement needed in the expansion project, significant economic benefits can be gained by optimizing the reinforcement design for the perimeter MSE berm. The proposed RBO design framework can be applied to modify the reinforcement design in the preceding MSE berm with an objective to optimize the geosynthetic cost while providing the required stability and reliability.

6.3.3.1. Sections for analysis. As illustrated in Figure 6.4, two typical MSE berm schemes are involved: (1) single tier; or (2) two-stepped tiers. A total of eight sections located in Phases III through V were selected for both design and analysis in consideration of the unique features of landfill geometry (e.g., maximum height, bench location), foundation stratigraphy (e.g., thickness of dredge/alluvium, thickness of the Potomac Formation), and the other subsurface features such as the distance to the river and wetlands. As mentioned in Section 5.3.2.2, among the multiple failure modes that may potentially occur in a GRES system, it is only the internal failure that has the failure surface passing all the

reinforcement layers. In other words, the internal failure mode is considered the most significant influence on the reinforcement design. Based on the ground improvements in the foundation soils and the high-strength geotextiles installed at the base of the berm, the design of the geosynthetic reinforcements inside of the MSE berm can be emphasized on the local stability that primarily occurs within the berm and is highly dependent on berm geometry. Therefore, due to the maximum MSE berm height of 60 ft, section A-A' with a single-tier geometry is selected as the most critical section to be designed and analyzed in the following case study by implementing the proposed RBO design framework.

6.3.3.2. Subsurface conditions. As illustrated in Figure 6.5, below the waste and the MSE berm, the stratigraphy at the CIL site includes dredge, alluvium, the Columbia Formation, and the Potomac Formation. The Columbia Formation, encountered under the dredge/alluvium, consists of poorly sorted, fine-to-coarse sand and gravel with silty sand,

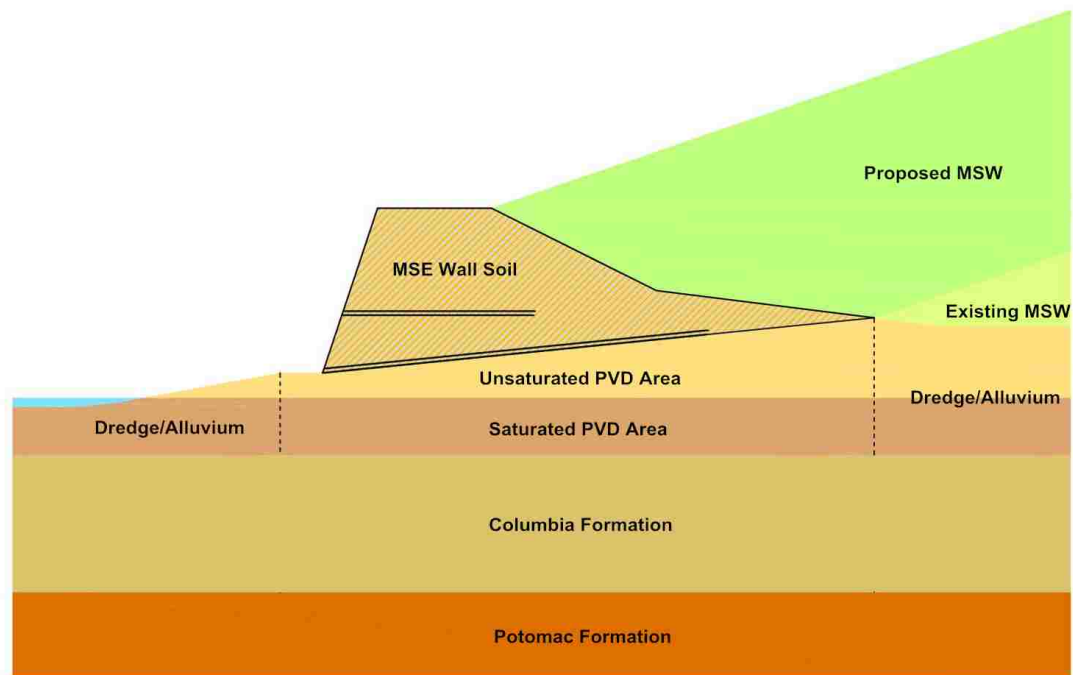


Figure 6.5: The configuration of section A-A'

silty clay, and clayey silt lenses of varying thicknesses. The Potomac Formation, which underlines the Columbia Formation, consists of a brownish red, stiff to hard, heavily over consolidated, clayey silt to silty clay, with traces of fine sand. On the river side of the berm, the soil above the Columbia Formation is assumed to be alluvium. Through the field investigations and laboratory testing performed by GeoSyntec in March and April 2002, the subsurface soil conditions were evaluated. A brief summary of the findings related to the properties for the selected section A-A' are listed in Table 6.2. The backfill

Table 6.2: The material properties for section A-A' at the CIL site

Material	Condition	c (psf)	ϕ (°)	γ (pcf)	γ_{sat} (pcf)
Waste	Drained	0	33	60	100
Dredge/Alluvium	Undrained	$0.29\sigma_v$	-	85	97
	Drained	0	34		
Columbia	Drained	0	40	125	125
Potomac	Undrained	4500	-	120	120
MSE Wall Soil ¹	Drained	0	29	90	90
MSE Wall Soil ²	Drained	0	35	120	120

of the MSE berm requires features to promote drainage. From the cost-effective perspective, non-traditional, cohesionless materials such as dredge and fly ash are considered for construction. The unit weight of the MSE wall soil is assumed to be 90 pcf with a friction angle of 29 degrees, as MSE wall soil¹ in Table 6.2; but for the lower 10 ft of the berm, the unit weight is assumed to be 120 pcf with a friction angle of 35 degrees, as MSE wall soil² in Table 6.2. As for the foundation soils, the dredge primarily consists of sandy silty

clay to clayey silt and varies in thickness from 30 to 40 feet. The alluvium is comprised of clayey silts and silty clays with varying amounts of sand, organic matter and silty sands. Because of the similar characteristics of the dredge spoils and the alluvium, these layers are combined as one soil type in design and analysis. A series of PVD will be installed underneath and beyond the MSE berm to enhance the dredge's ability to drain and accelerate the dissipation of excess pore pressures generated during berm construction and subsequent waste placement.

6.3.3.3. Simplified model. Based on the selected section A-A' and the preceding subsurface conditions, to implement the proposed design framework and improve design efficiency, some simplifications can be reasonably made in the following aspects of model geometry, optimized objectives, and loading conditions.

6.3.3.3.1. Model geometry. As shown in Figure 6.6, a single-tier berm is to be modeled with a total height of 60-ft. The MSE berm is 41.5-ft wide at the crest and the slopes on the external reinforced steepened slope at a 1H:3V and the internal slope at a 2H:1V.

6.3.3.3.2. Optimized objectives. In the proposed optimization design, the four main high-strength Mirafi® PET1170 geotextile reinforcement layers as used in the current design will remain, while the geogrid reinforcements will be optimized. Furthermore, as previously mentioned in Section 6.3.1, one of the purposes of the MSE berm is to counterbalance the lateral load caused by the proposed waste in the expanded landfill. In other words, the MSE berm is working as a gravity retaining wall, that has the external stability (i.e., sliding, overturning, bearing capacity, and deep-seated stability) mainly depending on its gravity, shearing resistance between foundation and reinforced soils, and the engineering properties of both foundation soils and backfill materials. Ground improvements

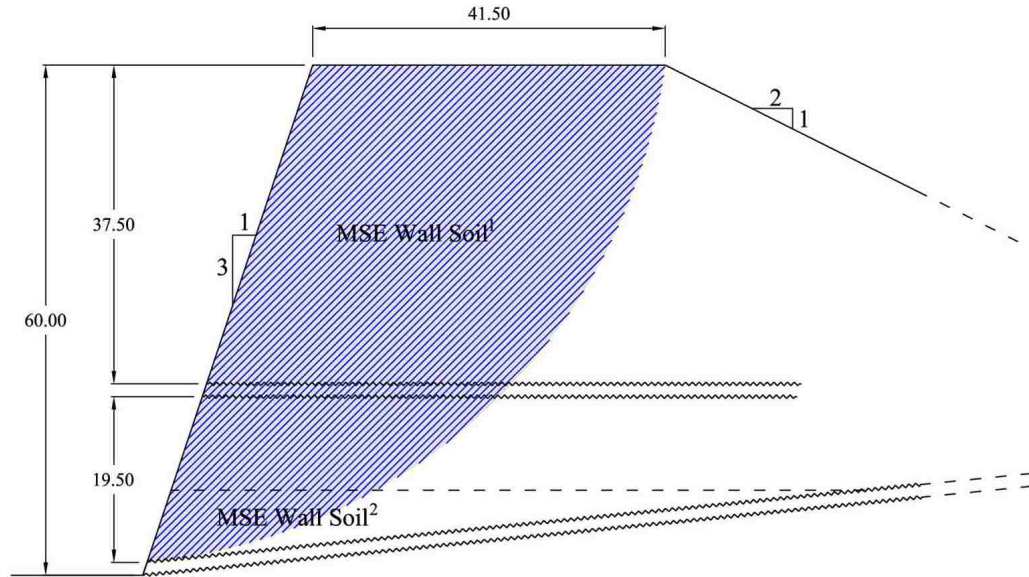


Figure 6.6: The configuration of MSE berm model for section A-A'

were achieved in the foundation soils for soil strength gain and high-strength geotextile reinforcements were installed for external stability. Therefore, the optimization design of geogrid reinforcements can be mainly emphasized from the internal stability of the berm to achieve a stable steep outer slope without considering the effects from the foundation soils. Accordingly, it is only the reinforced soils that the potential circular slip surfaces pass through, as in the area shaded in Figure 6.6.

6.3.3.3.3. Loading conditions. In view of the proposed MSW to be placed in the landfill, the local stability of the MSE berm may be influenced by the lateral forces produced by the proposed MSW disposal. However, by modeling the entire landfill in Slope/W, the proposed disposal seems hardly affect the local slope stability. Therefore, the main static load considered in the slope stability analysis and design for the MSE berm is the gravity alone. Furthermore, in view of the drainage features of the reinforced soils (e.g., cohesionless backfill, geocomposite drainage chimney, and a backdrain), drained

conditions of shear strength are considered in the optimization design.

6.3.3.4. Design parameters. According to the design recommendations stated in Section 5.3.2, with a berm height of 60-ft, multiple reinforcement zones may be considered. As shown in Figure 6.6, the berm can be basically divided into two primary reinforcement zones: 1) the bottom zone, which is below the middle geotextile layers with a height of 19.50-ft; and 2) the upper zone, which is above the middle geotextile layers with a height of 37.50-ft and can be further divided into several sub-reinforcement zones. The design variables can be accordingly defined as demonstrated in Table 6.3. As previously mentioned

Table 6.3: The reinforcement zones and design variables

Reinforcement Zone		Design Variables
Bottom		$n_b, T_{a(b)}$
Upper	uniform	$n_u, T_{a(u)}$
	2 zones	$n_{u_1}, T_{a(u)_1}, n_{u_2}, T_{a(u)_2}$
	3 zones	$n_{u_1}, T_{a(u)_1}, n_{u_2}, T_{a(u)_2}, n_{u_3}, T_{a(u)_3}$

in Section 5.3, to simplify the problem, the geosynthetic reinforcements are supposed to have the same tensile strength in each reinforcement zone. Therefore, two design variables are assigned per zone, including: 1) the number of reinforcement layers, n , and 2) the corresponding allowable tensile strength, T_a . For example, for the bottom zone, there are two design variables involved: $\mathbf{d} = \{n_b, T_{a(b)}\}$, where n_b is the number of reinforcement layers in the bottom zone, and $T_{a(b)}$ is the unique allowable tensile strength of the reinforcements. If the geogrid reinforcements are supposed to be uniformly distributed within the upper

zone, four design variables are involved in total: $\mathbf{d} = \{n_b, T_{a(b)}, n_u, T_{a(u)}\}$, where except for the two design variables assigned to the bottom zone, two more variables are included: n_u is the number of reinforcement layers in the upper zone, and $T_{a(u)}$ is the corresponding allowable tensile strength. If the upper zone is divided into two sub-reinforcement zones, there are six design variables involved in total as: $\mathbf{d} = \{n_b, T_{a(b)}, n_{u_1}, T_{a(u)_1}, n_{u_2}, T_{a(u)_2}\}$, where n_{u_1} and n_{u_2} are the numbers of reinforcement layers in the two sub-zones in the upper zone, and $T_{a(u)_1}$ and $T_{a(u)_2}$ are corresponding allowable tensile strengths. And if it is divided into three sub-reinforcement zones, a total of eight design variables are involved: $\mathbf{d} = \{n_b, T_{a(b)}, n_{u_1}, T_{a(u)_1}, n_{u_2}, T_{a(u)_2}, n_{u_3}, T_{a(u)_3}\}$, where n_{u_1} , n_{u_2} , and n_{u_3} are the numbers of reinforcement layers in the three sub-zones in the upper zone, and $T_{a(u)_1}$, $T_{a(u)_2}$, and $T_{a(u)_3}$ are the corresponding allowable tensile strengths. Since the reinforcement layers are supposed to be uniformly distributed within each zone, the spacing between the neighbored reinforcements can be accordingly calculated.

During the design stage, it is impossible to perform field exploration or lab testing to obtain the engineering properties of the embankment fills since the MSE berm has not been built yet. Therefore, the material properties are determined from the specified fill materials and reconstituted soil specimens in the lab. As mentioned in Section 6.3.3.2, from the cost-effective perspective, some non-traditional, cohesionless material such as dredge spoil is considered as the potential backfill for the MSE berm. Its probabilistic properties (e.g., the coefficient of variance) are assumed according to the statistical estimations on the numbers of the soil samples obtained from the dredge/alluvium layer in the foundation soils as published by Houlihan et al. (2010). As summarized in Table 6.4, both friction angle and unit weight of the MSE wall soils are considered as uncorrelated, normally-distributed probabilistic variables with the coefficient of variance assumed within some

published ranges (Houlihan et al. 2010).

Table 6.4: Summary of material parameters for design

Material	Parameter	Mean	COV	Distribution
MSE Wall Soil ¹	ϕ'	29°	10%	Normal
	γ	90 pcf	7.2%	Normal
MSE Wall Soil ²	ϕ'	35°	10%	Normal
	γ	120 pcf	7.2%	Normal
Mirafi® PET1170	T_a	21,000 lb/ft	Deterministic	

6.3.4. Results and Discussions. The analysis is first carried out on the basis of the current MSE berm design. With a total of 2,480 potential slip surfaces being searched, the critical deterministic and probabilistic slip surfaces are respectively located corresponding to internal and compound failure, as shown in Figure 6.7. The critical internal failure surfaces that pass all the reinforcement layers happen to be located at the same position in both deterministic and probabilistic analyses, with a minimum factor of safety equal to 1.94 and a probability of failure approaching zero. In other words, the total probability of failure regarding the internal failure is approaching zero as well since the rest of the internal failure surfaces all have a factor of safety even higher than 1.94 and thus a smaller probability of failure that can be considered as zero. The critical deterministic and probabilistic surfaces regarding the compound failure are slightly different but very close to each other with a minimum factor of safety equal to 1.38 and a maximum probability of failure as $2.1 \times 10^{-7}\%$. Since the search area is restricted within the MSE berm, neither deep-seated nor sliding failures are considered. As a result, the system reliability is ob-

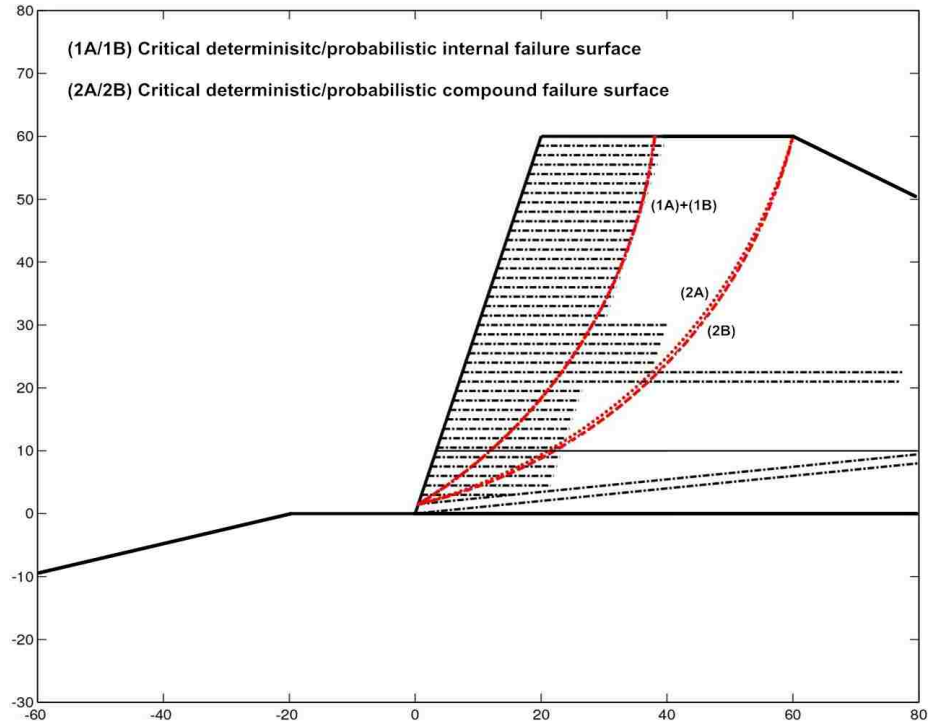


Figure 6.7: The critical deterministic and probabilistic slip surfaces for current design

tained as $6.7 \times 10^{-7}\%$, which is mainly coming from the compound failure. On the other hand, it is indicated the current reinforcement design guarantees a stable slope from both deterministic and probabilistic perspectives.

6.3.4.1. RBO optimization design. To achieve the same performance in the optimization design, the required minimum factor of safety and the target probability of failure can be set as same with the values obtained in the preceding analysis. Thereby, the optimization problem can be described by the following equations:

$$\min f(\mathbf{d}, \mathbf{X}, \mathbf{P}) = \text{Cost} \quad (6.1a)$$

$$\text{sub. to: } f_{s, \min} \geq f_{s, \text{req}} = 1.94 \quad (6.1b)$$

$$p_{f, \text{det}, i} = P\{g_{\text{internal}, \text{det}}(\mathbf{d}, \mathbf{X}, \mathbf{P}) \leq 0\} \leq p_{f, \text{cri}, \text{internal}} = 2.1 \times 10^{-7}\% \quad (6.1c)$$

$$p_{f_{pro,i}} = P \{g_{internal,pro}(\mathbf{d}, \mathbf{X}, \mathbf{P}) \leq 0\} \leq p_{f_{cri, internal}} = 2.1 \times 10^{-7}\% \quad (6.1d)$$

where the number of geogrid reinforcements and the corresponding allowable tensile strengths are considered as the design variables. As discussed in Section 6.3.3.4, more reinforcement zones assigned in the berm, more design variables are to be involved. Therefore, three different situations are to be taken into consideration for comparison as discussed below. Furthermore, with a target factor of safety set as 1.3 against sliding failure, the critical zone that needs to be reinforced is determined through performing the slope stability analysis on the original unreinforced slope as shown in Figure 6.8, where the critical zone has an

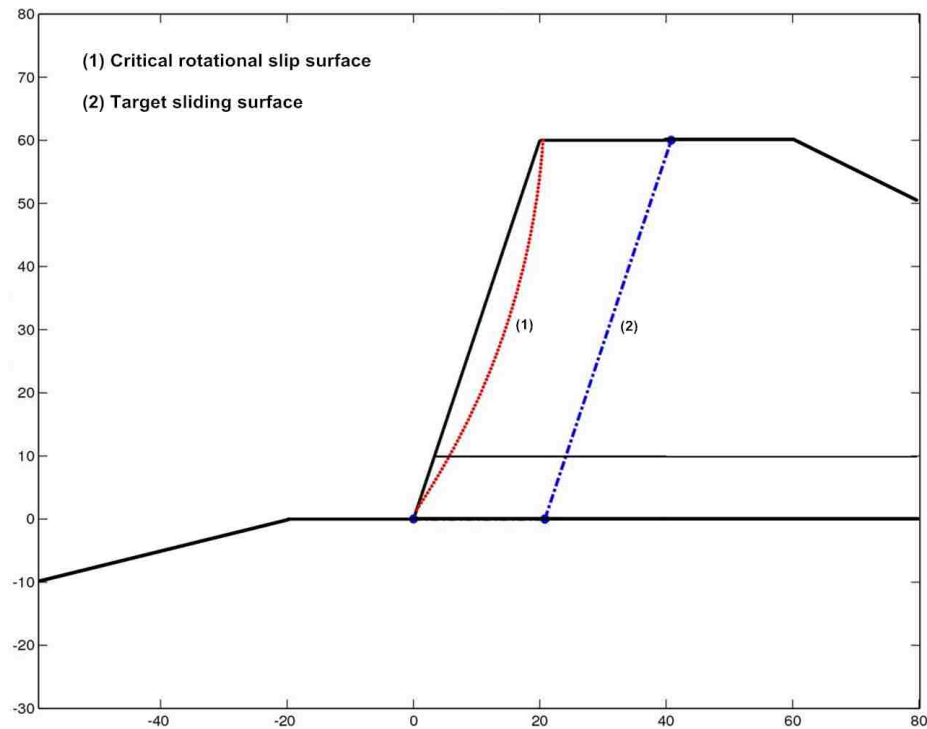


Figure 6.8: The critical zone and slip surface to be reinforced

average width equal to 20.8-ft throughout the whole berm; and the critical slip surface is located within the critical zone. Therefore, the geogrid reinforcements are supposed to extend to the limit of the critical zone.

6.3.4.1.1. Two reinforcement zones. If the geogrids are uniformly distributed throughout the upper zone, four design variables are involved and constrained as

$$T_{a(b)} \in [4000, 6000] \text{ lb/ft}, n_b \in [10, 18], \text{ for the bottom zone} \quad (6.2a)$$

$$T_{a(u)} \in [3000, 6000] \text{ lb/ft}, n_u \in [16, 36], \text{ for the upper zone} \quad (6.2b)$$

based on which the optimal design is derived as: in the bottom zone as highlighted in green in Figure 6.9, a total of 15 layers of geogrid reinforcements are required with an allowable tensile strength equal to 4060 lb/ft; and in the upper zone as highlighted in pink in Figure 6.9, 22 layers of geogrid reinforcements are needed with an allowable tensile strength equal to 3118 lb/ft. Since all the geogrid reinforcements are extended to the limits of the critical zone, the total usage and cost are respectively obtained as 974.52 ft² and \$419.12 per unit width of this cross section. Through performing slope stability analysis, the minimum factor of safety against internal failure is derived as 1.94 along with a zero probability of failure obtained from both deterministic and probabilistic perspectives. As for the compound failure, the critical deterministic and probabilistic failure surfaces are slightly different with the minimum factor of safety equal to 1.40 and the maximum probability of failure obtained as $2.3 \times 10^{-8}\%$, as shown in Figure 6.9.

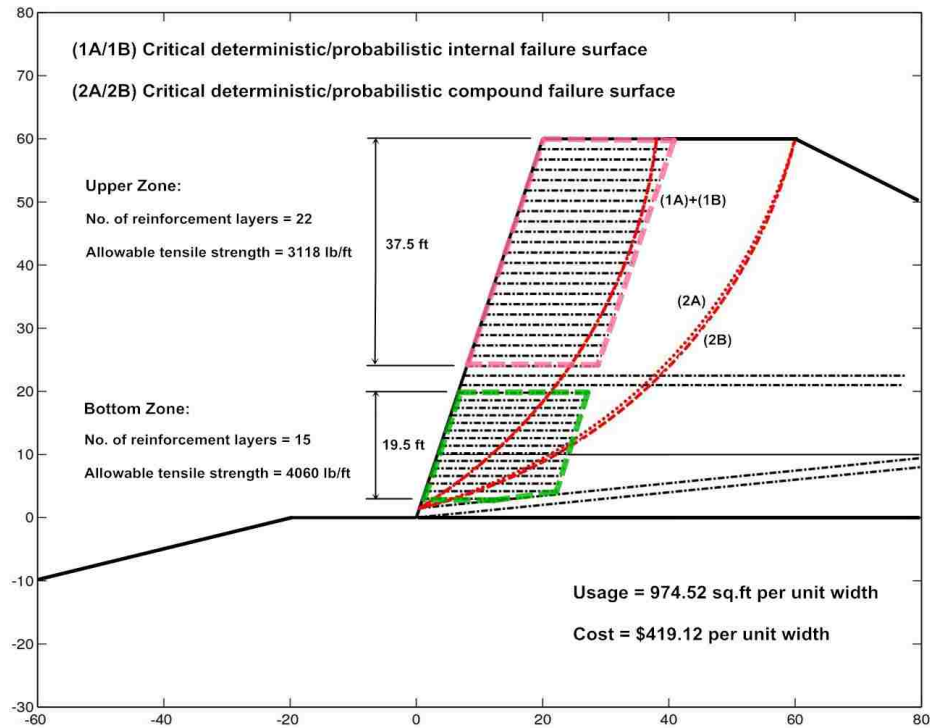


Figure 6.9: The optimized design with two reinforcement zones

6.3.4.1.2. Three reinforcement zones. If the upper reinforcement zone is divided into two equal parts, six design variables are involved and constrained as

$$T_{a(b)} \in [4000, 6000] \text{ lb/ft}, n_b \in [10, 18], \text{ for the bottom zone} \quad (6.3a)$$

$$T_{a(u)_1} \in [3500, 5500] \text{ lb/ft}, n_{u_1} \in [9, 18], \text{ for the upper zone 1} \quad (6.3b)$$

$$T_{a(u)_2} \in [3000, 4000] \text{ lb/ft}, n_{u_2} \in [8, 17], \text{ for the upper zone 2} \quad (6.3c)$$

based on which the optimal design is derived as: a total of 15 layers of geogrid reinforcements are required in the bottom zone as highlighted in green in Figure 6.10 with an allowable tensile strength equal to 4005 lb/ft. As for the upper zone, there are two sub-

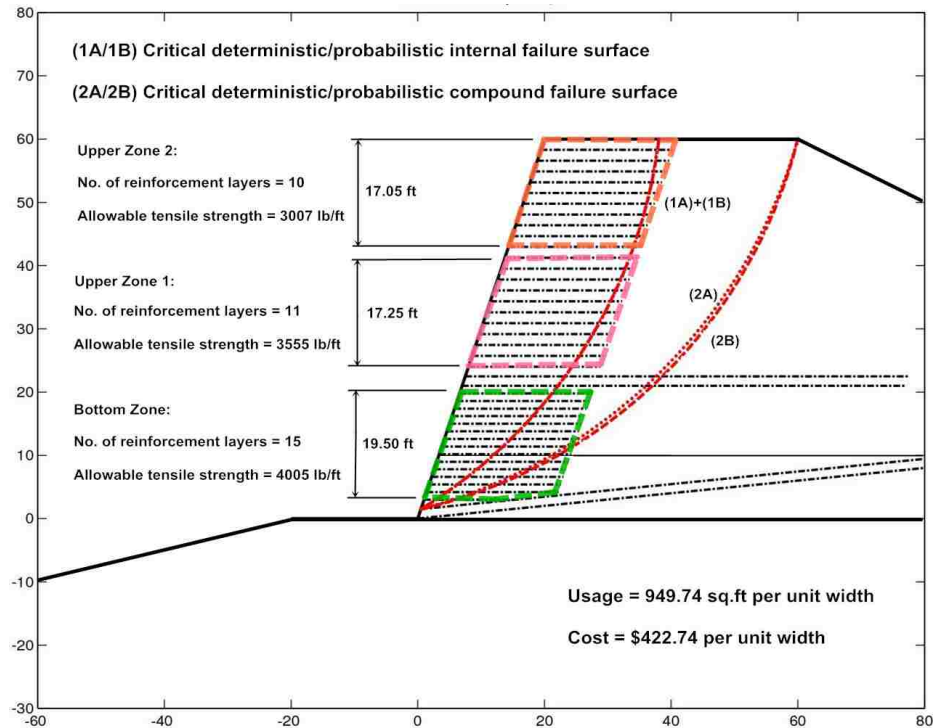


Figure 6.10: The optimized design with three reinforcement zones

reinforcement zones involved, that has 11 layers of reinforcements designed in the upper zone 1 as highlighted in pink in Figure 6.10 with an allowable tensile strength equal to 3555 lb/ft, and 10 layers of reinforcements for the upper zone 2 as highlighted in orange in Figure 6.10 with an allowable tensile strength equal to 3007 lb/ft. With all the geogrid reinforcements extended to the limits of the critical zone, the total usage and cost are derived as 949.74 ft² and \$422.75 per unit width of this cross section. Through performing slope stability analysis, the minimum factor of safety against internal failure is again derived as 1.94 along with a zero probability of failure in both deterministic and probabilistic aspects. And for the compound failure, the critical deterministic and probabilistic failure surfaces are located with the minimum factor of safety equal to 1.40 and the maximum probability of failure obtained as $3.4 \times 10^{-8}\%$, as shown in Figure 6.10.

6.3.4.1.3. Four reinforcement zones. If the upper reinforcement zone is divided into three equal parts, a total of eight design variables are involved and constrained as

$$T_{a(b)} \in [4000, 6000] \text{ lb/ft}, n_b \in [10, 18], \text{ for the bottom zone} \quad (6.4a)$$

$$T_{a(u)_1} \in [4000, 6000] \text{ lb/ft}, n_{u_1} \in [6, 12], \text{ for the upper zone 1} \quad (6.4b)$$

$$T_{a(u)_2} \in [3500, 4500] \text{ lb/ft}, n_{u_2} \in [6, 12], \text{ for the upper zone 2} \quad (6.4c)$$

$$T_{a(u)_3} \in [3000, 4000] \text{ lb/ft}, n_{u_3} \in [5, 11], \text{ for the upper zone 3} \quad (6.4d)$$

based on which the optimal design is derived as: a total of 14 layers of geogrid reinforcements are required in the bottom zone as highlighted in green in Figure 6.11 with

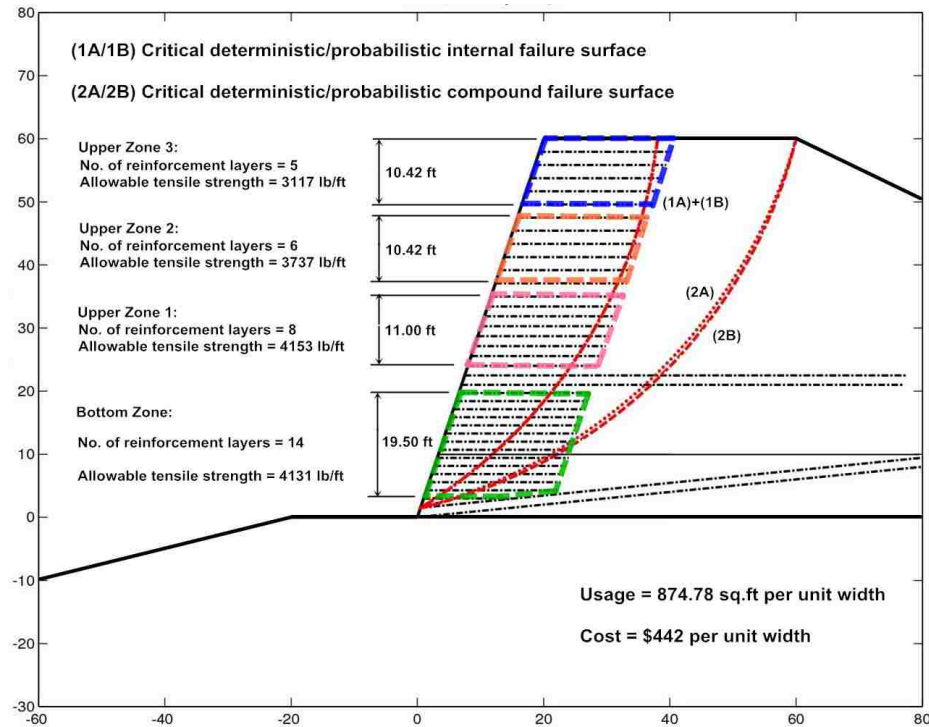


Figure 6.11: The optimized design with four reinforcement zones

an allowable tensile strength equal to 4131 lb/ft. As for the upper zone, there are three sub-reinforcement zones involved, that has 8 layers of reinforcements designed in the upper zone 1 as highlighted in pink in Figure 6.11 with an allowable tensile strength equal to 4153 lb/ft; 6 layers of reinforcements for the upper zone 2 as highlighted in orange in Figure 6.11 with an allowable tensile strength equal to 3737 lb/ft; and 5 layers of the reinforcements for the upper zone 3 as highlighted in blue in Figure 6.11 with an allowable tensile strength equal to 3117 lb/ft. With all the geogrid reinforcements extended to the limits of the critical zone, the total usage and cost are derived as 874.78 ft² and \$442 per unit width of this cross section. Through performing slope stability analysis, similar results are derived. The minimum factor of safety against internal failure is obtained as 1.94 with a zero probability of failure; while for the compound failure, the critical deterministic and probabilistic surfaces are slightly different with the minimum factor of safety equal to 1.39 and the maximum probability of failure obtained as $8.4 \times 10^{-8}\%$, as shown in Figure 6.11.

6.3.4.2. Results comparison. For comparison, the optimal results and slope performance are summarized in Table 6.5 and 6.6 along with the total usage and cost corresponding to the various reinforcement design alternatives. By comparing the RBO designs to the current design of the MSE berm, it can be noticed, with more reinforcement layers placed in the bottom zone, the requirements for the reinforcement strength is decreased; meanwhile, fewer reinforcement layers are needed in the upper zone provided a stable bottom zone that has sufficient numbers of reinforcements placed inside.

On the basis of the same cost function as demonstrated in Equation 5.20, the proposed RBO design always leads to a lower usage and cost regarding the geogrid reinforcements compared to the current design. As illustrated in Table 6.5, the total costs of the optimized designs are approximately 56% ~ 60% of the original as-built design. When

Table 6.5: Summary of slope performance, reinforcement usage and cost

Design alternatives		Usage (ft ²)	Cost (\$)	Internal		Compound		p_{fs}
				$f_{s, \min}$	$p_{f, \max}$	$f_{s, \min}$	$p_{f, \max}$	
Current Design		995.72	746.42	1.94	0	1.38	2.10	6.70
RBO Design	2 zones	974.52	419.12	1.94	0	1.40	0.23	0.68
	3 zones	949.74	422.75	1.94	0	1.40	0.34	1.02
	4 zones	874.78	442.00	1.94	0	1.39	0.84	2.87

Notes:

1. Both usage and cost are for berm cross section with unit width.
2. The maximum probability of failure ($p_{f, \max}$) and system probability of failure (p_{fs}) are in $10^{-7}\%$.

Table 6.6: Summary of reinforcement design for the MSE berm in CIL project

Design Alternatives		Reinforcement Zones		Layers
		Bottom Part	Upper Part	
Current Design		$n = 12, T_a = 5000$ lb/ft	$n = 24, T_a = 5000$ lb/ft	36
RBO Design	2 zones	$n = 15, T_a = 4060$ lb/ft	$n = 22, T_a = 3118$ lb/ft	37
	3 zones	$n = 15, T_a = 4005$ lb/ft	$n = 11, T_a = 3555$ lb/ft	36
			$n = 10, T_a = 3007$ lb/ft	
	4 zones	$n = 14, T_a = 4131$ lb/ft	$n = 8, T_a = 4153$ lb/ft	33
$n = 6, T_a = 3737$ lb/ft				
$n = 5, T_a = 3117$ lb/ft				

we take a look at the slope performance, the optimized designs have the minimum internal factors of safety maintained as 1.94 (the value in the original as-built design); while the minimum compound factors of safety are slightly higher than 1.38 (the value in the original as-built design) along with the maximum probabilities of failure that are approximately

60% ~ 90% lower than the original value of $2.10 \times 10^{-7}\%$. As a result, with saving around 40% ~ 44% of the reinforcement cost, the proposed RBO design not only maintains the slope performance at the same level, but offers an even more reliable slope system that has the system reliability higher than the original as-built design.

On the other hand, as shown in Table 6.6, in view of the three different reinforcement schemes considered in the RBO design, the more reinforcement zones assigned in the MSE berm, the lower the total usage is obtained; but the corresponding allowable tensile strengths are increased. Therefore, though the number of reinforcement layers is decreased, the design with more reinforcement zones leads to a higher total cost since the unit price is always proportional to the reinforcement strength. Among the three reinforcement design alternatives, the optimized design with two reinforcement zones has the lowest cost as \$419.12 per unit width of the berm along with a highest system reliability.

Since the proposed RBO framework is emphasized on the design of geosynthetic reinforcement, the total cost herein is only referring to the reinforcements; excludes the consideration of the installation costs, equipment and labor resources. As estimated by Elias et al. (2001), the installation cost of geosynthetics is typically ranging from \$0.30 to \$0.90 per square meter. In other words, increasing the number of reinforcement layers may lead to higher costs in labor work and more efforts in soil compaction and construction. As illustrated in Table 6.6, a total of 37 reinforcement layers are required in the optimized design with two reinforcement zones; 36 layers for the three-reinforcement-zone design; and 33 layers for the four-reinforcement-zone design. Therefore, provided similar slope performance, from the perspective of construction, the optimized design with four reinforcement zones may be recommended since it has the smallest amount of geogrid reinforcements to be installed and the reinforcement cost is approximately 40% lower than

the original as-built design.

6.4. SUMMARY

In this chapter, the proposed reliability-based optimization (RBO) framework is successfully implemented in an engineering case study for the design of the MSE berm in the Cherry Island Landfill expansion project. The optimization is mainly referring to the geosynthetic reinforcement cost. The cost of constructibility and the complication due to multiple zones and more layers in the cross-sections are not studied herein. Through comparing the RBO results with the current reinforcement design, it is shown the total cost regarding the geogrid reinforcements are significantly optimized; meanwhile, the slope performance is kept at the same level from both deterministic and probabilistic perspectives, and sometimes even improved. In this case study, with a minimum factor of safety as large as 1.94, the corresponding probability of failure is in a small magnitude of $10^{-7}\%$ or $10^{-8}\%$. Therefore, the optimal solution is primarily controlled by the target factor of safety instead of the probability of failure. When multiple reinforcement zones are taken into consideration, the number of design variables is increased. In this situation, the conventional, manually-performed optimization process can be very time-consuming and probably fails to locate the best solution due to the limited number of alternatives that can be manually tried. But the proposed RBO framework enables a more systematic and effective optimization to address the optimal design for the geosynthetic reinforced embankment slopes.

7. CONCLUSIONS AND RECOMMENDATIONS

7.1. CONCLUSIONS

In this study, a reliability-based optimization (RBO) design framework is proposed for the design of geosynthetic reinforced embankment slopes (GRES) with an intention to minimize the geosynthetic reinforcement cost. Meanwhile, the framework ensures all the design requirements are satisfied from both deterministic and probabilistic perspectives. The proposed RBO framework is developed on the basis of the conventional design procedure stated by FHWA Mechanically Stabilized Earth Walls and Reinforced Soil Slopes Design & Construction Guidelines (Elias et al. 2001); and primarily incorporates: 1) traditional deterministic slope stability analysis, 2) reliability-based (probabilistic) slope stability analysis, and 3) reliability-based optimization.

As discussed in Section 3, the probabilistic slope stability analysis is able to tell how probable the slope can fail associated with the uncertainties in soil properties. Unlike the traditional deterministic slope stability analysis that can only provide the factor of safety individually regarding the various failure modes (i.e., internal, compound, deep-seated, sliding, and etc.) that may potentially occur in a GRES structure, the proposed probabilistic slope stability analysis is able to estimate the reliability corresponding to the entire system, which is more thorough in evaluating the safety of the GRES. With different failure mechanisms involved in the slope stability analysis corresponding to the multiple failure modes, the formation of the limit state function varies. Therefore, the failure mode that has the minimum factor of safety may not be the most probable failure mode since it can still have a high probability of failure. Therefore, only considering the factor of safety, a thorough evaluation of the system reliability is not possible. Furthermore, since both the

factor of safety and the probability of failure aim at evaluating the slope safety, a lower factor of safety always comes along with a higher probability of failure. However, the factor of safety computed through the traditional deterministic analysis is always unable to consistently measure the risk associated with the uncertainties in soil properties. Therefore, it may happen the slip surface with the minimum factor of safety fails to be the one with the maximum probability of failure. This leads to two possible slip surfaces: the critical deterministic slip surface with the minimum factor of safety and the critical probabilistic slip surface with the maximum probability of failure.

In either design or analysis, from a reliability perspective, it is always essential to estimate the probabilistic properties of the random variables to make their variations well defined. Basically, it can be achieved by performing statistical inference on the basis of the data observed from site characterization. Increasing the number of soil samples and tests increases the confidence that the probabilistic characteristics of the soil properties are accurate. However, those information can frequently not available for statistical estimations; and sometimes, it can be even impossible to get any data for use. Often, assumptions have to be made first considering some available fill materials. And thus, it is important to know how those assumptions are going to influence the design and analysis. As presented in Section 4, it is proposed a probabilistic sensitivity analysis (PSA) that is developed on the basis of the most-probable point (MPP). Through performing the MPP-based PSA, sensitivity measurements can be computed regarding each random variable involved in the reliability-based design and analysis; and thus evaluate their significance on the slope performance.

In the proposed RBO design framework, the probabilistic slope stability is one of the primary sub-routines. It is embedded in not only the inner loop in the genetic algorithm

optimization to evaluate the probability of failure along the two critical slip surfaces but also the outer loop to check if the optimized design meets the design requirements. In the traditional procedure, the critical deterministic slip surface that is located in the original unreinforced slope is the only reference surface used for reinforcement design, and can probably lead to an unacceptable design that fails to meet the design requirements. But in the proposed RBO framework, the design is performed on a 'flexible' critical deterministic surface that varies with each optimization generation. Therefore, it always guarantees an optimal design that has the minimum factor of safety no less than the required value. Furthermore, as previously mentioned, when soil variability is taken into consideration, the critical deterministic and probabilistic slip surfaces may be located at different positions, where the probabilistic one can probably situate deeper in the slope. Therefore, the reinforcement layer may not be long enough if it is determined only based on the critical deterministic surface. In the proposed design framework, both critical deterministic and probabilistic slip surfaces are taken into consideration; and thus, such a problem is successfully resolved.

In practical design of geotechnical systems, optimization is conventionally performed by manually assigning various design alternatives in each trial; and thus select the one with the lowest cost as the optimal solution. However, according to the design recommendations (Elias et al. 2001), for the slopes higher than 6 m, it should be divided into two or three reinforcement zones for reinforcement design. Therefore, the design variables will be doubled or even tripled; and thus the number of potential combinations of the design alternatives significantly increases. In this situation, the conventional, manually performed optimization procedure can be very inefficient and probably fails to find the 'best' optimal result due to the limited number of trials. But by implementing the genetic algorithm (GA)

in the proposed RBO framework, such a problem can be resolved. And the design process becomes more systematic and effective to maximize the economic benefits regarding the geosynthetic reinforcement design; meanwhile, meets the technical design requirements in both deterministic and probabilistic aspects.

7.2. RECOMMENDATIONS FOR FUTURE WORK

This study has demonstrated the implementation of the reliability-based optimization in the design of geosynthetic reinforced embankment slope. However, there are some observations arising from the study that requires further investigation as stated below:

- With an emphasis on introducing the advanced numerical algorithms in GRES design, some simplifications were made on 1) the method of limit equilibrium, selected as the ordinary method of slices, and 2) the rotational slip surfaces, defined in shape of circular. In view of the preceding aspects, the proposed framework can be further improved by implementing some other commonly-used slice methods, e.g., Bishop simplified, Janbu simplified, Spencer, or Sarma, and taking non-circular slip surfaces into consideration.
- In either the preceding numerical examples or the engineering case study, the optimization design was performed on the basis of the cost functions estimated from limited data collected from the US Fabrics. The estimation approximately represents the trend between the unit price and the tensile strength of geosynthetic reinforcements: for the same type of products, a higher tensile strength always leads to a higher unit price. However, the cost information regarding the geosynthetic products are frequently varying with different projects, manufactures, and distributors. Therefore, when implementing the proposed RBO design framework in practical

cases, cost functions can be specifically estimated based on detail information.

- The application of the proposed study can be extended by incorporating the proposed RBO design with some other geotechnical engineering aspects, such as, earthquake, seepage, and etc..
- So far, most of the commercial slope stability design programs, e.g., Slope/W, Slide, SVSlope, etc., are unable to perform optimization design on geo-structures. Miraslope, which is a program published by Mirafi, is only for the deterministic design of reinforced slopes and walls. Since the proposed framework is developed on the basis of the current design manual, it can be expected to be embedded in some existing programs to make the optimization design more convenient and effective for designers.

APPENDIX A
VARIABLE TRANSFORMATION

This appendix presents demonstrates the mathematics involved in variable transformation in Section 3.3.1.1. This part of work is primarily summarized and concluded from some previous works as driven by Cruse (1997), Higham (2002), Griffiths and Fenton (2008), Du et al. (2010) and etc.. The variable transformation always varies with distribution types. As mentioned in Section 3.2.1, normal and log-normal are two most-commonly used distributions for Mohr-Coulomb (MC) strength parameters and soil unit weights in most of geo-related studies. Therefore, the following sections are discussed on the focus of these two distribution models.

A.1. INDEPENDENT RANDOM VARIABLES

For independent random variables, Rosenblatt transformation can be directly applied to convert the variables into a non-dimensional, standard normal space according to Equation 3.10, which is recalled and given below

$$u_i = \Phi^{-1} [F_i (x_i)] \quad (\text{A.1})$$

where $F_i(\cdot)$ is the cumulative distribution function (CDF) regarding random variable x_i with $\Phi(\cdot)$ representing its corresponding CDF in standard normal space.

A.1.1. Normal Distribution. If a random variable is normally distributed with $x_i \sim N(\mu_{x_i}, \sigma_{x_i})$, the transformation is derived as

$$u_i = \Phi^{-1} [F_i (x_i)] = \Phi^{-1} \left[\Phi \left(\frac{x_i - \mu_{x_i}}{\sigma_{x_i}} \right) \right] = \frac{x_i - \mu_{x_i}}{\sigma_{x_i}} \quad (\text{A.2})$$

A.1.2. Log-Normal Distribution. If a random variable is log-normally distributed with $x_i \sim LN(\mu_{x_i}, \sigma_{x_i})$, the transformation is derived as

$$u_i = \Phi^{-1} [F_i(x_i)] = \Phi^{-1} \left[\Phi \left(\frac{\ln x_i - \mu_{\ln x_i}}{\sigma_{\ln x_i}} \right) \right] = \frac{\ln x_i - \mu_{\ln x_i}}{\sigma_{\ln x_i}} \quad (\text{A.3})$$

where

$$\mu_{\ln x_i} = \ln \mu_{x_i} - \frac{1}{2} \sigma_{\ln x_i}^2 \quad (\text{A.4})$$

and

$$\sigma_{\ln x_i} = \sqrt{\ln \left(1 + \frac{\sigma_{x_i}^2}{\mu_{x_i}^2} \right)} \quad (\text{A.5})$$

where $\mu_{\ln x_i}$ and $\sigma_{\ln x_i}$ are the mean and standard deviation of random variable x_i in log-scale.

A.2. CORRELATED RANDOM VARIABLES

For correlated random variables, to convert the original variables to a set of uncorrelated ones in a non-dimensional, standard normal space, the covariance matrix needs to be transformed by going through the procedure as demonstrated in Figure 3.3 in Section 3.3.1.1.

A.2.1. Step 1: From $\{x\}$ To $\{\hat{x}\}$. The first step is to convert the original correlated random variables to a set of reduced ones that are in standard normal space. Leaving aside the covariance between the variables, the transformation in this step is exactly same as the one presented in Section A.1. But regarding the reduced variables, an essential issue is what happens to the covariance and correlated coefficient after the transformation. From Equation 3.12 and 3.13, it is easy to have

$$\rho_{x_i, x_j} = E \left[\frac{(x_i - \mu_{x_i})(x_j - \mu_{x_j})}{\sigma_{x_i} \sigma_{x_j}} \right] = E \left[\left(\frac{x_i - \mu_{x_i}}{\sigma_{x_i}} \right) \left(\frac{x_j - \mu_{x_j}}{\sigma_{x_j}} \right) \right] \quad (\text{A.6})$$

If two correlated random variables, x_i and x_j , are normally distributed, according to Equation A.2, we can derive

$$\rho_{x_i, x_j} = E [\hat{x}_i \hat{x}_j] = \hat{\rho}_{ij} \quad (\text{A.7})$$

where

$$\hat{x}_i = \frac{x_i - \mu_{x_i}}{\sigma_{x_i}} \quad (\text{A.8})$$

and

$$\hat{x}_j = \frac{x_j - \mu_{x_j}}{\sigma_{x_j}} \quad (\text{A.9})$$

are the reduced variables with a new correlated coefficient, $\hat{\rho}_{ij}$, that is exactly same with the original one. When x_i and x_j are log-normally distributed, $\ln x_i$ and $\ln x_j$ are both in normal distribution. Similar to Equation A.6, we can derive

$$\rho_{\ln x_i x_j} = E \left[\left(\frac{\ln x_i - \mu_{\ln x_i}}{\sigma_{\ln x_i}} \right) \left(\frac{\ln x_j - \mu_{\ln x_j}}{\sigma_{\ln x_j}} \right) \right] \quad (\text{A.10})$$

where

$$\rho_{\ln x_i x_j} = \frac{\ln \left(1 + \rho_{x_i x_j} \frac{\sigma_{x_i} \sigma_{x_j}}{\mu_{x_i} \mu_{x_j}} \right)}{\sqrt{\ln \left(1 + \frac{\sigma_{x_i}^2}{\mu_{x_i}^2} \right) \ln \left(1 + \frac{\sigma_{x_j}^2}{\mu_{x_j}^2} \right)}} \quad (\text{A.11})$$

According Equation A.3, it is easy to have

$$\rho_{\ln x_i x_j} = E [\hat{x}_i \hat{x}_j] = \hat{\rho}_{ij} \quad (\text{A.12})$$

where

$$\hat{x}_i = \frac{\ln x_i - \mu_{\ln x_i}}{\sigma_{\ln x_i}} \quad (\text{A.13})$$

and

$$\hat{x}_j = \frac{\ln x_j - \mu_{\ln x_j}}{\sigma_{\ln x_j}} \quad (\text{A.14})$$

are reduced variables with a new correlated coefficient, $\hat{\rho}_{ij}$, that is same with the original one in log-normal space. Accordingly, a new reduced covariance matrix, $\hat{\Sigma}$ ($= \text{Cov} [\hat{\mathbf{x}}]$), can be derived by being transformed from Σ ($= \text{Cov} [\mathbf{x}]$) based on Equation 3.14,

$$\hat{\Sigma}_{ij} = \text{Cov} [\hat{x}_i, \hat{x}_j] = \hat{\rho}_{ij} \quad (\text{A.15})$$

and when expanded in matrix form, it becomes

$$\hat{\Sigma} = \text{Cov} [\hat{\mathbf{x}}] = \begin{bmatrix} 1 & \hat{\rho}_{12} & \hat{\rho}_{13} & \cdots & \hat{\rho}_{1n} \\ \hat{\rho}_{21} & 1 & \hat{\rho}_{23} & \cdots & \hat{\rho}_{2n} \\ \hat{\rho}_{31} & \hat{\rho}_{32} & 1 & \cdots & \hat{\rho}_{3n} \\ \vdots & \vdots & \vdots & \vdots & \vdots \\ \hat{\rho}_{n1} & \hat{\rho}_{n2} & \hat{\rho}_{n3} & \cdots & 1 \end{bmatrix} \quad (\text{A.16})$$

where $\rho_{ij} = \rho_{ji}$, that makes the matrix a real symmetric one (Hermitian matrix).

A.2.2. Step 2: Cholesky Decomposition. In linear algebra, Cholesky decomposition is a decomposition of a Hermitian, positive-definite matrix into the product of a

lower triangular matrix and its conjugate transpose, as given by

$$\mathbf{A} = \mathbf{L}\mathbf{L}^T \quad (\text{A.17})$$

where \mathbf{A} is a Hermitian, positive-definite matrix, and \mathbf{L} is a lower triangular matrix with real and positive diagonal entries. In this situation, the algorithm for Cholesky decomposition is given by

$$L_{j,j} = \sqrt{A_{j,j} - \sum_{k=1}^{j-1} L_{j,k}^2}, \quad (\text{A.18})$$

$$L_{i,j} = \frac{1}{L_{j,j}} \left(A_{i,j} - \sum_{k=1}^{j-1} L_{i,k} L_{j,k} \right), \quad \text{for } i > j \quad (\text{A.19})$$

However, as mentioned in Section 3.3.1.1, covariance matrix that has been proved to be positive semi-definite may not be so ‘ideal’ for Cholesky decomposition. Thereby, unlike the positive-definite matrix, the eigenvalues of which are all positive, there is a chance that at least one eigenvalue of the matrix can be zero. In this condition, Cholesky decomposition still exists but with a form as

$$\mathbf{P}^T \mathbf{A} \mathbf{P} = \mathbf{L}\mathbf{L}^T \quad (\text{A.20})$$

where \mathbf{P} is the permutation matrix with real entries; \mathbf{L} is unique in the form as

$$\mathbf{L} = \begin{bmatrix} \mathbf{L}_{11} & 0 \\ \mathbf{L}_{12} & 0 \end{bmatrix} \quad (\text{A.21})$$

where \mathbf{L}_{11} is a lower triangular matrix with real and positive diagonal entries. This part of work has been maturely developed. Some computational packages, such as LINPACK and a more advanced one LAPACK, can be directly applied to achieve the decomposition in various situations.

A.2.3. Step 3: From $\{\hat{\mathbf{x}}\}$ To $\{\mathbf{u}\}$. Based on the previous preparation, the target variables that are uncorrelated and in a non-dimensional, standard normal space can be derived by

$$\{\mathbf{u}\} = \mathbf{L}_{\hat{\mathbf{x}}}^{-1} \{\hat{\mathbf{x}}\} \quad (\text{A.22})$$

where $\mathbf{L}_{\hat{\mathbf{x}}}$ is the lower triangular matrix with respect to the reduced variables $\hat{\mathbf{x}}$.

A.3. CALCULATION EXAMPLES

As discussed in Section 3.2, in probabilistic slope stability analysis, cohesion and friction angle are two primary random variables that are considered with a normal or log-normal distribution in most of the related studies. Therefore, a calculation example is demonstrated here as the practical application of the above algorithms.

A.3.1. Bivariate Normal Distribution. Given as c and ϕ are normally distributed with $c \sim N(\mu_c, \sigma_c)$ and $\phi \sim N(\mu_\phi, \sigma_\phi)$ and a correlated coefficient $\rho_{c\phi}$, the original co-

variance matrix is give by

$$\Sigma = \text{Cov} [c, \phi] = \begin{bmatrix} \sigma_c^2 & \varphi_{c\phi} \\ \varphi_{c\phi} & \sigma_\phi^2 \end{bmatrix} \quad (\text{A.23})$$

where $\varphi_{c\phi} = \sigma_c \sigma_\phi \rho_{c\phi}$. After transformed to standard normal space, the variables become to \hat{c} and $\hat{\phi}$ with $\mu = 0$ and $\sigma = 1$ and a correlated coefficient that is exactly same with the original one $\rho_{c\phi}$. Then the covariance matrix is converted to

$$\hat{\Sigma} = \text{Cov} [\hat{c}, \hat{\phi}] = \begin{bmatrix} 1 & \rho_{c\phi} \\ \rho_{c\phi} & 1 \end{bmatrix} \quad (\text{A.24})$$

Assume a perfect positive definite covariance matrix, through algorithm A.18 and A.19, the lower triangular matrix can be derived as

$$\mathbf{L}_{\hat{c}\hat{\phi}} = \begin{bmatrix} 1 & 0 \\ \rho_{c\phi} & \sqrt{1 - \rho_{c\phi}^2} \end{bmatrix} \quad (\text{A.25})$$

Therefore, the target variables can be derived by solving

$$\begin{Bmatrix} u_c \\ u_\phi \end{Bmatrix} = \mathbf{L}_{\hat{c}\hat{\phi}}^{-1} \begin{Bmatrix} \hat{c} \\ \hat{\phi} \end{Bmatrix} \quad (\text{A.26})$$

where

$$\hat{c} = \frac{c - \mu_c}{\sigma_c} \quad (\text{A.27})$$

$$\hat{\phi} = \frac{\phi - \mu_\phi}{\sigma_\phi} \quad (\text{A.28})$$

then finally given as

$$u_c = \frac{c - \mu_c}{\sigma_c} \quad (\text{A.29})$$

$$u_\phi = -\frac{\rho_{c\phi}}{\sqrt{1 - \rho_{c\phi}^2}} \frac{c - \mu_c}{\sigma_c} + \frac{1}{\sqrt{1 - \rho_{c\phi}^2}} \frac{\phi - \mu_\phi}{\sigma_\phi} \quad (\text{A.30})$$

where u_c and u_ϕ are uncorrelated, standard normal variables with respect to cohesion and friction angle respectively.

A.3.2. Bivariate Log-Normal Distribution. Given as c and ϕ are log-normally distributed with $c \sim LN(\mu_c, \sigma_c)$ and $\phi \sim LN(\mu_\phi, \sigma_\phi)$ and a correlated coefficient $\rho_{c\phi}$, the original covariance matrix is same as the one in the case of normal space (Equation A.23). After transformation, the reduced covariance matrix becomes

$$\hat{\Sigma} = \text{Cov} [\hat{c}, \hat{\phi}] = \begin{bmatrix} 1 & \rho_{\text{Inc}\phi} \\ \rho_{\text{Inc}\phi} & 1 \end{bmatrix} \quad (\text{A.31})$$

where $\rho_{\ln c \rho}$ can be computed based on Equation A.11. Similarly, assume a perfect positive definite matrix, through algorithm A.18 and A.19, the lower triangular matrix can be derived as

$$\mathbf{L}_{\hat{c}\hat{\phi}} = \begin{bmatrix} 1 & 0 \\ \rho_{\ln c \phi} & \sqrt{1 - \rho_{\ln c \phi}^2} \end{bmatrix} \quad (\text{A.32})$$

Through Equation A.26, where

$$\hat{c} = \frac{\ln c - \mu_{\ln c}}{\sigma_{\ln c}} \quad (\text{A.33})$$

$$\hat{\phi} = \frac{\ln \phi - \mu_{\ln \phi}}{\sigma_{\ln \phi}} \quad (\text{A.34})$$

the target variables can be finally derived as

$$u_c = \frac{\ln c - \mu_{\ln c}}{\sigma_{\ln c}} \quad (\text{A.35})$$

$$u_\phi = -\frac{\rho_{\ln c \phi}}{\sqrt{1 - \rho_{\ln c \phi}^2}} \frac{\ln c - \mu_{\ln c}}{\sigma_{\ln c}} + \frac{1}{\sqrt{1 - \rho_{\ln c \phi}^2}} \frac{\ln \phi - \mu_{\ln \phi}}{\sigma_{\ln \phi}} \quad (\text{A.36})$$

where u_c and u_ϕ are uncorrelated, standard normal variables with respect to cohesion and friction angle respectively.

APPENDIX B

LATERAL EARTH PRESSURE THEORY

This appendix presents the generalized extension of two classical lateral earth pressure theories: Coulomb's theory and Rankine's theory, that are involved in the sliding analysis of geosynthetic reinforced slope system in Section 3.4.2.2.1. This part of work is primarily developed based on the previous works summarized by Leshchinsky and Boedeker (1989), Leshchinsky et al. (1995), Elias et al. (2001), Craig (2004), Naresh and Edward (2006), Coduto et al. (2011), and Das (2011) and the manuals of some geotechnical design software that are specialized on reinforced slopes, such as MiraSlope, ReSSA, etc..

B.1. COULOMB'S THEORY

Basically, Coulomb's theory is proposed to calculate the lateral earth pressure on a retaining wall with granular soil backfill, when extended to slope stability analysis, it is suitable for a uniform slope consisting of granular materials in dry condition. The derivation of active force P_a and Coulomb's active earth pressure coefficient K_a has been concluded in Section 2.2.1. But in a more generalized situation, that involves both cohesive soils and groundwater, the active force and the lateral coefficient need to be re-derived by taking equilibrium of the wedges. The procedure is demonstrated in the following sections.

B.1.1. Equilibrium of Backfill Wedge. As shown in Figure B.1, the failure plane in the backfill is assumed inclined at an angle β with the horizontal, on which there are normal force N_a , shearing force T_a and the force due to the pore pressure U_a acting. From Mohr-Coulomb failure criteria, for any point on the failure plane, we have

$$\tau = c'_b + \sigma' \tan \phi'_b \quad (\text{B.1})$$

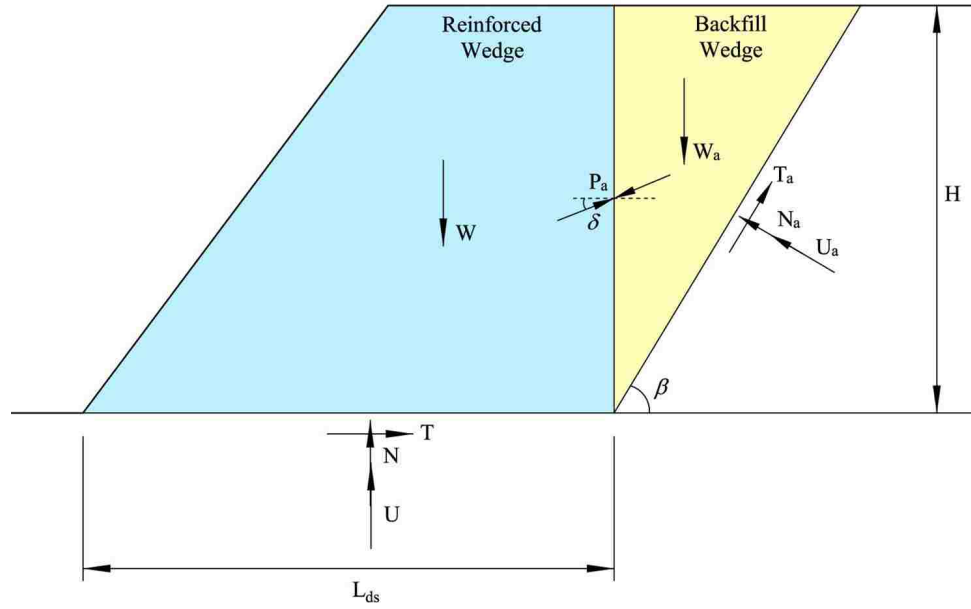


Figure B.1: The two-part wedge mechanism for sliding analysis in a generalized case

where c'_b and ϕ'_b are the effective cohesion and friction angle of backfill soil, respectively.

If the soil properties are constant, it is easy to obtain

$$T_a = C_a + N_a \tan \phi'_b \quad (\text{B.2})$$

where T_a , N_a and C_a can be derived by the integral as

$$T_a = \int \tau ds \quad (\text{B.3})$$

$$C_a = \int c'_b ds \quad (\text{B.4})$$

$$N_a = \int \sigma' ds \quad (\text{B.5})$$

Based on Equation B.2, the forces acting on the failure plane can be conveniently represented by the cohesive force C_a and the resistance force R_a which is a combined of T_a and N_a and inclined at an angle of ϕ'_b with normal direction, as shown in Figure B.2. Taking

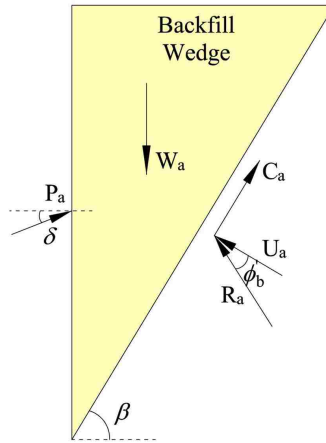


Figure B.2: The forces acting on the backfill wedge

the equilibrium of backfill wedge, we have

$$\begin{cases} W_a = P_a \sin \delta + R_a \cos (\beta - \phi'_b) + C_a \sin \beta + U_a \cos \beta \\ P_a \cos \delta + C_a \cos \beta = R_a \sin (\beta - \phi'_b) + U_a \sin \beta \end{cases} \quad (\text{B.6})$$

By solving Equation B.6, P_a can be derived as

$$P_a = \frac{W_a - \left[\sin \beta + \frac{\cos \beta}{\tan (\beta - \phi'_b)} \right] C_a - \left[\cos \beta - \frac{\sin \beta}{\tan (\beta - \phi'_b)} \right] U_a}{\sin \delta + \frac{\cos \delta}{\tan (\beta - \phi'_b)}} \quad (\text{B.7})$$

where

$$C_a = \frac{c'_b}{\sin \beta} \int_0^H dz = \frac{c'_b H}{\sin \beta} \quad (\text{B.8})$$

and

$$U_a = \frac{\gamma_w}{\sin \beta} \int_{\bar{z}}^H z dz = \frac{\gamma_w}{2 \sin \beta} (H - \bar{z})^2 \quad (\text{B.9})$$

and

$$W_a = \frac{1}{2 \tan \beta} [\gamma'_b (H - \bar{z})^2 + \gamma_b (2H - \bar{z}) \bar{z}] \quad (\text{B.10})$$

with γ_b and γ'_b representing the bulk and buoyant unit weight of backfill respectively; \bar{z} is the depth of ground water table; if $\bar{z} > H$, it means the groundwater is located beneath the slope and its effects are not taken into consideration. By changing β , the failure plane is altered until the maximum P_a is located; on the other hand, this problem can be solved by addressing

$$\frac{dP_a}{d\beta} = 0 \quad (\text{B.11})$$

Once the maximum P_a is derived, it will be considered as the driving force when taking the equilibrium of reinforced wedge.

B.1.2. Equilibrium of Reinforced Wedge. From Equation 2.1, the factor of safety against sliding is computed by summing the horizontal forces that are acting on the reinforced wedge as shown in Figure B.1 and is given by

$$f_s = \frac{T}{P_a \cos \delta} = \frac{C + N \tan \phi'}{P_a \cos \delta} = \frac{c' L_{ds} + (W + P_a \sin \delta - u L_{ds}) \tan \phi'}{P_a \cos \delta} \quad (\text{B.12})$$

where c' is the smaller cohesion of either foundation or reinforced soil; ϕ' is the minimum angle of either the shearing friction between reinforced soil and reinforcements or the friction of foundation soil; u is the pore pressure acting along the base of reinforced mass; and W is the weight of reinforced wedge.

B.2. RANKINE'S THEORY

In Rankine's theory, the wall is assumed frictionless; therefore, the δ that represents the wall friction as shown in Figure B.1 is zero, which produces a horizontal active force P_a that can be computed by Equation 2.6 and 2.7. Therefore, the factor of safety that against sliding can be derived as

$$f_s = \frac{T}{P_a} = \frac{C + N \tan \phi'}{P_a} = \frac{c' L_{ds} + (W - u L_{ds}) \tan \phi'}{P_a} \quad (\text{B.13})$$

where c' is the smaller cohesion of either foundation or reinforced soil; ϕ' is the minimum angle of either the shearing friction between reinforced soil and reinforcements or the fric-

tion of foundation soil; u is the pore pressure acting along the base of reinforced mass; and W is the weight of reinforced wedge.

APPENDIX C
GEOSYNTHETIC PRODUCTS

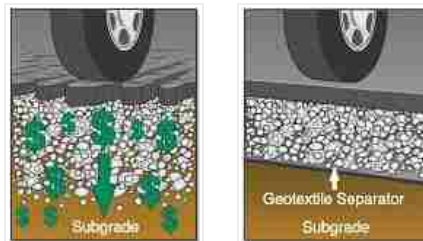
The information of the geosynthetic products used in this study are all collected from US Fabrics (www.usfabricsinc.com). Two types of geosynthetics that are frequently used as reinforcing elements in embankment slopes are woven geotextiles and bi-axial knitted geogrids. To estimate the relationship between price and tensile strength of geosynthetic reinforcements, three woven geotextiles and three bi-axial knitted geogrids are studied with the engineering properties summarized in the following manufacturers data sheets.

US 2600

Woven Geotextile



US 2600 is a woven geotextile made of 100% high-tenacity polypropylene yarns. US 2600 resists ultraviolet and biological deterioration, rotting, naturally encountered basics and acids. Polypropylene is stable within a pH range of 2 to 13. US 2600 meets the following M.A.R.V. values except where noted:



PROPERTY	TEST METHOD	ENGLISH	METRIC
Wide Width Tensile	ASTM D-4595	2,640 x 2,460 lbs/ft (220 x 205 lbs/in)	38.5 x 35.9 kN/m
Tensile Strength @ 2% Strain	ASTM D-4595	480 x 588 lbs/ft (40 x 49 lbs/in)	7.0 x 8.6 kN/m
Wide Width Tensile @ 5% Strain	ASTM D-4595	1,212 x 1,356 lbs/ft (101 x 113 lbs/in)	17.7 x 19.8 kN/m
Wide Width Tensile @ 10% Strain	ASTM D-4595	2,340 x 2,412 lbs/ft (195 x 201 lbs/in)	34.1 x 35.2 kN/m
Apparent Opening Size	ASTM D-4751	30 US Sieve	0.600 mm
Permittivity	ASTM D-4491	0.70 Sec-1	0.70 Sec-1
Permeability	ASTM D-4491	0.04 Sec-1	0.04 Sec-1
Water Flow Rate	ASTM D-4491	50 g/min/sf	2,037 l/min/sm
UV Resistance @ 500 Hours	ASTM D-4355	80%	80%

ROLL SIZE	ROLL DIAMETER	AREA	WEIGHT
15' x 300'	11.0 in	500 sys	240 lbs

This information is provided for reference only and is not intended as a warranty or guarantee. US Fabrics assumes no liability in connection with the use of this information (1/2014).

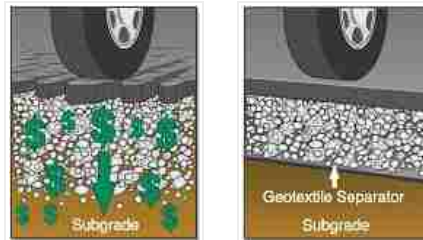
US Fabrics, Inc. | 3904 Virginia Avenue | Cincinnati, OH 45227 (USA) | Phone: 800-518-2290 | Fax: (513) 271-4420

US 3600

Woven Geotextile



US 3600 is a woven geotextile made of 100% high-tenacity polypropylene yarns. US 3600 resists ultraviolet and biological deterioration, rotting, naturally encountered basics and acids. Polypropylene is stable within a pH range of 2 to 13. US 3600 meets the following M.A.R.V. values except where noted:



PROPERTY	TEST METHOD	ENGLISH	METRIC
Wide Width Tensile	ASTM D-4595	3,600 x 3,300 lbs/ft (300 x 275 lbs/in)	52.5 x 48.2 kN/m
Wide Width Tensile @ 2% Strain	ASTM D-4595	540 x 540 lbs/ft (45 x 45 lbs/in)	7.9 x 7.9 kN/m
Wide Width Tensile @ 5% Strain	ASTM D-4595	1,500 x 1,560 lbs/ft (116 x 130 lbs/in)	21.9 x 22.8 kN/m
Wide Width Tensile @ 10% Strain	ASTM D-4595	2,400 x 2,400 lbs/ft (200 x 200 lbs/in)	35 x 35 kN/m
Apparent Opening Size	ASTM D-4751	30 US Sieve	0.60 mm
Permittivity	ASTM D-4491	0.52 Sec-1	0.52 Sec-1
Permeability	ASTM D-4491	0.05 cm/sec	0.05 cm/sec
Water Flow Rate	ASTM D-4491	40 g/min/sf	1,630 l/min/sm
UV Resistance @ 500 Hours	ASTM D-4355	80%	80%

ROLL SIZE	ROLL DIAMETER	AREA	WEIGHT
15' x 300'	13.0 in	500 sys	320 lbs

This information is provided for reference only and is not intended as a warranty or guarantee. US Fabrics assumes no liability in connection with the use of this information (1/2014).

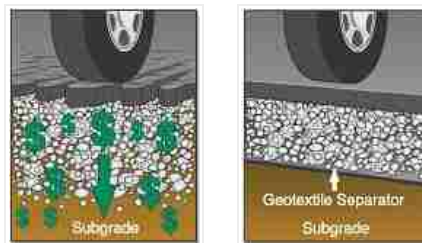
US Fabrics, Inc. | 3904 Virginia Avenue | Cincinnati, OH 45227 (USA) | Phone: 800-518-2290 | Fax: (513) 271-4420

US 4800

Woven Geotextile



NTPEP APPROVED - GTX-2013-01-035. US 4800 is a woven geotextile made of 100% high-tenacity polypropylene yarns. US 4800 resists ultraviolet and biological deterioration, rotting, naturally encountered basics and acids. Polypropylene is stable within a pH range of 2 to 13. US 4800 meets the following M.A.R.V. values except where noted:



PROPERTY	TEST METHOD	ENGLISH	METRIC
Tensile Strength	ASTM D-4632	600 x 600 lbs	2,669 x 2,669 N
Elongation @ Break	ASTM D-4632	20 x 15%	20 x 15%
Wide Width Tensile	ASTM D-4595	4,800 x 4,800 lbs/foot (400 x 400 lbs/in)	70 x 70 kN/m
Wide Width Elongation	ASTM D-4595	10.2 x 7.2%	10.2 x 7.2%
CBR Puncture	ASTM D-6241	1,400 lbs	6,228 N
Trapezoidal Tear	ASTM D-4533	200 x 200 lbs	890 x 890 N
Apparent Opening Size	ASTM D-4751	80 US Sieve	0.18 mm
Permittivity	ASTM D-4491	0.15 Sec-1	0.15 Sec-1
Water Flow Rate	ASTM D-4491	10 g/min/sf	407 l/min/sm
UV Resistance @ 500 Hours	ASTM D-4355	80%	80%

ROLL SIZE	ROLL DIAMETER	AREA	WEIGHT
15' x 300'	16.0 in	500 sys	420 lbs
17.06' x 328'	18.0 in	621.7 sys	540 lbs

This information is provided for reference only and is not intended as a warranty or guarantee. US Fabrics assumes no liability in connection with the use of this information (1/2014).

US Fabrics, Inc. | 3904 Virginia Avenue | Cincinnati, OH 45227 (USA) | Phone: 800-518-2290 | Fax: (513) 271-4420

Microgrid

Bi-Axial Knitted Geogrid



STRATAGRID Microgrid™ is geogrid reinforcement for soil. These high performance geogrids are constructed of high molecular weight and high tenacity polyester yarns utilizing a complex knitting process and polymer coating to provide superior engineering properties. Yarns are precision knitted into a dimensionally stable, uniform network of apertures providing significant tensile reinforcement capacity. STRATAGRID is engineered to be mechanically and chemically durable, in both the harsh construction installation phase and in aggressive soil environments (pH range from 3-9).

PROPERTY	TEST METHOD	ENGLISH	METRIC
Ultimate Strength	ASTM D-6637 Method A	2,000 lbs/ft	29.2 kN/m
Creep Limited Strength	ASTM D-5262/D-6992	1,149 lbs/ft	16.8 kN/m
LTDS (SW, SP, SM, SC)	LTDS or Tal	871 lbs/ft	12.7 kN/m
LTDS (GP, GW, GM, GC, SW, SP, SM, SC)	LTDS or Tal	550 lbs/ft	8.0 kN/m
LTDS (GW, GP, GM, GC)	LTDS or Tal	550 lbs/ft	8.0 kN/m
Molecular Weight (min.)	GRI GG8	-	25,000 g/mol
Carboxyl End Group Count (max.)	GRI GG7	-	30 Meg/kg
Aperture Size	Measured	.10 x .25 in	2.54 x 6.35 mm

ROLL SIZE	ROLL DIAMETER	AREA	WEIGHT
8' x 225'	12.0 in	200 sys	65 lbs

REDUCTION FACTOR	VALUE
RF(id) Soil - 20mm minus, D50 ≤ 0.2mm (SW, SP, SM, SC)	1.20
RF(id) Soil - 25mm minus, D50 ≤ 8mm (GP, GW, GM, GC, SW, SP, SM, SC)	1.90
RF(id) Soil - 50mm minus, D50 ≤ 20mm (GW, GP, GM, GC)	1.90
RF(d) (3 ≤ pH ≤ 9) (PET - CEG < 30, MW > 25,000)	1.10

SOIL INTERACTION COEFFICIENT	VALUE
Silts/Clay (ML, CL)	0.6 - 0.7
Sandy Silts & Clay (SC,GC)	0.7 - 0.8
Poorly-Graded Sand & Gravel, Silty Sand (GP, GM, SP, SM)	0.8 - 0.9
Well-Graded Gravel, Sand Gravel Mix, Well-Graded Sand (SW, GW)	0.9 - 1.0

This information is provided for reference only and is not intended as a warranty or guarantee. US Fabrics assumes no liability in connection with the use of this information (1/2014).

US Fabrics, Inc. | 3904 Virginia Avenue | Cincinnati, OH 45227 (USA) | Phone: 800-518-2290 | Fax: (513) 271-4420

SG 200

Uni-Axial Knitted Geogrid



STRATAGRID is geogrid reinforcement for soil. These high performance geogrids are constructed of high molecular weight and high tenacity polyester yarns utilizing a complex knitting process and polymer coating to provide superior engineering properties. Yarns are precision knitted into a dimensionally stable, uniform network of apertures providing significant tensile reinforcement capacity. STRATAGRID is engineered to be mechanically and chemically durable, in both the harsh construction installation phase and in aggressive soil environments (pH range from 3-9).

PROPERTY	TEST METHOD	ENGLISH	METRIC
Ultimate Strength	ASTM D-6637 Method A	3,600 lbs/ft	52.5 kN/m
Creep Limited Strength	ASTM D-5262/D-6992	2,323 lbs/ft	33.9 kN/m
LTDS (SW, SP, SM, SC)	LTDS or Tal	1,919 lbs/ft	28.0 kN/m
LTDS (GP, GW, GM, GC, SW, SP, SM, SC)	LTDS or Tal	1,836 lbs/ft	26.8 kN/m
LTDS (GW, GP, GM, GC)	LTDS or Tal	1,564 lbs/ft	22.8 kN/m
Molecular Weight (min.)	GRI GG8	-	25,000 g/mol
Carboxyl End Group Count (max.)	GRI GG7	-	30 Meg/kg
Aperture Size	Measured	.72 x .65 in	18.3 x 16.5 mm

ROLL SIZE	ROLL DIAMETER	AREA	WEIGHT
6' x 300'	15.0 in	200 sys	96 lbs
12' x 225'	13.0 in	300 sys	142 lbs

REDUCTION FACTOR	VALUE
RF(id) Soil - 20mm minus, D50 \leq 0.2mm (SW, SP, SM, SC)	1.10
RF(id) Soil - 25mm minus, D50 \leq 8mm (GP, GW, GM, GC, SW, SP, SM, SC)	1.15
RF(id) Soil - 25mm minus, D50 \leq 8mm (GP, GW, GM, GC, SW, SP, SM, SC)	1.35
RF(d) (3 \leq pH \leq 9) (PET - CEG < 30, MW > 25,000)	1.10

SOIL INTERACTION COEFFICIENT	VALUE
Silts/Clay (ML, CL)	0.6 - 0.7
Sandy Silts & Clay (SC,GC)	0.7 - 0.8
Poorly-Graded Sand & Gravel, Silty Sand (GP, GM, SP, SM)	0.8 - 0.9
Well-Graded Gravel, Sand Gravel Mix, Well-Graded Sand (SW, GW)	0.9 - 1.0

This information is provided for reference only and is not intended as a warranty or guarantee. US Fabrics assumes no liability in connection with the use of this information (1/2014).

US Fabrics, Inc. | 3904 Virginia Avenue | Cincinnati, OH 45227 (USA) | Phone: 800-518-2290 | Fax: (513) 271-4420

SG 550

Uni-Axial Knitted Geogrid



STRATAGRID is geogrid reinforcement for soil. These high performance geogrids are constructed of high molecular weight and high tenacity polyester yarns utilizing a complex knitting process and polymer coating to provide superior engineering properties. Yarns are precision knitted into a dimensionally stable, uniform network of apertures providing significant tensile reinforcement capacity. STRATAGRID is engineered to be mechanically and chemically durable, in both the harsh construction installation phase and in aggressive soil environments (pH range from 3-9).

PROPERTY	TEST METHOD	ENGLISH	METRIC
Ultimate Strength	ASTM D-6637 Method A	8,150 lbs/ft	118.9 kN/m
Creep Limited Strength	ASTM D-5262/D-6992	5,258 lbs/ft	76.7 kN/m
LTDS (SW, SP, SM, SC)	LTDS or Tal	4,346 lbs/ft	63.4 kN/m
LTDS (GP, GW, GM, GC, SW, SP, SM, SC)	LTDS or Tal	4,157 lbs/ft	60.7 kN/m
LTDS (GW, GP, GM, GC)	LTDS or Tal	3,541 lbs/ft	51.7 kN/m
Molecular Weight (min.)	GRI GG8	-	25,000 g/mol
Carboxyl End Group Count (max.)	GRI GG7	-	30 Meg/kg
Aperture Size	Measured	0.85/0.35 x 0.95 in	21.6/8.9 x 24.1 mm

ROLL SIZE	ROLL DIAMETER	AREA	WEIGHT
6' x 300'	15.5 in	200 sys	145 lbs
12' x 225'	13.0 in	300 sys	216 lbs

REDUCTION FACTOR	VALUE
RF(id) Soil - 20mm minus, D50 \leq 0.2mm (SW, SP, SM, SC)	1.10
RF(id) Soil - 25mm minus, D50 \leq 8mm (GP, GW, GM, GC, SW, SP, SM, SC)	1.15
RF(id) Soil - 50mm minus, D50 \leq 20mm (GW, GP, GM, GC)	1.35
RF(d) (3 \leq pH \leq 9) (PET - CEG < 30, MW > 25,000)	1.10

SOIL INTERACTION COEFFICIENT	VALUE
Silts/Clay (ML, CL)	0.6 - 0.7
Sandy Silts & Clay (SC,GC)	0.7 - 0.8
Poorly-Graded Sand & Gravel, Silty Sand (GP, GM, SP, SM)	0.8 - 0.9
Well-Graded Gravel, Sand Gravel Mix, Well-Graded Sand (SW, GW)	0.9 - 1.0

This information is provided for reference only and is not intended as a warranty or guarantee. US Fabrics assumes no liability in connection with the use of this information (1/2014).

US Fabrics, Inc. | 3904 Virginia Avenue | Cincinnati, OH 45227 (USA) | Phone: 800-518-2290 | Fax: (513) 271-4420

REFERENCE

- Ang, A. and W. Tang (2007). *Probability Concepts in Engineering: Emphasis on Applications on Civil and Environmental Engineering*. 2nd. Wiley.
- Arai, K. and K. Tagyo (1985). "Determination of Non-circular Slip Surface Giving the Minimum Factor of Safety in Slope Stability Analysis." In: *Soils and Foundations* 25.1, pp. 43–51.
- Babu, G. and B. Basha (2008). "Optimum Design of Cantilever Sheet Pile Walls in Sandy Soils Using Inverse Reliability Approach." In: *Computers and Geotechnics* 35.2, pp. 134–143.
- Baecher, G. and J. Christian (2003). *Reliability and Statistics in Geotechnical Engineering*. John Wiley and Sons Ltd.
- Basha, B. and G. Babu (2008). "Target Reliability Based Design Optimization of Anchored Cantilever Sheet Pile Walls." In: *Canadian Geotechnical Journal* 45.4, pp. 535–548.
- Basha, B. and G. Babu (2010). "Optimum Design for External Seismic Stability of Geosynthetic Reinforced Soil Walls : Reliability Based Approach." In: *Journal of Geotechnical and Geoenvironmental Engineering* 136.6, pp. 797–812.
- Bhattacharya, G., D. Jana, S. Ojha, and S. Chakraborty (2003). "Direct Search for Minimum Reliability Index of Earth Slopes." In: *Computers and Geotechnics* 30.6, pp. 455–462.
- Bygness, R. (2012). "Massive Soil Reinforcement at Cherry Island Extends Landfill's Use for Decades." In: *Geosynthetics* 30.5, pp. 13–19.
- Chan, C., L. Zhang, and J. Ng (2009). "Optimization of Pile Groups Using Hybrid Genetic Algorithms." In: *Journal of Geotechnical and Geoenvironmental Engineering* 135.4, pp. 497–505.
- Chapra, S. (2008). *Applied Numerical Methods with MATLAB for Engineers and Scientists*. Mc Graw Hill.
- Chen, X. and T. Hasselman (1997). "Reliability Based Structural Design Optimization for Practical Applications." In: *38th AIAA Structures, Structural Dynamics, and Materials Conference*.
- Chen, Z. and C. Shao (1988). "Evaluation of Minimum Factor of Safety in Slope Stability Analysis." In: *Canadian Geotechnical Journal* 25.4, pp. 735–748.

- Cheng, Y. (2003). "Location of critical failure surface and some further studies on slope stability analysis." In: *Computers and Geotechnics* 30.3, pp. 255–267.
- Cheng, Y. and C. Lau (2008). *Slope Stability Analysis and Stabilization New Methods and Insight*. Routledge, p. 260.
- Ching, J. (2009). "Equivalence Between Reliability and Factor of Safety." In: *Probabilistic Engineering Mechanics* 24.2, pp. 159–171.
- Ching, J., K. Phoon, and Y. Hu (2009). "Efficient Evaluation of Reliability for Slopes with Circular Slip Surfaces Using Importance Sampling." In: *Journal of Geotechnical and Geoenvironmental Engineering* 135.6, pp. 768–777.
- Cho, S. (2007). "Effects of Spatial Variability of Soil Properties on Slope Stability." In: *Engineering Geology* 92.3-4, pp. 97–109.
- (2013). "First-Order Reliability Analysis of Slope Considering Multiple Failure Modes." In: *Engineering Geology* 154, pp. 98–105.
- Chowdhury, R. and D. Xu (1994). "Rational Polynomial Technique in Slope-Reliability Analysis." In: *Journal of Geotechnical Engineering* 119.12, pp. 1910–1928.
- Christian, J., C. Ladd, and G. Baecher (1995). "Reliability Applied to Slope Stability Analysis." In: *Journal of Geotechnical and Geoenvironmental Engineering* 120.12, pp. 2180–2207.
- Christopher, B., D. Leshchinsky, and R. Stulgis (2005). "Geosynthetic-Reinforced Soil Walls and Slopes: US Perspective." In: *International Perspectives on Soil Reinforcement Applications*. Austin, Texas, pp. 1–12.
- Coduto, D., M. Yeung, and W. Kitch (2011). *Geotechnical Engineering Principles and Practices*. 2nd. Pearson Education, Inc.
- Coley, D. (1999). *An Introduction to Genetic Algorithms for Scientists and Engineers*. World Scientific Publishing Co. Pte. Ltd.
- Cornell, C. (1971). "First Order Uncertainty Analysis of Soils Deformation and Stability." In: *International Conference on Application of Statistics and Probability to Soil and Structural Engineering*, pp. 129–144.
- Craig, R. (2004). *Craig's Soil Mechanics*. 7th. Spon Press.
- Cruse, T. (1997). *Reliability-Based Mechanical Design*. Marcel Dekker, Inc.
- Das, B. (2011). *Principles of Foundation Engineering*. Cengage Learning.

- Deng, M. and R. Luna (2013). "Probability of Failure for Slopes with Sensitivity Analysis." In: *Geo-Congress 2013: Stability and Performance of Slopes and Embankments III*, pp. 925–961.
- Du, X., J. Guo, and H. Beeram (2007). "Sequential Optimization and Reliability Assessment for Multidisciplinary Systems Design." In: *Structural and Multidisciplinary Optimization* 35.2, pp. 117–130.
- Du, X., W. Chen, and Y. Wang (2010). "Most Probable Point-Based Methods." In: *Extreme Statistics in Nanoscale Memory Design (Integrated Circuits and Systems)*. Ed. by A. Singhee and R. Rutenbar. Springer.
- Duncan, J. (1996). "State of the Art: Limit Equilibrium and Finite-Element Analysis of Slopes." In: *Journal of Geotechnical Engineering* 122.7, pp. 577–596.
- Duncan, J. and S. Wright (1980). "The Accuracy of Equilibrium Methods of Slope Stability Analysis." In: *Engineering Geology* 16, pp. 5–17.
- EI-Ramly, H., N. Morgenstern, and D. Cruden (2004). "Probabilistic Stability Analysis of an Embankment on Soft Clay." In: *57th Canadian Geotechnical Conference*, pp. 14–21.
- Elias, V., B. Christopher, and R. Berg (2001). *Mechanically Stabilized Earth Walls and Reinforced Soil Slopes Design and Construction Guidelines*. Tech. rep. 132042. Washington DC: U.S. Department of Transportation Federal Highway Administration.
- Elkateb, T., R. Chalaturnyk, and P. Robertson (2003). "An Overview of Soil Heterogeneity : Quantification and Implications on Geotechnical Field Problems." In: *Canadian Geotechnical Journal* 15, pp. 1–15.
- Gasser, M. and G. Schueller (1997). "Reliability-Based Optimization of Structural Systems." In: *Mathematical Methods of Operations Research* 46.3, pp. 287–307.
- Gong, J.-X. and P. Yi (2010). "A Robust Iterative Algorithm for Structural Reliability Analysis." In: *Structural and Multidisciplinary Optimization* 43.4, pp. 519–527.
- Grandhi, R. and L. Wang (1998). "Reliability-Based Structural Optimization Using Improved Two-Point Adaptive Nonlinear Approximations." In: *Finite Elements in Analysis and Design* 28.1, pp. 35–48.
- Greco, V. (1996). "Efficient Monte Carlo Technique for Locating Critical Slip Surface." In: *Journal of Geotechnical Engineering* 122.7, pp. 517–525.
- Griffiths, D. and G. Fenton (2004). "Probabilistic Slope Stability Analysis by Finite Elements." In: *Journal of Geotechnical and Geoenvironmental Engineering* 130.5, pp. 507–518.

- Griffiths, D. and G. Fenton (2007). *Probabilistic Methods in Geotechnical Engineering*. Springer Wien New York.
- (2008). *Risk Assessment in Geotechnical Engineering*. John Wiley and Sons Ltd.
- Guo, J. and X. Du (2009). “Reliability Sensitivity Analysis with Random and Interval Variables.” In: *International Journal for Numerical Methods in Engineering* 78, pp. 1585–1617.
- Hassan, A. and T. Wolff (1999). “Search Algorithm for Minimum Reliability Index of Earth Slopes.” In: *Journal of Geotechnical and Geoenvironmental Engineering* 125.4, pp. 301–308.
- Higham, N. (2002). *Accuracy and Stability of Numerical Algorithms*. 2nd. Philadelphia, PA: Society for Industrial and Applied Mathematics.
- Houlihan, M. et al. (2010). “Use of Reliability Methods as a Project Management Tool: The Cherry Island Landfill Expansion Project.” In: *GeoFlorida2010: Advances in Analysis, Modeling and Design*. GSP 199, pp. 1924–1933.
- Jacques, J., C. Lavergne, and N. Devictor (2006). “Sensitivity Analysis in Presence of Model Uncertainty and Correlated Inputs.” In: *Reliability Engineering and System Safety* 91.10-11, pp. 1126–1134.
- Jiang, H., C. Lee, and D. Zhu (2003). “Generalised Framework of Limit Equilibrium Methods for Slope Stability Analysis.” In: *Géotechnique* 53.4, pp. 377–395.
- Koerner, R. (2005). *Designing with Geosynthetics*. 5th. Pearson Education, Inc.
- Krounis, A. and F. Johansson (2011). “The Influence of Correlation between Cohesion and Friction Angle on the Probability of Failure for Sliding of Concrete Dams.” In: *Risk Analysis, Dam Safety, Dam Security and Critical Infrastructure Management; Proceedings of the 3rd International Forum on Risk Analysis, Dam Safe*. Valencia, pp. 75–80.
- Kullback, S. and R. Leibler (1951). “One Information and Sufficiency.” In: *The Annals of Mathematical Statistics* 22.1, pp. 79–86.
- Leshchinsky, D. and R. Boedeker (1989). “Geosynthetic Reinforced Soil Structures.” In: *Journal of Geotechnical Engineering* 115.10, pp. 1459–1478.
- Leshchinsky, D., H. Ling, and G Hanks (1995). “Unified Design Approach to Geosynthetic Reinforced Slopes and Segmental Walls.” In: *Geosynthetics International* 2.5, pp. 845–881.

- Leshchinsky, D., B. Kang, J. Han, and H. Ling (2014). “Framework for Limit State Design of Geosynthetic-Reinforced Walls and Slopes.” In: *Transportation Infrastructure Geotechnology* 1.2, pp. 129–164.
- Li, K. and R. Cheung (2001). “Discussion: Search Algorithm for Minimum Reliability Index of Earth Slopes.” In: *Journal of Geotechnical and Geoenvironmental Engineering* 127.2, pp. 194–200.
- Li, K. and P. Lumb (1987). “Probabilistic Design of Slopes.” In: *Canadian Geotechnical Journal* 24.4, pp. 520–535.
- Li, W. and L. Yang (1994). “An Effective Optimization Procedure Based on Structural Reliability.” In: *Computer and Structures* 52.5, pp. 1061–1067.
- Liu, H., W. Chen, and A. Sudjianto (2004). “Probabilistic Sensitivity Analysis Methods for Design Under Uncertainty.” In: *10th AIAA/ISSMO Multidisciplinary Analysis and Optimization Conference*, pp. 1–15.
- Loehr, J., C. Finley, and D. Huaco (2006). *Procedures for Design of Earth Slopes Using LRFD*. Tech. rep. January, p. 82.
- Low, B. and W. Tang (1997). “Probabilistic Slope Analysis Using Janbu’s Generalized Procedure of Slices.” In: *Computers and Geotechnics* 21.2, pp. 121–142.
- (2007). “Efficient Spreadsheet Algorithm for First-Order Reliability Method.” In: *Journal of Engineering Mechanics* 133.12, pp. 1378–1387.
- Martinez, W. and A. Martinez (2002). *Computation Statistics Handbook with MATLAB*. Chapman and Hall/CRC, pp. 280–285.
- McCombie, P. and P. Wilkinson (2002). “The Use of the Simple Genetic Algorithm in Finding the Critical Factor of Safety in Slope Stability Analysis.” In: *Computers and Geotechnics* 29.8, pp. 699–714.
- Melanie, M. (1999). *An Introduction to Genetic Algorithms*. 5th. Massachusetts Institute of Technology.
- Melchers, R. (1999). *Structural Reliability Analysis and Prediction*. John Wiley and Sons Ltd.
- Morgenstern, N. and D. Cruden (2002). “Probabilistic Slope Stability Analysis for Practice.” In: *Canadian Geotechnical Journal* 683, pp. 665–683.
- Naresh, C. and A. Edward (2006). *FHWA Soils and Foundations Reference Manual - Volume I*. Tech. rep. 132012. U.S. Department of Transportation Federal Highway Administration.

- Nguyen, V. (1985). "Determination of Critical Slope Failure Surface." In: *Journal of Geotechnical Engineering* 111.2, pp. 238–250.
- Onyejekwe, S. (2012). "Characterization of Soil Variability for Reliability-Based Design." PhD thesis. Missouri University of Science and Technology.
- Phoon, K. (2008). *Reliability-Based Design in Geotechnical Engineering Computations and Applications*. Taylor and Francis, p. 545.
- Phoon, K. and F. Kulhawy (1999a). "Characterization of Geotechnical Variability." In: *Canadian Geotechnical Journal* 36.4, pp. 612–624.
- (1999b). "Evaluation of Geotechnical Property Variability." In: *Canadian Geotechnical Journal* 36.4, pp. 625–639.
- Rackwitz, R. and B. Fiessler (1978). "Structural Reliability Under Combined Random Load Sequences." In: *Computers and Structures* 9, pp. 489–494.
- Reddy, M., R. Granhdi, and D. Hopkins (1994). "Reliability Based Structural Optimization: A Simplified Safety Index Approach." In: *Computer and Structures* 53.6, pp. 1407–1418.
- Rethati, L. (1988). *Probabilistic Solutions in Geotechnics*. Amsterdam.
- Santosh, T., R. Saraf, A. Ghosh, and H. Kushwaha (2006). "Optimum Step Length Selection Rule in Modified HL–RF Method for Structural Reliability." In: *International Journal of Pressure Vessels and Piping* 83.10, pp. 742–748.
- Sengupta, A. and A. Upadhyay (2009). "Locating the Critical Failure Surface in A Slope Stability Analysis by Genetic Algorithm." In: *Applied Soft Computing* 9.1, pp. 387–392.
- Silvestri, V. (1983). "The Bearing Capacity of Dykes and Fills Founded on Soft Soils of Limited Thickness." In: *Canadian Geotechnical Journal* 20.3, pp. 428–436.
- Su, X. (2008). *Global Optimization in Slope Analysis by Simulated Annealing*. Tech. rep., p. 45.
- Talebizadeh, P., M. Mehrabian, and M. Abdolzadeh (2011). "Prediction of the Optimum Slope and Surface Azimuth Angles Using the Genetic Alogrithm." In: *Energy and Buildings* 43.11, pp. 2998–3005.
- Tu, J., K. Choi, and Y. Park (1999). "A New Study on Reliability- Based Design Optimization." In: *Journal of Mechanical Design* 121.4, pp. 557–564.

- Uzielli, M., S. Lacasse, and F. Nadim (2007). "Soil Variability Analysis for Geotechnical Practice." In: *Characterisation and Engineering Properties of Natural Soils*. Taylor and Francis, pp. 1653–1754.
- Valdebenito, M. and G. Schuëller (2010). "A Survey on Approaches for Reliability-based Optimization." In: *Structural and Multidisciplinary Optimization* 42.5, pp. 645–663.
- Vanmarcke, E. (1977). "Reliability of Earth Slopes." In: *Journal of the Geotechnical Engineering Division* 103.11, pp. 1247–1265.
- Wang, L., R. Grandhi, and D. Hopkins (1995). "Structural Reliability Optimization Using An Efficient Safety Index Calculation Procedure." In: *International Journal for Numerical Methods of Engineering* 38.10, pp. 1721–1738.
- Wang, Y. (2009). "Reliability-Based Economic Design Optimization of Spread Foundations." In: *Journal of Geotechnical and Geoenvironmental Engineering* 135.7, pp. 954–959.
- Wang, Y. and F. Kulhawy (2008). "Economic Design Optimization of Foundations." In: *Journal of Geotechnical and Geoenvironmental Engineering* 134.8, pp. 1097–1105.
- Wolff, T. (1985). "Analysis and Design of Embankment Dam Slopes: A Probabilistic Approach." Ph.D. Thesis. Purdue University.
- Wu, Y. (1994). "Computational Methods for Efficient Structural Reliability and Reliability Sensitivity Analysis." In: *AIAA Journal* 32.8, pp. 1717–1723.
- Xu, B and B. Low (2006). "Probabilistic Stability Analyses of Embankments Based on Finite-Element Method." In: *Journal of Geotechnical and Geoenvironmental Engineering* 132.11, pp. 1444–1454.
- Xue, J. and K. Gavin (2007). "Simultaneous Determination of Critical Slip Surface and Reliability Index for Slopes." In: *Journal of Geotechnical and Geoenvironmental Engineering* 133.7, pp. 878–886.
- Yamagami, T. and J. Jiang (1997). "A Search for the Critical Slip Surface in Three-Dimensional Slope Stability Analysis." In: *Soils and Foundations* 37.3, pp. 1–16.
- Yang, D., G. Li, and G. Cheng (2006). "Convergence Analysis of First Order Reliability Method Using Chaos Theory." In: *Computers and Structures* 84.8-9, pp. 563–571.
- Yates, D., D. Moore, and D. Starnes (2003). *The Practice of Statistics*. 2nd. New York: Freeman.
- Yu, H., R. Salgado, S. Sloan, and J. Kim (1998). "Limit Analysis versus Limit Equilibrium for Slope Stability." In: *Journal of Geotechnical and Geoenvironmental Engineering* 124.1.

- Zhang, J., L. M. Zhang, and W. Tang (2009). "Bayesian Framework for Characterizing Geotechnical Model Uncertainty." In: July, pp. 932–940.
- Zhang, J., L. Zhang, and W. Tang (2011a). "Reliability-Based Optimization of Geotechnical Systems." In: *Journal of Geotechnical and Geoenvironmental Engineering* 137.12, pp. 1211–1221.
- (2011b). "Slope Reliability Analysis Considering Site-Specific Performance Information." In: *Journal of Geotechnical and Geoenvironmental Engineering* 137.3, pp. 227–238.
- Zhang, J., H. Huang, C. Juang, and D. Li (2013). "Extension of Hassan and Wolff method for system reliability analysis of soil slopes." In: *Engineering Geology* 160, pp. 81–88.
- Zolfaghari, A., A. Heath, and P. McCombie (2005). "Simple Genetic Algorithm Search for Critical Non-Circular Failure Surface in Slope Stability Analysis." In: *Computers and Geotechnics* 32.3, pp. 139–152.

VITA

Michelle (Mingyan) Deng was born in Shanghai, China in 1987. She got her start in civil engineering at Tongji University in Shanghai, China, where she earned a B.S. degree in civil engineering in June 2009. After graduating from Tongji University, she attended Missouri University of Science and Technology (formerly University of Missouri at Rolla) for advanced degrees. Michelle received a non-thesis, M.S. degree in civil engineering with a geotechnical emphasis in May 2011; and subsequently began her Ph.D. studies in the same research program and received her degree in August 2015. In addition to her studies and research, Michelle served as a teaching assistant and a lecturer from 2010 to 2014 at Missouri University of Science and Technology.